

**COMPUTATIONAL AND EXPERIMENTAL
STUDY OF AIR HYBRID ENGINE
CONCEPTS**

A thesis submitted for the degree of Doctor of Philosophy

by

Cho-Yu Lee

School of Engineering and Design

Brunel University

West London, United Kingdom

March 2011

Brunel University

School of Engineering and Design

West London, United Kingdom

Cho-Yu Lee

COMPUTATIONAL AND EXPERIMENTAL

STUDY OF AIR HYBRID ENGINE

CONCEPTS

March 2011, PhD

Abstract

The air hybrid engine absorbs the vehicle kinetic energy during braking, stores it in an air tank in the form of compressed air, and reuses it to start the engine and to propel a vehicle during cruising and acceleration. Capturing, storing and reusing this braking energy to achieve stop-start operation and to give additional power can therefore improve fuel economy, particularly in cities and urban areas where the traffic conditions involve many stops and starts. In order to reuse the residual kinetic energy, the vehicle operation consists of 3 basic modes, i.e. Compression Mode (CM), Expander Mode (EM) and normal firing mode, as well as stop-start operation through an air starter.

A four-cylinder 2 litre diesel engine has been modelled to operate in four air hybrid engine configurations so that the braking and motoring performance of each configuration could be studied. These air hybrid systems can be constructed with production technologies and incur minimum changes to the existing engine design. The regenerative engine braking and starting capability is realised through the employment of an innovative simple one-way intake system and a production cam profile switching (CPS) mechanism. The hybrid systems will allow the engine to be cranked by the compressed air at moderate pressure without using addition starters or dedicated valves in the cylinder head. Therefore, the proposed air hybrid engine systems can be considered as a cost-effective regenerative hybrid powertrain and can be implemented in vehicles using existing production technologies.

A novel cost-effective pneumatic regenerative stop-start hybrid system, Regenerative Engine Braking Device (RegenEBD), for buses and commercial vehicles is presented. RegenEBD is capable of converting kinetic energy into pneumatic energy in the compressed air saved in an air tank using a production engine braking device and other production type automotive components and a proprietary intake system design. The compressed air is then used to drive an air starter to achieve regenerative stop-start operations. The proposed hybrid system can work with the existing vehicle transmission system and can be implemented with the retro-fitted valve actuation device and a sandwich block mounted between the cylinder head and the production intake manifold.

Compression mode operation is achieved by keeping the intake valves from fully closed throughout the four-strokes through a production type variable valve exhaust brake (VVEB) device on the intake valves. As a result, the induced air could be compressed through the opening gap of intake valves into the air tank through the intake system of proprietary design. The compressed air can then be used to crank the engine directly through the air expander operation or indirectly through the action of an air starter in production.

A single cylinder camless engine has been set up and operated to evaluate the compression mode performance of two air hybrid concepts. The experimental results are then compared with the computational output with excellent agreement.

In order to evaluate the potential of the air hybrid engine technologies, a new vehicle driving cycle simulation program has been developed using Matlab Simulink. An air hybrid engine sub-model and methodology for modelling the air hybrid engine's performance have been proposed and implemented in the vehicle driving cycle simulation. The NEDC analysis of a Ford Mondeo vehicle shows that the vehicle can achieve regenerative stop-start operations throughout the driving cycle when it is powered by a 2.0litre diesel engine with air hybrid operation using a 40litre air tank of less than 10bar pressure. The regenerative stop-start operation can lead to 4.5% fuel saving during the NEDC. Finally, the Millbrook London Transport Bus (MLTB) driving cycle has been used to analyse the effectiveness of RegenEBD on a double deck bus powered by a Yuchai diesel engine. The results show that 90% stop-starts during the MLTB can be accomplished by RegenEBD and that a significant fuel saving of 6.5% can be obtained from the regenerative stop-start operations.

Acknowledgments

I would like to express my most gratitude to my supervisor, Professor Hua Zhao, whose expertise, understanding, and patience, added considerably to me who was new to the project. After writing up my thesis, I have found out how much work I have done so far all guided under Prof. Zhao who has given me full support on the scholarship as well as computational and experimental facilities.

I would like to thank members of Brunel engine group. First of all, I must acknowledge Professor Tom Ma who is always giving professional comments on my research. Furthermore, a very special thank goes to Dr. Yan Zhang, without whose assistance of experimental work I would have had hard time on my research process. Last, but not least, I would like to thank my good friends and colleagues, Andrew Selway, Dr. Navin Kalia, Dr. Montajir Rahman, Dr. Changho Yang, Dr. Seong-Ho Jin, Haofan Zhang, Norman Hung, Wade Lai, and Dr. Ali Persian for their kindly help and friendship to enrich my life experience.

Finally, I would like to express my gratitude and appreciation to my family for the support they have provided me through my entire life and in particular, I must acknowledge my mother, Li-Fen Lin, my brother Cho-Hao Lee, my sister, Cho-Ying Lee, my grandfather, Bing-Shen Lee, my grandmother, Ren-Qing Zheng, my auntie, Pei-Zhi Lee, my uncle, I-Chih Yang, and my wife, Pei-Lan Wu, without whose love, encouragement and financial support, I would not have finished this thesis.

Nomenclature

Abbreviations

ABDC	After Bottom Dead Centre
ATDC	After Top Dead Centre
BBDC	Before Bottom Dead Centre
BDC	Bottom Dead Centre
bmep	brake mean effective pressure
BTDC	Before Top Dead Centre
CA	Crank Angle
CATC	Compressed Air Transfer Coefficient
CI	Compression Ignition
CM	Compressor Mode
CPS	Cam Profile Switching
ECV	Energy Control Valve
EM	Expander Mode
EUDC	European Urban Driving Cycle
FTP	Federal Test Procedure
FVVA	Fully Variable Valve Actuation
FVVT	Fully Variable Valve Train
HDV	Heavy Duty Vehicle
HEV	Hybrid Electric Vehicle
imep	indicated mean effective pressure
IC	Internal Combustion
IVC	Intake Valve Close
IVO	Intake Valve Open
MIPS	Million Instructions per Second
NEDC	New European Driving Cycle
PC	Personal Computer
rpm	revolutions per minute
SI	Spark Ignition
TDC	Top Dead Centre
UPS	Uninterruptible Power Supply

Notation

a	acceleration
α_d	rotational acceleration of the driveshaft
α_e	rotational acceleration of the engine
A	piston area
Amp	ampere
A_f	vehicle frontal area
Ah	ampere hours
$bmep_b$	braking brake mean effective pressure
$bmep_m$	motoring brake mean effective pressure
C_d	aerodynamic drag coefficient
$CATC_b$	braking compressed air transfer coefficient
$CATC_m$	motoring compressed air transfer coefficient
E_s	starting energy
F_a	aerodynamic drag force
F_d	disturbance force
F_G	gas force
F_r	rolling resistance
F_t	traction force
F_T	tangential force
g	gravitational acceleration
LHV	lower heating value
I_d	rotational inertia of the driveshaft
I_e	rotational inertia of the engine
I_w	rotational inertia of the wheels
m_c	mass of the air charge
m_f	fuel mass
m_t	mass of the air stored
m_v	vehicular mass
N_f	numerical ratio of the final drive
N_t	numerical ratio of the transmission
p	pressure
p_t	absolute airtank pressure
R	universal gas constant

R_c	compression ratio
r_w	wheel radius
t	time
T	temperature
T_d	torque demand on the driveshaft
T_e	torque demand on the engine
T_f	friction torque
T_t	airtank temperature
v	vehicle speed
V	volt
V_c	volume of the cylinder
V_t	airtank volume
ω_w	speed of all wheels
ρ_a	air density
α	crankshaft angle
β	pivoting angle of the connecting rod
γ	half stroke
l	length of the connecting rod
λ	ratio of γ and l
μ_r	rolling drag coefficient
η_{al}	alternator efficiency
η_b	engine braking efficiency
η_{ch}	battery charging efficiency
η_{dis}	battery discharging efficiency
η_{st}	starter motor efficiency

Chemical symbols

CO	carbon monoxide
CO ₂	carbon dioxide
HC	hydrocarbons
NO _x	nitrogen oxides

Table of Contents

Abstract	i
Acknowledgments	iii
Nomenclature	iv
Chapter 1: Introduction	1
1.1 Overview	1
1.2 Objectives	4
1.3 Structure of thesis	4
Chapter 2: Literature Review	6
2.1 Introduction	6
2.2 Hybrid electric vehicles	7
2.2.1 Benefits of hybrid electric vehicles	7
2.2.2 Electric hybrid vehicle powertrain systems	9
2.2.2.1 Series hybrids	9
2.2.2.2 Parallel hybrids	10
2.2.2.3 Series-parallel hybrids	11
2.2.3 Hybrid Electric Commercial Vehicles	11
2.2.4 Mild Hybrid Electric Vehicles	12
2.3 Hydraulic hybrid vehicles	13
2.4 Air hybrid engine concepts	17
2.4.1 Theoretical studies of idealized air hybrid concepts	17
2.4.2 Air hybrid engine concepts based on the use of camless valve train system	19
2.4.3 Air hybrid engine with pneumatic actuator	23
2.4.4 The Downsized and supercharged hybrid pneumatic engine	24
2.5 Summary	24
Chapter 3: Analytical Studies of Air Hybrid Concepts for a Light Duty Diesel Engine	27
3.1 Introduction	27
3.2 Air Hybrid Engine with split intake ports	28
3.2.1 Description of the concept	28
3.2.2 The principle of operation	30
3.2.3 Overview of three concepts	34

3.2.4	Engine simulation setup.....	34
3.2.5	Simulation Results.....	38
3.2.5.1	<i>Valve timing optimization for CM</i>	38
3.2.5.2	<i>Valve timing optimization for the cranking mode</i>	41
3.2.5.3	<i>Comparison between an insulated airtank and a normal airtank</i>	43
3.2.6	Conclusions	48
3.3	Ford PUMA air hybrid engine with joint intake ports.....	48
3.3.1	Description of the concept	48
3.3.2	The Principle of operation.....	49
3.3.3	Engine simulation setup.....	51
3.3.4	Simulation Results.....	54
3.3.4.1	<i>Intake valves timing for CM</i>	54
3.3.4.2	<i>Valves timing optimization for the cranking mode</i>	58
3.3.5	Conclusions	61
3.4	Summary	62
Chapter 4: Analytical Studies of Air Hybrid Concepts for a Medium Duty Diesel Engine.....		
4.1	Introduction.....	65
4.2	YUCHAI air hybrid engine with a Variable Valve Exhaust Braking device	65
4.2.1	Description of the Air Hybrid Engine Setup	65
4.2.2	The Principle of operation.....	67
4.2.3	Engine simulation setup.....	68
4.2.4	Simulation Results.....	72
4.2.4.1	<i>Compression mode operation</i>	72
4.2.4.2	<i>Cranking mode operation</i>	75
4.2.4.3	<i>Regenerative stop-start system with an air starter</i>	78
4.3	YUCHAI air hybrid engine with Jacobs brake.....	79
4.3.1	Description of the Air Hybrid Engine Setup	80
4.3.2	The Principle of operation.....	81
4.3.3	Engine simulation setup.....	82
4.3.4	Simulation Results.....	85
4.3.4.1	<i>Compression mode operation</i>	85
4.3.5	Conclusions	88

Chapter 5: Experimental Studies of the Air Hybrid Engine Operation	90
5.1 Introduction	90
5.2 Engine Testing Equipment and Facility	90
5.2.1 The Single Cylinder Camless Engine	90
5.2.2 Engine Control Module	91
5.2.2.1 R-Cube and Valve Control Unit	91
5.2.2.2 Electro hydraulic valve actuator	92
5.2.2.3 Hydraulic pump unit	93
5.2.3 Air intake system	94
5.3 Experimental Measurement and Data Analysis	95
5.3.1 Mass flow meter	95
5.3.2 In-cylinder pressure measurement	95
5.3.3 Data Acquisition System	96
5.3.4 The daily checks	97
5.4 Experiments on the air hybrid engine operation with a Reed Valve	97
5.4.1 Compression mode operation with an intake Reed Valve	97
5.4.2 Experimental results	101
5.5 Experiments on the air hybrid engine with a split intake runner block ...	105
5.5.1 Principle of the operation	105
5.5.2 Experimental results	107
5.6 Evaluation of the engine simulation for the air hybrid engine with a split intake runner block	114
5.6.1 Engine simulation setup	114
5.6.2 Comparison between predicted and experimental results	116
5.7 Summary	119
Chapter 6: Driving Cycle Analysis of Air Hybrid Vehicles	120
6.1 Introduction	120
6.2 Driving Cycle Simulation Model of an Air hybrid vehicle	120
6.2.1 Model Overview	120
6.2.2 Sub-models of normal vehicle operations	124
6.2.2.1 Longitudinal dynamics sub-model	124
6.2.2.2 Aerodynamic drag force	124
6.2.2.3 Rolling resistance	124
6.2.2.4 Disturbance force	125

6.2.2.5	<i>Final drive control sub-model</i>	125
6.2.2.6	<i>Transmission control sub-model</i>	126
6.2.3	Air Hybrid Control sub-model	130
6.2.4	Airtank pressure control loop	131
6.3	Driving cycle analysis of an air hybrid Light Duty Diesel Vehicle	131
6.3.1	Vehicle data	131
6.3.2	Engine response map for the compressor mode operation	132
6.3.3	Engine response maps for the cranking mode operation	133
6.3.4	New European Driving Cycles for light duty vehicles	138
6.3.5	Results and analysis	138
6.3.5.1	<i>Air Hybrid Vehicle Speed and Load Analysis</i>	138
6.3.5.2	<i>Compression braking</i>	140
6.3.5.3	<i>Engine cranking and compressed air usage</i>	143
6.3.5.4	<i>Fuel consumption</i>	144
6.4	Driving Cycle Analysis of a City Bus	145
6.4.1	Bus data	145
6.4.2	YUCHAI YC6A 7.25 litre diesel engine response map for the compressor mode operation	146
6.4.3	Engine response maps for the cranking mode operation	146
6.4.4	Millbrook London Transport Bus (MLTB) Drive Cycle	147
6.4.5	Results and discussion on YUCHAI air hybrid engine	147
6.4.5.1	<i>Air Hybrid Vehicle Speed and Load Analysis</i>	147
6.4.5.2	<i>Compression braking</i>	149
6.4.5.3	<i>Engine cranking and compressed air usage</i>	151
6.4.5.4	<i>Fuel consumption</i>	153
6.4.6	Analysis of the potential of the current alternator/battery system for HGVs	154
6.4.6.1	<i>Reality check for starting energy and hence equivalent fuel required for starting</i>	154
6.4.6.2	<i>Battery charging ability</i>	155
6.4.6.3	<i>Durability of Battery and Starter Motors</i>	155
6.5	Summary	156
Chapter 7:	Conclusions and Further Work	158
7.1	Conclusions	158
7.1.1	Predicted Air Hybrid Engine Performance	158

7.1.1.1	<i>Air hybrid concept 1 with Reed valve for a light duty diesel engine</i>	158
7.1.1.2	<i>Air hybrid engine concept 2 with a port throttle for a light duty diesel engine</i>	159
7.1.1.3	<i>Air hybrid engine concept 3 for a light duty diesel engine.</i>	159
7.1.1.4	<i>Air hybrid engine 4 with joint intake ports for a light duty diesel engine</i>	160
7.1.1.5	<i>RegenEBD Technology with VVEB</i>	160
7.1.1.6	<i>RegenEBD Technology with a compression release engine braking device</i>	160
7.1.2	Experimental Validation of Air Hybrid Concepts	161
7.1.2.1	<i>The air hybrid engine operation with a Reed Valve</i>	161
7.1.2.2	<i>The air hybrid engine with a split intake runner block</i>	161
7.1.3	Vehicle simulation	161
7.1.3.1	<i>Driving cycle analysis of an air hybrid Light Duty Diesel Vehicle</i>	161
7.1.3.2	<i>Driving cycle analysis of a city bus</i>	162
7.2	Further work	163
	References	165
	Appendix	172

Chapter 1: Introduction

1.1 Overview

Almost all automotive vehicles are powered by internal combustion (IC) engines. Due to the combustion of hydrocarbon fuels, automotive vehicles emit harmful emissions, such as Carbon monoxide (CO), Oxides of Nitrogen (NO_x), particulate matter (PM) and Unburned Hydrocarbon (uHC). Over the last few decades, significant progress has been made in reducing vehicle exhaust emissions through a combination of engine technologies and after-treatment systems in order to meet ever stringent emission legislations. Compared to the Euro 4 standard for light duty diesel engines implemented in 2005, the Euro 5 standard introduced in 2010 represents an 80% and a 25% reduction in PM and NO_x emissions respectively [1]. The Euro 6 standard, which is expected to be introduced in 2014 will impose another 50% reduction in NO_x emissions in Euro 5 standard. Commercial vehicles are subject to similar stringent emission legislations. The recent developments in PM traps and SCR NO_x or NO_x traps will enable automotive vehicles to meet such emission legislations.

Climate change and energy security are among the critical social issues in recent years. Carbon dioxide (CO₂) emissions of the transport sector, which are one of the most important anthropogenic sources, have significant impacts on not only climate change but also energy security, as lower CO₂ emission means lower fuel consumption. An initiative has been taken from the EU by committing to cut its emissions of CO₂ and other greenhouse gases by at least one fifth of their 1990 levels by 2020 [2].

Within the European Union (EU), road transport contributes about one fifth of the total EU's CO₂ emissions and passenger cars are responsible for around 12% [3]. The heavy duty vehicle (HDV) fleet contributes a disproportionately large percentage to the overall carbon emissions. For example, the UK HDV fleet currently consumes more than 13.5 billion litres of liquid fuel each year and contributes 8.96 percent to overall UK carbon emissions. According to the European Union [4], freight traffic is forecast to grow, measured in tonne-kilometres, by 63% across the main European markets by 2030. Transport growth, and therefore strong demand for trucks and buses, comes also from emerging economies like Brazil, Russia, India and China. For many transport companies, fuel is the main operating cost. For others, it constitutes a significant part of their overall

budget. There is a strong environmental as well business case for fuel efficiency. For every litre of diesel burnt, 2.6 kg of carbon dioxide is released into the atmosphere. Therefore, less fuel used means lower emissions and lower costs for business. Significant CO₂ reductions from such vehicles are therefore important to achieving the overall CO₂ reduction target given the large population of buses and delivery vehicles.

Over the past few decades, the Internal Combustion (IC) engine, both gasoline and diesel, has performed considerably and continuously improved on both fuel economy and emissions. Nowadays, the gasoline engine can incorporate a broad range of options, including variable geometry intake systems, Variable Valve Timing (VVT), gasoline direct injection, turbo-charging and port deactivation for better performance. Similarly, many technologies, including VVT, advanced boost, homogeneous combustion and advanced Exhaust Gas Recirculation (EGR) systems, have been developed to improve diesel engine out emissions and fuel economy. However, some of the advanced technologies to reduce CO₂ emissions from light-duty vehicles are not feasible for heavy duty vehicles. Due to their high energy usage, strategies such as electrification are unlikely to be commercially viable for heavy duty vehicles, so alternative solutions should be researched and then developed.

For buses and delivery vehicles, engine part-load efficiency contributes significantly towards the vehicle's overall fuel economy and can be improved by engine downsizing, which involves the use of a smaller engine of higher specific power in place of a larger engine. In addition, the vehicle's fuel economy can also be improved by down-speeding through early gear shift. However, the diesel engine downsizing and down-speeding are often accompanied by inadequate performance during acceleration due to turbo-lag, which can be minimised if instant supply of compressed air can be provided during the transient operation.

While the traffic conditions involve frequent vehicle stops and starts, redundant vehicle kinetic energy is converted to heat in brake friction during deceleration. Furthermore, a large amount of fuel is needed to keep the engine idling when stationary and power the vehicle during acceleration. Vehicle hybridization is able to absorb and store vehicle kinetic energy during deceleration and reuse it to either power the engine or cruise the vehicle during acceleration.

At present, the Hybrid Electric Vehicle (HEV) is the dominant production hybrid technology. In order to regenerate kinetic energy, an additional electrical propulsion and drivetrain system and high capacity batteries are used in the HEV. With the additional power input, the HEV can install a downsize engine and run it in the efficiency region. The most notable advantages of the HEV are the lower fuel consumption and lower emissions. Furthermore, when the HEV is running with electric motor solely, it contributes to a lessening of noise pollution. However, the application of electric hybrid powertrain to buses and delivery vehicles is severely limited by the huge additional cost associated with the engineering complexities of the combined electric and mechanical powertrain and transmission systems, making them unsuitable for commercially viable large volume production. The battery's typical life span is 6 to 10 years, and therefore, the high maintenance costs ensue due to the imperative battery replacement.

Similarly, the hydraulic hybrid powertrain will involve a completely new transmission system and additional power units to the existing vehicle, for example, a single hydraulic pump/motor, a high pressure storage accumulator and a low pressure storage accumulator. The hydraulic fluid is pumped into the high pressure storage accumulator during deceleration and can then be reused to operate the pump/motor to propel the vehicle. The high pressure accumulator could operate up to 5000 psi and therefore the hydraulic hybrid powertrain has the characteristic of high energy density which makes it particularly suited for benefits stop-start mode operation of heavy duty vehicles. Compared to the HEV, the hydraulic hybrid powertrain has even higher regenerative efficiency. The hydraulic hybrid powertrain can also achieve significant fuel saving. However, the cost and weight would be high though perhaps less than the equivalent electric hybrid for a commercial vehicle. The noise is also one of drawbacks.

An air hybrid powertrain can be achieved with a standard vehicle transmission and would require low cost modification to the engine. The system is able to convert braking energy into pneumatic energy of compressed air stored in an air tank during deceleration. It saves fuels at every stop by eliminating engine idle, i.e. switching off the engine. The stored compressed air can then be reused either to start the engine in every stop/start operation for the biggest fuel saving or to be used as boost air for eliminating the turbo lag. However, as it will be discussed in Chapter 2, the previous proposed air hybrid engine concepts mandates the use of an additional valve and complex and expensive camless valve train system. The innovative concepts presented in this work challenge both assumptions and make use of practical valve train technologies that are already in production with simple

switching controls. In fact, as it will be described later in the thesis, the proposed concepts can be implemented on a production engine through retrofitting without affecting the engine's design and architecture. Therefore, it could be implemented at low cost.

1.2 Objectives

The objectives of this study are to:

- i) Provide a detailed description of production oriented air hybrid engine concepts including alternative engine technologies implemented, additional modification needed and working principles for various traffic conditions.
- ii) Model and predict different air hybrid engine concepts to identify optimized engine valve timings for achieving the best regenerative efficiency by using 1D gas dynamics simulation.
- iii) Carry out experimental studies of the air hybrid engine performance in a single cylinder engine, and validate the engine simulation results.
- iv) Develop an air hybrid vehicle driving cycle simulation program, including a new air hybrid engine operation model, in order to evaluate the effectiveness of air hybrid operation.
- v) Analyse the performance and effect of air hybrid operations of a light duty vehicle and a London bus on their fuel savings through stop-start operations.

1.3 Structure of thesis

Chapter 2 contains a brief introduction to combustion engine history and their fundamental operating principle. This is followed by an overview of Hybrid Electric Vehicles, including benefits of HEVs, hybrid engine propulsion system and limitations of HEVs. The hydraulic hybrid vehicle technologies are then presented. This is followed by a review of previous air hybrid engine concepts and their implementation through sophisticated valve train technologies. The final part presents the recent hybrid electric bus trials in London and potential air hybrid bus in order to illustrate the potential fuel savings from regenerative stop-start operations.

Chapter 3 presents four design iterations of the air hybrid engine based on a Ford PUMA 2.0L diesel engine with separate intake ports. Appropriate Reed valves, check valves, throttle valves, the airtank and pressure regulators are selected and included to achieve air hybrid engine operation. The Variable Valve Timing (VVT) technology and Cam Profile

Switching (CPS) are also utilised to enable compression mode and expansion mode operations of the air hybrid engine. Systematic analysis of the air hybrid concepts is then carried out to understand the underlying fluid flow processes, as well as to identify the most effective air hybrid engine setup.

Chapter 4 considers how to adopt a commercial diesel engine to operate as an air hybrid engine. The first part presents the principle of operation of a YUCHAI YC6A 7.25L diesel engine with regenerative engine braking and starting through a Variable Valve Exhaust Brake (VVEB) device on the intake valves. The engine braking torque and air tank charging process are calculated and analysed during the vehicle deceleration and braking operation. In the second part of the chapter, the combined use of split intake ports and a more generic engine braking device, Jake brake, on the engine braking torque and regenerative air production is presented.

Chapter 5 details experimental facilities and hybrid engine results from a single cylinder engine. In order to investigate the effect of valve timings on the regenerative engine braking and compressed air storage, an electro-hydraulic camless system is used to control the intake and exhaust valves. Results of in-cylinder pressure, air flow rate and air tank pressure are presented and then compared with the simulation results.

An air hybrid vehicle driving cycle simulation programme in MATLAB Simulink developed by the author is described in the first part of Chapter 6. The methodology and implementation of an air hybrid engine sub-model is presented. Then the NEDC driving cycle analysis of a Ford Mondeo car is shown and discussed. In the last section of Chapter 6, the performance and potential of a double deck bus equipped with RegenEBD, a simplified version of air hybrid concept, through the London bus driving cycle is analysed and presented.

Chapter 7 summarises the main findings and major conclusions from this work. Recommendations and suggestions are made for future work.

Chapter 2: Literature Review

2.1 Introduction

A heat engine is designed to convert the chemical energy of fuel into thermal energy and uses this energy to produce mechanical work. Heat engines can be classified into two broad types, the external combustion (EC) engine and IC engine.

A steam engine is one of the EC engines in which combustion of fuel transfers the heat generated to a second fluid which is the working fluid of the cycle. Steam, generated from water, is the working fluid of the steam engine for powering the piston or a turbine. In a steam engine, fuel combustion takes place outside the engine cylinder.

In IC engines, fuel combustion takes place inside the engine cylinder. The expansion of combustion products powers the piston of the engine directly in IC engines. Compared to EC engines, primary disadvantages of IC engines are considered to be high exhaust emissions (particularly NO_x emission) and higher requirements in terms of type and quality of fuel. However, one major advantage of IC engines is better thermal efficiency and, therefore, lower fuel consumption than EC engines. Two more benefits of IC engines are quick engine start and elimination of an additional tank for secondary working fluid.

IC engines have been developed for more than 100 years as the powertrain for most ground vehicles. Since their invention, IC engines have been subject to continued improvement in performance, efficiency, and emission, the priority of which changes with time.

As early as 1860, Jean Joseph Etienne Lenoir designed an illuminating gas engine without mixture compression but utilized with electric spark ignition [5]. Furthermore, the characteristics of four-stroke engine, consisting of four-stroke process and pre-compression of the air/gas mixture, were firstly described by Beau de Rochas in 1862 [5]. Finally, Nikolaus August Otto is the first person who actually built a four-stroke engine at Deutz in 1876 [5]. This four-stroke engine is also a Spark Ignition (SI) engine, where the fuel is ignited by a spark in the cylinder. Due to this important invention, the creation of first automobiles with gasoline engines had been developed by Carl Benz, Gottlieb Daimler and Wilhelm Maybach in 1886 [5].

The other important invention, the world's first diesel engine, was produced by Rudolf Diesel in 1897. The diesel engine is also a Compression Ignition (CI) engine and its fuel would be ignited by using the heat of compression.

The initial development of IC engines was focused on the performance and engine efficiency. Since late 1960s, in particular, over the last two decades, substantial effort had been devoted to the reduction of harmful exhaust emissions. As a result, a Euro V compliant vehicle produced in 2010 emits only a fraction of the emissions from a Euro I car in 1990. However, with increasing concern with the greenhouse gas emission (CO₂) and higher fuel prices, the automotive industry has moved their emphasis to improve the fuel economy and reduce CO₂ emission. Amongst an array of technologies, hybrid powertrains and engine downsizing are considered as most effective means to the production of low carbon vehicles in the short and medium terms. In the rest of this chapter, recent developments in hybrid powertrain will be presented and discussed. In particular, the research on air hybrid engines will be reviewed with regard to their potential and limitations in order to demonstrate the need and merit of the current work [6].

2.2 Hybrid electric vehicles

2.2.1 Benefits of hybrid electric vehicles

The hybrid electric vehicle (HEV) is characterised with excellent fuel economy and low emissions. It is powered by a combination of either a petrol engine or a diesel engine and one or more electric motor. Vehicle's kinetic energy, which is normally lost as heat in the brakes during the vehicles deceleration process, is converted into electricity by the electric motor/generator and stored in an electrochemical (battery) or electrostatic storage (capacitor) system. The recovered braking energy can then be used to start the engine and provide the propulsion power during the initial period of the vehicle operation, if there is sufficient recovered energy stored.

Figure 2.1 shows that up to 87% energy is lost in the energy conversion process from fuel energy to the wheel torque on the road for a typical vehicle driving through Federal Test Procedure (FTP) driving cycle [7]. Heat dissipation and idling engine operation occupies a high percentage of total energy loss.

As shown in Figure 2.2, the electric hybrid can lead to significant reduction in fuel consumption through two major approaches, including reduced idle consumption (5% to 10%) through regenerative stop-start operations and improved overall engine efficiency by optimised engine design due to less stringent performance requirement that is enabled by the addition power to be provided by the electric motor [7]. However, it is important to note that the battery state of charge after the drive cycle assessment has not been clarified in this paper.

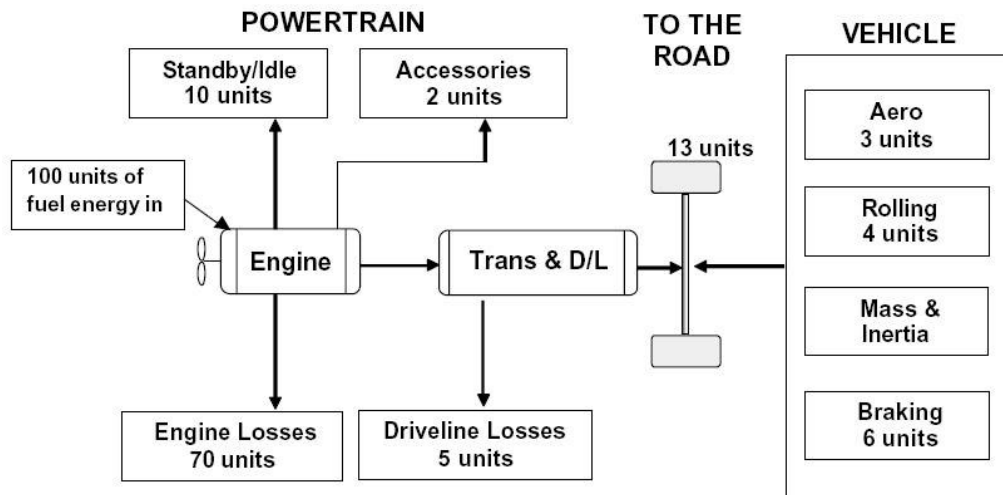


Figure 2.1: Energy loss model for a typical vehicle [7]

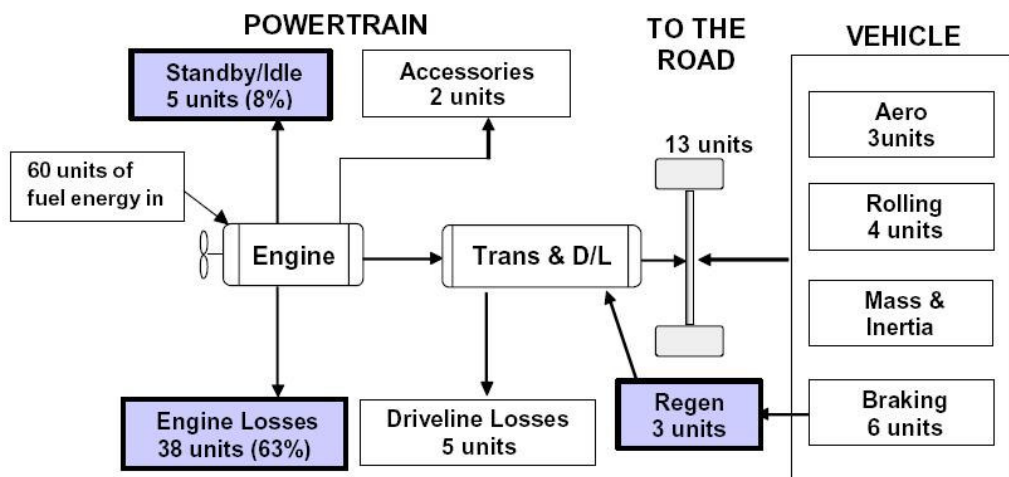


Figure 2.2: Energy loss model for a typical hybrid vehicle [7]

2.2.2 Electric hybrid vehicle powertrain systems

HEVs are classified into three main types, series hybrid, parallel hybrid and series-parallel hybrid. Their configurations and characteristics will be discussed below.

2.2.2.1 Series hybrids

The internal combustion engine is used as an auxiliary power unit to extend the driving range of the pure electric vehicle in the series hybrid propulsion systems. Figure 2.3 shows that the engine is utilized to power the generator from which electricity is generated. The output of the generator can either feed directly to the electric motor to drives the wheels or charge batteries, via a power electronic module. In parallel, the battery also supplies electric power to the motor when the maximum power output is required from the electric motor. Since the engine is not the propulsion system it can be designed and operated at its optimum efficiency and low emission points.

The system is able to absorb and store the regenerative braking as electricity in the battery by using the traction motor as a generator during deceleration.

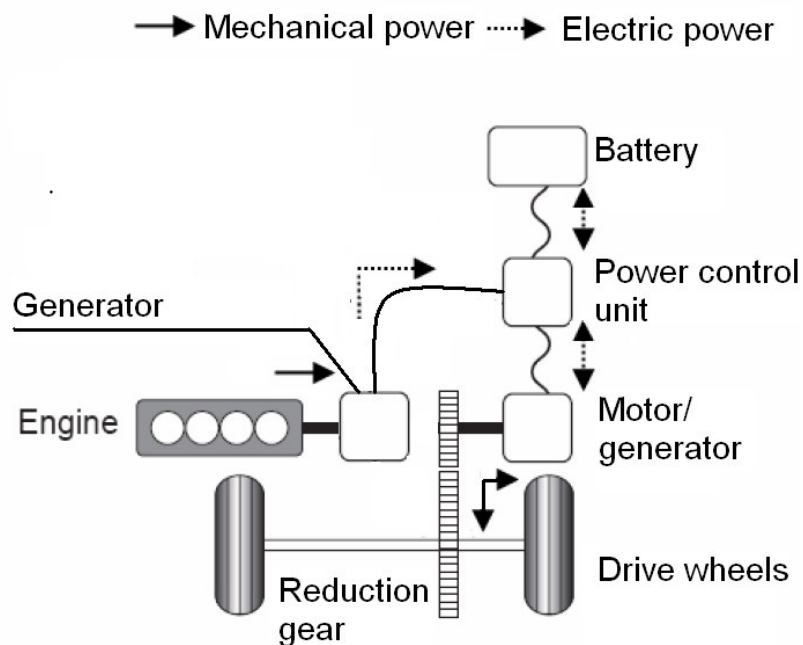


Figure 2.3: Series hybrid system

2.2.2.2 Parallel hybrids

In the parallel hybrid system, the IC engine is the primary power source with supplementary power from the electric motor. Figure 2.4 shows that the parallel hybrid system consists of additional batteries and the electric motor as the second power source.

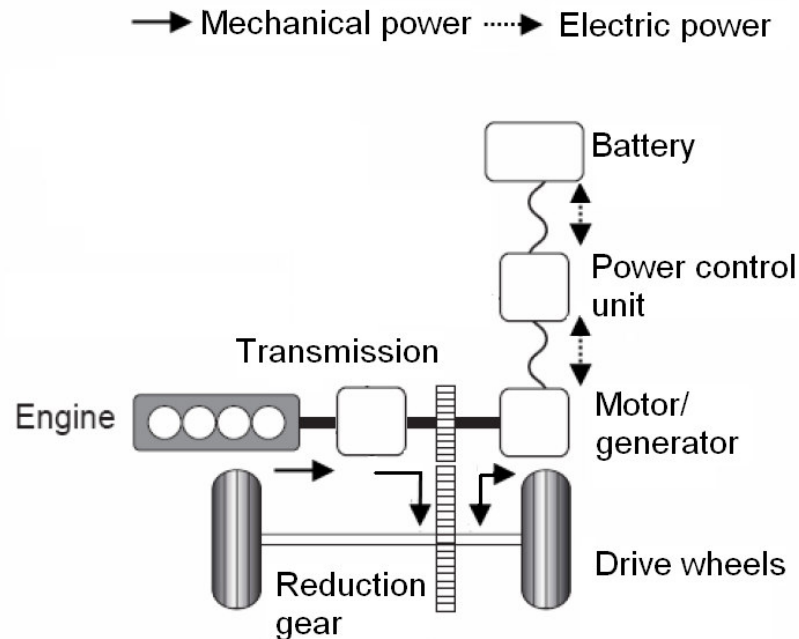


Figure 2.4: Parallel hybrid system

Since the engine and the electric motor can supply the traction power either alone or in combination, flexible power distribution between these two paths can be achieved which enables both of them to be operated at optimum efficiency. In addition, the system can achieve the regenerative stop-start mode by turning the engine off at idle and then cranking the engine by the electric motor using the electricity produced during the vehicle's braking process. Finally, the electric motor can be used as a generator to charge the battery from either regenerative braking or the engine power output. For example, the Honda Insight, an electric parallel hybrid production car, utilizes its electric motor to function as either a generator for the charging system during deceleration or a starter for the stop-start mode at the idling speed [8]. The electric motor, in the parallel hybrid system, has another additional function of providing propulsion assist during acceleration which is different from the mild parallel hybrid system.

2.2.2.3 Series-parallel hybrids

The series-parallel hybrid system, shown in Figure 2.5, is able to operate as series or parallel hybrids. With a power split device, the combustion engine can provide power via either the mechanical path or the electrical path. Therefore, as the system drives the wheels, the combustion engine can drive a generator to simultaneously generate electricity to recharge the battery.

Typically, the system utilizes the electric motor to drive the vehicle alone at low loads and low speeds with a better efficiency and the engine as high loads and speeds required. In addition, the electric motors are capable of regenerative braking energy during decelerations and therefore with better fuel consumption achieved [9-11]. The Toyota Prius is the most successful fully electric hybrid vehicle of such a design.

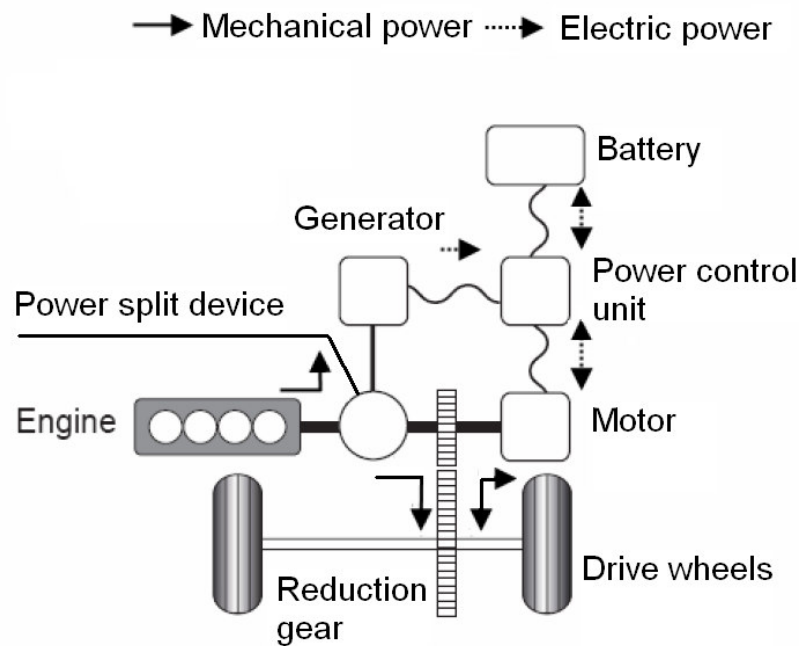


Figure 2.5: Series-parallel hybrid system

2.2.3 Hybrid Electric Commercial Vehicles

As the major fuel savings come from regenerative stop-start operations, it would be most beneficial for the hybrid powertrain to be used in city buses which have the most frequent stop-start operations and long idle periods. This has resulted in the development and deployment of a number of electric hybrid buses in New York and London over the last few years. Figure 2.6 shows that the buses with hybrid powertrain in London achieved on

average around 15% fuel saving compare to diesel buses [12]. However, it is noted that in some cases the installation of the electric hybrid powertrain caused higher fuel consumption because of inadequate calibration and optimisation. However, the fuel saving is obtained at a hefty price of addition £100,000 for a full hybrid powertrain. That is, hybrid double-decker costs GBP 300,000 as against GBP 200,000 for one with a conventional diesel engine [13]. For a hybrid bus with 30% reduction in fuel consumption, the annual saving is around GBP4,500-GBP5,000 a year in London [13] and the payback period is 20 years.

A fuel economy comparison of hybrid buses operating in London by route and vehicle type										
route number	276	360	371	E8	129	141	328	24	482	16
single-/double-deck	S	S	S	S	S	D	D	D	D	D
hybrid bus mpg	7.4	7.2	10.9	6.4	8.5	5.8	4.8	6.6	9.1	6.4
diesel bus mpg	5.6	7.3	8.0	7.8	7.5	4.9	4.2	5.6	6.9	5.5
percentage change	31	-2	37	-15	15	18	14	18	31	16
hybrid bus lit/100km	38.2	39.2	25.9	44.1	33.2	48.7	58.8	42.8	31.0	44.1
diesel bus lit/100km	50.4	38.7	35.3	37.2	37.7	57.6	67.3	50.4	40.9	51.4
percentage change	24	-1	27	-19	12	16	13	15	24	14
hybrid bus type	Optare Tempo	Wrightbus Electricity	ADL E200H	Optare Tempo	Wrightbus Electricity	Wrightbus Gemini 2H/ Volvo B5L	Wrightbus Gemini 2H	ADL E400H	ADL E400H	ADL E400H
hybrid driveline	Allison	Enova	BAE Systems	Allison	Enova	Siemens/ Volvo ISAM	Siemens	BAE Systems	BAE Systems	BAE Systems
hybrid's diesel engine	Cummins 6.7-litre	GM1.9-litre/ Ford 2.4-litre	Cummins 4.5-litre	Cummins 6.7-litre	Ford 2.4-litre	Ford 2.4-litre/ Volvo 4.8-litre	Ford 2.4-litre	Cummins 4.5-litre	Cummins 4.5-litre	Cummins 4.5-litre
series/parallel	parallel	series	series	parallel	series	series/ parallel	series	series	series	series
operating company	East London	London Central	Transdev	Metroline	Abellio	Arriva	First	London General	Transdev	Metroline

Figure 2.6: A fuel economy comparison of hybrid buses operating in London by route and vehicle type [12]

2.2.4 Mild Hybrid Electric Vehicles

A mild parallel hybrid system utilizes the electric path mainly to crank the engine from stop up to the cranking speed so that the stop-start mode operation can be achieved. For example, the Toyota Crown implements the Toyota THS-M system with the functions of stop-start mode operation, initial vehicle launch assist and regenerative braking [14]. In order to provide sufficient torque to re-start the 3.0 litre engine, the Toyota THS-M system operates at 42V with an additional 36V battery. However, the function of vehicle launch assist is limited due to the sizing of the system relative to the vehicle mass.

In the case of the integrated starter alternator [15], an electric motor-generator is installed and replaces the conventional alternator and starter motor. In addition, three 12V lead-acid batteries are connected in series to produce a 36V nominal supply and a 36V-12V DCDC converter is utilized to step down the 36V bus to 12 V to power the vehicle accessories. The system can provide stop-start mode operation by transferring the electric motor-generator torque to the crankshaft or obtain regenerative braking from the wheels to the electric motor-generator (through the transmission and engine).

Another example of the mild hybrid electric technologies is the Integrated Motor Assist (IMA) system employed on the Honda Insight, which has a downsized engine (from 1.5 litre to 1 litre) and an electric motor with a 144V battery pack as an auxiliary power source [16]. Since the IMA system is able to provide overall torque by over 50% in the lower rpm range, Honda Insight achieves its fuel saving by significant reduction of engine displacement. Furthermore, with assist from the electric motor the engine is able to broaden the lean-burn operating range and therefore further fuel saving can be achieved. Finally, as with most HEVs, the IMA system is also capable of regenerative engine braking and stop and start operations.

Over the last couple of years, an increasing number of smaller passenger cars is equipped with the belt driven stop-start system, which features a larger capacity and more durable battery as well as more reliable starter motors. As such a system has little regenerative braking capability, the fuel savings during an NEDC cycle is typically limited to a few percent.

2.3 Hydraulic hybrid vehicles

The Hydraulic Hybrid Vehicle (HHV) is capable of absorbing and storing the kinetic energy as high pressure hydraulic oil in the accumulator filled with nitrogen gas during deceleration and then reusing it to propel the vehicle with high regenerative efficiency during acceleration. With the ability of recovery of brake energy, the HHV can achieve not only the fuel saving but also the reduction of brake wear.

Basically, the HHV can be classified into two types, the parallel hydraulic hybrid and the series hydraulic hybrid. The HHV in a parallel hybrid hydraulic system maintains its original vehicle drive-line and allows the vehicle to operate normally when the system is deactivated. When the system is activated during deceleration, brake energy regeneration

can be achieved. The HHV in a series hydraulic hybrid system replaces the entire conventional drive-line by the additional hydraulic system.

A parallel hydraulic hybrid system consists of the working fluid (hydraulic oil), reservoir, pump/motor and high pressure and low pressure hydraulic bladder accumulators. Figure 2.7 shows the basic principle of operation of the HHV with a parallel hydraulic hybrid system [17]. During deceleration, hydraulic oil is pumped into the high pressure hydraulic accumulator and increases the pressure of the gas due to the volume reduction. During acceleration, the high pressure hydraulic accumulator discharges the hydraulic oil and then motors the drive-line to propel the vehicle which results in gas volume decrease. In [17], Bosch Rexroth has demonstrated the Hydrostatic regenerative Brake (HRB) system for garbage trucks and lift trucks in extremely short work cycles which drops fuel consumption by up to 30 percent.

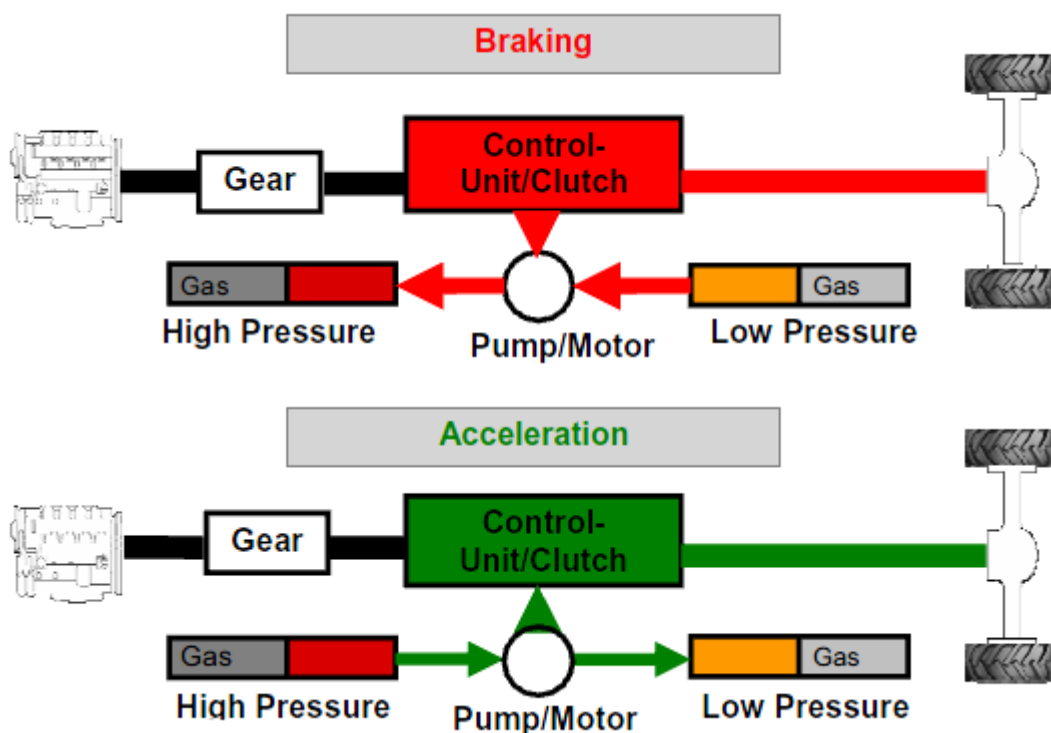


Figure 2.7: Operating method of hydraulic hybrid vehicles [17]

In [18], Ford Motor Company and United States Environmental Protection Agency (USEPA) built a Hydraulic Power Assist (HPA) demonstration vehicle which performs 23.6% fuel consumption improvement from the EPA city cycle test results. Figure 2.8 shows the system layout of the HHV which shows integration with conventional powertrain and braking system. The HHV featured a smaller 4.0L engine and could

achieve 0-30 mph acceleration in 3.5 seconds, 1.3 seconds faster than the original vehicle with a 5.4L engine [18].

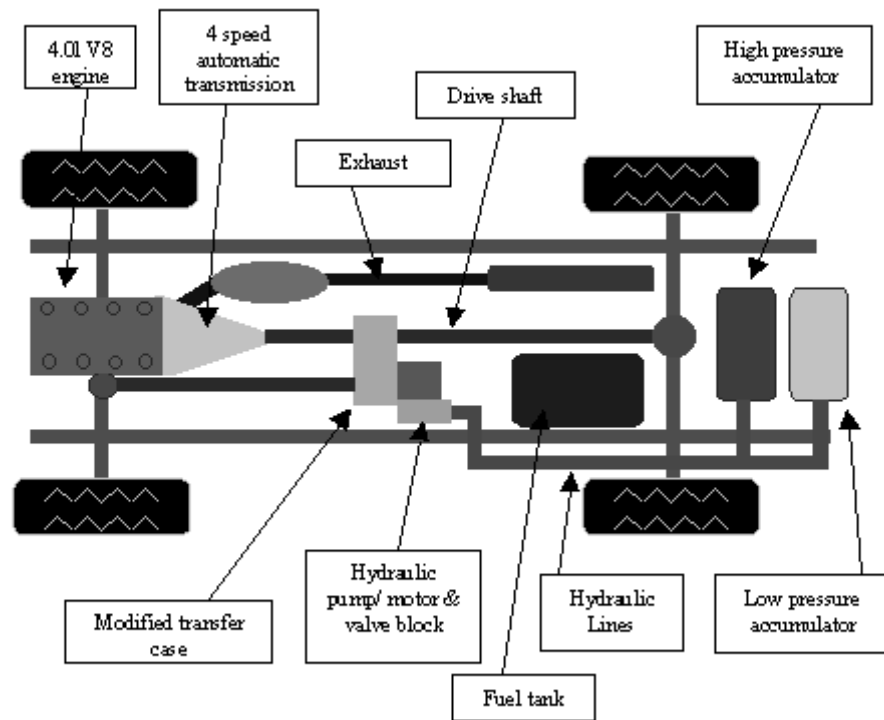


Figure 2.8: HHV with an automotive HPA system [18]

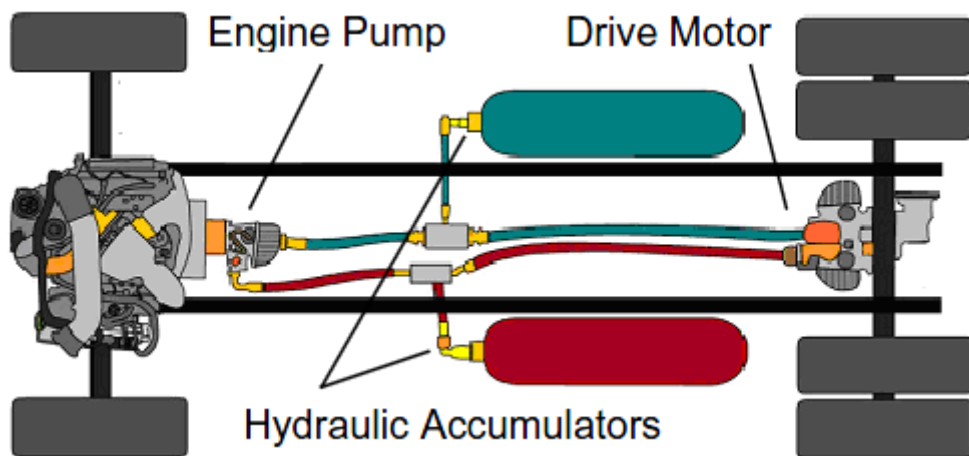


Figure 2.9: Primary components of the series hydraulic hybrid vehicle [19]

Figure 2.9 shows configuration of series HHV components which has been developed by Eaton Corporation et al and utilized in first real world parcel delivery vehicles owned by United Parcel Service (UPS) [19]. In this series HHV, the engine, linked to the drive wheels only by the hybrid hydraulic drive system components, indicates that the base

vehicle transmission has been replaced. This series HHV demonstrated up to 50% fuel saving and 30% reduction in carbon emissions in real world use. Figure 2.10 shows regenerative efficiency is up to 71% for the UPS parcel delivery vehicles [20]. In addition, the Dutch company Innas also develops its series HHV and predicted results show that more than 50% of fuel saving for a 1450 kg passenger car could be achieved throughout the NEDC [21-22]. Furthermore, Parker has also developed a series hydraulic hybrid vehicle system for refuse truck. The system is able to capture and reuse more than 70% of braking energy [23].

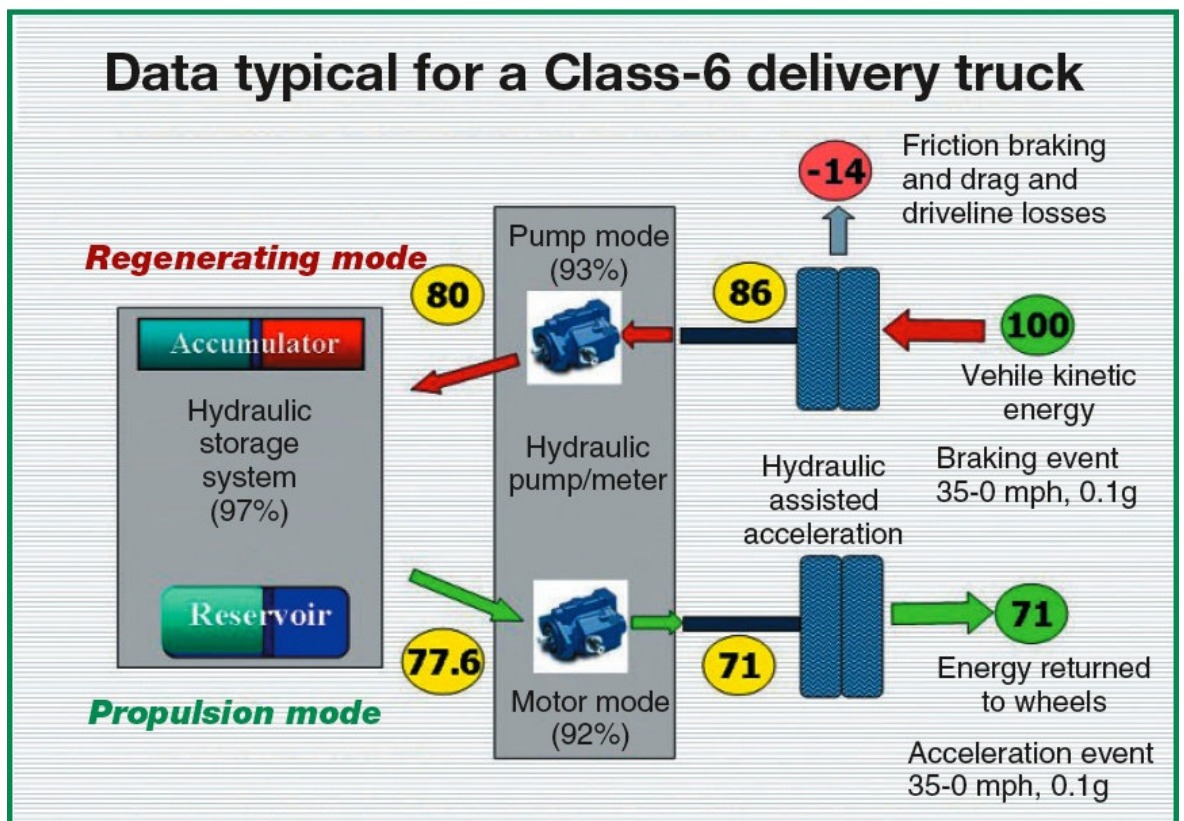


Figure 2.10: Regenerative efficiency through all components [20]

The hydraulic hybrid vehicle has advanced characteristics including high regenerative efficiency, high power density and significant fuel saving. In [24], Chrysler has started cooperation with the USEPA to develop a hydraulic hybrid minivan. Compared to the costly batteries and other electric drive components, a hydraulic system is estimated 50 percent cheaper to install [24]. The current challenges of hydraulic hybrid drivelines are hefty and size for the small passenger car. Furthermore, the noise issue comes with the high pressure hydraulic accumulator will be another challenge for the future development.

2.4 Air hybrid engine concepts

In France, the Frenchmen Andraud and Tessie of Motay built the first recorded compressed air vehicle in 1838 [25]. The vehicle showed good test results on a test track at Chaillot on the 9th July 1840.

In 1872, the Mekarski air engine, a single stage engine, was used for street transit [25-26]. The advantage of the engine is that the compressed air was preheated before entering the engine from the air supply tank. For the power generating process, the hot compressed air expands in one piston and is then exhausted.

In 1909 [27], John K. Broderick had invented a combined internal combustion and compressed air engine. In his application, some of the cylinders of an internal combustion engine can be operated as normal and remaining cylinders can be utilized as air compressors for compressing the air into the air storage tank when the vehicle is stationary or driving down a hill. The function of the compressed air is to assist the main engine in driving the vehicle under heavy loads or to actuate the vehicle brake system. Furthermore, it can propel the vehicle alone.

In 1972 [28], Russel R. Brown filed his patent of a compressed air engine powered by the compressed air. The air engine has an auxiliary electric air compressor which is capable of charging the air supply tank to build up the maximum predetermined air pressure level and maintaining this level during the engine operation.

In the recent research, the air hybrid engine concept utilizes an airtank to store vehicle kinetic energy in the form of compressed air. The engine can either work as an air compressor to convert vehicle kinetic energy into compressor air, stored in the airtank during deceleration. The compressed air can then be used to start the vehicle using an air starter, or operate the engine as an air expander during stop-start operation and to provide instant boost or propulsion force.

2.4.1 Theoretical studies of idealized air hybrid concepts

It can be seen from Figure 2.11, the air hybrid operation can be realised using an additional air transfer valve in the cylinder head, which is actuated by an additional camshaft, in a similar way to engine starting by compressed air as used in some marine applications [29-31]. The air transfer valve, which connects the combustion chamber of each cylinder to an

airtank, can also be electrically or hydraulically actuated. Besides the normal firing mode operation, the additional 2-stroke pneumatic pump operation during the vehicle's deceleration operation is to charge the compressed air into the high pressure air tank via the charging valve and therefore kinetic energy can be absorbed and stored. During the two-stroke pneumatic motor operation, the amount of stored compressed air in the high pressure air tank is released into the cylinder via the charging valve and then the expansion work generates power to propel the vehicle. Vehicle simulation predicted 12% fuel consumption improvement throughout the NEDC for an 800 kilogram passenger car [31].

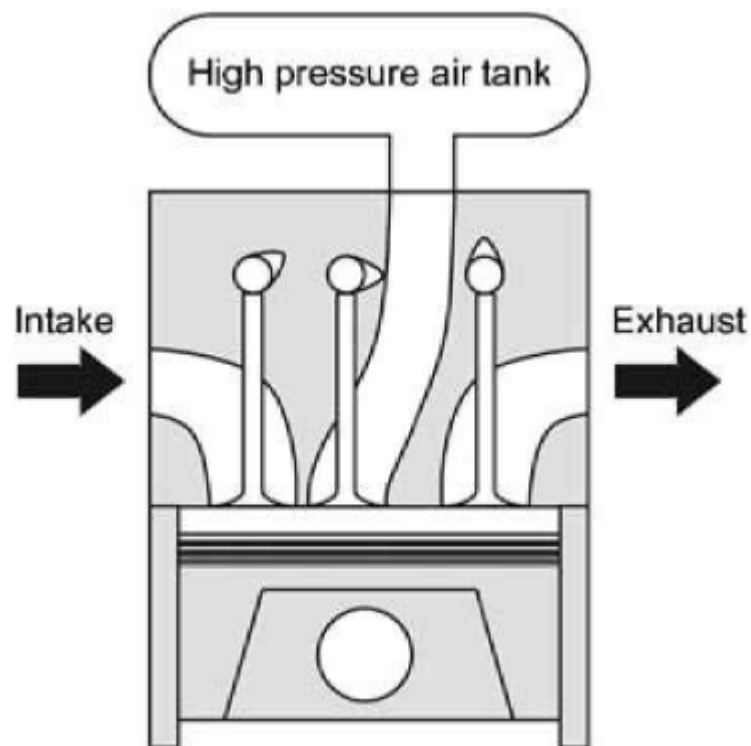


Figure 2.11: The connection between the high pressure air tank and each combustion chamber is via an additional valve and pipe [31]

Compared to previous research [29-31], in order to make the pneumatic motor and pneumatic pump cycle effective, the authors [32-34] indicate that the opening and closing timings of the charging valve have to be variable with engine speed and tank pressure. Therefore, the charge valve has to utilize a fully variable actuator. Furthermore, intake and exhaust valves utilizing different technologies can achieve various pneumatic cycles. First, in order to achieve the two-stroke pump cycle and two-stroke motor cycle, all valves need a fully variable valvetrain. Second, if the intake and exhaust valves utilize a conventional camshaft system, four-stroke pump cycle and four-stroke motor cycle can be achieved. Finally, an improved pneumatic cycle is obtained with requirement of one camshaft (intake

or exhaust) disengaged. For a 1.5 tonne passenger car, a simplified vehicle simulation program predicted up to 30% fuel saving [33]. It does not show that the weight of additional components have been added up to the weight of the selected vehicle.

Although good predicted results have been shown above, the additional valve is difficult to be fitted onto the limited space of the cylinder head together with other four valves, the spark plug and the possible direct injector. In addition, the fully variable valvetrain is necessary in this concept.

2.4.2 Air hybrid engine concepts based on the use of camless valve train system

In order to realise various air hybrid mode operations, a camless electro-hydraulic valvetrain system has often been considered as necessary. In [35], Ford developed an experimental electro-hydraulic valve train system at Ford Research Laboratory. The system provides a continuously variable and independent control of virtually all parameters of valve motion. Figure 2.12 shows the hydraulic pendulum concept. Two solenoid valves are utilized to control either the high pressure or the low pressure in the volumes below and above the piston. In addition, the low volume below the piston is always connected to the high pressure source. Since the pressure area above the piston is much bigger than the pressure area below the piston, opening of a high pressure solenoid valve is activated in order to open the engine valve. A low pressure solenoid valve is activated to close the engine valve. Additional high pressure and low pressure check valves are assisted in valve opening and closing control.

Figure 2.13 shows the unequal lift modifier installed with paired valves (either intake valves or exhaust valves). The unequal lift modifier is rotatable to control the connection between the high pressure reservoir and the volume below two pistons. Therefore, a partially blocked connection of the high pressure reservoir and the volume below one piston would reduce one valve lift and allows the other valve to operate normally. Furthermore, when the connection of the high pressure reservoir and the volume of the piston is completely blocked, it would deactivate one valve opening and allow the other valve operate normally. Lotus Engineering has also developed a similar electro-hydraulic Fully Variable Valve Actuation (FVVA) system for both single cylinder and multi-cylinder engines [36-37].

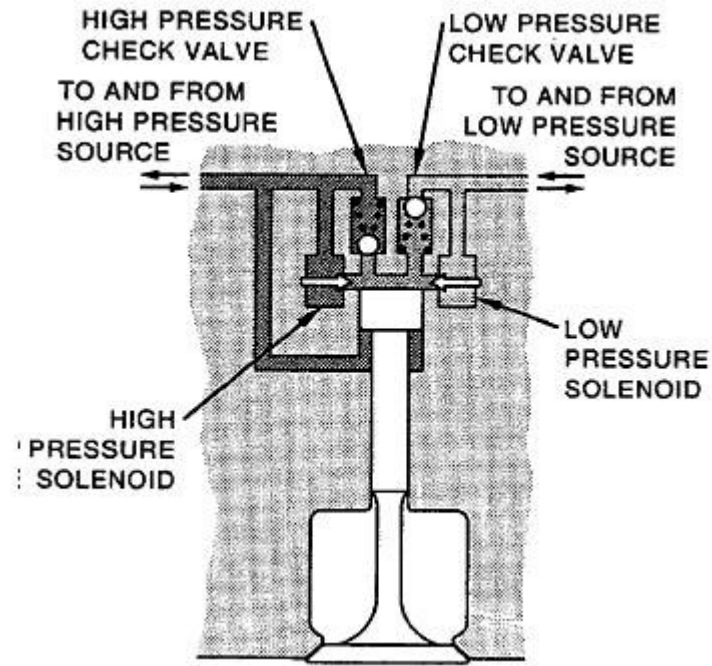


Figure 2.12: Hydraulic Pendulum [35]

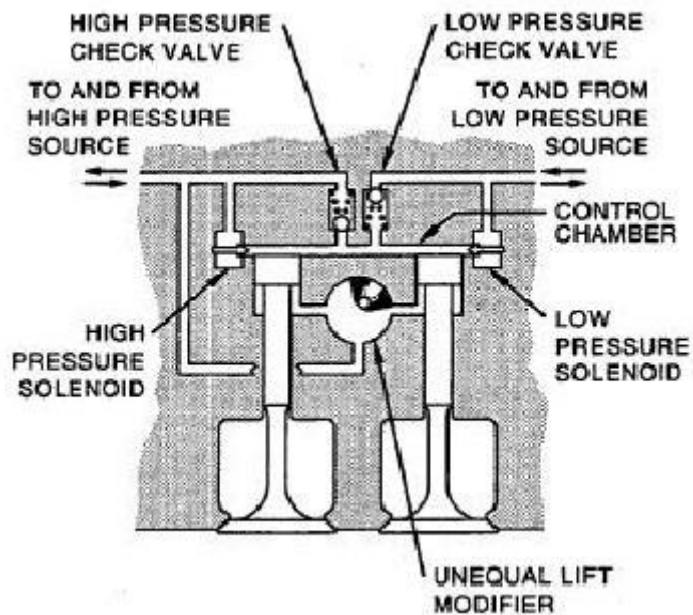


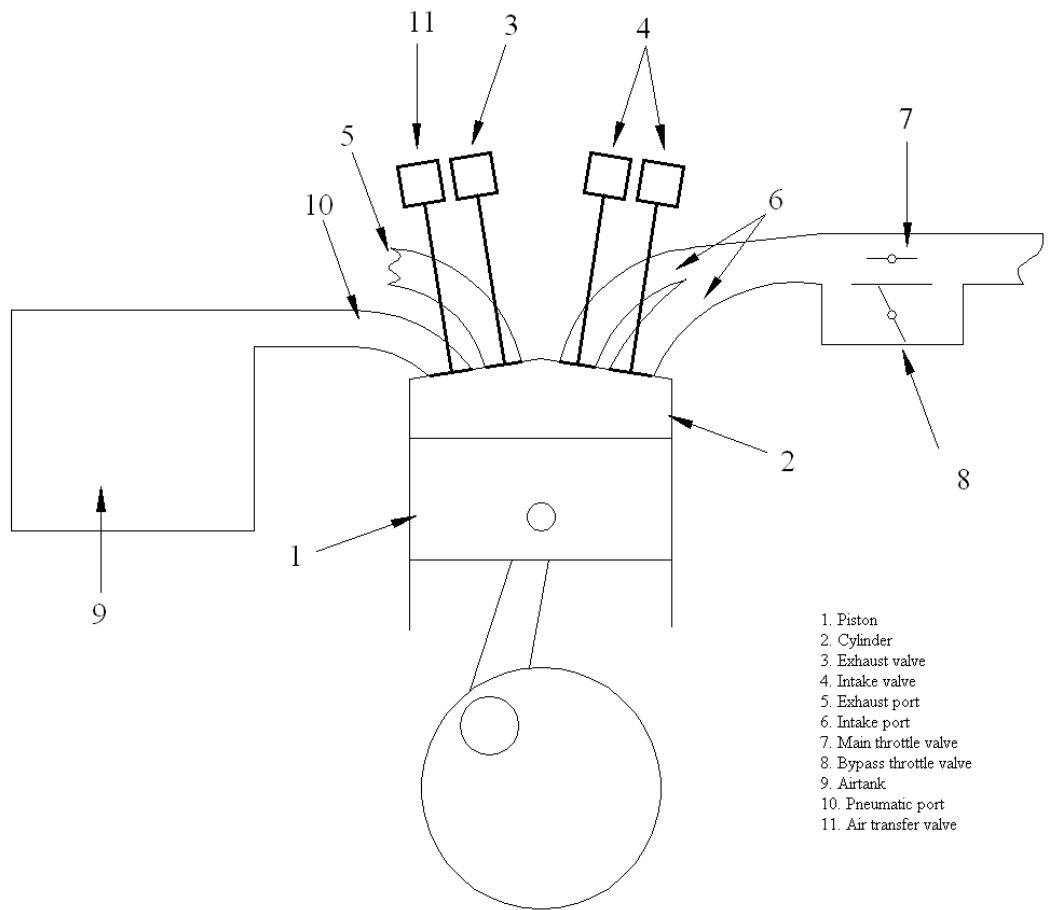
Figure 2.13: Pair valves with unequal lift control [35]

Authors from UCLA and the Ford Company [38] investigated the potential of the application of such a camless electro-hydraulic valve train and a sophisticated air-switching intake system to achieve various air hybrid operations. Each cylinder of the air hybrid engine consists of one electro-hydraulic intake valve connecting ambient via the first inlet manifold and the other electro-hydraulic intake valve connecting either ambient

or the airtank via second inlet manifold controlled by switchable intake port valves. During the normal firing mode, the switchable intake port valve is closed and therefore each cylinder is able to induce air from ambient via both intake valves. During the vehicle deceleration, the switchable valve is open and therefore the induced air can be compressed into the airtank. When the vehicle is stationary, the engine will be shut off. In order to restart the engine if needed, the switchable valve is open to release the compressed air from the airtank into the cylinder via one intake valve and the expanding power will crank the engine. The vehicle will be propelled by the compressed air until the airtank reaches its minimum tank pressure, 6 bar. One important characteristic is that the air-switching intake system does not interfere with the exhaust system of the engine. The air tank utilized in the simulation model adds roughly 30 kg to the weight of the selected vehicle. The modelling results predicted a 36% round-trip efficiency of air hybrid operation and 38% reduction in fuel consumption. To obtain the predicted results, a 1.5 tonne passenger car with a 2.5 litre air hybrid engine was simulated throughout the FTP city driving cycle in MATLAB Simulink.

The camless electro-hydraulic valve train requires substantial hydraulic power. The hydraulic oil leakage and noise issue are also a challenge in reality. As report in [39], in order to achieve the air hybrid operations, a camless system consisting of hydraulic pumps and motors and expensive hydraulic accumulators had to be used.

In 2007, Dr. Psanis from Brunel University had done the modelling and experimental work on various air hybrid concepts. A single cylinder engine with a camless hydraulic valve train was modelled in Ricardo WAVE. Figure 2.14 shows the schematic of the air hybrid engine equipped with the Lotus FVVA camless system. The air transfer valve, modified from one of the exhaust valve, was utilized to control the flow direction of the compressed air between the airtank and the cylinder. When the vehicle decelerates, the engine works as an air compressor. As shown in Figure 2.15, during the compression mode operation the air transfer valve opens in the compression stroke so that air can be compressed into the airtank. When the vehicle start-up or accelerates, the air transfer valve opens during the expansion stroke and compressed air expands in the cylinder. The residual air in the cylinder will be expelled out from the exhaust manifold by opening the other exhaust valve. Valve timings for the compressor mode and the expander mode were investigated and optimized. A simplistic vehicle driving simulation predicted that 68.0% brake energy could be captured throughout the NEDC [40].



- 1. Piston
- 2. Cylinder
- 3. Exhaust valve
- 4. Intake valve
- 5. Exhaust port
- 6. Intake port
- 7. Main throttle valve
- 8. Bypass throttle valve
- 9. Airtank
- 10. Pneumatic port
- 11. Air transfer valve

Figure 2.14: Schematic of the air hybrid engine [40]

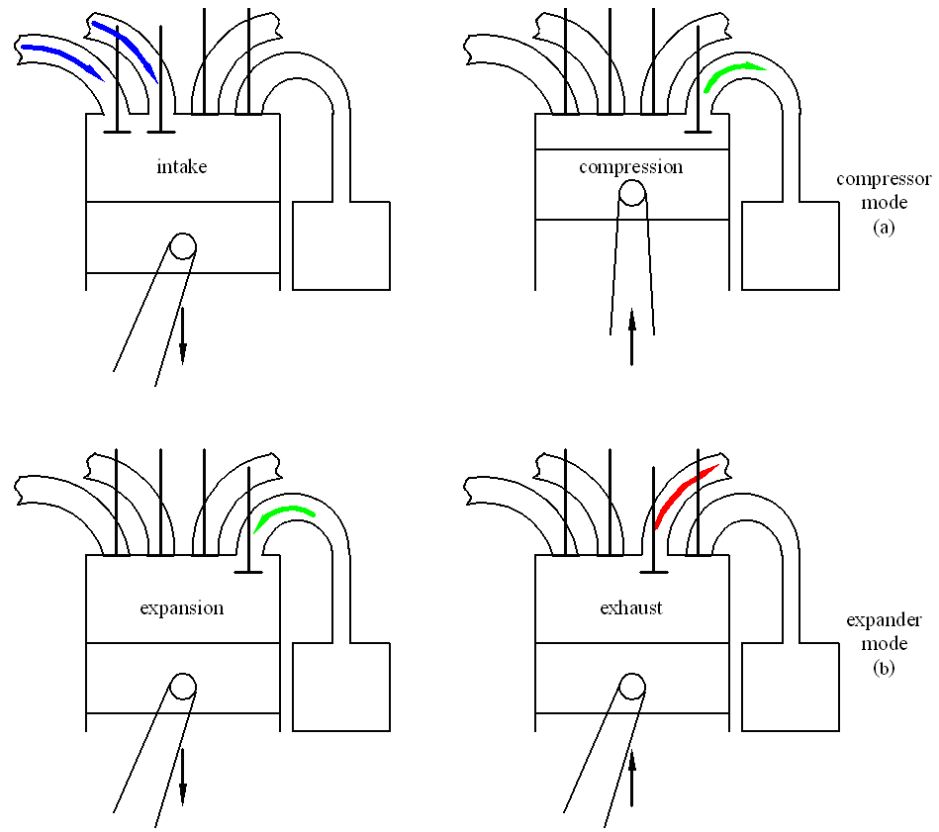


Figure 2.15: Two-stroke compressor cycle (a) and two-stroke expander (b) [40]

In addition to the requirement of a camless system, the deactivation of one exhaust valve may lead to the remaining burned gases expelled from the cylinder incompletely during the normal firing mode. Thus the high temperature residual exhaust gas will cause knock and reduce volumetric efficiency which refers to the low vehicle performance.

2.4.3 Air hybrid engine with pneumatic actuator

Authors from Lund University [41-45] have done the modelling and experimental work on the air hybrid engine with pneumatic valve actuators. The pneumatic valve actuation system, shown in Figure 2.16, consists of two solenoids to operate the actuator, can achieve valve lift between 2 and 12 mm, and one hydraulic brake with a function of slowing down the valve landing speed before seating [41]. All valves are equipped with pneumatic actuators. One intake valve is modified as a tank valve connecting between the airtank and the cylinder which is very similar to Dr. Psanis' work as mentioned above. Therefore, both of them have the same valve strategy for the two-stroke compressor mode and two-stroke expander mode. In the experimental work, the tank valve timing is optimized according to practical results. The practical experiment results showed that the regenerative efficiency of 40-48% could be achieved. The vehicle driving simulation of a 15 tonne bus powered by a 12 litre SCANIA engine was carried out over the Braunschweig duty cycle. The results showed that 28.5% reduction in fuel consumption could be achieved mostly from the stop-start functionality [44].

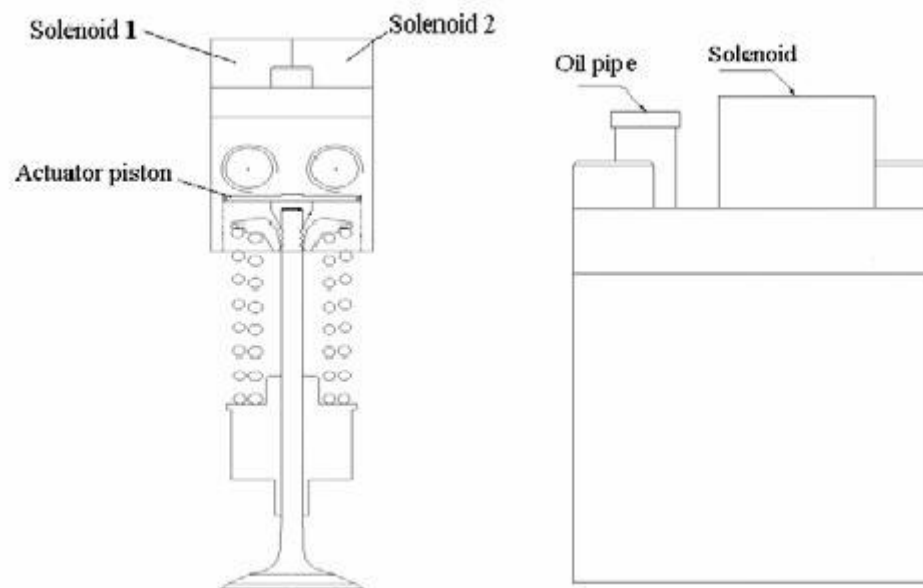


Figure 2.16: Schematic diagram of the pneumatic valve actuator [41]

2.4.4 The Downsized and supercharged hybrid pneumatic engine

The principle of engine downsizing is to use a smaller engine and operate the engine at its most efficient operation points at higher load conditions. However, in order to maintain the vehicle's performance, the downsized engine needs to be boosted, typically through turbocharging. For example, MAHLE Powertrain [46, 47] has developed a 3 cylinder 1.2l DI gasoline engine with a power density of 120kW/l. Their vehicle simulation results showed that if this engine were used to power a 1600kg passenger car in place of 2.4 litre 25-30% fuel saving could be achieved over the NEDC.

Although the downsized engine can lead to significant reduction in fuel consumption and CO₂ emissions, highly downsized engines can suffer from low starting torque and turbo-lag, as well as limited full load performance due to knocking combustion [48]. However, the air hybrid powertrain technology offers the opportunity to overcome such shortcomings by supplying instant boost from the compressed air tank.

Authors [49] from ETH Zurich have demonstrated an air hybrid operation and its potential for highly downsized engine operation in a single cylinder SI engine. Although it was proposed that one additional flexibly controlled valve would be required for the air hybrid operation. In the experiment, one exhaust valve was modified to act as the air charge valve controlled by an electro-hydraulic actuator, as there was sufficient space to add another valve and valve actuator in the cylinder head. The other intake and exhaust valves were actuated by conventional camshafts and hence only four-stroke air compression mode and air expander mode were achievable. During the compression mode, air was charged to the air tank via the charge valve in the normal compression stroke. In the four-stroke air motor mode, the compressed air was injected into the cylinder in the normal expansion stroke. In addition, the supercharged mode was realised by using the air injection during the compression stroke. Comparative relatively low regenerative efficiency of 13.8% was achieved due to the heat loss from the airtank. However, it was claimed that up to 32% fuel saving could be achieved due to the downsized engine, stop-start and hybridization.

2.5 Summary

Many hybrid systems, which have been discussed above, have various methods of energy storage and reuse. HEVs, the mature production vehicles, are usually advertised themselves as environmental friendly cars due to their ability of good regenerative

efficiency and reduction in fuel consumption and emissions. Furthermore, a distinguishing characteristic of the HEV is that it can cruise quietly with no emissions at low speed by using electric power. However, the main deterrent for most of potential customers is the purchase cost of a HEV. In addition, it is also important to extend the short battery service time of the HEV.

HEVs are able to supply large amounts of energy over long periods of time but perform a smaller rate of energy conversion process from electro-chemical energy to mechanical energy. On the other hand, HHVs have a faster rate of energy conversion process from hydraulic energy to mechanical energy but store relative small amount of energy. Compared to HEVs, HHVs have higher braking power and hence particularly suited for heavy vehicles. The main challenges of HHVs are noise issue and the production cost. The high pressure hydraulic blade accumulator normally stores 200-400 bar hydraulic pressure which make significant noise while releasing the energy.

Table 2.1: Summary of hybrid system advantages and disadvantages [50]

	Control	Simplicity	Energy Density	Mass	Cost
Electric	+	--	-	--	--
Mechanical	+	+	+	-	-
Hydraulic	-	-	++	--	-
Pneumatic	--	++	-	++	+

The air hybrid engine research mentioned above shows good experimental and predicted results. Compared to HEVs and HHVs, the air hybrid concept retains the standard vehicle transmission. Authors [50] from Lotus Engineering have summarised the advantages and disadvantages of hybrid systems shown in Table 2.1. In the table, the Toyota Prius and Honda Insight are used as models of the HEVs and their electrical hybrid systems have been considered as having high Bill of Material (BOM) cost. Furthermore, Ford F-350 Mighty Tonka concept has been chosen as a model of the HHV in [50]. The concept demonstration vehicle used was a 1999 Lincoln Navigator Sport Utility Vehicle with a 2379 kg curb weight [18]. The air hybrid operation was based on the use of a camless valve train system in a 1531 kg passenger car [38]. The pneumatic hybrid concept has advantages of simple configuration, light weight and low cost. However, the implementation of electro-hydraulic actuators and additional valve are a major deterrent for the air hybrid technologies to be adopted in production engines.

In order to approach an air hybrid engine with reliable and simple design, the current research project was commenced with the support from EPSRC and Yuchai Machinery Ltd. As it will be discussed in the rest of this thesis, a number of innovative air hybrid engine concepts have been generated and analysed for both light duty and commercial vehicles. All these concepts are aimed at achieving air hybrid operations with production components. Through modelling and experimental studies, two concepts have been identified suited for commercial exploitation and were used in the estimation of fuel savings through appropriate vehicle driving cycles.

Chapter 3: Analytical Studies of Air Hybrid Concepts for a Light Duty Diesel Engine

3.1 Introduction

In this chapter, air hybrid concepts are proposed for a modern light duty diesel engine and analysed using the engine simulation software, WAVE.

WAVE is the 1D engine and gas dynamics simulation software package developed by Ricardo Inc [51, 52]. It is able to analyze the dynamics of pressure waves, mass flows, and energy losses in ducts, plenums, and the manifolds of IC engines and associated components. A one-dimensional formulation is utilized by WAVE to provide a completely integrated treatment of time-dependent fluid dynamics and thermodynamics which incorporate the general treatment of working fluids including air, air-hydrocarbon mixtures, combustion products, liquid fuels, and Freon gases.

Gathering geometric data, engine data and operating parameters are necessary before the hybrid engine model is constructed. WaveBuild is the pre-processor which provides a Graphical User Interface (GUI) for users to build the geometric models with a 'select and paste' function. WAVE flow elements are utilized to model the piping and manifolds of the intake and exhaust systems. Compressible-flow fluid pipe networks can be attached with machinery components such as engine cylinders, piston compressors, turbochargers/supercharger compressors and turbines, and pumps.

Users are able to control the solver behaviour via tabs of simulation control. The start mode and time step of the simulation are controlled by the general parameters tab. Users can specify convergence criteria via the convergence tab. WAVE could halt a simulation earlier than the user-defined simulation duration if the simulation has achieved a converged condition.

In a time-based simulation, WAVE provides time plots to show plots of time-varying values at a given location within the WAVE model. WAVE also provides sweep plots to show plots of summary quantities such as pressures, temperatures and flow rates at many locations within the duct/ manifold network.

A Ford PUMA 2L diesel engine was selected as the base engine because of the availability of the relevant data supplied by Ford Motor Company. In this chapter, each air hybrid engine concept will be presented first and followed by description of their simulation models in WAVE. The modelling results will be analysed and used to identify the optimised parameters for optimum air hybrid engine performance and the best energy regenerative efficiency.

3.2 Air Hybrid Engine with split intake ports

3.2.1 Description of the concept

Figure 3.1 shows an air hybrid engine [53] having a piston (1) reciprocating in a cylinder (2). Intake valves (5 and 6) connect the cylinder with intake ports (7 and 8 respectively) and exhaust valves (3) connect the cylinder with exhaust ports (4). Active intake valve 6 is timed to open and close by a CPS device. A non-return Reed valve (12) is additionally provided in the intake port 8 connected to the active intake valve 6. While air pressure (inside the auxiliary chamber) is lower than atmosphere pressure, the Reed valve petals open and air is induced into intake port 8. On the other hand, the Reed valve petals close and air can be kept without escaping out of intake port 8 to atmosphere while the air pressure (inside the auxiliary chamber) is higher than atmosphere pressure.

An air tank (9), stores high-pressure air, connected to intake port 8 through an Energy Control Valve (ECV) into an auxiliary chamber (10 and 11 respectively). A solenoid valve has been adopted to be the ECV (10) that controls air flow out of the air tank for EM. Furthermore, a check valve has been adopted to be the SSV (self-sealing valve) 13 that controls air flow in to the air tank during the CM operation. In the simulation, the air tank was assumed adiabatic, and therefore, high temperature and high pressured compressed air could be reused.

The engine also includes three more cylinders, a fuel system and an ignition system which are not shown in Figure 3.1 for highlighting the main subject of the present study. In [54], authors have shown the detailed simulation results of air hybrid engine concept 1. A brief overview of all design evolutions will be presented later in this chapter.

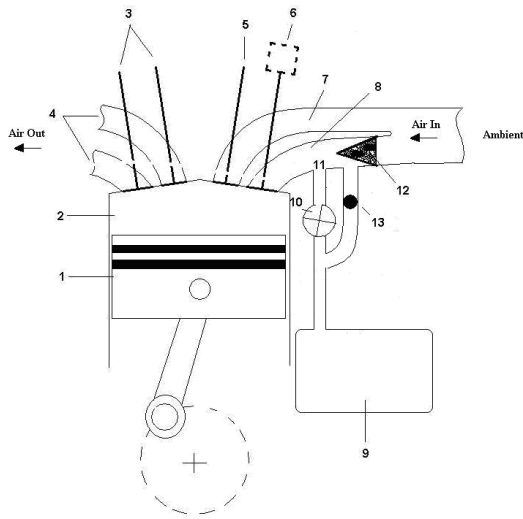


Figure 3.1: Air hybrid engine concept 1 with a Reed valve

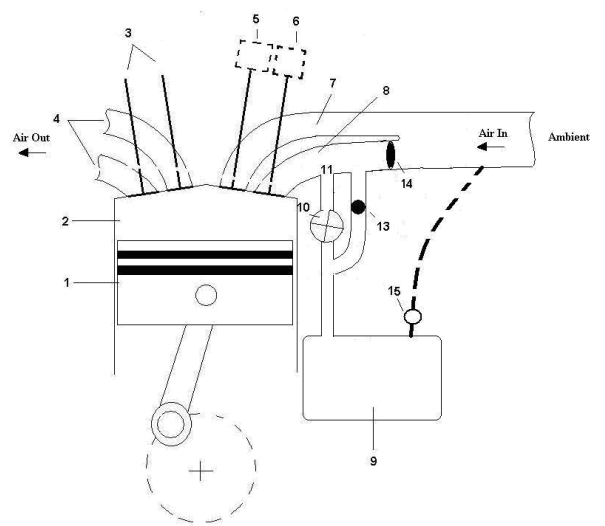
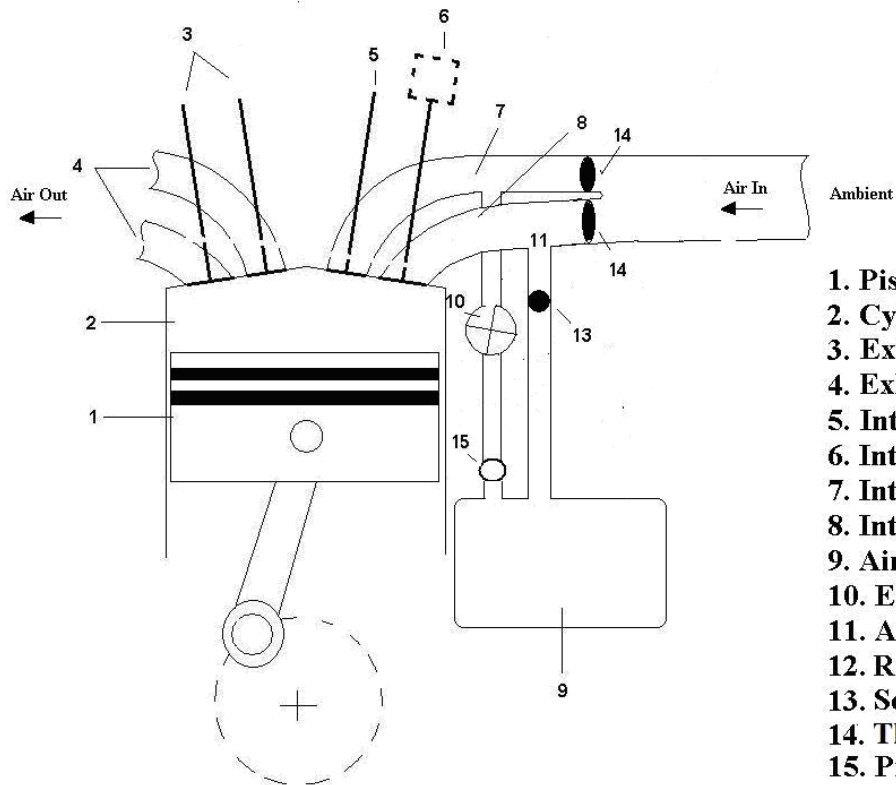


Figure 3.2: The 2nd air hybrid engine concept



1. Piston
2. Cylinder
3. Exhaust valves
4. Exhaust ports
5. Intake valve
6. Intake valve with CPS
7. Intake port 7
8. Intake port 8
9. Air tank
10. ECV
11. Auxiliary chamber
12. Reed valve
13. Self-sealing valve
14. Throttle valve
15. Pressure regulator

Figure 3.3: The 3rd air hybrid engine concept

Figure 3.2 shows the improved air hybrid engine concept. Compared to the 1st design, the Reed valve in each cylinder is replaced by a port throttle valve (14). While the engine is running in the normal firing mode, the throttle valve remains fully open and air can be induced into each cylinder through the upper intake port (7) and the lower intake port (8). For the CM and EM operations, the throttle valve is shut and air is trapped without escaping out of the lower intake port to atmosphere. The advantage of replacing the Reed valve with a throttle valve is to avoid restricted flow for the normal firing mode as well as durability issue of a Reed valve. Since the Reed valve is not designed to withstand high pressure and therefore its petals might be broken while operating in the air hybrid engine. Furthermore, the petals are bent to open while the vacuum is created in the cylinder. Thus the petals suffer from fatigue failure. The detailed simulation results of air hybrid engine concept 2 have been shown in [55].

Figure 3.3 shows the latest design [56] of the air hybrid engine. Compared to 2nd design, in order to operate in the expander mode the compressed air is supplied to the intake port 7 through the ECV and a pressure regulator 15 for all cylinders. The relocation of the ECV reduces the auxiliary chamber volume, resulting in higher compression ratio and hence greater peak tank pressure during the CM operation. With the addition of a pressure regulator, the compressed air could be supplied at preset pressure as required to operate the engine either in the cranking mode or the boost mode. One additional throttle valve 14 is added to the intake port 7.

3.2.2 The principle of operation

Figures 3.4 and 3.5 show the valve timing diagrams and air flow direction of 3rd design respectively, for the normal firing mode, CM and EM/cranking mode. Throttle 13 and throttle valve 12 controls air flow in and out of the intake port 7 and intake port 8 respectively. Both throttle valves are fully open and intake valves are actuated with default timings during the normal firing mode.

The engine can be operated in the CM the same way as 2nd concept, by closing port throttle 12 and shift the IV6 to open in the compression stroke through a CPS device. During the CM operation, throttle valve 13 remains fully open and the IV5 operates normally to allow air to be induced in the intake stroke. As shown in Figure 3.5, in the subsequent stop-start operation, the engine can be motored by the high pressure air supplied through the ECV

with the same IV6 and IV5 timings as those for the CM. In the engine starting process, the ECV remains open to allow the compressed air to flow in the intake port 7 and through the IV5 during the intake stroke, forcing the piston down and crankshaft rotate. Furthermore, IV6 opens in the forthcoming compression stroke to release in-cylinder air and hence minimise the negative work. Compared to 2nd air hybrid engine concept, the current design dispenses with the need of another active valve actuation device for IV5, resulting in a more cost-effective and simpler system.

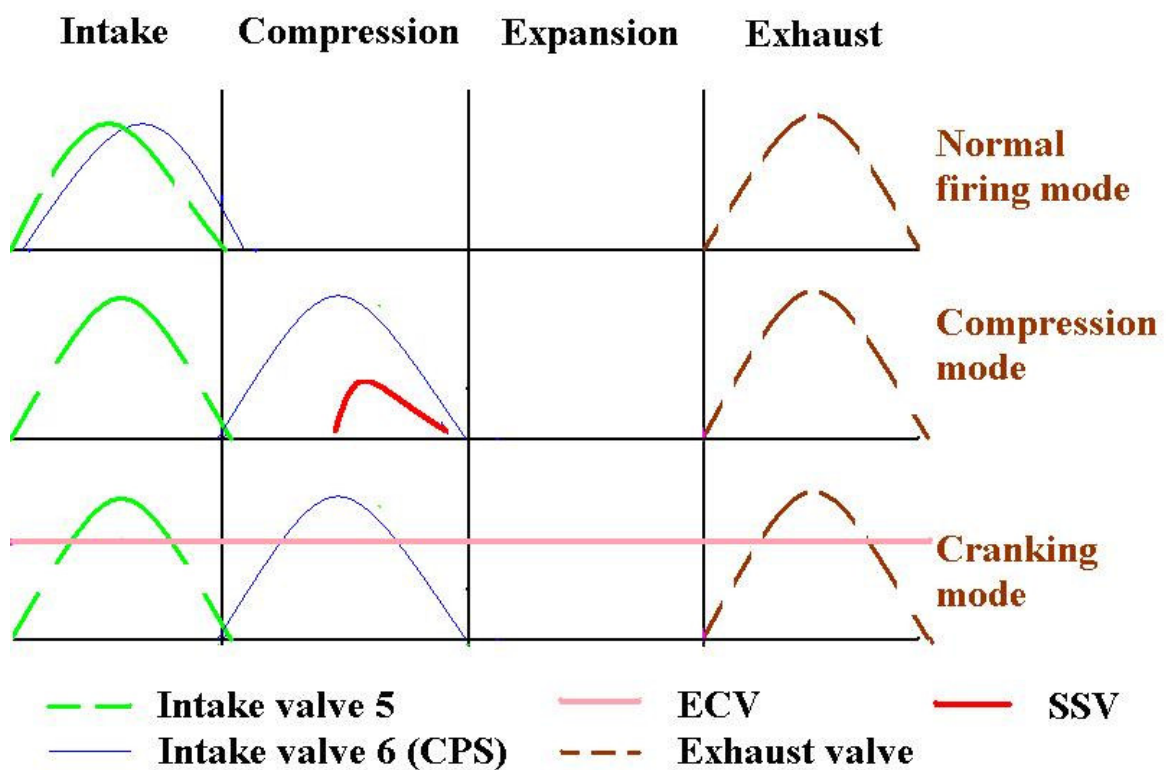


Figure 3.4: Engine valves timing for normal firing mode, CM and the cranking mode

The possible CPS device utilized for active intake valve 6 could be AVS (Audi Valvelift System) or the Honda V-TEC. Figure 3.6 shows the mechanism of AVS. The four cam lobes for two valves are mounted on a cam element (1), which can be shifted sideways on the teathed camshaft (2). The longitudinal position of the cam element decides that which cam acts on the roller cam follower. By adopting electromagnetic actuators, a pair of metal pins is able to move along the spiral groove in either way and therefore the operating cam can be changed from one set to another set. Thus the intake valve 6 can be actuated with two independent cam lobes to achieve different valve timing.

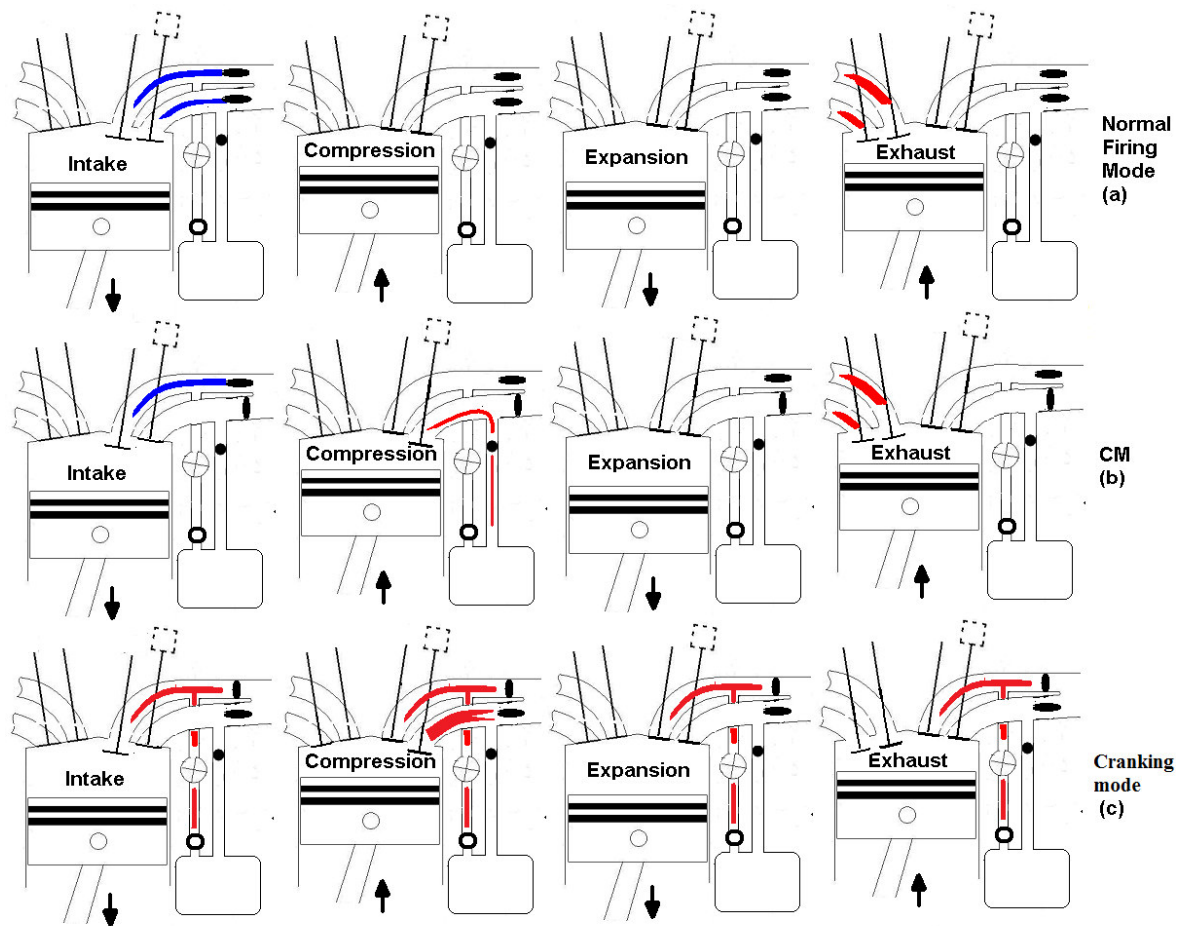


Figure 3.5: Four-stroke engine cycle for normal firing mode (a), CM (b) and cranking mode (c)

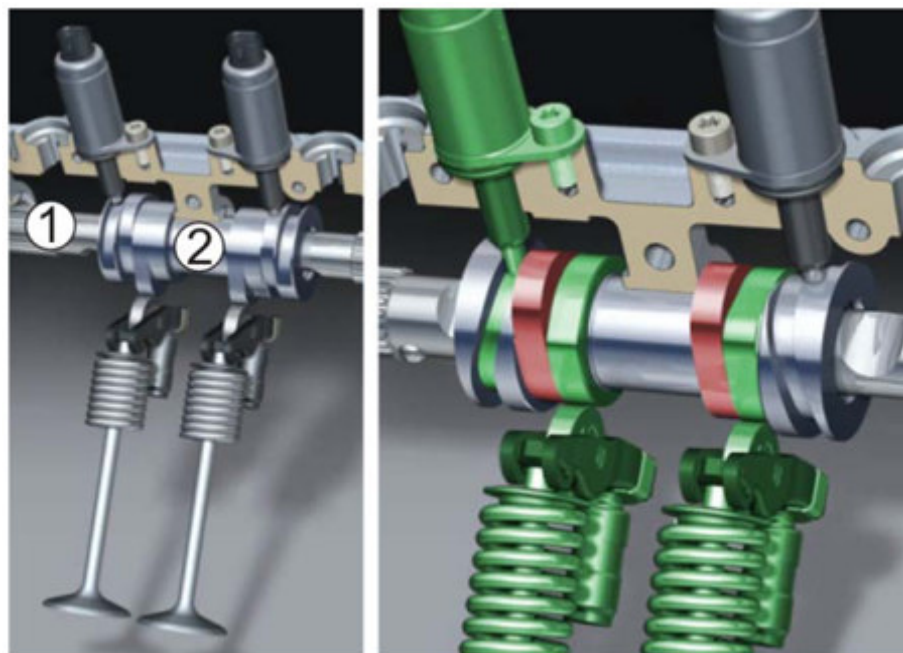


Figure 3.6: Mechanism of the AVS system [57]

Indicated mean effective pressure (imep) can be an indication of engine load in a 4-stroke engine. It is determined by the ratio of area enclosed by the pressure curve, shown in A1 in Appendix, and the cylinder displacement volume.

$$imep = \frac{1}{V_d} \oint P dV \quad \text{Equation 3.1}$$

Compressed Air Transfer Coefficient (CATC) is introduced to indicate the efficiency of the air hybrid braking process. In [40], it is defined as the ratio of air mass transferred to the air tank from the cylinder to air mass sucked into the cylinder from the atmosphere, as given by Equation 3.2:

$$CATC_b = \frac{m_{air,gtv}}{m_{air,in}} \quad \text{Equation 3.2}$$

which is a measure of the fraction of the vehicle's kinetic energy which can be stored in the air reservoir in the form of potential energy.

In [54], the potential of work of each unit of air mass captured during the compression mode is described by the braking specific indicated mean effective pressure (imep_b), which is the ratio of imep and air mass transferred to the air tank,

$$\text{Specific imep}_b = \frac{|imep_b|}{m_{air,gtv}} \quad \text{Equation 3.3}$$

The output of work per unit mass during the expansion mode is represented by the motoring specific indicated mean effective pressure (imep_m) [54],

$$\text{Specific imep}_m = \frac{imep_m}{m_{air,gtv}} \quad \text{Equation 3.4}$$

Furthermore, the regenerative efficiency is defined as the ratio of the motoring specific imep and braking specific imep [54],

$$\eta_{regen} = \frac{\text{Specific imep}_m}{\text{Specific imep}_b} \quad \text{Equation 3.5}$$

3.2.3 Overview of three concepts

Following the introduction of the configuration and the principle of operation of three air hybrid engine concepts, a brief summary of reasons for the design iterations is given here. First, air hybrid engine concept 1 utilizes a Reed valve in an intake port which causes a reduction in the air flow rate. The smaller amount of the induced air affects engine performance but also its emissions. Thus, the port throttle valve is included in the later air hybrid concepts in place of the Reed valve. In order to simplify the control and hardware requirement, a simple on-and-off valve is implemented in the concept 3 to achieve the stop-start operation by sacrificing the ability to motor the engine by the compressed air, which may be feasible for high storage and most frequent braking applications.

Compared to 2nd design, concept 3 adopts the same CPS device in only one intake valve in each cylinder for both the compressor mode operation and the expander mode operation. It saves the cost and simplifies the valve actuation mechanism. Furthermore, compressed air can be captured and stored at higher pressure because of the reduced auxiliary volume due to the relocation of the compressed air supply line to the other intake port for the expander mode operation.

3.2.4 Engine simulation setup

Table 3.1: Engine dimensions and characteristics

Number of cylinders	4
Cylinder bore	86mm
Piston stroke	86mm
Connecting rod length	160mm
Displacement volume	500cm ³
Clearance volume	28.7cm ³
Total volume of one cylinder	528.7cm ³
Compression ratio	18.4:1
R _c for air hybrid mode	5.0:1

The modelled air hybrid engine is based on a Ford PUMA 2L diesel engine with four cylinders. Each cylinder has a stroke of 86 mm, a bore of 86 mm and a displacement volume of 500 cm³. Its connecting rod length is 160 mm and its intake and exhaust valve diameters are 23.5 mm and 23.4 mm respectively. The engine speed range during the air hybrid engine operation is between 1000 and 2000 rpm. For a normal passenger vehicle, this engine speed range occupies more engine working range in a city driving cycle.

Engine and valves data are given in Table 3.1 and Table 3.2 respectively. A 40 litre air tank is used in this model.

Table 3.2: Valves dimensions and operating characteristics

Intake valve	2
Diameter	23.5 mm
Opening point (normal)	20° BTDC
Closing point (normal)	60° ABDC
Maximum lift	8.75 mm
Exhaust valve	1
Diameter	23.4 mm
Opening point	60° BBDC
Closing point	35° ATDC
Maximum lift	8.75 mm
Throttle valve	1
Diameter	25 mm
ECV count	1
Diameter	24.9 mm
SSV count	1
Diameter	12.7 mm

The size of the auxiliary chamber volume is an important parameter in this concept. It is determined by the position of the SSV and the position of the throttle valve. The geometric compression ratio of the engine is 18.4:1 for this CI engine in the normal firing mode (The engine displacement volume and clearance volume are 500 cm³ and 28.7 cm³ per cylinder respectively). However, when the engine is switched to the compression mode, the actual compression ratio (R_c) decreases as the volume of the auxiliary chamber is included in the cylinders' total clearance volume. It can be seen from Figure 3.3, the auxiliary chamber volume is decided by the position of the throttle valve and the SSV. The smallest auxiliary chamber can be easily found by installing both valves as close to the cylinder as possible. The potential highest tank pressure can be achieved with minimum auxiliary chamber due to high actual compression ratio. For the minimum auxiliary chamber volume of 56.2 cm³ examined below, the actual compression ratio is calculated as:

$$R_c = \frac{500 + 28.7 + 56.2}{28.7 + 56.2} = 6.8 : 1 \quad \text{Equation 3.6}$$

During CM, air is compressed into the auxiliary chamber isolated by the SSV from the air storage tank, and then released by the SSV into the air storage tank due to the pressure difference between the auxiliary chamber and the air storage tank. During EM, the ECV

controls the amount of compressed air released from the air storage tank to the intake port 8 and then goes into the cylinder after the intake valve 5 is opened.

Without the auxiliary chamber and ECV, the intake valve has to be able to vary its opening profile in order to control the amount of compressed air released from the air storage tank. By adopting the auxiliary chamber and the ECV, the complicated and expensive active valve control system used by other researchers [38-40] could be avoided in the engine design.

The simulation canvas of the WAVE hybrid engine model is shown in Figure 3.7. Four Energy Control Valves (“ECV1”, “ECV2”, “ECV3” and “ECV4”) have been implemented to connect the other four intake ports (“Intakeport2”, “Intakeport4”, “Intakeport6” and “Intakeport8”), though such valve would be sufficient if no individual cylinder control is required. In addition, each of these four intake ports (“Intakeport2”, “Intakeport4”, “Intakeport6” and “Intakeport8”) are equipped with one throttle valve (“T2”, “T4”, “T6” and “T8”). Whilst, the right intake ports, labelled “intakeport1”, “intakeport3”, “intakeport5”, and “intakeport7”, are connected to the intake network through “T1”, “T3”, “T5” and “T7” (throttle valves) respectively. All intake ports are connected to the atmosphere (“amb”). The right intake ports (“intakeport1”, “intakeport3”, “intakeport5”, and “intakeport7”) are connected to the air tank (“Airtank”) through Self-sealing valves (“SSV1”, “SSV2”, “SSV3” and “SSV4”) respectively. The air tank is modelled as a duct of defined volume and initial pressure. All exhaust ports are connected to a single exhaust pipe to the atmosphere (“amb2”). It is noted that the two exhaust valves and ports are modelled as one exhaust of equivalent flow area for computational efficiency.

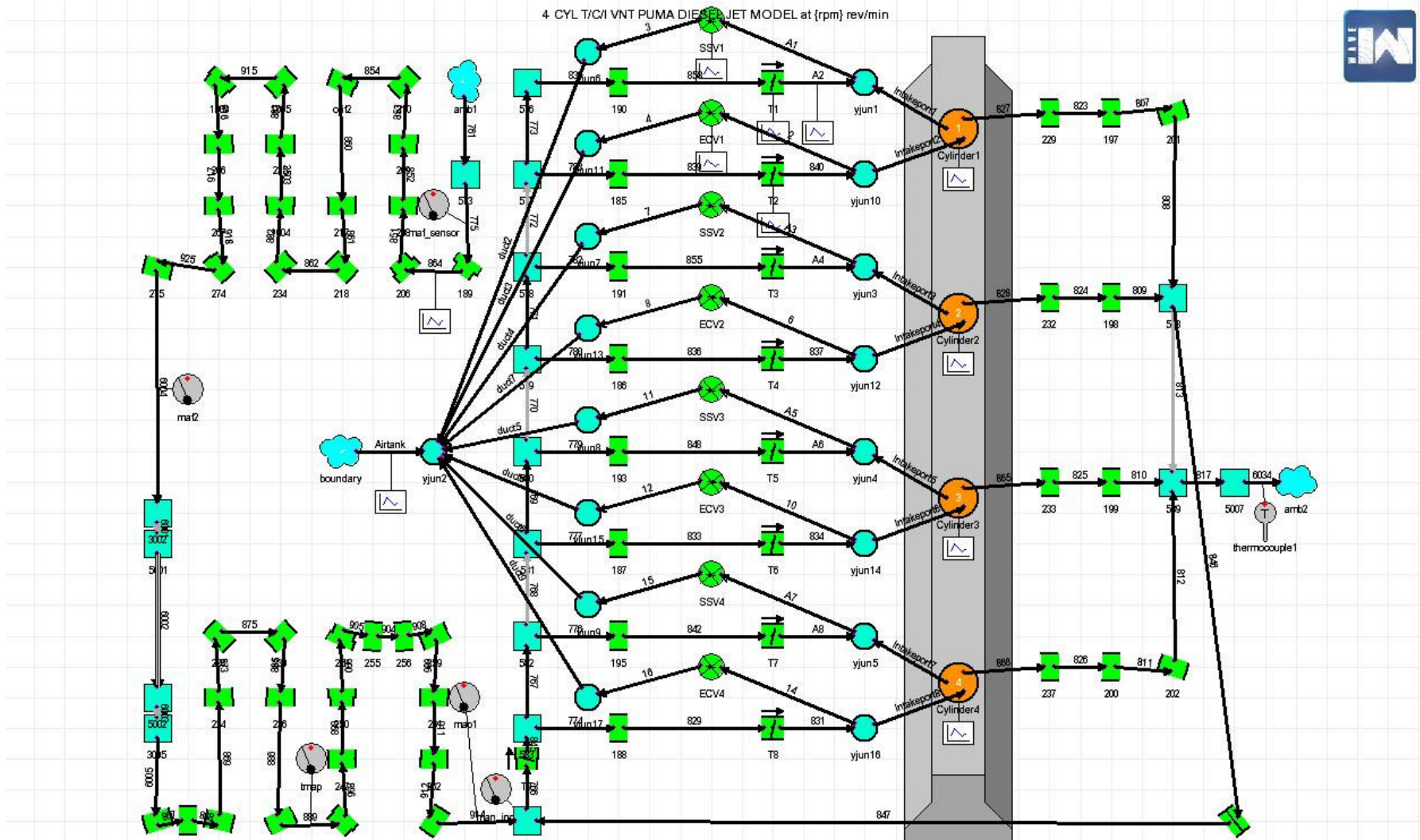


Figure 3.7: WAVE model of 3rd air hybrid engine concept

3.2.5 Simulation Results

3.2.5.1 Valve timing optimization for CM

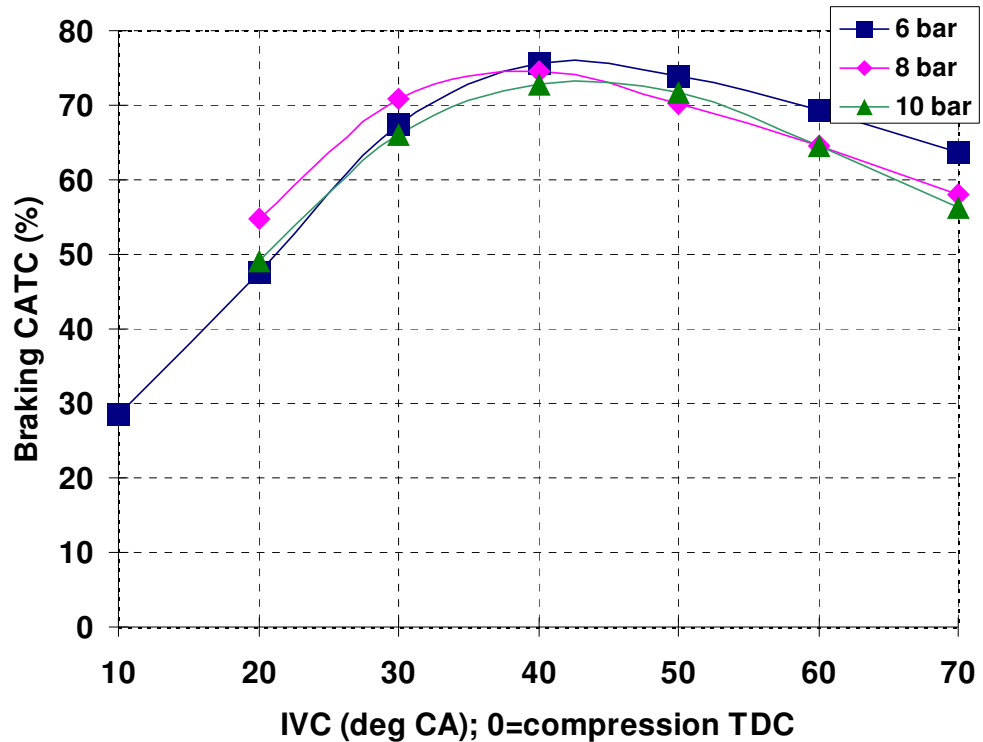


Figure 3.8: Predicted $CATC_b$ for 1500 rpm engine speed

During the compression mode operation, the IV6 opening duration should ideally extend over the whole compression stroke to allow the air to be compressed into the airtank. However, the IV6 closing timing can not go further than 70° ATDC for a typical valve lift profile otherwise the valve clash will occur. In this simulation, the IV6 closing points have been set in the range between 10° ATDC and 70° ATDC to optimize the IV6 timing.

Figure 3.8 shows that the maximum $CATC_b$ is realized when the IV6 is set to close at 40° ATDC and its Intake Valve Open (IVO) at 40° BBDC. For earlier IVCs, there is not enough time for the compressed air to flow from cylinders to the tank due to short opening duration from TDC to IVCs when the air flows due to the ramming effect. On the other hand, very late IVC timings result in compressed air flowing back into the cylinder during the expansion stroke.

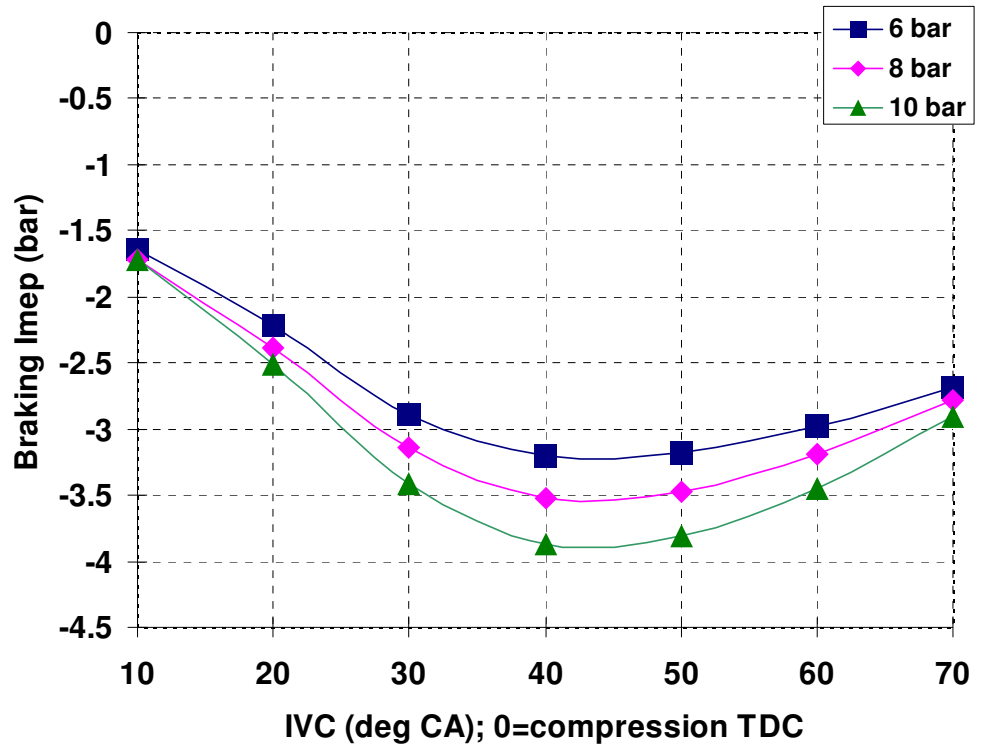


Figure 3.9: Predicted imep_b for 1500 rpm engine speed

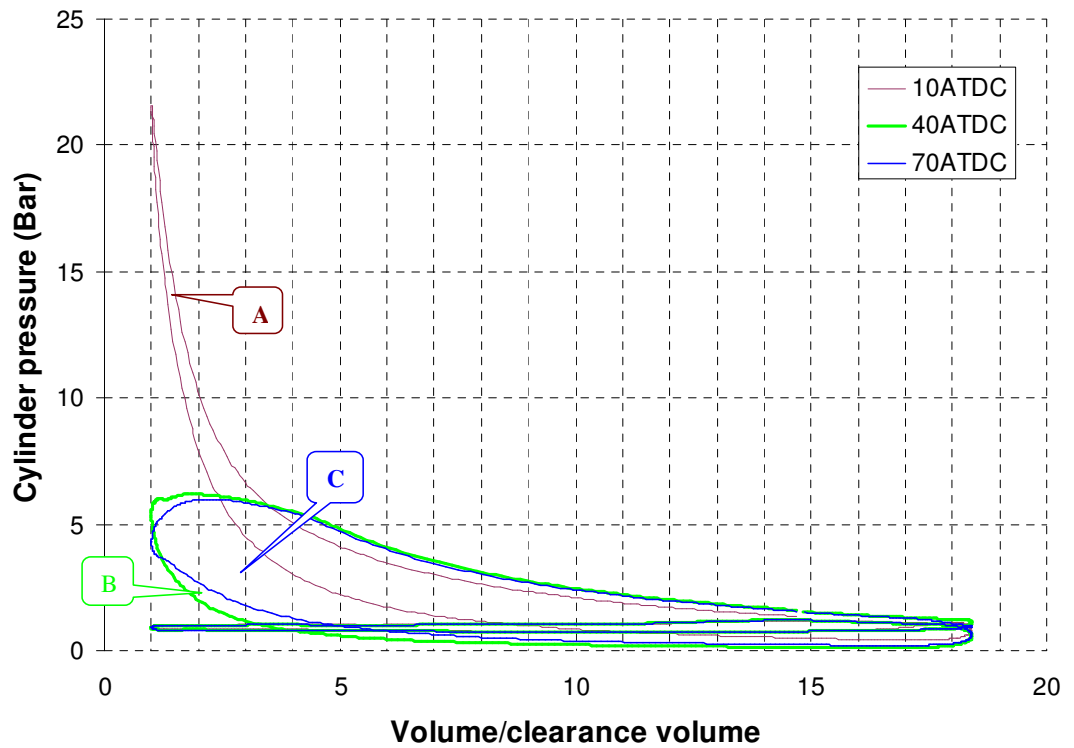


Figure 3.10: P-V diagram for various IV6 closing timings

The corresponding variation of imep_b with the IV6 closing timing is plotted in Figure 3.9. It can be seen from the results that the optimal braking performance is achieved between $30^\circ - 50^\circ$ CA ATDC. Maximum imep_b is achieved at IV6 closing time of 40° CA ATDC, regardless of the tank pressure. It should note that the actual braking torque exerted to the vehicle will include the frictional torque and hence the braking bmeP will be roughly 1 bar above the values shown in Figure 3.9.

In order to understand the effect of IV6 timing, the predicted cylinder indicator diagrams for three IV6 timings are shown in Figure 3.10 at 1500 rpm engine speed and 4 bar tank pressure. It can be seen that peak cylinder pressure is much higher when IV6 is closed earlier due to more air being compressed in the cylinder and then expanded, which results in less compressed air flowing into the air tank and reduced braking torque. As IV6 is more retarded to close at 70° CA ATDC, the backflow of the compressed air into the cylinder from the auxiliary volume increases the expansion work and hence reduces the braking work. With IV6 closing at 40° CA ATDC, compressed air continues to flow into the auxiliary volume beyond TDC due to the ramming effect but it is prevented from flowing back into the cylinder by the closing valve, resulting in the most compressed air being supplied to the air tank and maximum braking work as indicated by Area B.

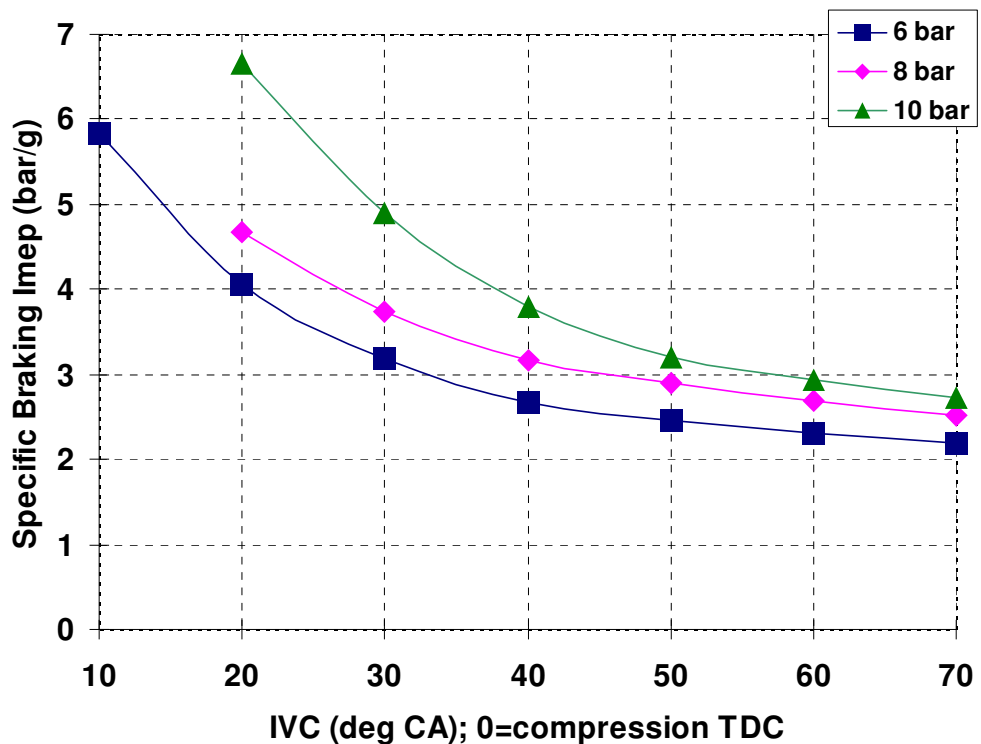


Figure 3.11: Braking specific imep for 1500 rpm engine speed

As a result, its energy capture and storage ability, as measured by the specific braking imep, is optimised when IV6 closing time is set at after 40° CA ATDC, as shown in Figure 3.11.

Based on the above investigation, the optimised IV6 timing is plotted in Figure 3.12 together with other valves timing and SSV opening period that is determined by the pressure drop between the auxiliary chamber and the air tank.

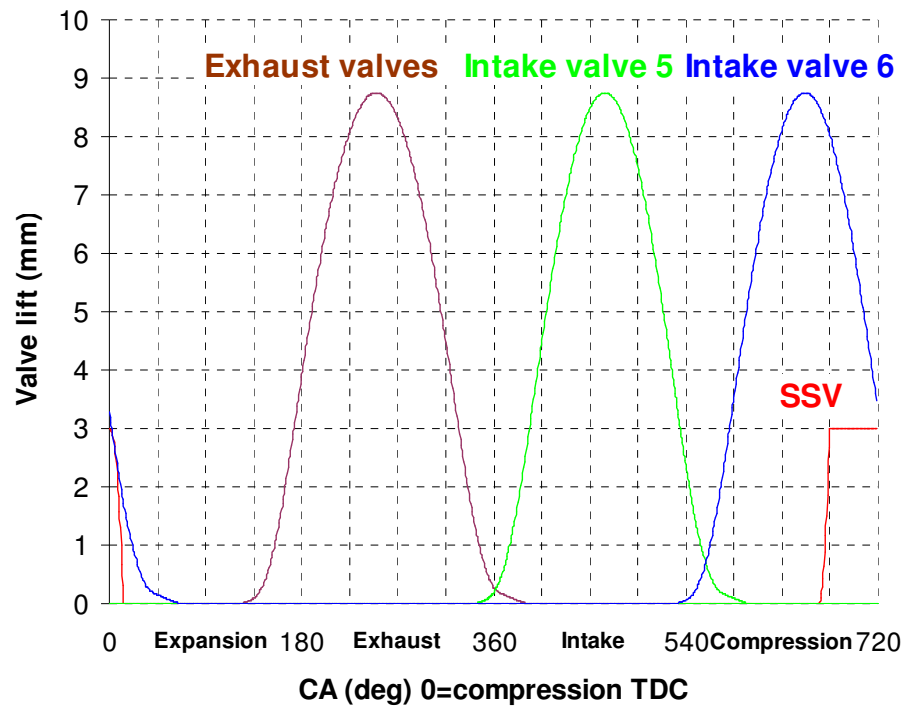


Figure 3.12: Optimal IV6 timing for air compressor mode

3.2.5.2 Valve timing optimization for the cranking mode

An effective and simple application of the compressed air is to provide the cranking torque for stop-start operation in the hybrid vehicle. The light-duty diesel engine has the idle speed 750 rpm. During the cranking mode operation, the compressed air is utilized to crank the engine from stop to the idle speed. Ricardo's WAVE can not model the engine at 0 rpm engine speed, and therefore, the mean speed 375 rpm has been chosen for the cranking mode. The sensitivity of predicted mass of air transferred during one engine cycle to IV6 closing points for various air tank pressures is shown in Figure 3.13.

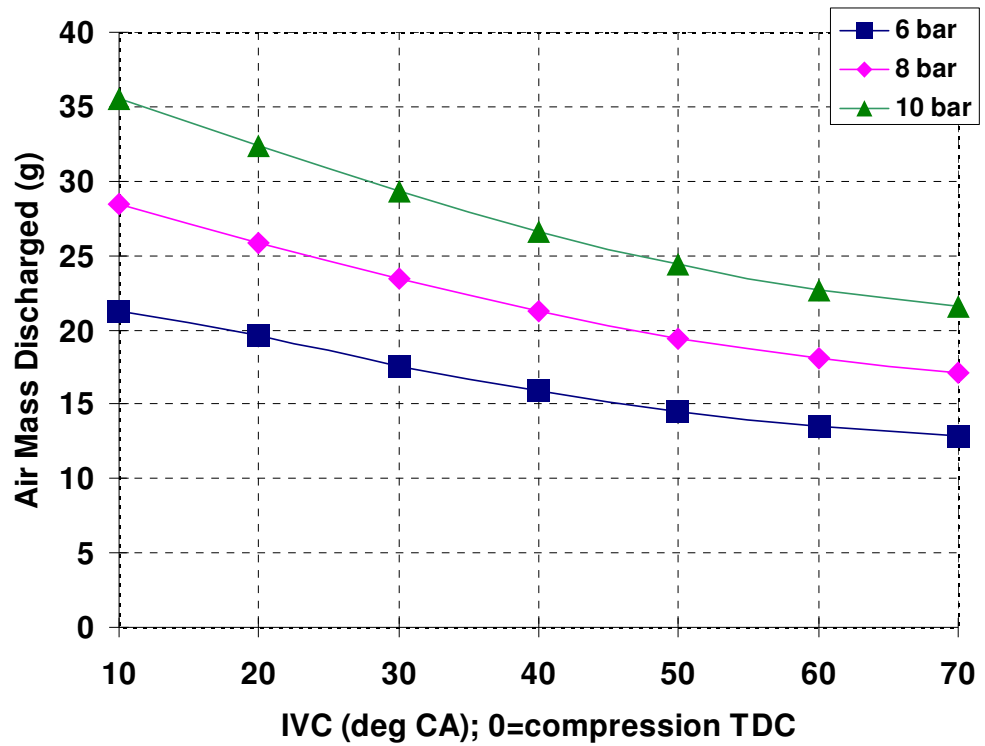


Figure 3.13: Compressed air expenditure for 375 rpm engine speed

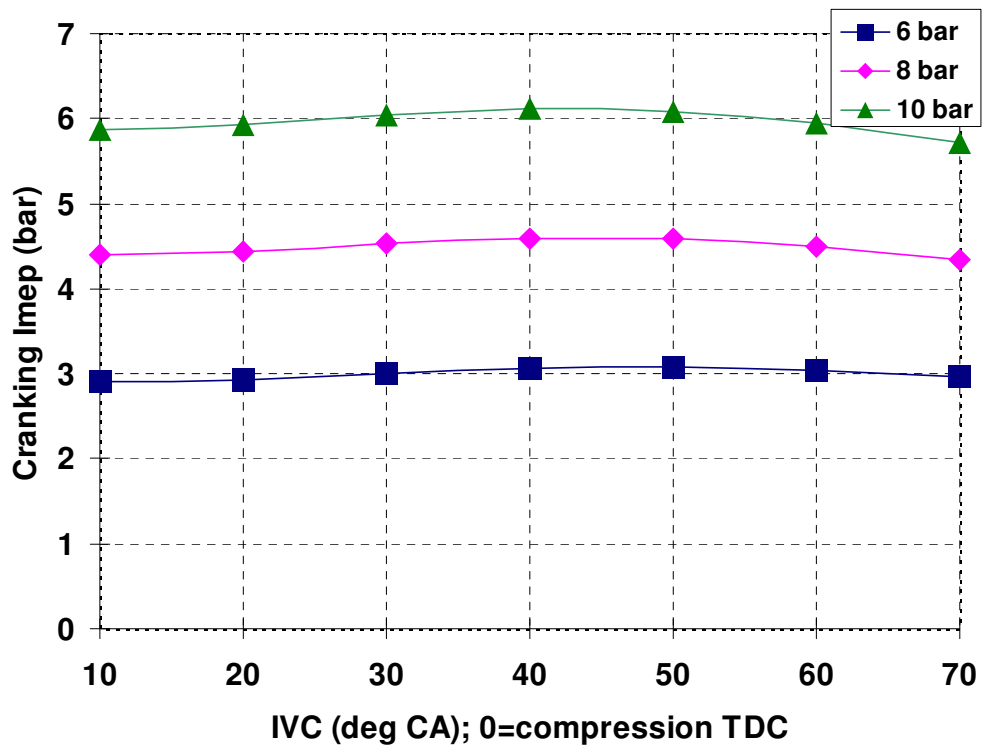


Figure 3.14: Predicted imep_m for 375 rpm engine speed

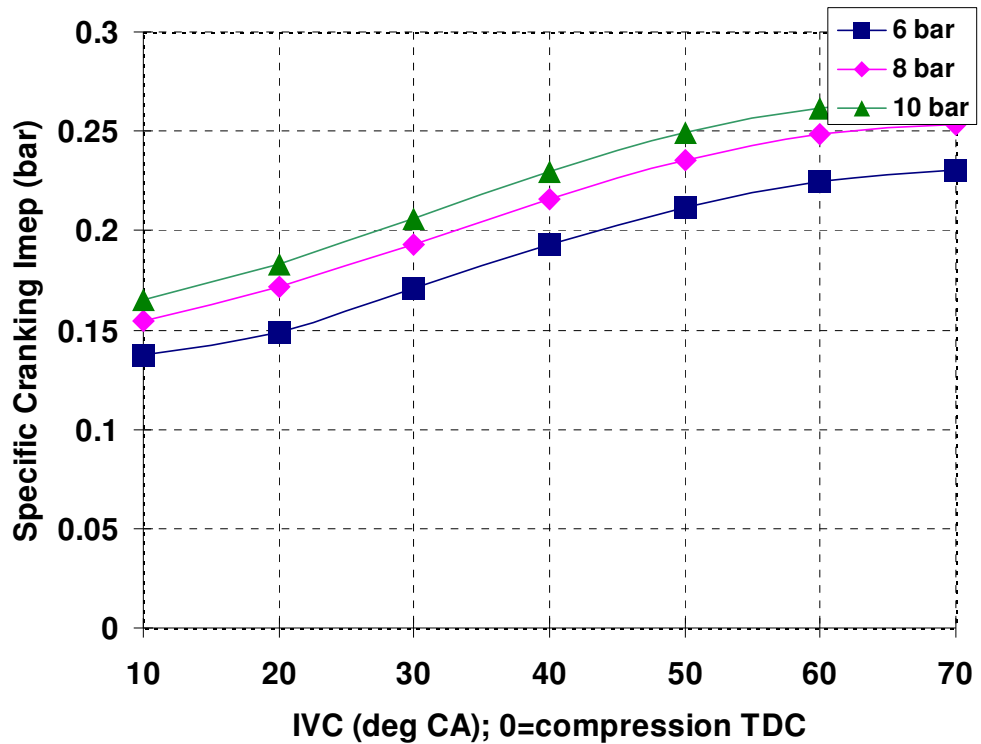


Figure 3.15: specific cranking imep for 375 rpm engine speed

It can be seen that compressed air expenditure decreases with the retarded IV6 closing point because of the smaller overlap between IV5 and IV6. The latest IV6 closing point is at 70° CA to avoid collision between the IV6 and the piston.

Figure 3.14 shows the sensitivity of the predicted $imep_m$ to IV6 closing points for various air tank pressures. It can be seen that $imep_m$ is strongly dependent on the tank pressure but varies slightly with various IV6 closing points.

The efficiency of the expander mode operation is represented by the ratio of compressed air expenditure to $imep_m$. Figure 3.15 shows that the best efficiency is achieved when IV6 is closed at 70°, regardless of tank pressures.

Based on the results in Figures 3.11 and 3.15, when IV6 is set to close at 70° CA both air compressor mode and air cranking mode will be operating most effectively.

3.2.5.3 Comparison between an insulated airtank and a normal airtank

The simulation done above is using an insulated airtank. Thus heat can be stored and reused in an adiabatic condition. However, the normal airtank without insulation may

decrease the regenerative efficiency but save the cost and simplify the manufacturing process. A comparison between an insulated airtank and a normal airtank will be analyzed here. First of all, it is necessary to find out if there is any difference during the valve timing optimization process. The simulation has been done at 8 bar tank pressure for 1500 rpm engine speed. Values of predicted $CATC_b$ and $imep_b$ are similar between the adiabatic and isothermal process. The results show that the amount of air charged into the airtank and the braking $imep$ absorbed by the engine are not affected by the air temperature in the air tank. The efficiency of the compressor mode operation is represented in Figure 3.16. It can be seen that the best efficiency for both airtanks is achieved when IV6 is closed at 70°, regardless of the tank insulation.

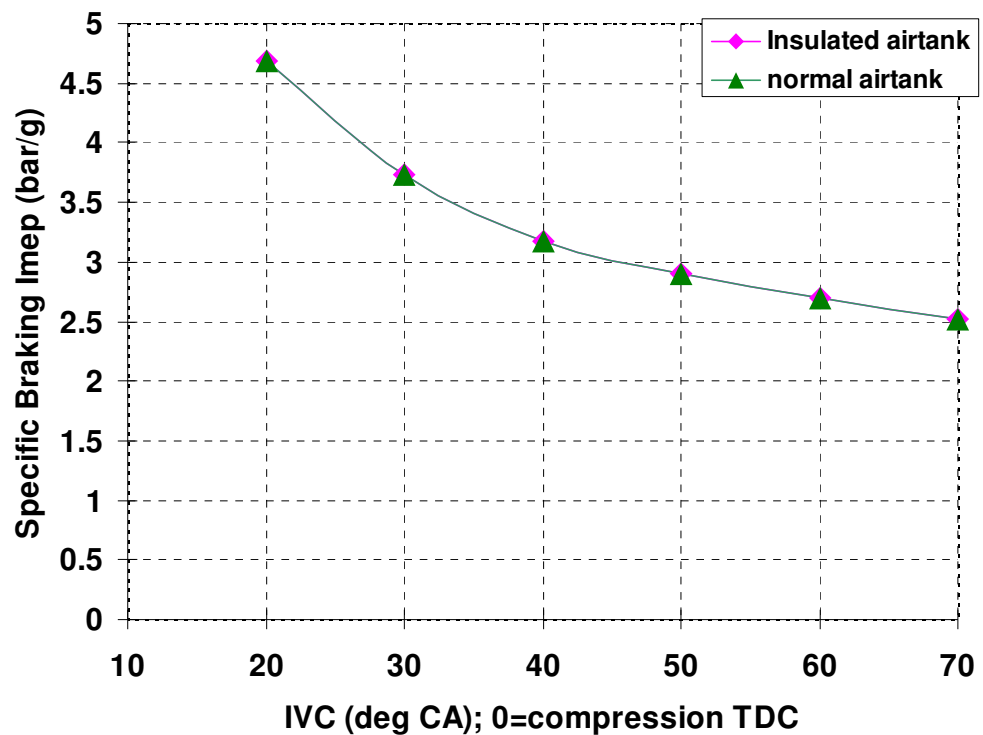


Figure 3.16: Predicted specific $imep_b$ for 1500 rpm engine speed at 8 bar tank pressure

Figure 3.17 shows the tank pressure increase with time during the CM operation. It is noted that it takes 90 and 210 engine revolutions to charge the tank pressure from 5 bar to 8 bar at 1500 rpm engine speed for the insulated airtank and the normal airtank respectively. Compared to the normal airtank, the insulated airtank can be charged 4.8 seconds faster from 5 bar to 8 bar for 1500 rpm engine speed due to the absence of heat and hence energy losses. The compressed air temperature has increased from the initial

tank temperature, 298.15 K, to the final tank temperature, 387.18 K after 90 engine revolutions.

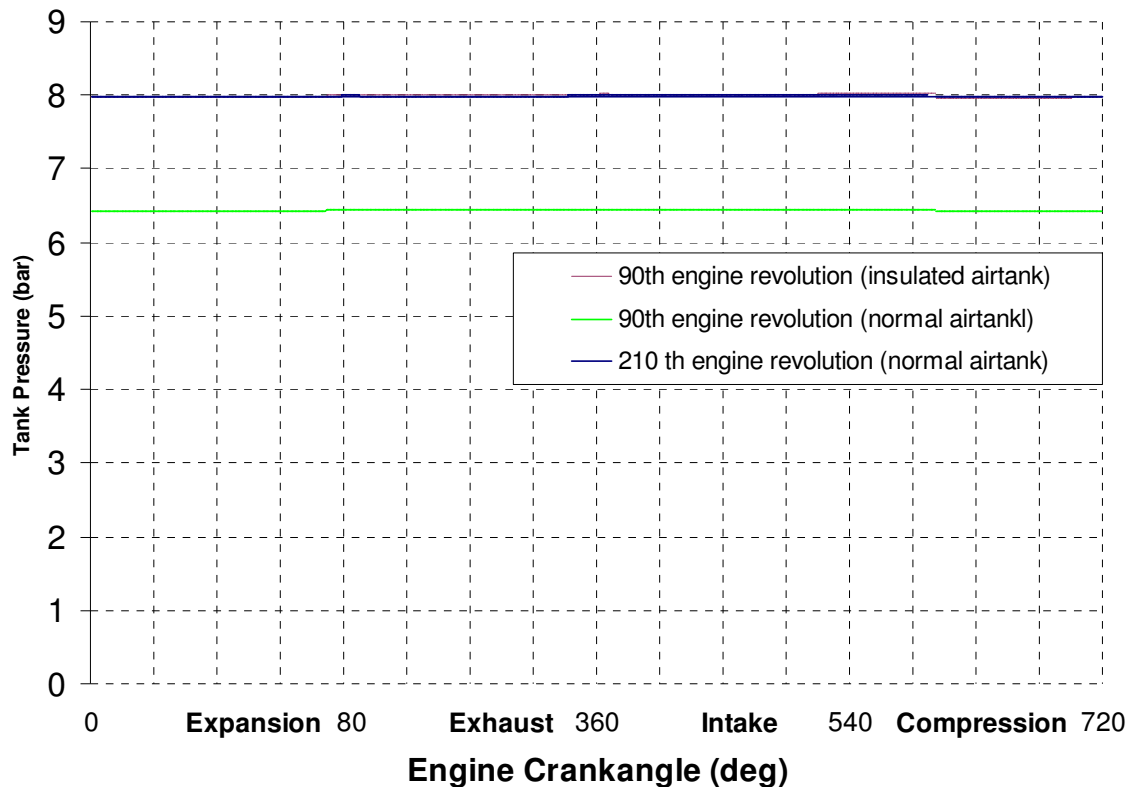


Figure 3.17: Predicted tank pressure for 1500 rpm engine speed

The effect of compressed air temperature on the expander mode operation is shown in Figures 3.18 and 3.19. Figure 3.18 shows the sensitivity of predicted mass of air transferred during one engine cycle to IV6 closing points from the insulated airtank at 387K and the normal airtank at 298K. Although the least air consumption occurs at IV6 closure of 70° CA, less hot air is consumed to produce similar cranking imep, Figure 3.19. As Figure 3.20 shows, the insulated airtank leads to more than 20% improvement in specific cranking imep.

The simulation done above uses a 40 litre airtank which had been chosen to be of the same size as the fuel tank volume in a small passenger car. The effect of tank volume does not affect the charging and discharging process in the compressor and expander mode operations. However, it will affect the storage and usage of the compressed air during the stop-start operations and hence its effect on the vehicles performance will be modelled in the chapter 6.

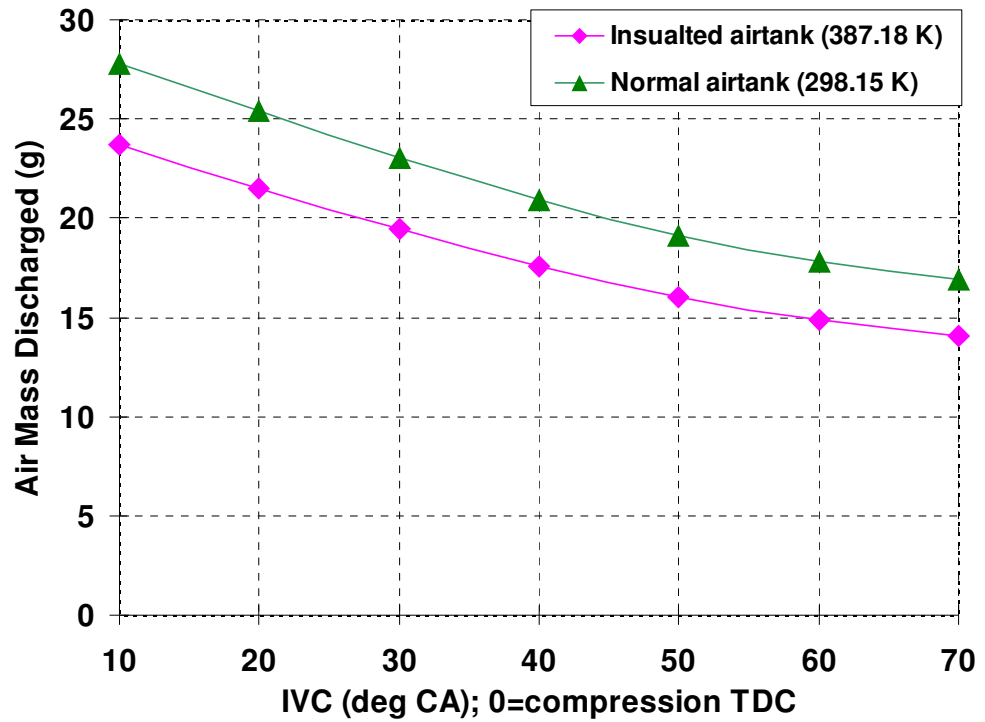


Figure 3.18: Compressed air expenditure for 375 rpm engine speed at 8 bar tank pressure

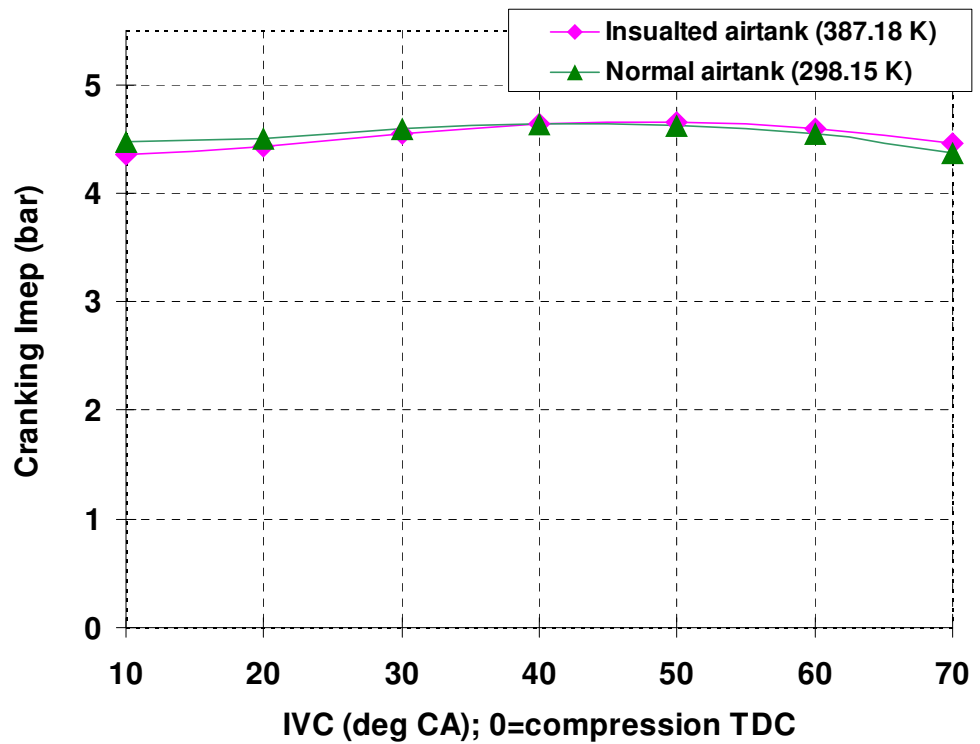


Figure 3.19: Predicted $imep_m$ for 375 rpm engine speed at 8 bar tank pressure

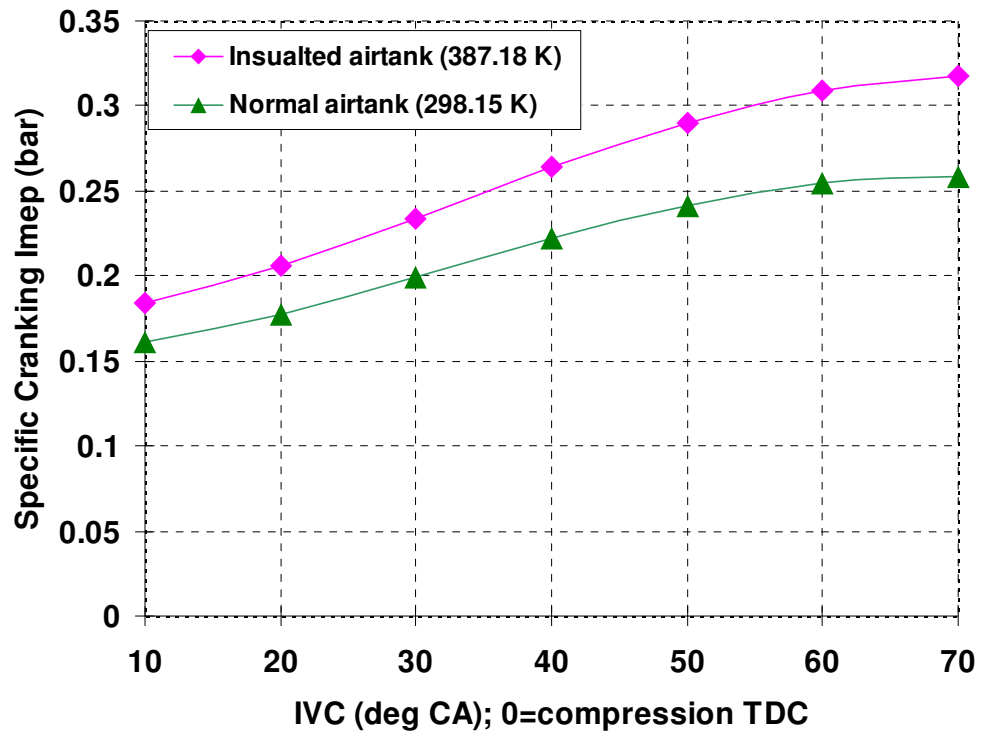


Figure 3.20: Specific cranking imep for 375 rpm engine speed at 8 bar tank pressure

In the above analysis, the insulated airtank was assumed adiabatic, and therefore, high temperature and high pressured compressed air could be reused. The air hybrid engine implements the insulated airtank which is more efficiency than the one with the normal airtank. However, the rise of the tank temperature limits the amount of the compressed air stored in the airtank. Figure 3.21 shows additional recuperator 16 implemented between the engine and the airtank. Recuperator 16, made of a ceramic matrix could absorb and store heat energy when compressed air is stored from the cylinder to the airtank in the compressor mode process. The minor rise of the tank temperature has smaller affection on the amount in the compressed air stored in the airtank. The heat stored in the recuperator can be reused in the expander mode process while the compressed air is released into the cylinder through the recuperator. The possible drawback is that the restricted flow will occur if the effective opening area is smaller than the default pipe size in the intake manifold. It will be important to pick the right size of the recuperator for the air hybrid engine. Due to the difficulty of modelling the recuperator with precise structure, the air hybrid engine concept modelled in this thesis has no recuperator.

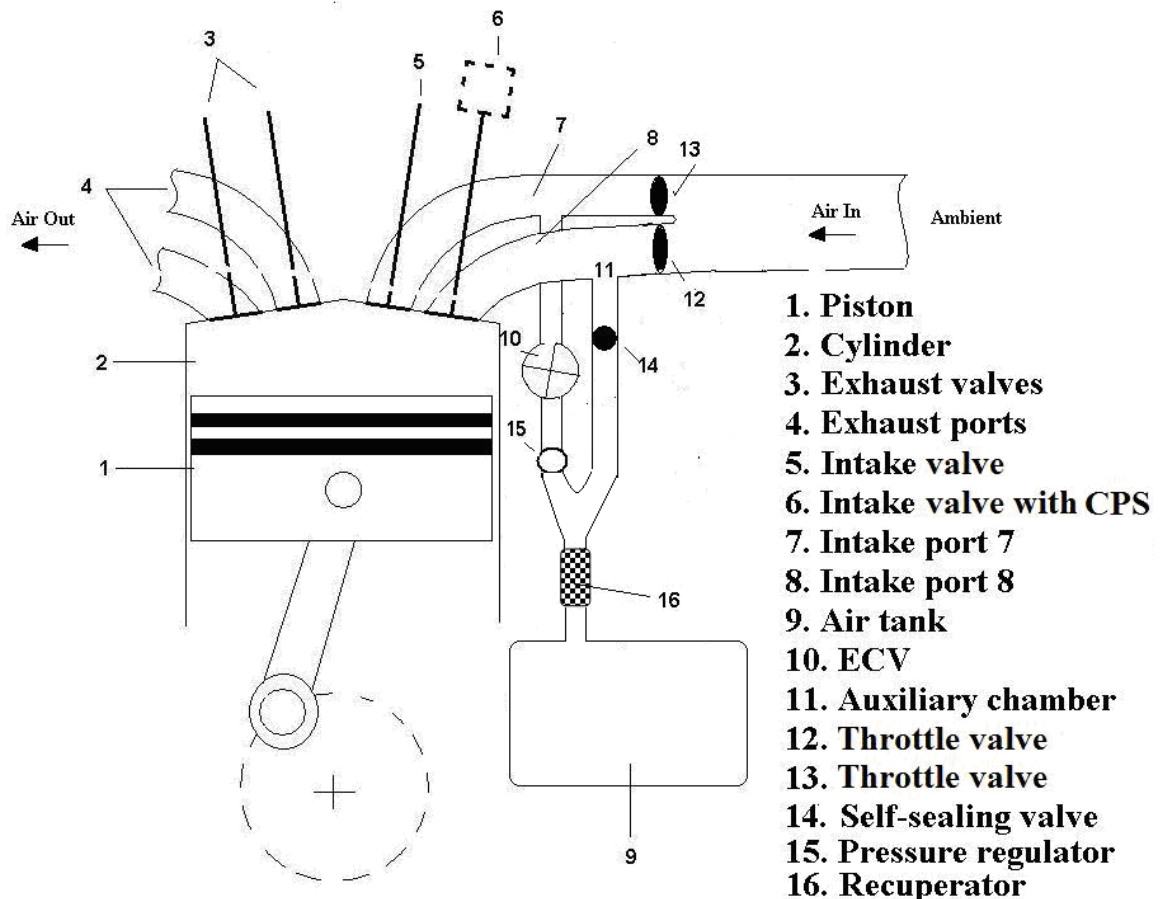


Figure 3.21: 3rd air hybrid engine concept with a recuperator

3.2.6 Conclusions

The systematic study has been done on the 3rd design revolution of the air hybrid engine concept. The concept can be achieved by adopting production valve technologies without modifying the engine and transmission system. This air hybrid concept will be selected in the vehicle driving simulation in Chapter 6 to evaluate its potential.

3.3 Ford PUMA air hybrid engine with joint intake ports

3.3.1 Description of the concept

In order to evaluate the potential of the air hybrid concept to an engine with joint intake ports, Ford PUMA engine's intake was first modelled with joint intake ports in this section. Figure 3.22 shows an air hybrid engine with a joint intake port for each cylinder. Both intake valves and exhaust valves are assumed to be operated with CPS system so that their times can be shifted for air hybrid operations. Compared to the engine with split

intake ports, a Reed valve (12) is placed in the intake port. While air pressure (inside the auxiliary chamber) is lower than the manifold pressure, the Reed valve petals open and air is induced into joint intake port 7. On the other hand, the Reed valve petals close and air can be kept without escaping out of intake port 7 to atmosphere while the air pressure (inside the auxiliary chamber) is higher than the manifold pressure.

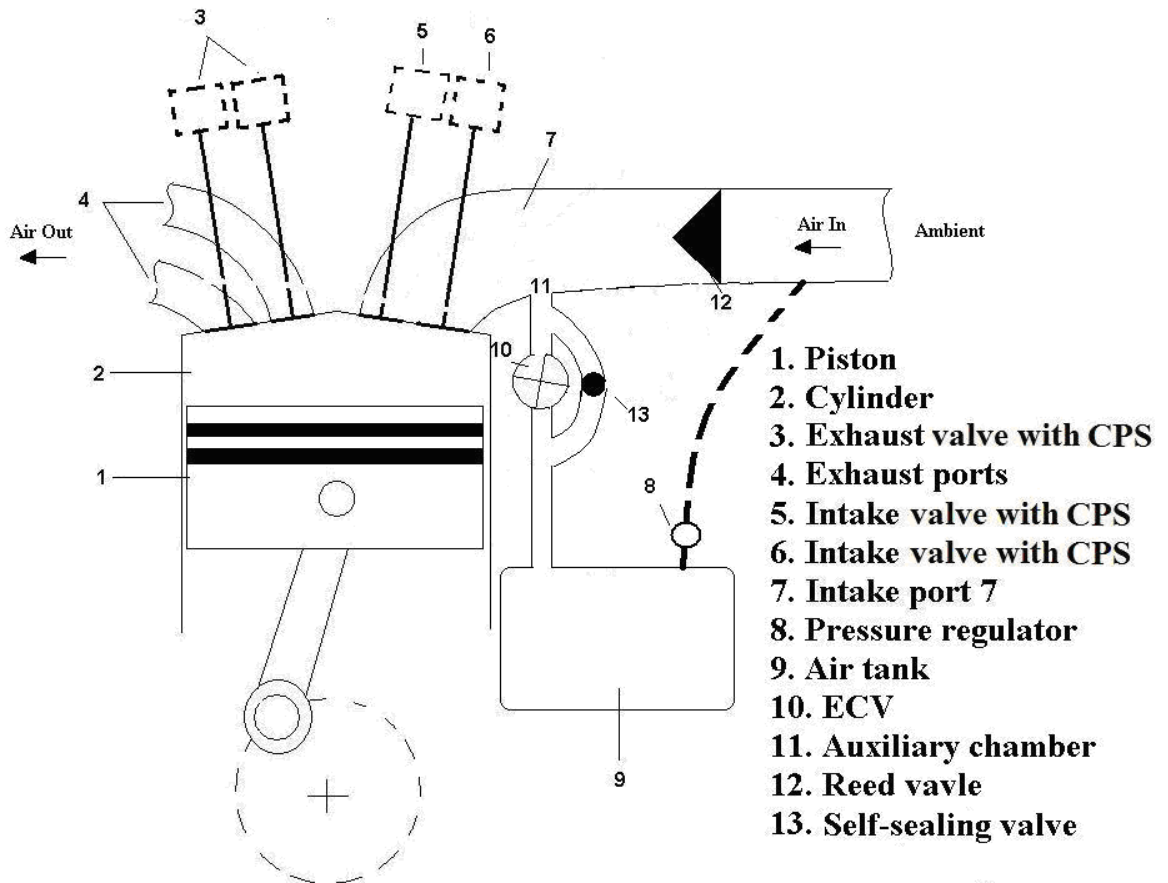


Figure 3.22 Ford PUMA 2L air hybrid engine cylinder with a joint intake port

3.3.2 The Principle of operation

Figure 3.23 and Figure 3.24 show the valve timing diagrams and air flow direction respectively for the normal firing mode, CM and the expander mode. During the normal firing mode, both intake and exhaust valves operate at their default settings. During deceleration and braking, the engine switches from the normal firing mode to the compression mode and both intake valves start opening in the normal intake stroke and therefore the air can be induced through the joint intake port into the cylinder. Both intake valves are assumed to open by means of a CPS device until the end of the compression

stroke so that air is compressed and stored in the auxiliary chamber formed by the Reed Valve, SSV and ECV so that engine braking is realised. For the expander mode, the engine is turned into an air expander by opening the ECV and both intake valves during the normal intake stroke so that high pressure air forces the piston down and generate the motoring work. In order to minimise the parasitic compression work followed, it is assumed that both exhaust valves can be opened by means of a similar CPS device, as shown in Figure 3.23.

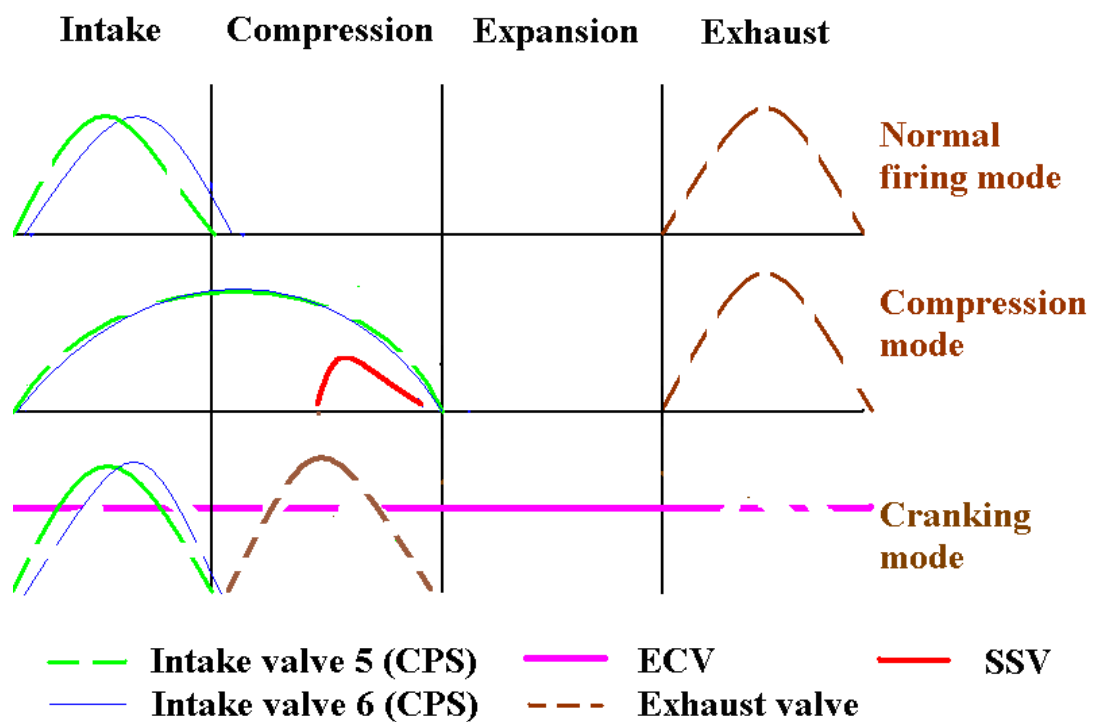


Figure 3.23: Engine valves, active intake valve and ECV timing for normal firing mode, CM and the cranking mode

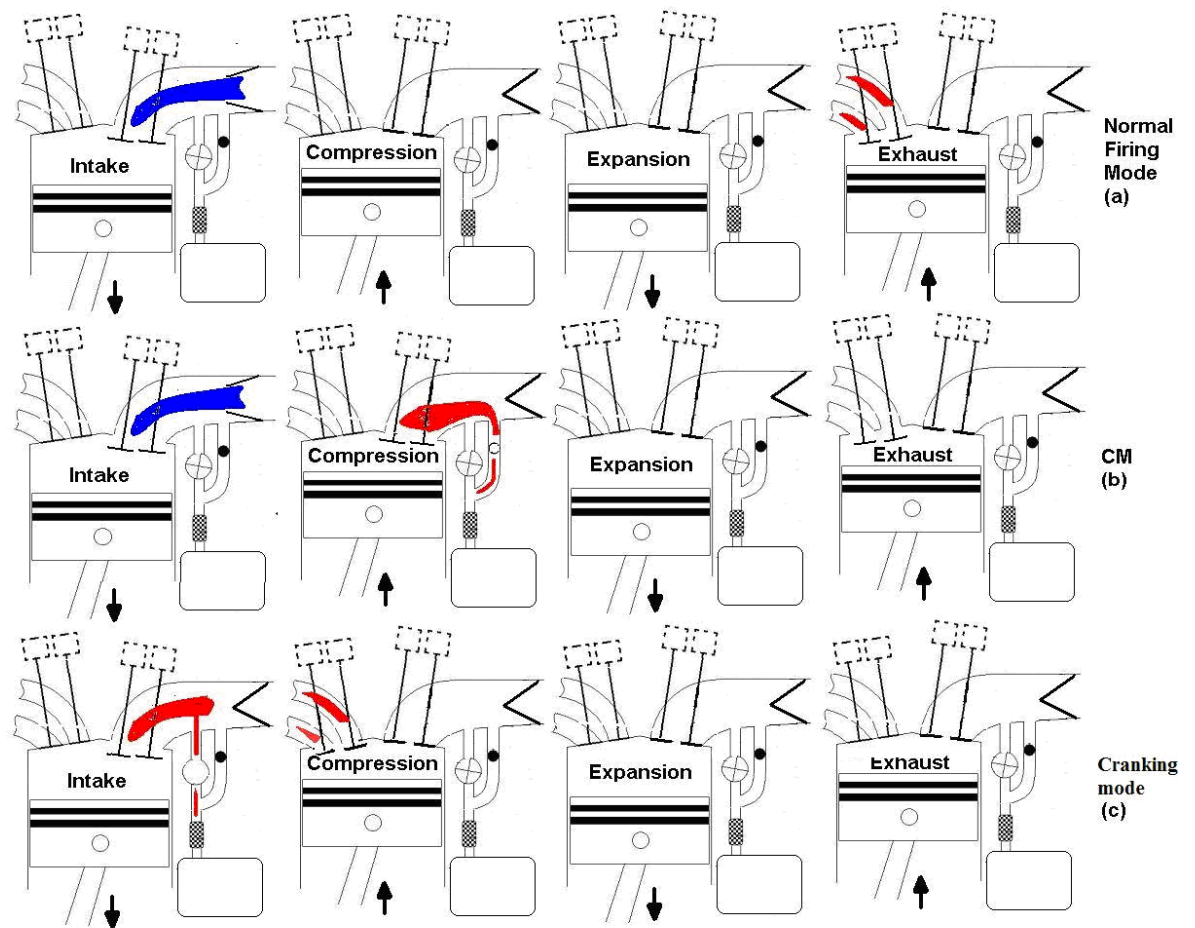


Figure 3.24: Four-stroke engine cycle for the normal firing mode (a), CM (b) and the cranking mode (c)

3.3.3 Engine simulation setup

The simulation canvas of the air hybrid engine's model is shown in Figure 3.25. The modelled air hybrid engine was modified from the Ford PUMA 2L diesel engine with split intake ports. The cylinders, labelled "cylinder1, cylinder 2, cylinder 3 and cylinder 4" are connected to the intake network through "reedvalve1", "reedvalve2", "reedvalve3" and "reedvalve4" (non-return valves) respectively for inducing air from atmosphere ("amb1"). The cylinder ("cylinder1, cylinder 2, cylinder 3 and cylinder 4") are connected to the air tank ("Airtank") through Energy Control Valves ("ECV1", "ECV2", "ECV3" and "ECV4") and Self-sealing valves ("SSV1", "SSV2", "SSV3" and "SSV4") for releasing compressed air from the air tank and compressing air into the air tank respectively. The air tank is modelled as a duct of defined volume and initial pressure. All exhaust ports are connected to a single exhaust pipe to the atmosphere ("amb2").

Engine and valves data are given in Table 3.1 and Table 3.2 respectively. The size of the auxiliary chamber volume is an important parameter in this concept. It is determined by the position of the non-return Reed valve, the position of the SSV and the position of the ECV. However, when the engine is switched to the compression mode, the actual compression ratio (R_c) decreases as the volume of the auxiliary chamber is included in the cylinders' total clearance volume. For the auxiliary chamber volume of 80.6 cm^3 examined below, the actual compression ratio is calculated as:

$$R_c = \frac{500 + 28.7 + 80.6}{28.7 + 80.6} = 5.6 : 1$$

Compared with the air hybrid engine with the split intake ports, the significant reduction in the effective compression ratio will reduce the maximum air tank pressure and hence the amount of braking energy as to be discussed below.

3.3.4 Simulation Results

3.3.4.1 Intake valves timing for CM

Figure 3.26 shows the maximum $CATC_b$ is realized when the IV5 and IV6 are set to close to 50° ATDC (compression stroke) and both of their IVO at 20 Before Top Dead Centre (BTDC) (exhaust stroke). For earlier IVCs, there is not enough time for the compressed air to flow from cylinders to the tank due to short opening duration from TDC to IVCs and the ramming effect of flowing air. On the other hand, very late IVC timings result in compressed air flowing back into the cylinder during the expansion stroke.

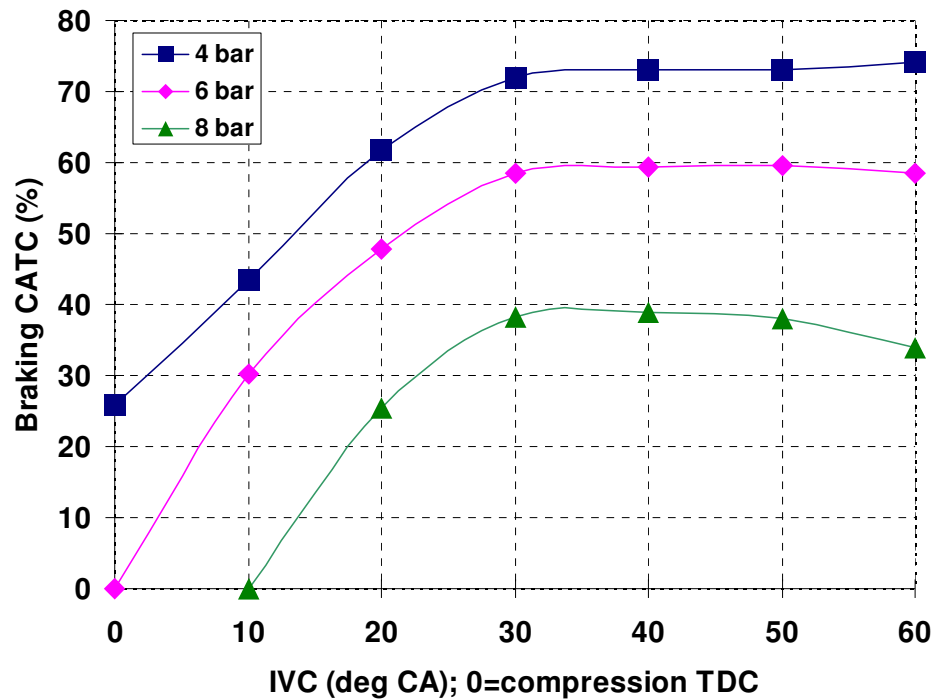


Figure 3.26: Predicted $CATC_b$ for 1500 rpm engine speed

Figure 3.27 shows the predicted variation of $imep_b$ (with absolute values shown) with regard to IVC points for the tank pressure range between 4 and 8 bar, at intervals of 2 bar. It can be seen from the results that high braking performance is achieved for a range of active IVC timings between $30^\circ - 40^\circ$ CA ATDC, where increased $imep_b$ (and hence braking torque) is realized. The maximum air tank pressure is 9.3 bar, compared with over 15 bar with the air hybrid engine concepts with split intake ports, because of the reduced effective compression ratio caused by the enlarged auxiliary chamber volume of the joint intake port.

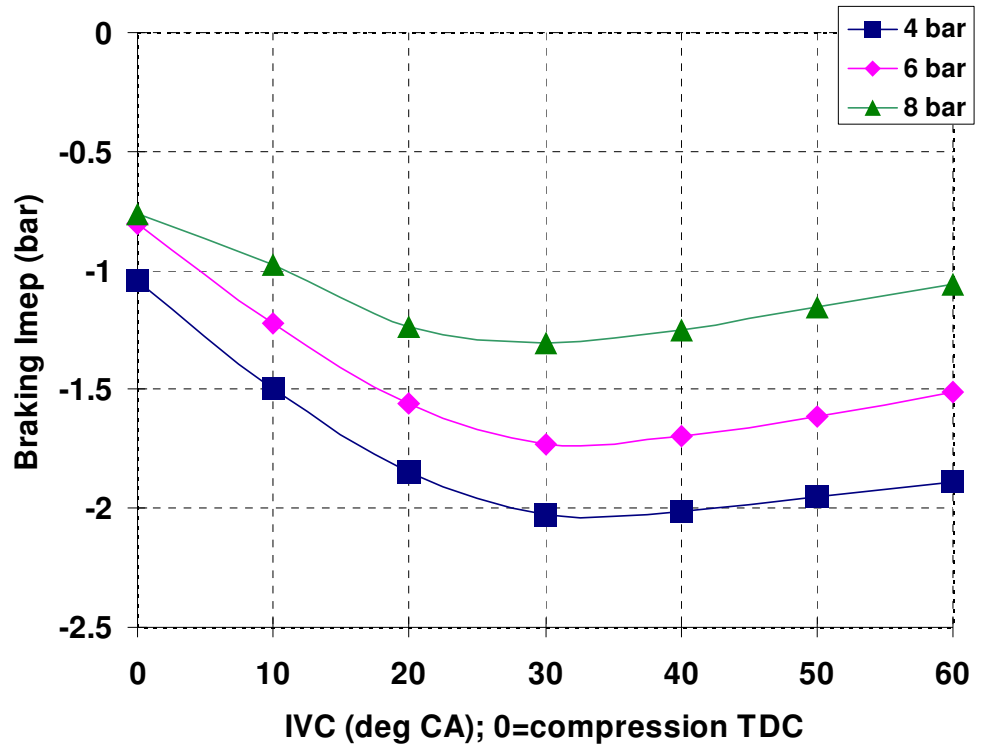


Figure 3.27: Predicted $imep_b$ for 1500 rpm engine speed

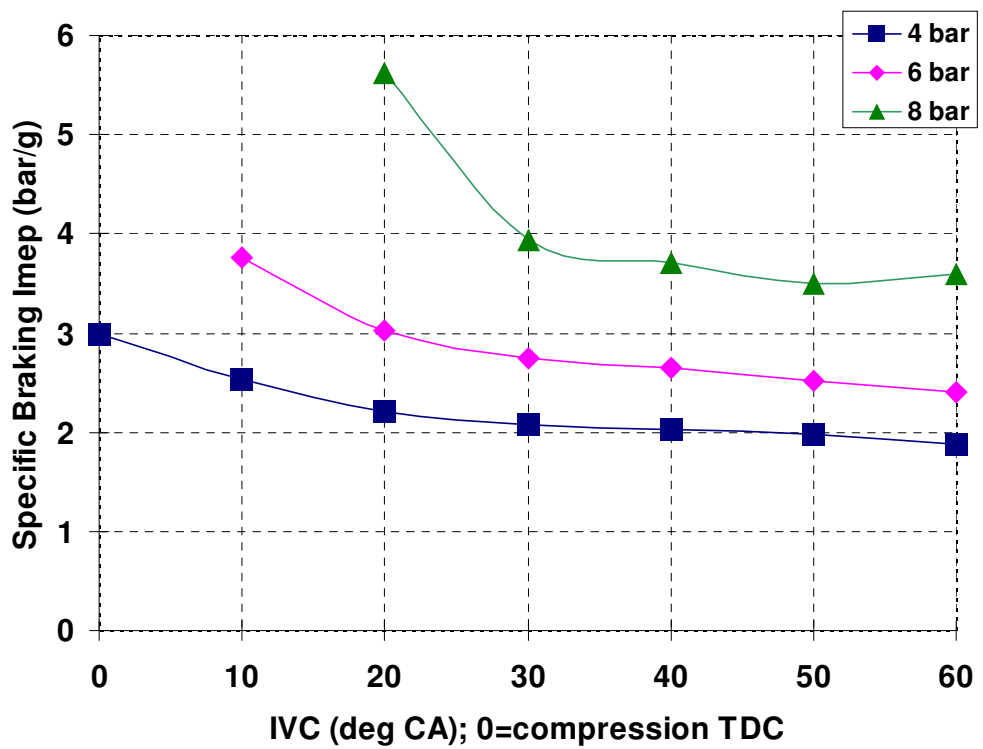


Figure 3.28: Braking specific imep for 1500 rpm engine speed

As a result, its energy capture and storage ability, as measured by the specific braking imep, is optimised when IV5 and IV6 closing time is set at after 40° CA ATDC, as shown in Figure 3.28.

Figure 3.29 shows air tank pressure for various IVC timings after running 60 revolutions at 1500 rpm with an initial air tank pressures of 4 bar, 6 bar and 8 bar respectively. It is noted that the largest rise in the tank pressure is achieved at IVC timing 40° ATDC, independent of the initial tank pressure. As discussed in previous concepts, too advanced IVC timing results in less air being compressed into the air tank due to insufficient valve opening duration whilst the retarded IVC timings beyond 40° ATDC causes some of the compressed air to flow back into the cylinder as the air expands in the cylinder.

In addition, it is found that some of the compressed air is left in the auxiliary chamber after the IVC and will flow back into the cylinder during the initial period of the intake stroke, as shown in Figure 3.30. As a result, lesser amount of induced air in every normal intake stroke is the reason that the air hybrid system has a limitation for maximum air tank pressure.

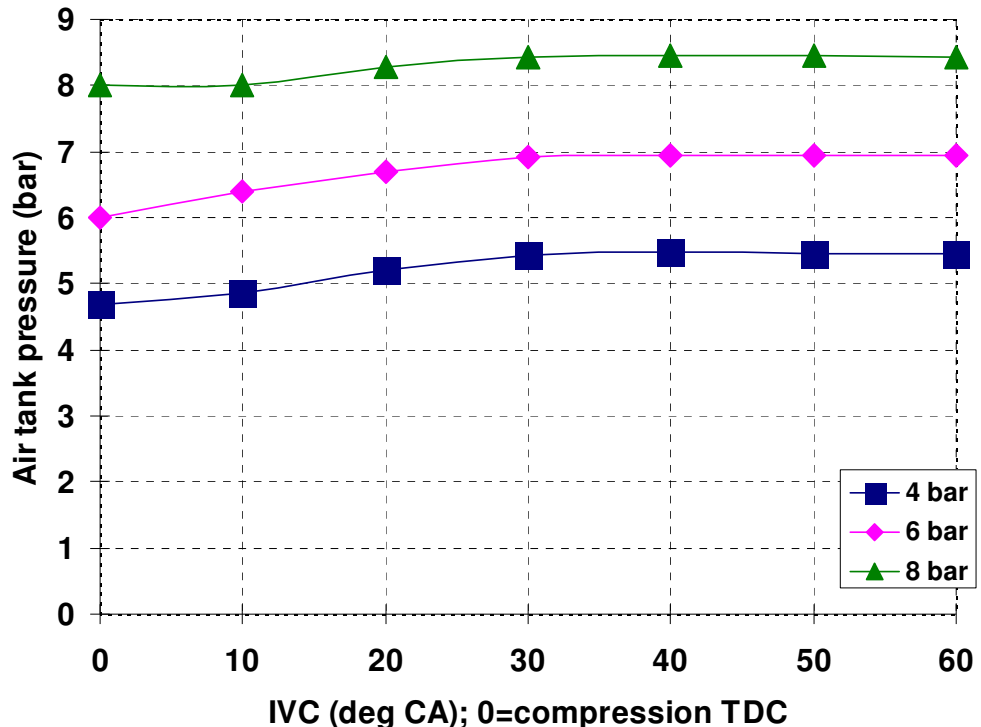


Figure 3.29: Air tank pressure for various IVC timings

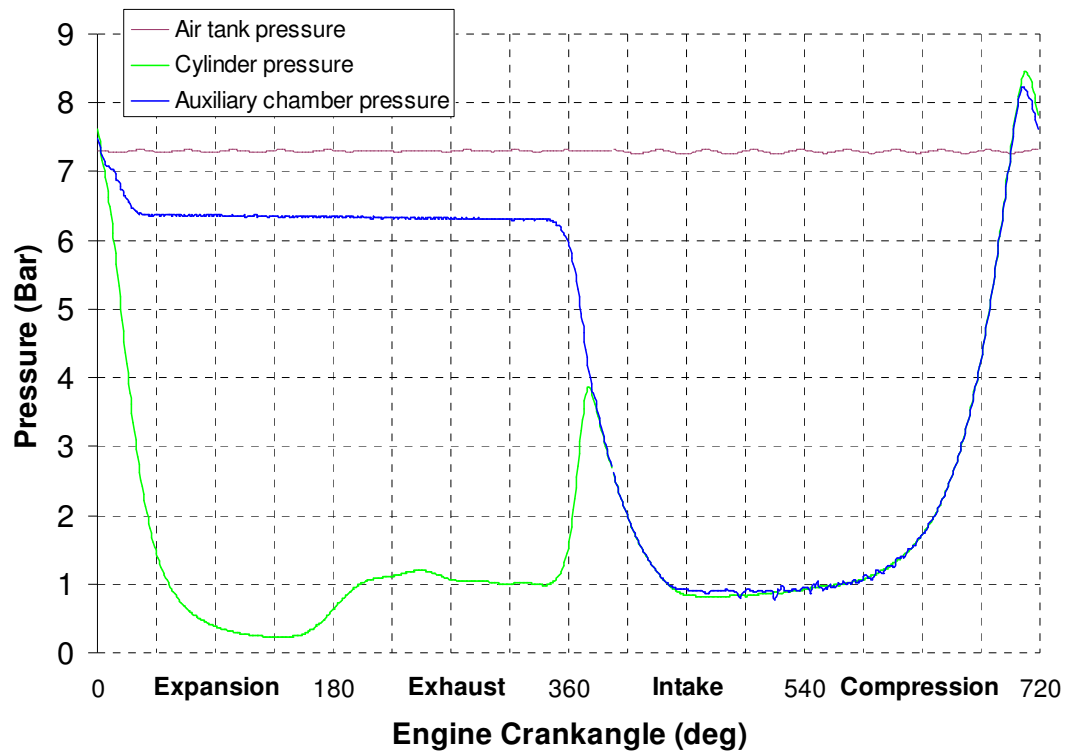


Figure 3.30: Pressure diagrams of air tank, cylinder and auxiliary chamber

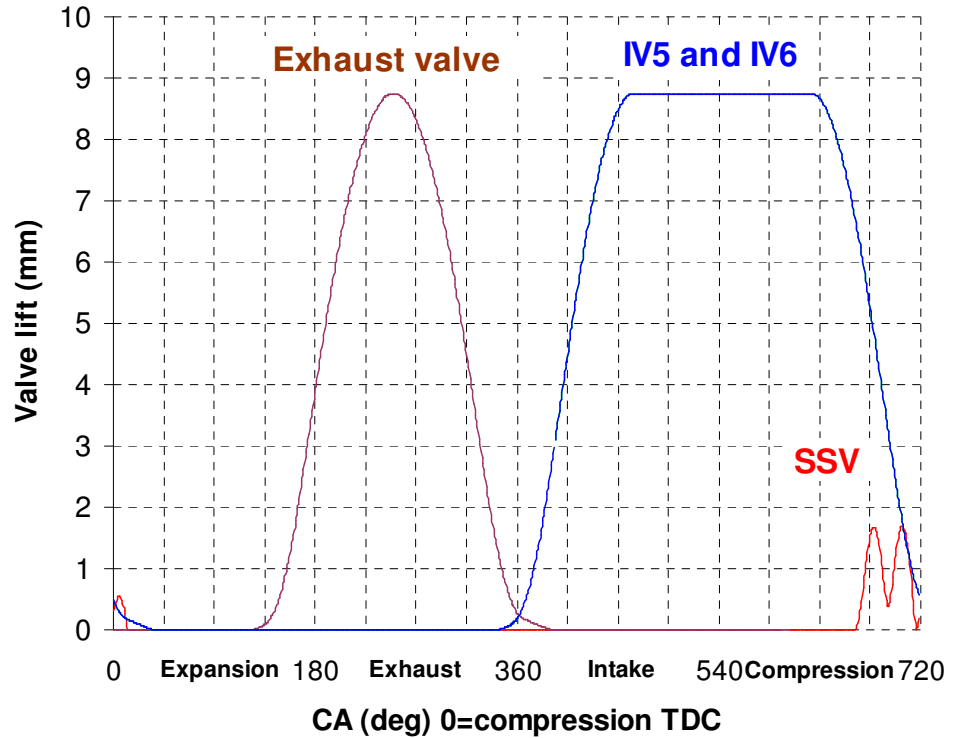


Figure 3.31: Optimal both intake valves timing for air compressor mode

Based on the above investigation, the optimal intake valves lift profile is plotted in Figure 3.31 together with other valve timing diagrams. For a simple CPS device of a fixed switching profile, the optimal intake valves closing timing can be set at 60° ATDC at any tank pressure and engine speed.

3.3.4.2 Valves timing optimization for the cranking mode

For the purpose of simplified hardware and control, the intake valves operate with default valve timings and the ECV is assumed to open during the EM operation. Exhaust valves start to open during the normal compression stroke in order to minimise the compression work. Therefore, the only variable is the opening time of the switched exhaust cams.

The sensitivity of predicted mass of air transferred during one engine cycle to EV closing points for various air tank pressures is shown in Figure 3.32. It can be seen that compressed air expenditure decreases for the late EV closing point because of smaller overlap between both Intake valves and EV for the cranking mode. The latest EV closing point is at 70° CA to avoid collision between the EV and the piston.

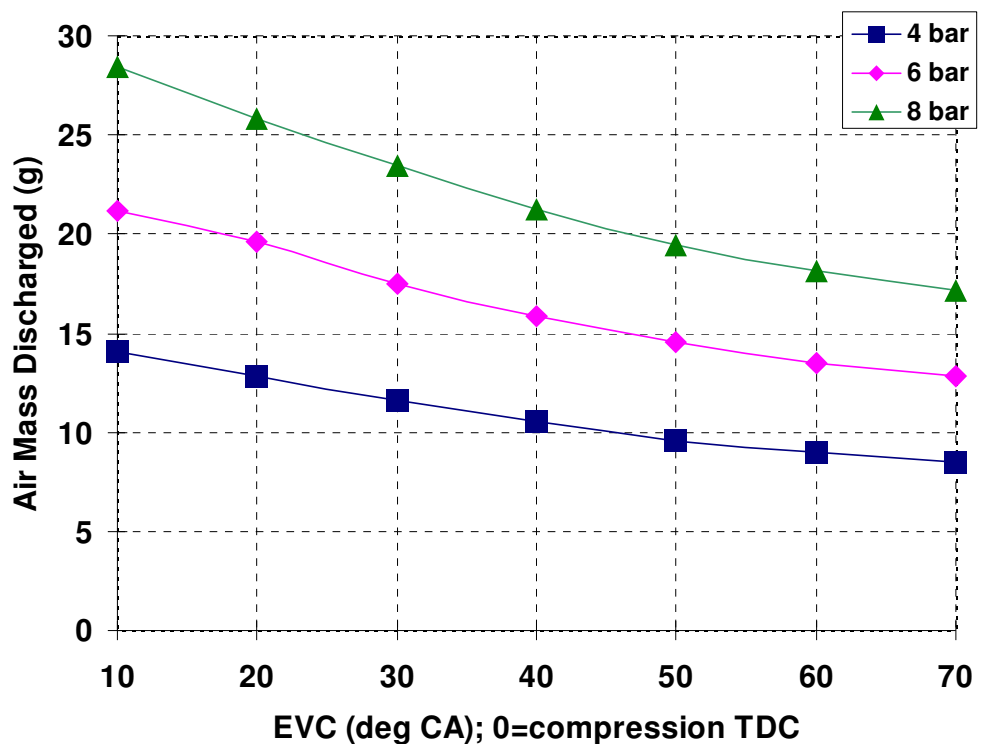


Figure 3.32: Compressed air expenditure for 375 rpm engine speed

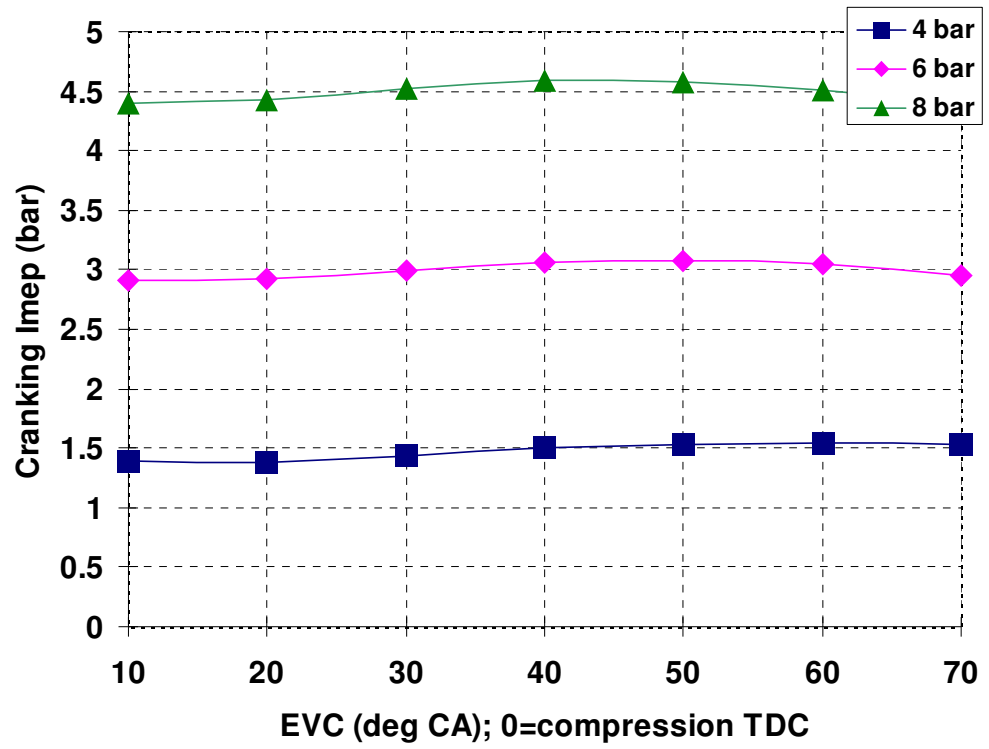


Figure 3.33: Predicted imep_m for 375 rpm engine speed

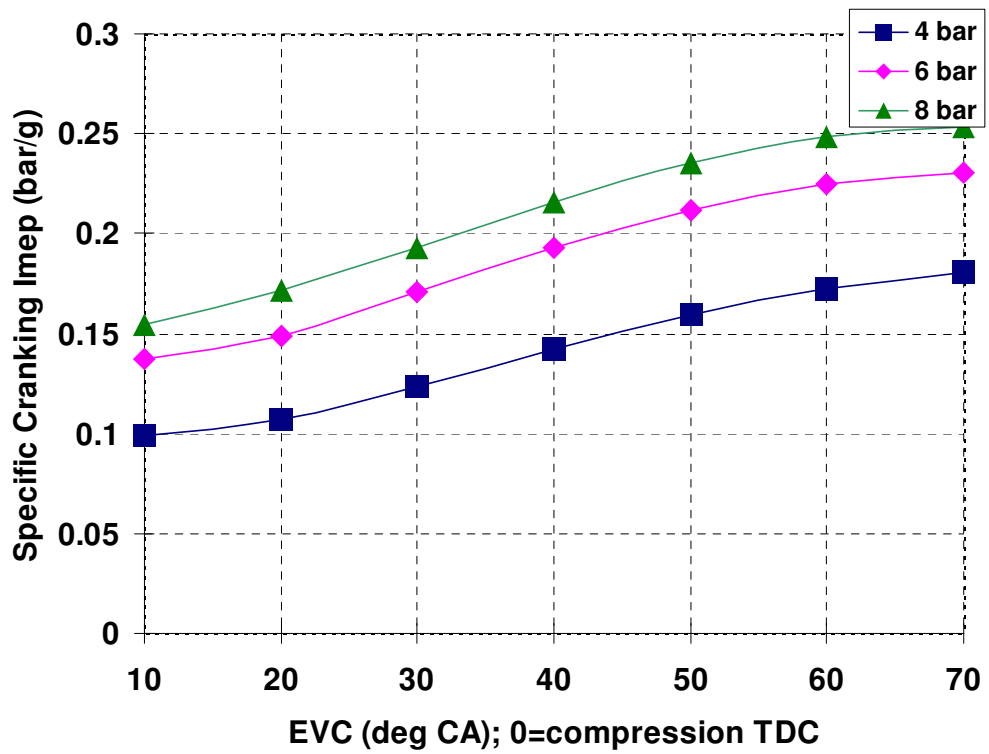


Figure 3.34: motoring specific imep for 375 rpm engine speed

Figure 3.33 shows the sensitivity of the predicted $imep_m$ to EV closing points for various air tank pressures. It can be seen that $imep_m$ depends strongly on the air tank pressure and but varies little with IV5 closing points. Therefore the efficiency for the cranking mode will mainly rely on the values of compressed air expenditure, which can be measured by the ratio of the compressed air expenditure to $imep_m$ practically represents the ability of the air expander. As shown in Figure 3.34, for various air tank pressures and EV closing points, higher motoring specific $imep$ and hence high efficiency is achieved when EV closes at 70° , regardless of tank pressures.

Figure 3.35 shows the corresponding P-V diagram of cylinder 1 at 375 rpm engine speed. It can be seen that cylinder pressure is equal to the air tank pressure throughout the intake stroke and then the cylinder pressure drops to ambient pressure when intake valve 5 is opened. The cylinder pressure remains at about 1 bar throughout the normal compression stroke and therefore the parasitic lose is eliminated.

Based on the above analysis, the optimal EV shifting timing is plotted in Figure 3.36 together with other valve lift curves.

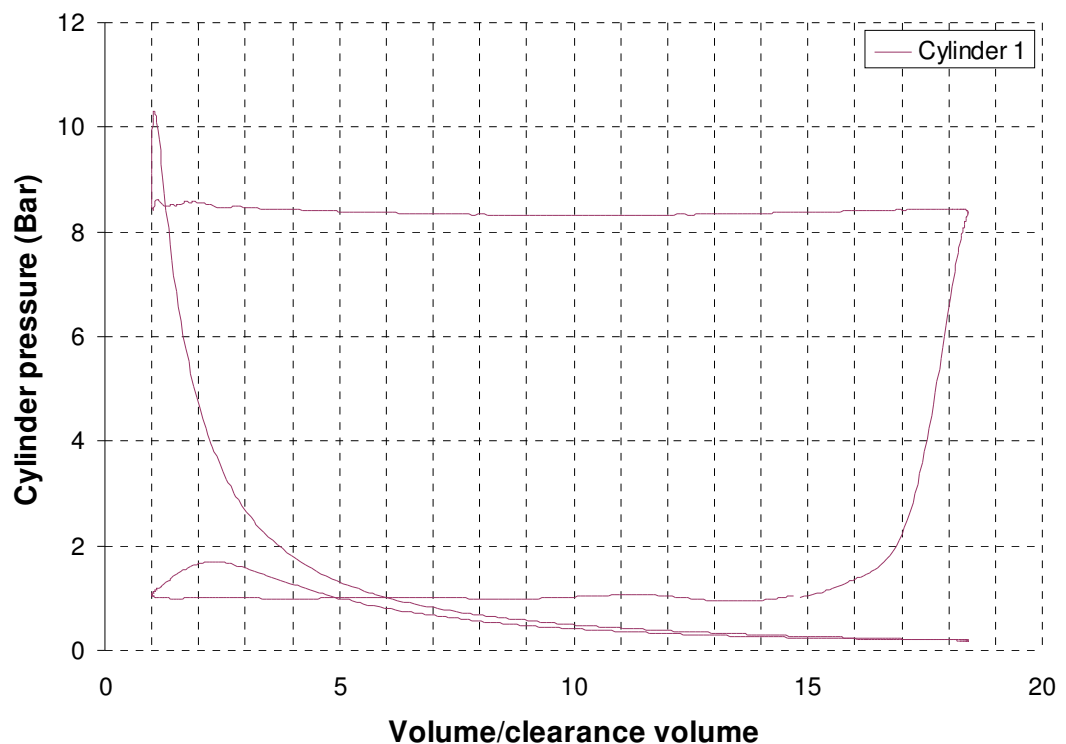


Figure 3.35 P-V diagram of Cylinder 1

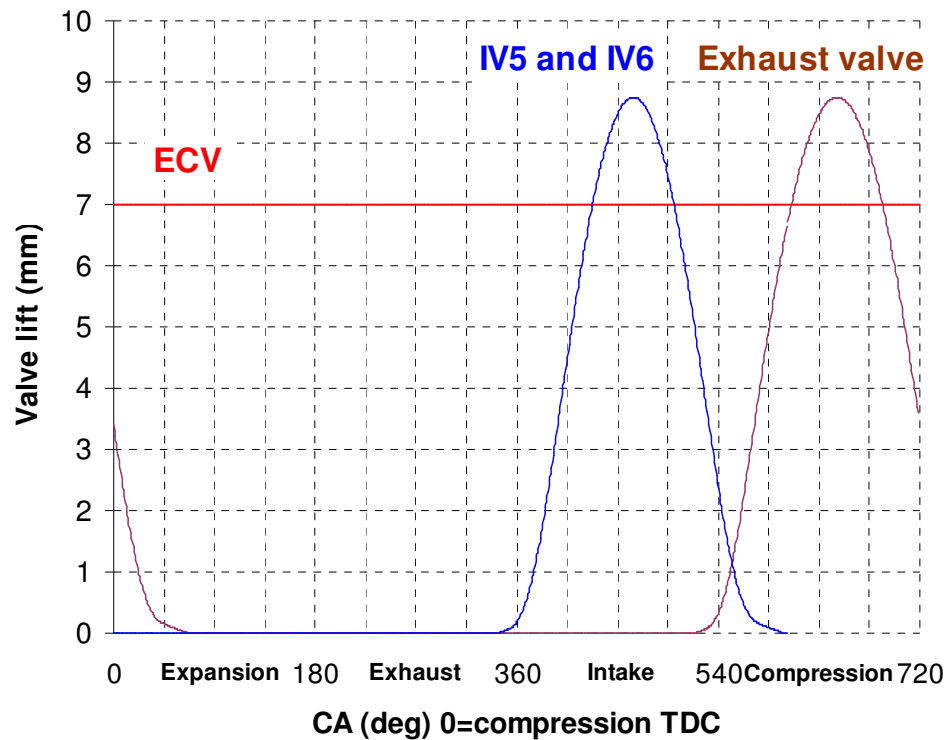


Figure 3.36 Optimal IV5 opening timing for cranking mode

3.3.5 Conclusions

The air hybrid engine concept with joint intake port has been proposed and analysed. It can be realised with current production technologies. Both compression mode and cranking mode operations can be effectively operated with the use of a CPS system on intake valves and exhaust valves for transferring the compression air between the cylinders and the air tank.

The air hybrid system is able to charge its 40 litre air tank from 6.8 bar tank pressure to 8 bar tank pressure in 4.8 seconds in CM. However, it suffers from much reduced maximum air tank pressure due to the larger auxiliary chamber volume of the joint intake port.

3.4 Summary

Performance of four air hybrid engine concepts is summarised in Table 3.3. For the air hybrid engine with split intake ports, their maximum tank pressures are all above 15 bar. During the CM operation, induced air is compressed into the airtank via the auxiliary chamber where some compressed air resides after both the active intake valve and one-way valve are shut. In the next engine cycle, the fresh air is induced into the cylinder and compressed together with the residual compressed air in the auxiliary chamber into the air tank. As a result more compressed air and higher braking engine torque is produced by the engine with split intake ports. The maximum air tank pressure is higher than the peak pressure calculated from the polytropic compression based on the effective compression ratio determined by the auxiliary chamber volume.

Air hybrid engine concept 1 with a Reed valve is the only air hybrid engine concept which is able to motor the engine during cruised vehicle operation by controlling the ECV opening duration. Its regenerative efficiency achieves 19-25% while tank pressure works between 5-15 bar. Compared to other air hybrid engines [38, 42], 1st air hybrid engine concept has lower regenerative efficiency. However, its simple modification makes the production achievable. Because of the presence of a Reed valve in one of split intake ports, air flow rate can be affected during the normal firing mode. In addition, the calculated CATC values demonstrate that lesser air induced will be compressed into the airtank while the tank pressure increases.

The air hybrid engine concept 2 with a port throttle has the same effective compression ratio as the air hybrid engine concept 1 and therefore they have the same optimized valve timing for CM. Compare to the air hybrid concept 1, it is capable of generating higher cranking torque, because its expanding duration is controlled by the opening of intake valve which is longer than the expanding duration of the air hybrid engine concept 1. 1st air hybrid engine has shorter expanding duration in order to minimise the overlap between the opening of ECV and the intake valve. However, default intake valve closing point of 2nd air hybrid concept is at 60° after TDC which results in negative work in the beginning of the compression stroke during the cranking mode operation. This is reflected by Table 3.3 the lower specific cranking imep in Table 3.3, which indicates lower efficiency.

Compared to 1st and 2nd air hybrid concept, the air hybrid engine concept 3 adopts a CPS devise for only one intake valve which makes its system simpler. The compressed air

supply is supplied to the other intake port by eliminating the volume upstream of the ECV and therefore its real compression ratio is increased from 6.2 to 6.8. With higher real compression ratio, it is characterised with better energy capture efficiency as represented by the values of specific braking imep in Table 3.3. It has similar cranking engine torque and cranking specific imep to 2nd air hybrid concept. Since the same valve settings will be used for both the regenerative braking operation and the subsequent cranking operation, it requires much simpler valve train and control optimisation. In addition, with the same valve setting, it enables the instant supply of the compressed air to the cylinder during a brief period of the transient operation when turbo lag is present in the highly downsized engines.

Compared to the air hybrid engine with split intake ports, the air hybrid engine with joint intake ports has a lower real compression ratio of 5.6 which results in lower maximum tank pressure at 9.3 bar. Its braking engine torque reduces while the tank pressure increases due to lesser amount of compressed air charged as shown by its CATC values.

Cranking tests done on a 3-cylinder engine at room temperature showed that 42 Nm engine torque was able to crank the engine from zero speed to 950 rpm engine speed [58]. Static maximum engine cranking torque requirement at 24° C is 20.3 Nm which is 83% of static maximum engine cranking torque requirement at -25° C [58]. In their analysis [59], Zhou and Houldcroft showed that the minimum required turning torque was strongly related to the gas resistance torque due to the presence of trapped air in the cylinders. Some of the cylinders could retain gas pressure well above the ambient, resulting in significant gas resistance torque. All of the air hybrid engine concepts, discussed in this chapter, would have much lower torque demand for the subsequent stop-start operation due to the absence of trapped air at high pressure following the regenerative braking operation, when any remaining compressed air would have exhausted either from one intake port for the air hybrid engine with split intake port or from exhaust ports for the air hybrid engine with joint intake ports. Therefore, the regenerative air hybrid engine stop-start operation requires less cranking power than the other forms of stop-start systems.

Since engine speed is a necessary input, not an output, in WAVE model, the cranking simulation done in this chapter is using half cranking speed as engine speed input during the cranking mode operation to optimize engine valve timing. Engine cranking speed and acceleration are functions of gas torque during the cranking mode operation, which will be

discussed in Chapter 6, where the air hybrid engine concept 3 is utilized in the vehicle driving simulation modelling studies.

Table 3.3: Summary table

Classification	Concept of engine with split intake ports			Concept of engine with joint intake ports
	Concept 1	Concept 2	Concept 3	
maximum tank pressure	Over 15 bar	Over 15 bar	Over 15 bar	9.3 bar
real compression ratio	6.2	6.2	6.8	5.6
braking engine torque (6 bar)	-56 Nm	-56 Nm	-43 Nm	-27 Nm
braking engine torque (8 bar)	-63 Nm	-63 Nm	-44 Nm	-20 Nm
braking engine torque (10 bar)	-63 Nm	-63 Nm	-46 Nm	X
specific braking imep (6 bar)	2.8 bar/g	2.8 bar/g	2.2 bar/g	2.4 bar/g
specific braking imep (8 bar)	3.4 bar/g	3.4 bar/g	2.5 bar/g	3.6 bar/g
specific braking imep (10 bar)	3.4 bar/g	3.4 bar/g	2.7 bar/g	X
cranking engine torque (6 bar)	35 Nm	48 Nm	47 Nm	56 Nm
cranking engine torque (8 bar)	53 Nm	70 Nm	69 Nm	81 Nm
cranking engine torque (10 bar)	72 Nm	92 Nm	91 Nm	X
specific cranking imep (6 bar)	0.34 bar/g	0.24 bar/g	0.23 bar/g	0.23 bar/g
specific cranking imep (8 bar)	0.38 bar/g	0.26 bar/g	0.25 bar/g	0.25 bar/g
specific cranking imep (10 bar)	0.41 bar/g	0.27 bar/g	0.27 bar/g	X
CATC values (6 bar)	71%	71%	64%	59%
CATC values (8 bar)	66%	66%	58%	34%
CATC values (10 bar)	64%	64%	56%	X
regenerative efficiencies	19-25%	X	X	X
Motoring mode available	Yes	No	No	No
Restricted air flow rate	Yes	No	No	Yes

Chapter 4: Analytical Studies of Air Hybrid Concepts for a Medium Duty Diesel Engine

4.1 Introduction

As discussed in Chapter 2, the hybrid powertrain technology reduces a vehicle's fuel consumption principally by means of regenerative stop-start operations. Buses and delivery vehicles are characterised with frequent stop and start operations and hence they will benefit the most from the air hybrid engine technology. In this chapter, a YUCHAI YC6A 7.25 litre diesel engine widely used in the city buses in China has been modelled as an air hybrid engine. The principle of operation of two air hybrid engine setups will be presented and their performance will be analysed and compared.

4.2 YUCHAI air hybrid engine with a Variable Valve Exhaust Braking device

4.2.1 Description of the Air Hybrid Engine Setup

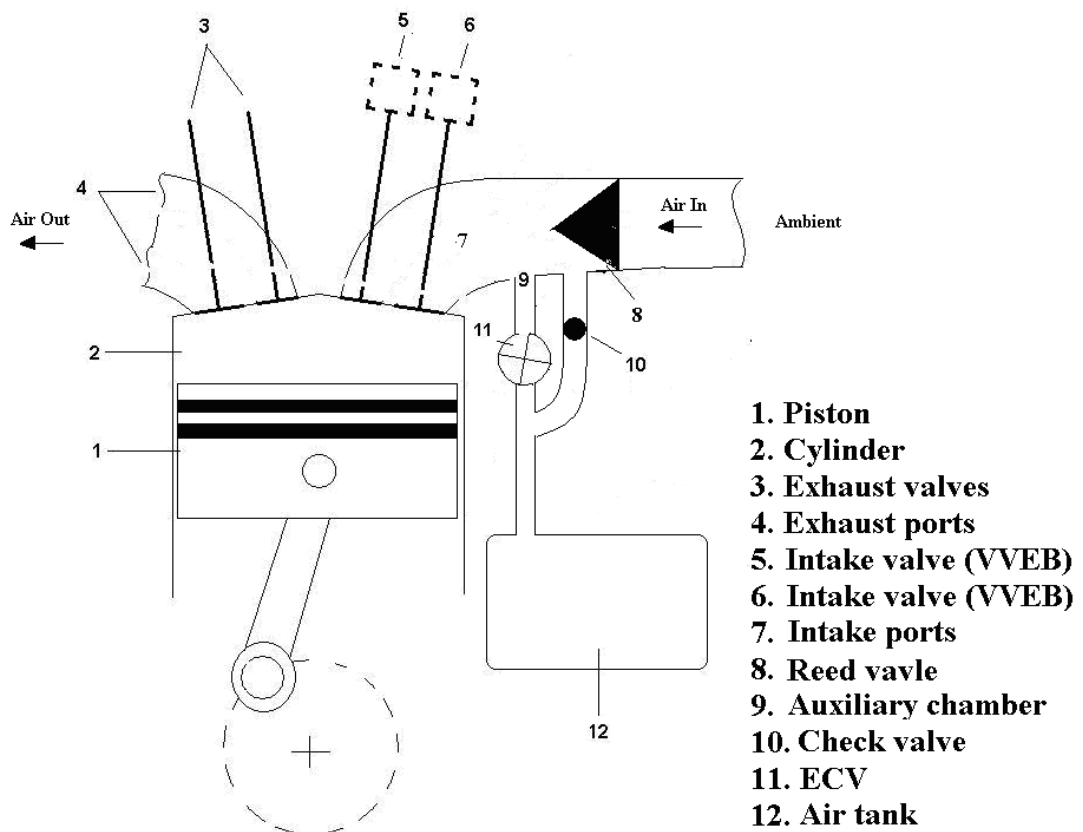


Figure 4.1: YUCHAI Air Hybrid Engine with the intake VVEB device

Figure 4.1 shows one of the 6-cylinders of a YUCHAI diesel engine in production modified for the air hybrid engine operation. Air flows through the intake valves (5 and 6) via a siamesed intake port (7) and leaves exhaust valves (3) via exhaust port (4). Intake valve 5 and Intake valve 6 can be actuated jointly by a variable valve exhaust braking (VVEB) device. The VVEB device is designed for engine braking applications and is normally installed on the exhaust valves as shown in Figure 4.2. When it is actuated, the small piston is forced down by the hydraulic pressure and the valve will be stopped with a 1-2mm adjustable lift. A non-return Reed valve (8) is additionally provided in the intake port (7). While air pressure downstream of the Reed valve is lower than the pressure in the intake manifold, the reed valve petals open and air is induced into Intake port 7. On the other hand, if air pressure inside the auxiliary chamber formed between the intake valves and the Reed valve is higher than the pressure in the intake manifold, the Reed valve petals close and air will be kept within the intake port.

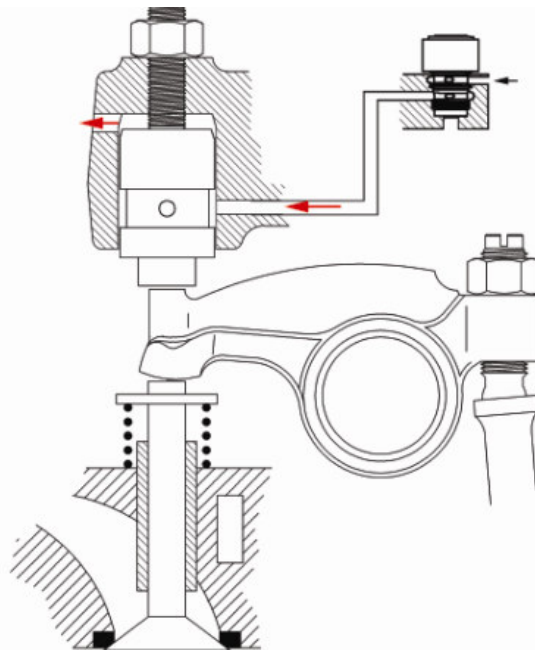


Figure 4.2: Schematic of the VVEB device [60]

The energy control valve ECV (11) is a solenoid valve that controls air flow out of the air tank (12) for the cranking mode operation. In addition, a check valve (10) has been adopted to be a one way valve that controls air flow into the air tank (12) for CM. The air tank 12 is insulated and therefore the heat of the compressed air can be stored in it.

The engine also includes five more cylinders, a fuel system and an ignition system which are not shown in Figure 4.1 for highlighting the main subject of the present study.

4.2.2 The Principle of operation

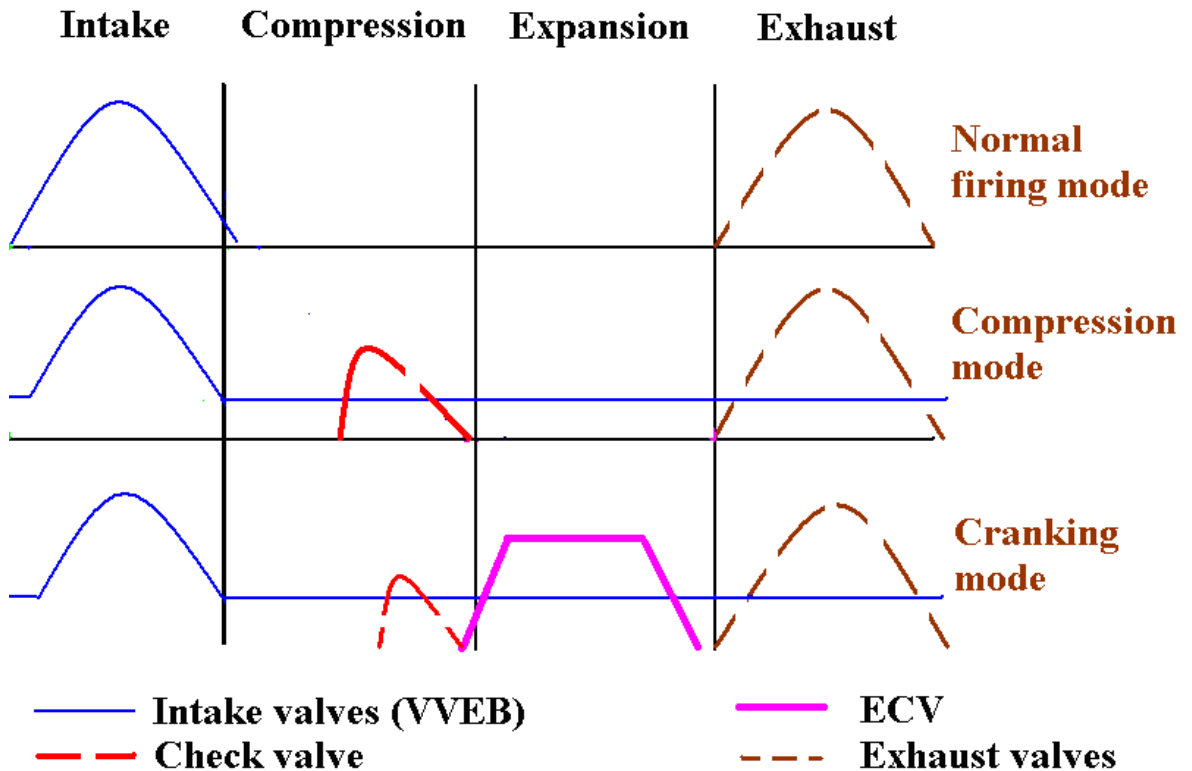


Figure 4.3: Engine valves, SSV and ECV timing for the normal firing mode, CM and the cranking mode

Figure 4.3 and 4.4 show the valve timing diagrams and flow direction respectively for the normal firing mode, CM and the cranking mode. During the normal firing mode, both intake and exhaust valves operate with their default lift profiles. During deceleration and braking, both intake valves are opened by the stock cam through the pushrod and rock arm during the intake stroke and then remain slightly open (1.25 mm lift) by the action of the VVEB device throughout the rest of the four-stroke cycle so that the air is compressed and stored in the auxiliary chamber formed by the one-way Reed Valve, the Check Valve and the ECV. As a result, the engine will be operated as a compressor driven by the kinetic energy of the moving vehicle. When the cranking operation is desired, the ECV opens during the normal expansion stroke so that the compressed air can flow through the opening intake valves due to the action of the VVEB system and forces the piston down

and generate the motoring work. However, as it will be shown later that the net cranking torque is reduced by the compression work done on the air inducted during the intake stroke.

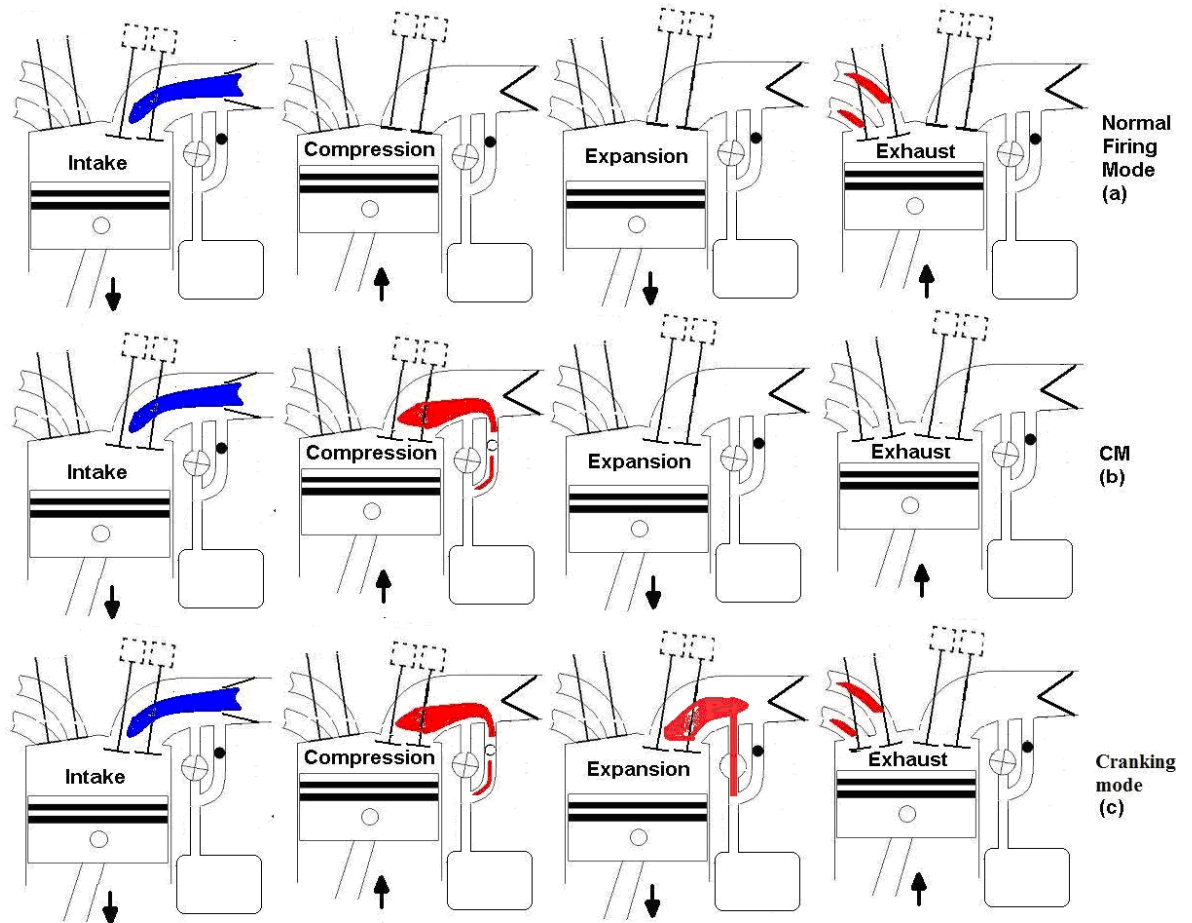


Figure 4.4: Four-stroke engine cycle for the normal firing mode (a), CM (b) and the cranking mode (c).

4.2.3 Engine simulation setup

A YUCHAI YC6A 7.25 litre diesel engine widely used in the inner city buses in China has been chosen for the modelling studies. Details of the engine and characteristics of various valves are given in Table 4.1 and Table 4.2 respectively. A standard 151 Litre air tank as used on a bus has been used in the model. The air tank is designed to have an operation pressure of 10 bar. The engine simulation programme, WAVE, is used to study the gas dynamics of the 6-cylinder engine and its air hybrid operations. The initial implementation of the proposed intake system is realised by adding a sandwich block, which

accommodates Reed valves and check valves, between the cylinder head and intake manifold, without altering the engine block or the existing intake system.

Table 4.1: Engine dimensions and characteristics

Number of cylinders	6
Cylinder bore	105mm
Piston stroke	132mm
Connecting rod length	210mm
Displacement volume	1143cm ³
Clearance volume	69cm ³
Total volume of one cylinder	1212cm ³
Compression ratio	17.5:1
R _c for air hybrid mode	4.5:1

Table 4.2: Valves dimensions and characteristics for each cylinder

Intake valve	2
Diameter	32.5 mm
Opening point (normal)	61° BTDC
Closing point (normal)	91° ABDC
Maximum lift	9.6 mm
Exhaust valve	2
Diameter	29.5 mm
Opening point	105° BBDC
Closing point	67° ATDC
Maximum lift	9.7 mm
Reed valve	1
Petal stiffness	1900 N/m
Maximum lift	9 mm
ECV count	1
Diameter	25.4 mm

The size of the auxiliary chamber volume is determined by the position of the non-return Reed valve, the position of the check valve and the position of the ECV. The geometric compression ratio of the engine is 17.5:1 for the normal firing mode. However, when the engine is switched to the compression mode, the actual compression ratio (R_c) decreases as the volume of the auxiliary chamber is included in the cylinders' total clearance volume. The size of the auxiliary chamber volume is determined by the position of the check valve, the position of the ECV and the position of the throttle valve. For the engine to be examined, the minimum auxiliary chamber volume is 260cm³, the actual compression ratio of CM is calculated as:

$$R_c = \frac{1143 + 69 + 260}{69 + 260} = 4.5 : 1$$

During CM, air is compressed into the auxiliary chamber isolated by the ECV and the check valve from the air storage tank, and then released by the check valve into the air storage tank due to the pressure difference between the auxiliary chamber and the air storage tank. During the cranking mode, the ECV controls the amount of compressed air released from the air storage tank to the auxiliary chamber and then flows into the cylinder after the intake valve is opened.

The simulation canvas of this design is shown in Figure 4.5. The modelled air hybrid engine was modified from a YUCHAI YC6A 7.25 litre diesel engine with six cylinders. Each cylinder has a stroke of 132 mm, a bore of 105 mm and a displacement volume of 1143 cm³. Its connecting rod length is 210 mm and its intake and exhaust valve diameters are 32.5 mm and 29.5 mm respectively. The engine speed range is between 1000 and 2000 rpm. The cylinders, labelled “cylinder1, cylinder 2, cylinder 3, cylinder 4, cylinder 5 and cylinder 6” are connected to the intake network through “reedvalve1”, “reedvalve2”, “reedvalve3”, “reedvalve4”, “reedvalve5” and “reedvalve6” (non-return valves) respectively for inducing air from atmosphere (“amb1”). The cylinder are connected to the air tank (“Airtank”) through Energy Control Valves (“ECV1”, “ECV2”, “ECV3”, “ECV4”, “ECV5”, and “ECV6”) and check valves (“SSV1”, “SSV2”, “SSV3”, “SSV4”, “SSV5” and “SSV6”) for releasing compressed air from the air tank and compressing air into the air tank respectively. All exhaust ports are connected to a single exhaust pipe to the atmosphere (“amb2”).

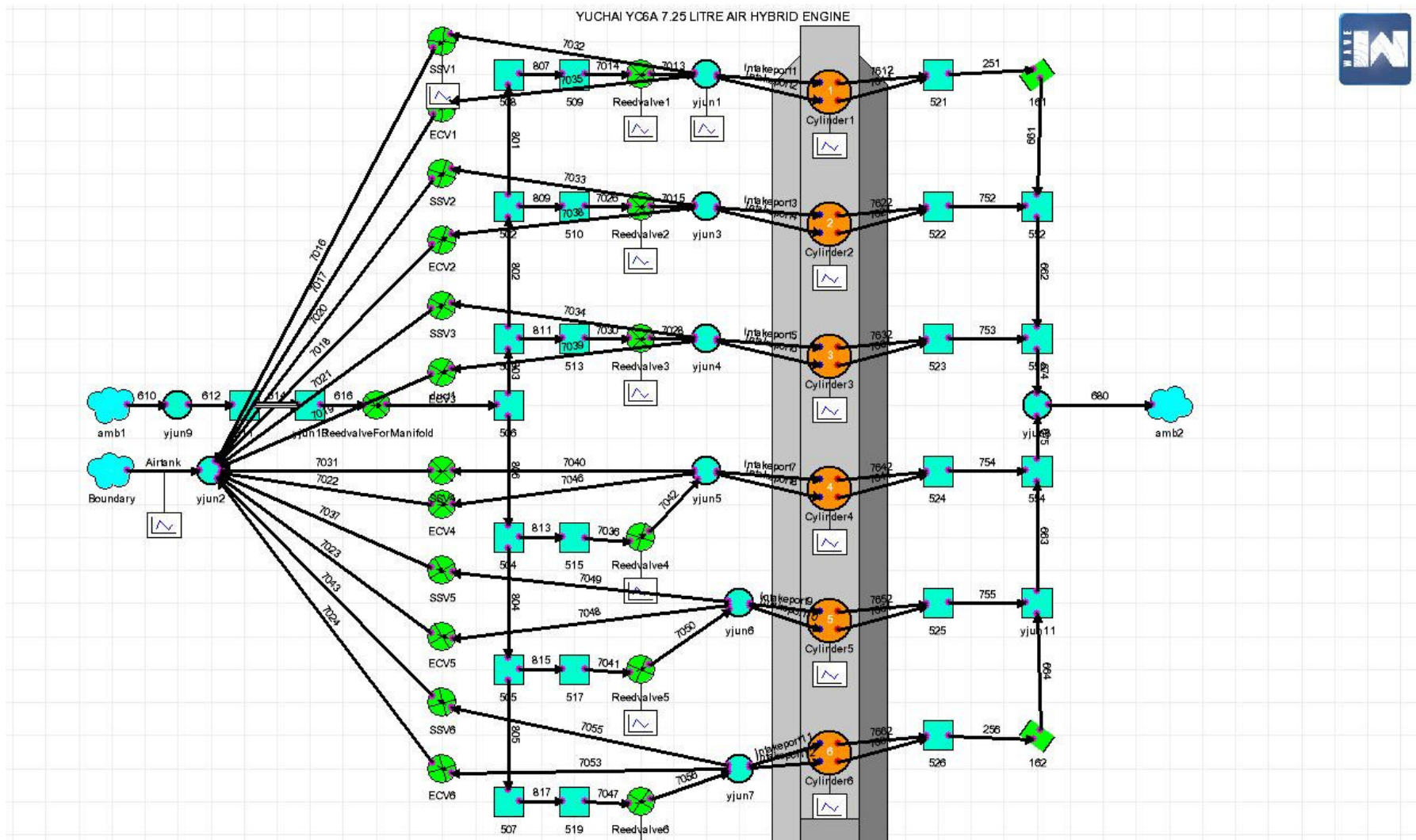


Figure 4.5: WAVE model of the YUCHAI air hybrid engine with VVEB

4.2.4 Simulation Results

4.2.4.1 Compression mode operation

Figure 4.6 shows the intake valve lift diagram, check valve opening period, and the standard exhaust valve lift diagram. During the CM operation, the VVEB device is actuated on both intake valves so that they will remain open at 1.25mm above the valve seats after the intake process.

Figure 4.7 shows that the auxiliary chamber pressure trace overlaps with the in-cylinder pressure profile because of the opening intake valves by the action of VVEB. Comparing Figure 4.6 and Figure 4.7, it can be seen that the check valve opens close to TDC in the compression stroke when the auxiliary chamber pressure becomes higher than the tank pressure.

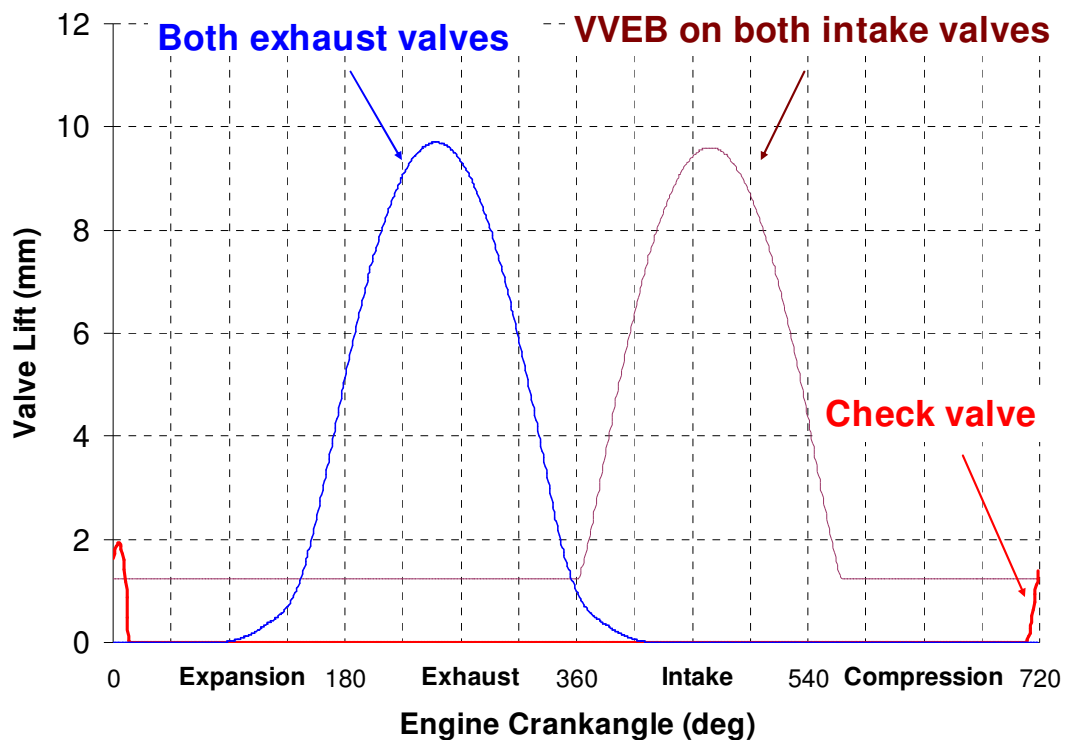


Figure 4.6: Valve timing diagram for compression mode

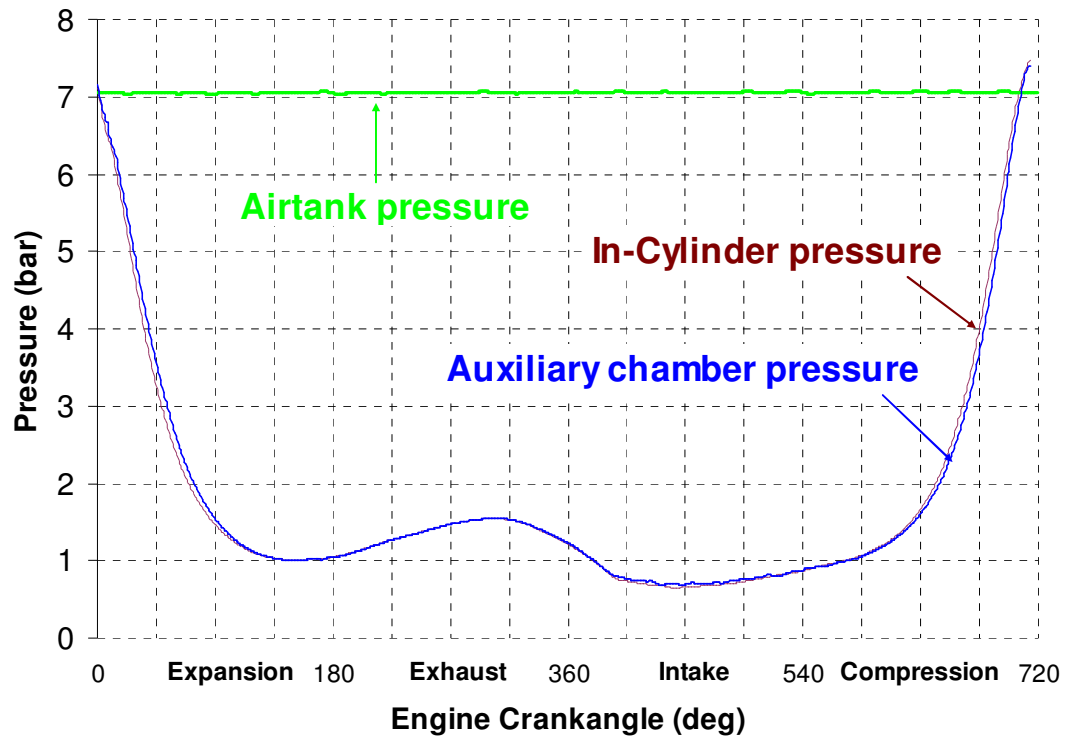


Figure 4.7: Pressure diagram for compression mode

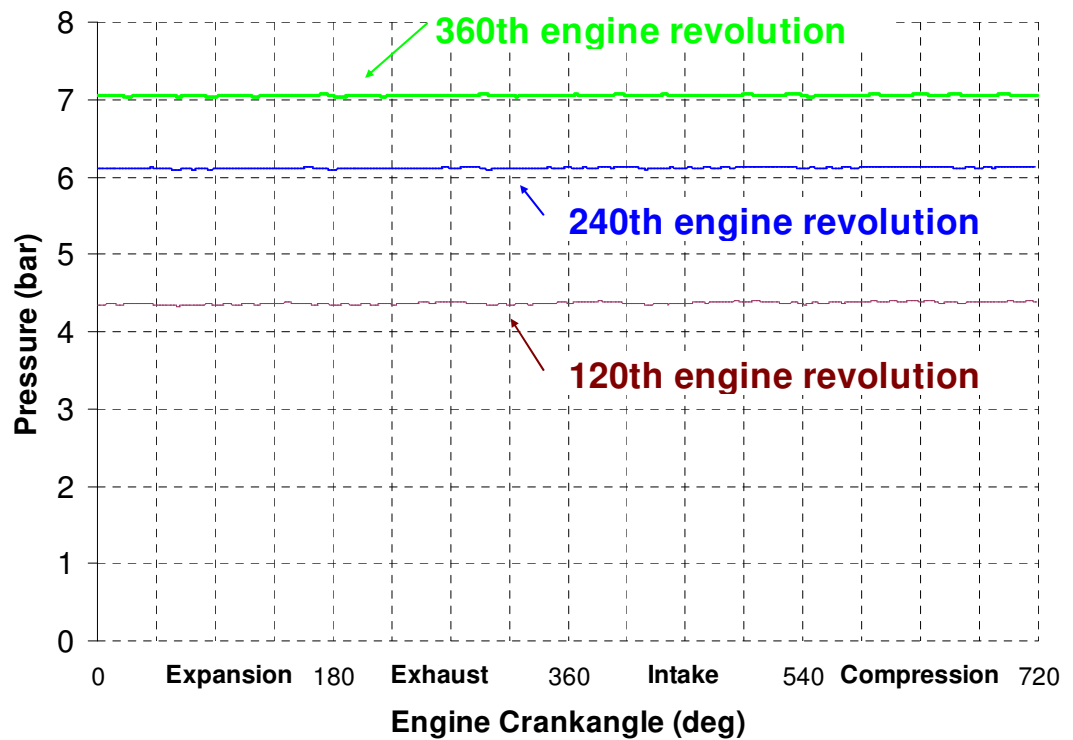


Figure 4.8: Air tank pressure during the CM operation at 1500 rpm

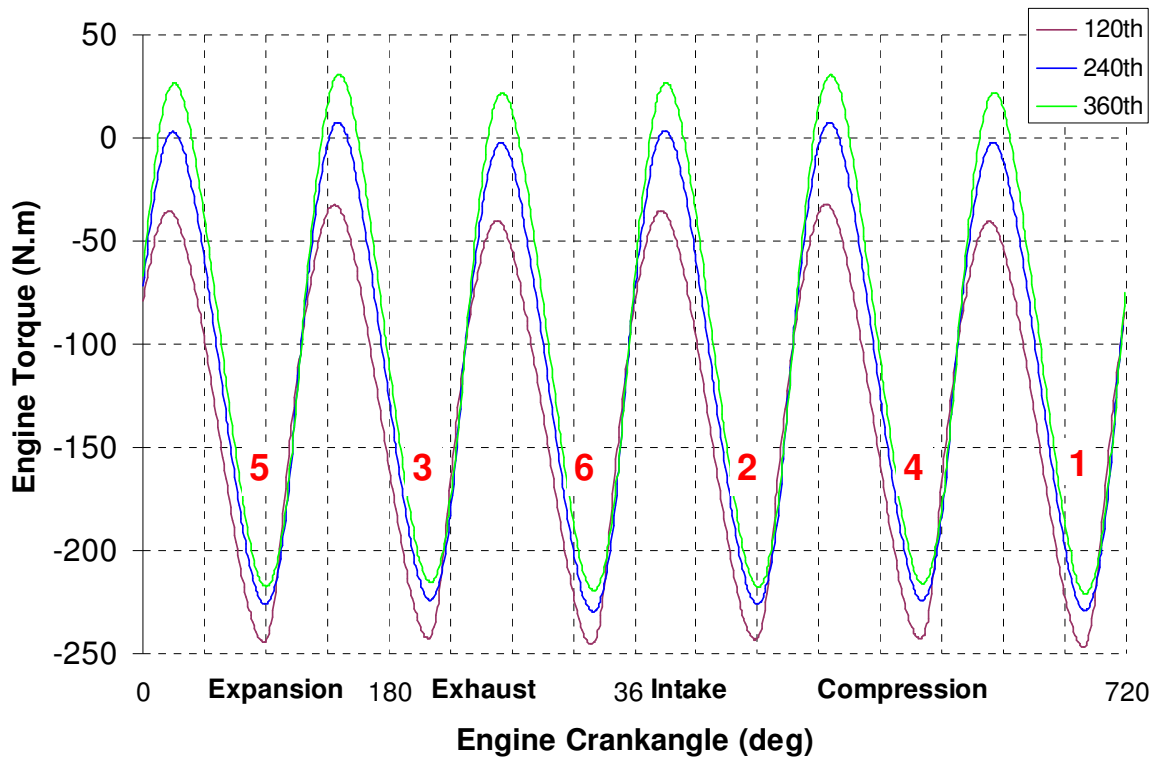


Figure 4.9: Engine braking torque at 1500 rpm during CM operation

Figure 4.8 shows air tank pressure at 120th, 240th and 360th engine revolutions at 1500rpm engine speed during the CM operation. The results show that the air tank can be charged from 1bar to 6.1bar within 9.6 seconds at 1500rpm engine speed. However, it is more important to note that it takes 4.8 seconds to charge the air tank from 4.3 bar to 6.1 bar. As to be discussed later, when a typical air starter is used for stop-start operations, the supply pressure should be above 4.5 bar and the pressure would drop by roughly 0.5 bar after each start. Thus, after less than 5 seconds braking, the air tank would have been charged sufficiently to start the engine.

Figure 4.9 shows the corresponding engine braking torque values for the 6 individual cylinders at 120th, 240th and 360th engine revolutions at 1500rpm engine speed. The cylinder number is included in the diagram to show the firing order of 6 cylinders. At 120th engine revolution, according to Fig.4.8 and Figure 4.9, the tank pressure has reached to 4.3 bar and the peak engine braking torque reaches 250 Nm. The tank pressure reaches 7.1 bar after 360 engine revolutions, the peak engine braking torque approaches 210 Nm. Before the air tank is fully charged, the compressed air is captured by the check valve when the auxiliary chamber pressure is higher than the air tank pressure. As the air tank pressure increases, the check valve opening period decreases. As a result, greater expansion takes

place after TDC, resulting in lower engine braking torque seen. The maximum air tank pressure is limited to 7.4 bar by the effective compression ratio defined by the auxiliary chamber volume depending on the dimension of the sandwich block and the position of the check valve, Reed valve and ECV if it is include. If a new device can be designed so that the auxiliary volume is only dependent on the existing intake port dimension, the effective compression ratio can be increased to 5.6 and the maximum air tank pressure will be 10.2 bar, resulting in higher pneumatic energy storage.

4.2.4.2 Cranking mode operation

As mentioned in Chapter 3, engine speed is required to model the cranking mode. In this study, half of the engine idling speed, 325 rpm is used during the cranking mode operation. During the cranking mode operation, intake valve lift diagram and exhaust valve lift profile are the same as those for the CM operation as shown in Figure 4.10. However, the ECV is actuated to open at 10° BTDC at the end of the compression stroke to allow it open fully during the expansion stroke. As a result, the compressed air flows through intake ports and expands in the cylinder before it escapes to exhaust ports in the exhaust stroke.

As shown in Figure 4.11, when the ECV opens, both auxiliary chamber pressure and cylinder pressure reaches to the air tank pressure. For the given 1.25mm intake valve lift, these two overlapping pressure traces indicate that there is negligible pressure drop across such a small gap. The high pressure forces the piston down and produces the expansion work. However, as shown in Figure 4.12, the next work output of the engine during the expander mode is reduced by the compression work done on the air inducted during the intake stroke. Because of almost constant high pressure acting throughout the expansion stroke, a positive output is produced.

Figure 4.13 shows that the air tank pressure drops from 7.1 bar to 6.3 bar during the first 6 engine revolutions at 325 rpm engine speed during the crank mode operation. The corresponding cranking torque values for the first 6 engine revolutions are shown in Fig.4.14. The numbers represent the cylinder number and their sequence indicates the firing order of 6 cylinders. It is noted that the first cylinder produces about 230 Nm peak torque at 7.1 bar tank pressure and the number 4 cylinder generates a reduced peak torque of 174 Nm as the tank pressure has dropped to 6.8 bar. At the end of the 6th engine revolution, the peak torque output from cylinder number 4 is about 150 Nm at an air tank pressure of 6.3 bar.

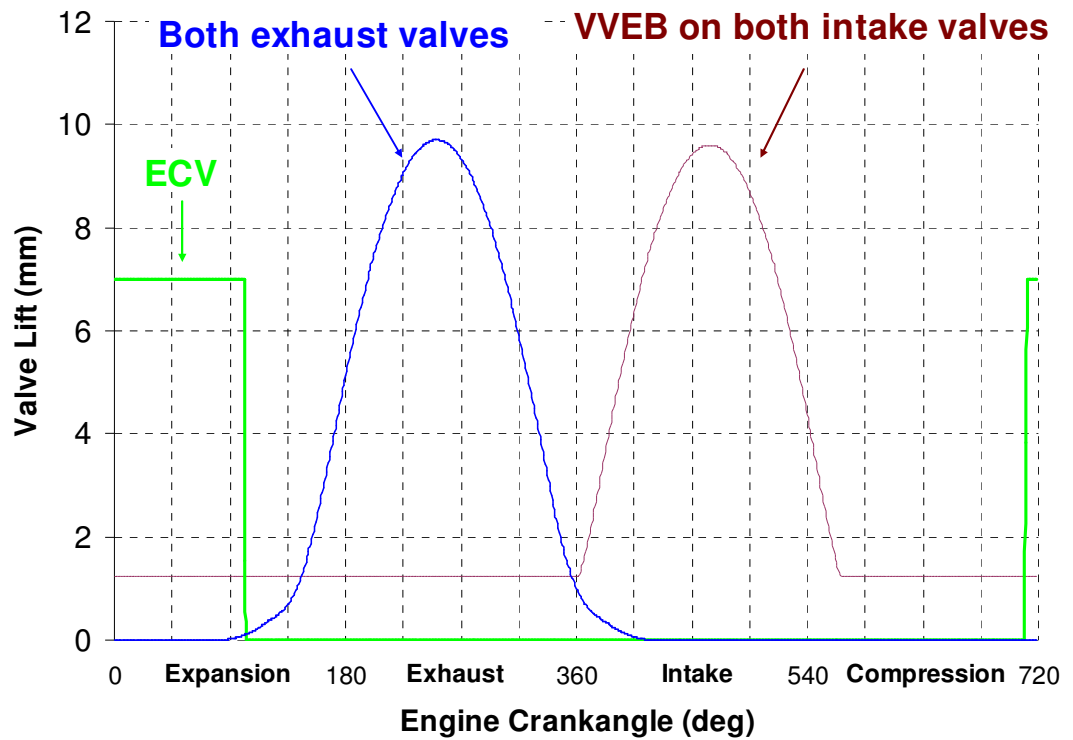


Figure 4.10: Valve timing diagram for expander mode

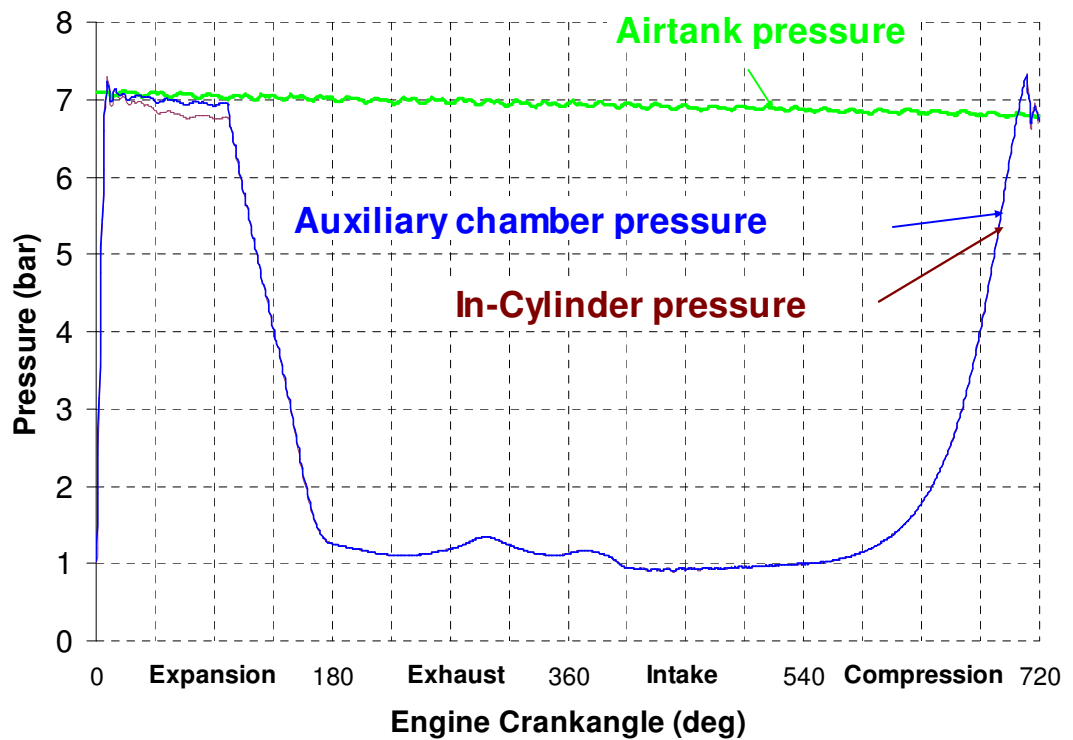


Figure 4.11: Pressure diagram during cranking mode

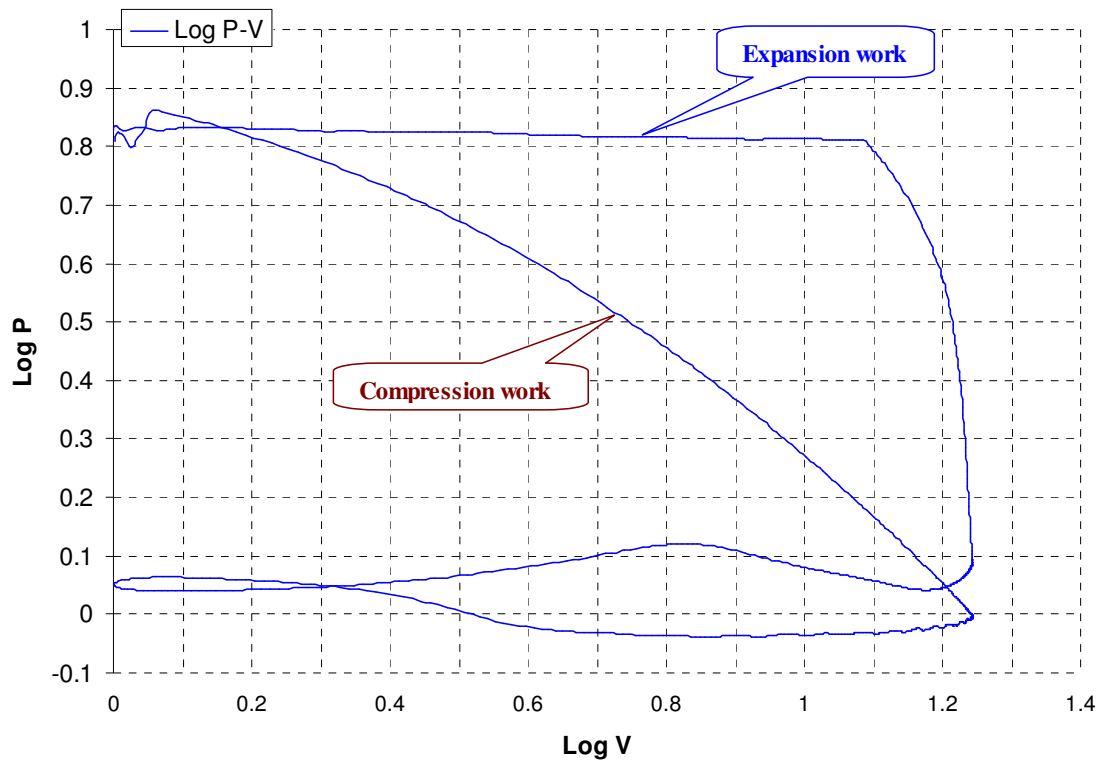


Figure 4.12: Log P-V diagram

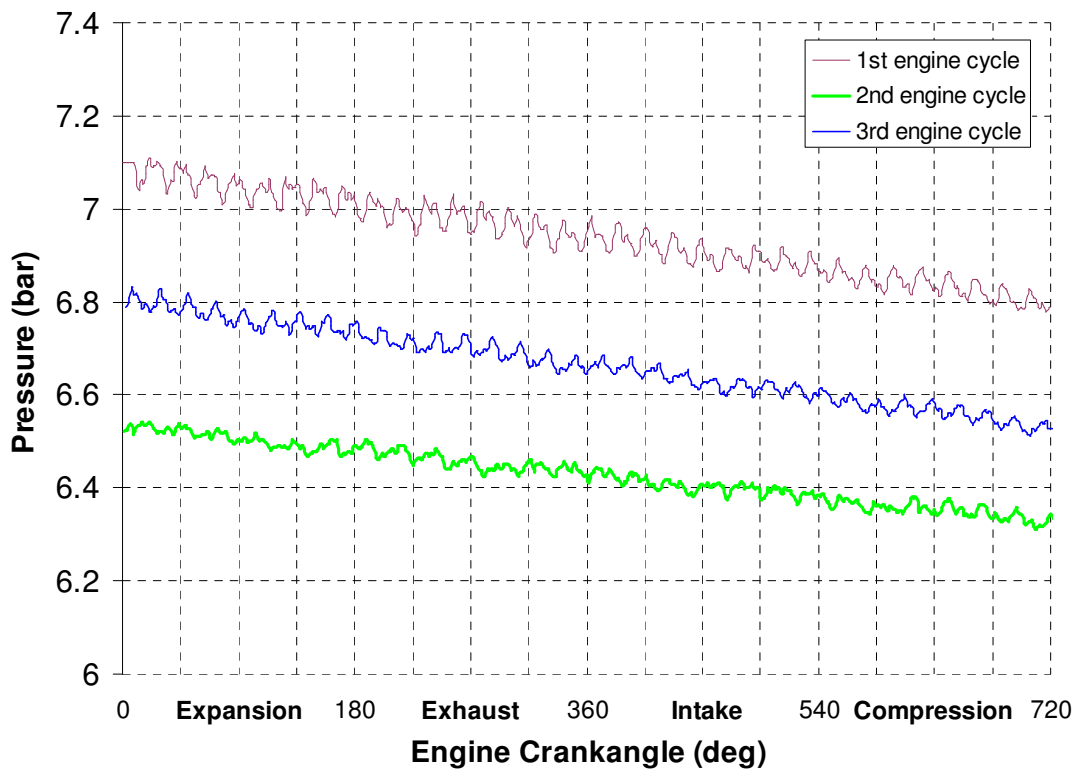


Figure 4.13: Air tank pressure changes for the first 6 revolutions at 325 rpm engine speed

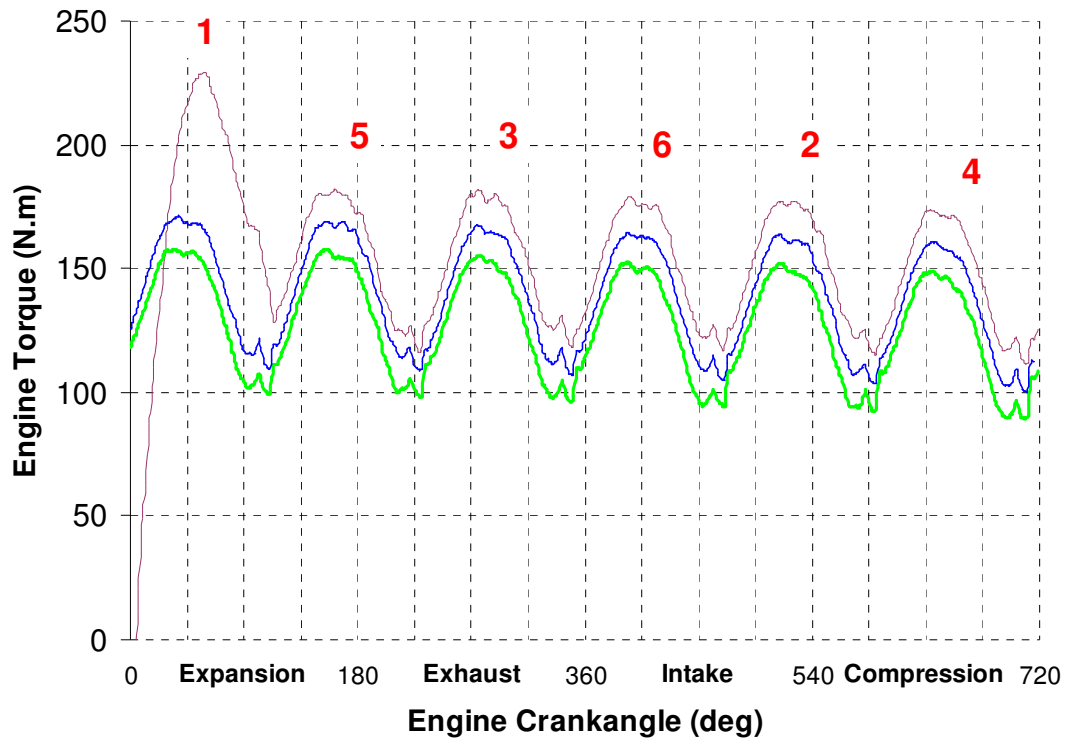


Figure 4.14: Cranking torque for the first 6 revolutions at 325 rpm engine speed

4.2.4.3 *Regenerative stop-start system with an air starter*

In order to start the engine using the compressed air in the cranking mode, it would require 6 fast acting solenoid valves. Because they have to be operated individually to release the compressed air into the cylinder and timed to synchronize with the firing order of the engine for the cranking mode, complex control would be also needed.

However, it will be simpler if an air starter can be used to achieve regenerative stop-start operation. As shown in Figure 4.15, a standard production air starter, e.g. the SS175 by Ingersoll Rand [61], can be readily employed to crank start the engine using the compressed air produced during the compression mode operation. The air hybrid operation based on this configuration is referred as RegenEBD (Regenerative Engine Braking).

Assuming 1-second crank time, the air starter is able to provide 2 start-up operations with a 151 litres air tank at 6.2 bar [61].

Compared to the direct use of compressed air to crank start the engine, the employment of an air starter is a much simpler system and easier to implement, by dispensing with the need of fast acting ECVs and sophisticated controls.

This configuration has therefore been adopted by Yuchai in their demonstration vehicle and will be used as the air hybrid vehicle driving cycle simulation studies in Chapter 6.

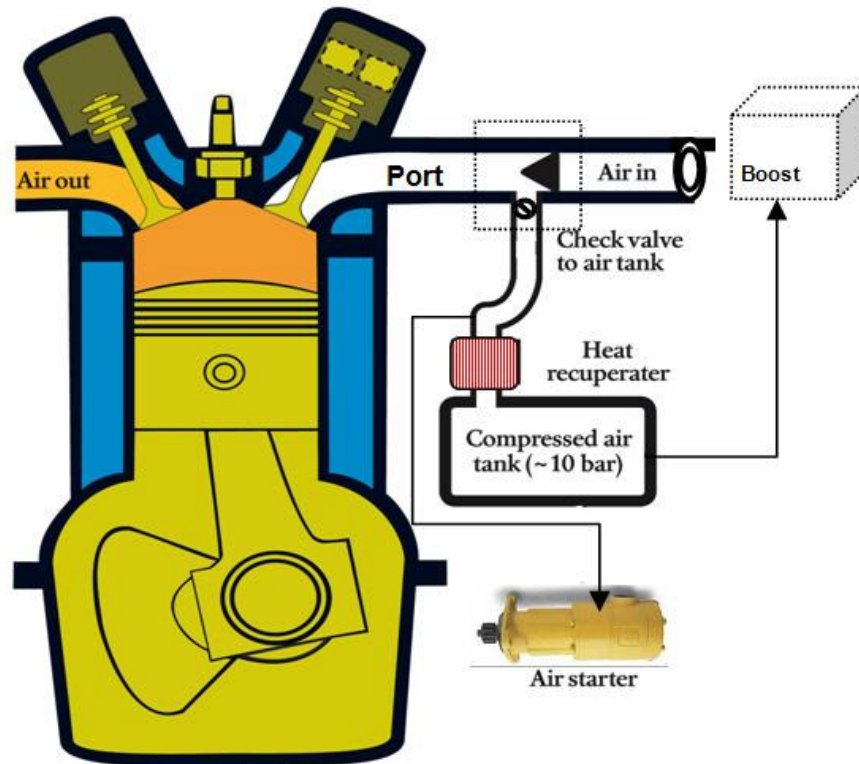


Figure 4.15: Schematic diagram of an air hybrid engine with an air starter

4.3 YUCHAI air hybrid engine with Jacobs brake

As mentioned in Section 4.2, a VVEB device is able to prevent the intake valves from fully closing during the compression mode operation. In this section, a Jacobs engine brake is used in place of a VVEB device. Normally, the Jacobs engine brake configuration is utilized on the exhaust valves. During the vehicle deceleration, the Jacobs engine brake allows the exhaust valve to have one more small lift near TDC in the compression stroke and therefore the high pressure compressed air will be released through the exhaust system. Without the Jacobs engine brake, the high pressure compressed air will force the piston down and accelerate the vehicle in the expansion stroke during the vehicle deceleration. To adopt Jacobs brake, this stored energy will be dissipated through the exhaust system. By adopting the Jacobs brake mechanism in the air hybrid engine configuration, the second opening of an intake valve during the compression stroke is used to capture compressed air during the engine braking process.

4.3.1 Description of the Air Hybrid Engine Setup

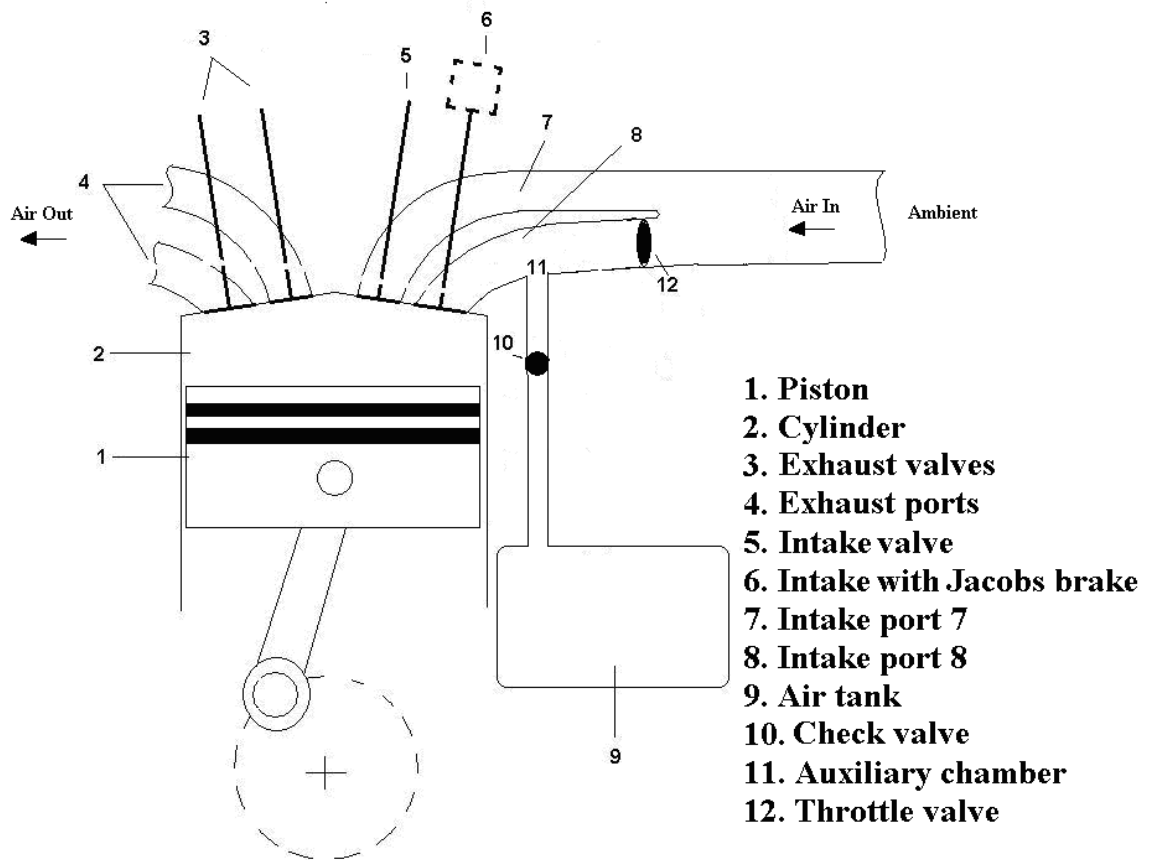


Figure 4.16: YUCHAI Air Hybrid Engine with the intake Jacobs brake device

Figure 4.16 shows one of the 6-cylinders of a modified version of the YUCHAI diesel engine with split intake ports. Air flows through the intake valves (5 and 6) via a separate intake ports (7 and 8) and leaves exhaust valves (3) via exhaust port (4). Intake valve 6 can be actuated by a Jacobs brake device. The Jacobs brake device is designed for engine braking applications and is normally installed on the exhaust valves. A throttle valve (12) is additionally provided in the intake port (8). For the normal firing mode, the throttle valve 12 is fully open. During the CM operation, Throttle valve 12 is fully closed to stop the compressed air escaping out of the intake manifold. The air tank 9 is insulated and therefore the heat of the compressed air can be stored in it.

The engine also includes five more cylinders, a fuel system and an ignition system which are not shown in Figure 4.16 for highlighting the main subject of the present study.

4.3.2 The Principle of operation

Figure 4.17 and 4.18 show the valve timing diagrams and flow direction respectively for the normal firing mode and CM. During the normal firing mode, both intake and exhaust valves operate with their default lift profiles. During deceleration and braking, the second opening of Intake valve 6 is in the normal compression stroke near TDC by activating the Jacobs brake device during the normal compression so that the air is compressed and stored in the auxiliary chamber formed by the throttle valve and the check valve. As a result, the engine will be operated as a compressor driven by the kinetic energy of the moving vehicle. An air starter is utilized for the cranking mode operation and therefore it simplifies the valve control strategy.

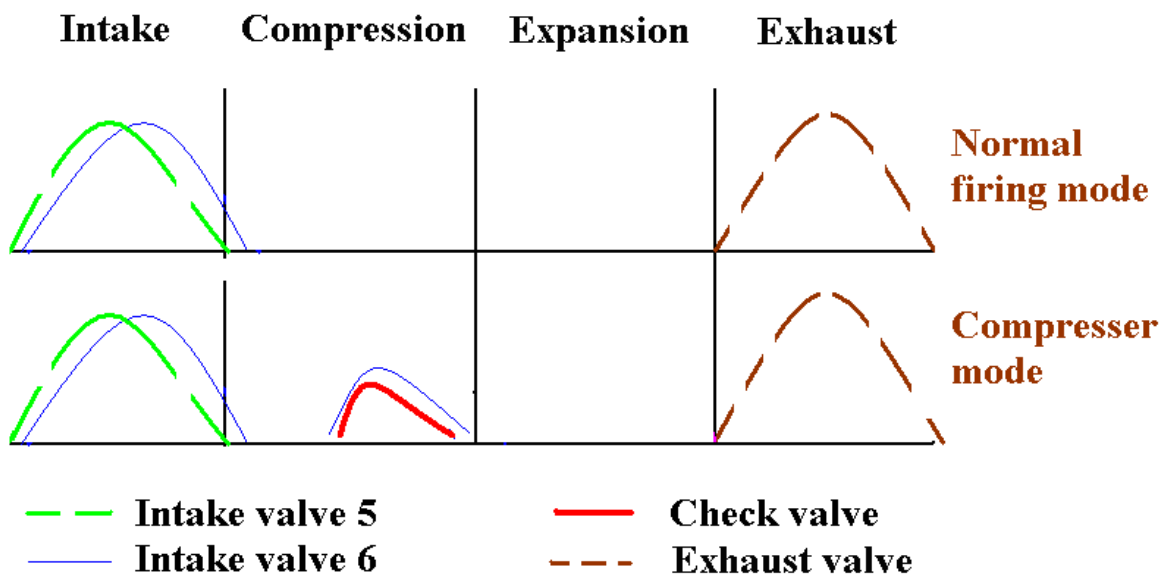


Figure 4.17: Engine valves, Check Valve and ECV timing for the normal firing mode and CM

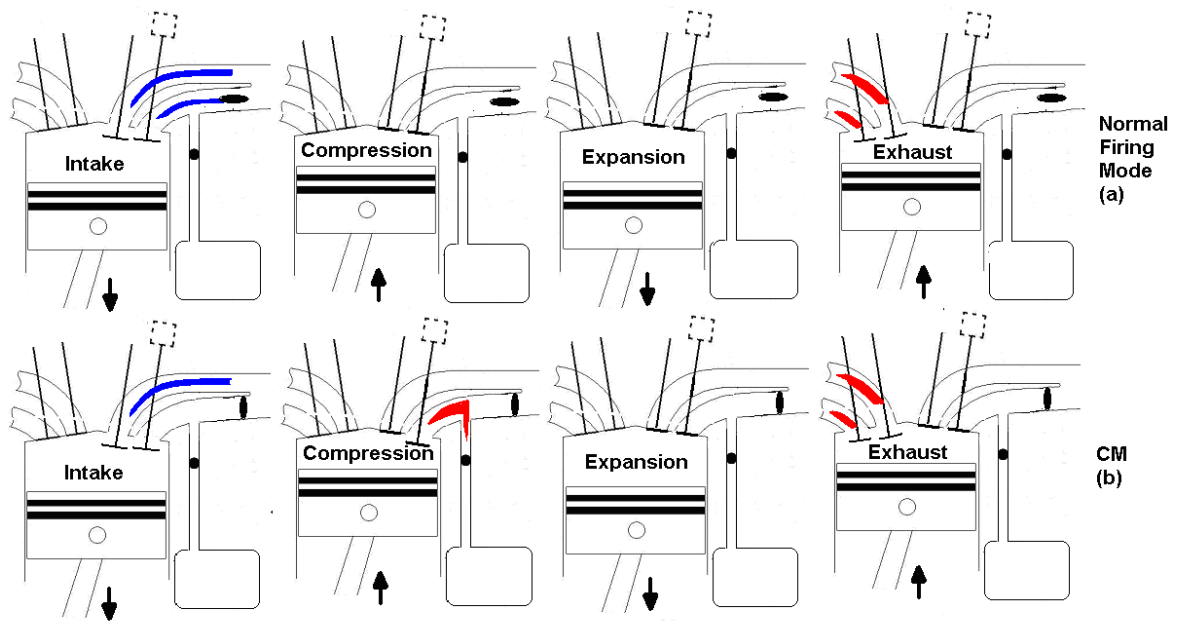


Figure 4.18: Four-stroke engine cycle for the normal firing mode (a), and CM (b).

4.3.3 Engine simulation setup

The size of the auxiliary chamber volume is determined by the position of the throttle valve and the position of the SSV. The geometric compression ratio of the engine is 17.5:1 for the normal firing mode. However, when the engine is switched to the compression mode, the actual compression ratio (R_c) decreases as the volume of the auxiliary chamber is included in the cylinders' total clearance volume. For the engine to be examined, the auxiliary chamber volume is 198.4 cm^3 , the actual compression ratio of CM is calculated as:

$$R_c = \frac{1143 + 69 + 198.4}{69 + 198.4} = 5.3 : 1$$

During CM, air is compressed into the auxiliary chamber isolated by the throttle valve and the Check Valve from the air storage tank, and then released by the CHECK VALVE into the air storage tank due to the pressure difference between the auxiliary chamber and the air storage tank.

The simulation canvas of this design is shown in Figure 4.19. The engine speed range is between 1000 and 2000 rpm. The cylinders, labelled "cylinder1, cylinder 2, cylinder 3, cylinder 4, cylinder 5 and cylinder 6" are connected to the intake network through "T1", "T2", "T3", "T4", "T5", and "T6" (throttle valves) respectively for inducing air from

atmosphere (“amb1”). The cylinder (“cylinder1, cylinder 2, cylinder 3, cylinder 4, cylinder 5 and cylinder 6”) are connected to the air tank (“Airtank”) through Check valves (“SSV1”, “SSV2”, “SSV3”, “SSV4”, “SSV5” and “SSV6”) for compressing air into the air tank. All exhaust ports are connected to a single exhaust pipe to the atmosphere (“amb2”). Based on the published information of Jakes Brake, the intake valve 6 is assume to reopen at 70° CA BTDC for a period of 100° CA and maximum lift 3 mm.

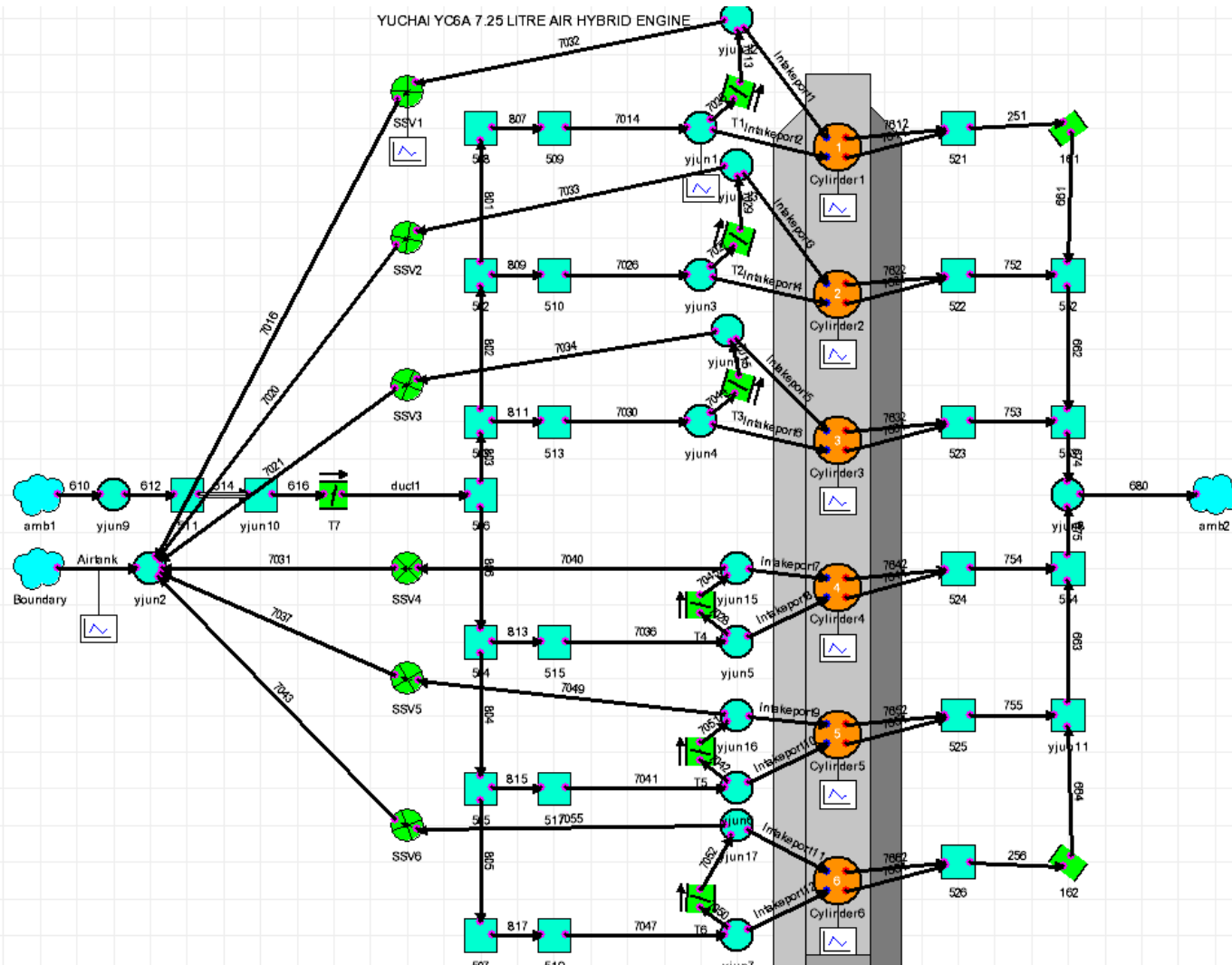


Figure 4.19 WAVE model of the YUCHAI air hybrid engine with Jacobs brake

4.3.4 Simulation Results

4.3.4.1 *Compression mode operation*

Figure 4.20 shows the valve lift diagrams of intake valve 6 and intake valve 5, Check Valve opening period, and the standard exhaust valve lift diagram. During the CM operation, Jacobs brake mechanism is actuated on only Intake valves 6 so that it will have the second opening in the compression stroke. During the compression mode operation, the IV6 second opening duration should ideally close to compression stroke TDC to allow the air to be compressed into the airtank. However, the IV6 closing timing can not go further than 30° ATDC for its second lift otherwise the valve clash will occur. In this simulation, the IV6 closing points have been set in the range between 10° ATDC and 30° ATDC to optimize the IV6 timing. The heavy duty vehicles normally supply significant kinetic energy and therefore the valve timing optimization is for the fast charging ability rather than the better specific braking imep. Figure 4.21 shows that the fastest charging ability is achieved while the IV6 closes at 30° ATDC after 120 engine revolutions at 1500 rpm engine speed during the compressor mode operation. In Figure 4.20, the second opening of IV6 closes at 30° ATDC with the duration of 100° CA and 3mm lift.

Figure 4.22 shows that the auxiliary chamber pressure, in-cylinder pressure and the air tank pressure during one engine cycle. It can be seen that in-cylinder pressure rises after both intake valves have closed after BDC and the air pressure in the auxiliary chamber goes up rapidly soon after the reopening of intake valve 6. Both pressures remain the same during the opening period of the check valve near TDC when the auxiliary chamber pressure becomes higher than the tank pressure. After TDC, the air flow stops when the air tank pressure exceeds that of the auxiliary chamber, which remains constant until the intake valves open again in the next cycle.

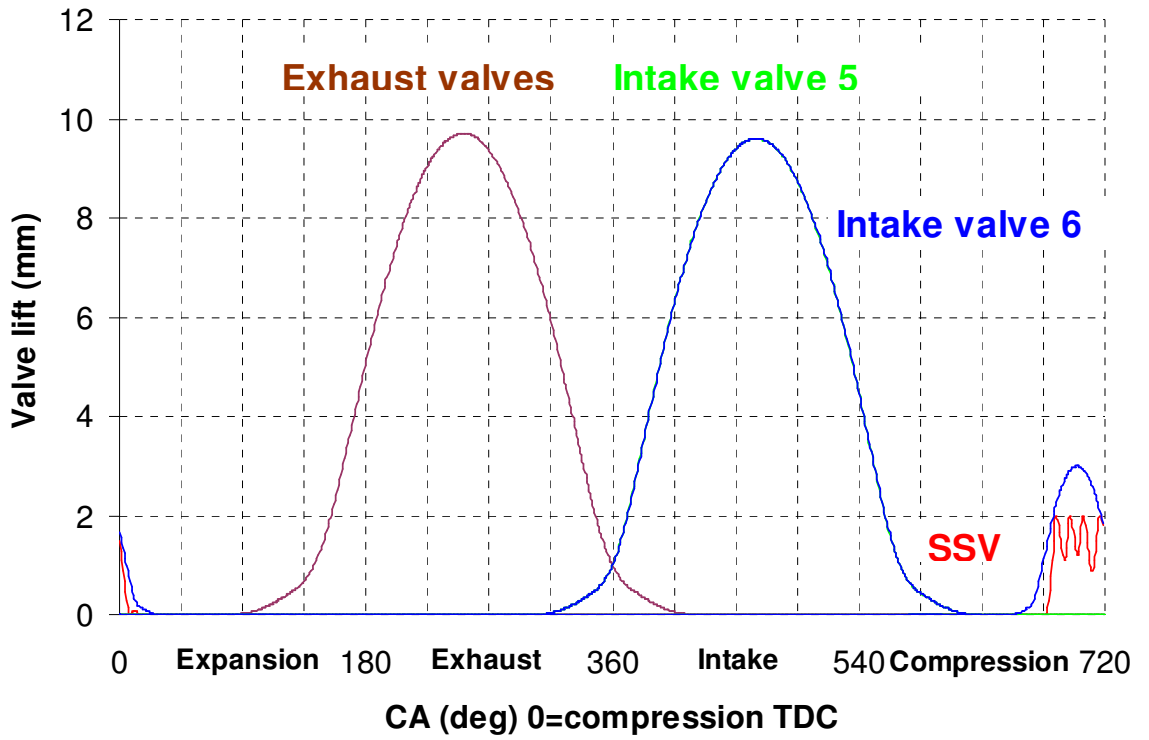


Figure 4.20: Valve timing diagram for compression mode

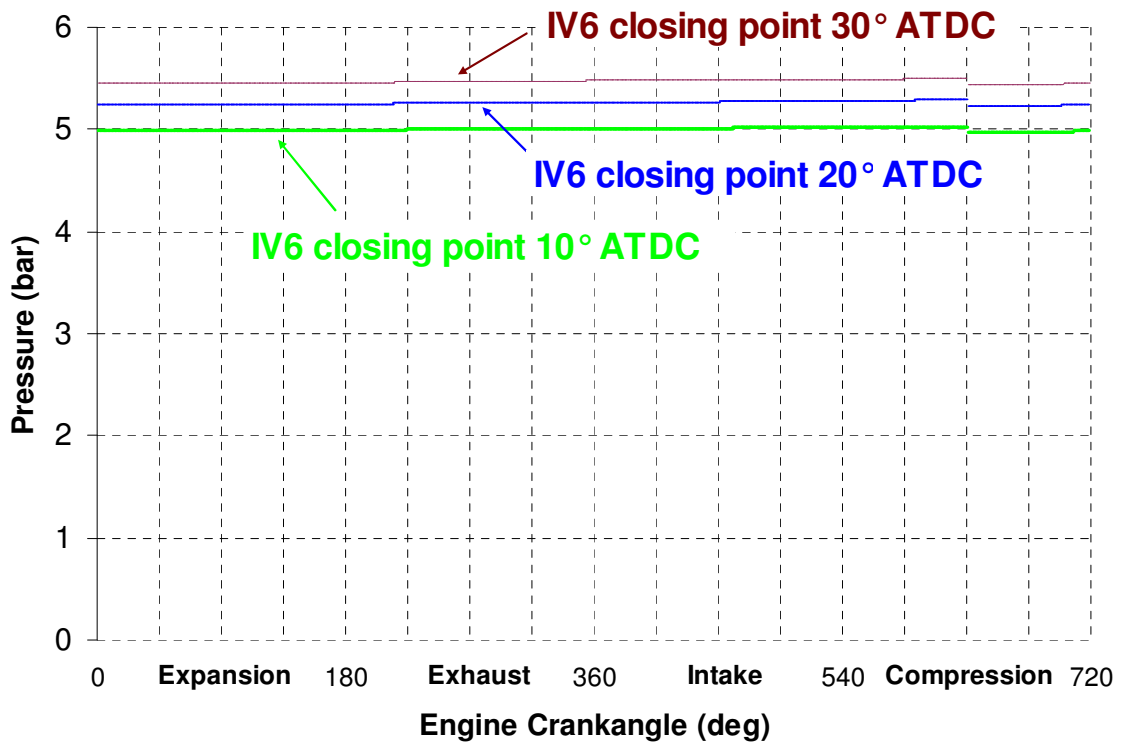


Figure 4.21: Air tank pressure at 120th engine revolution during the CM operation at 1500 rpm

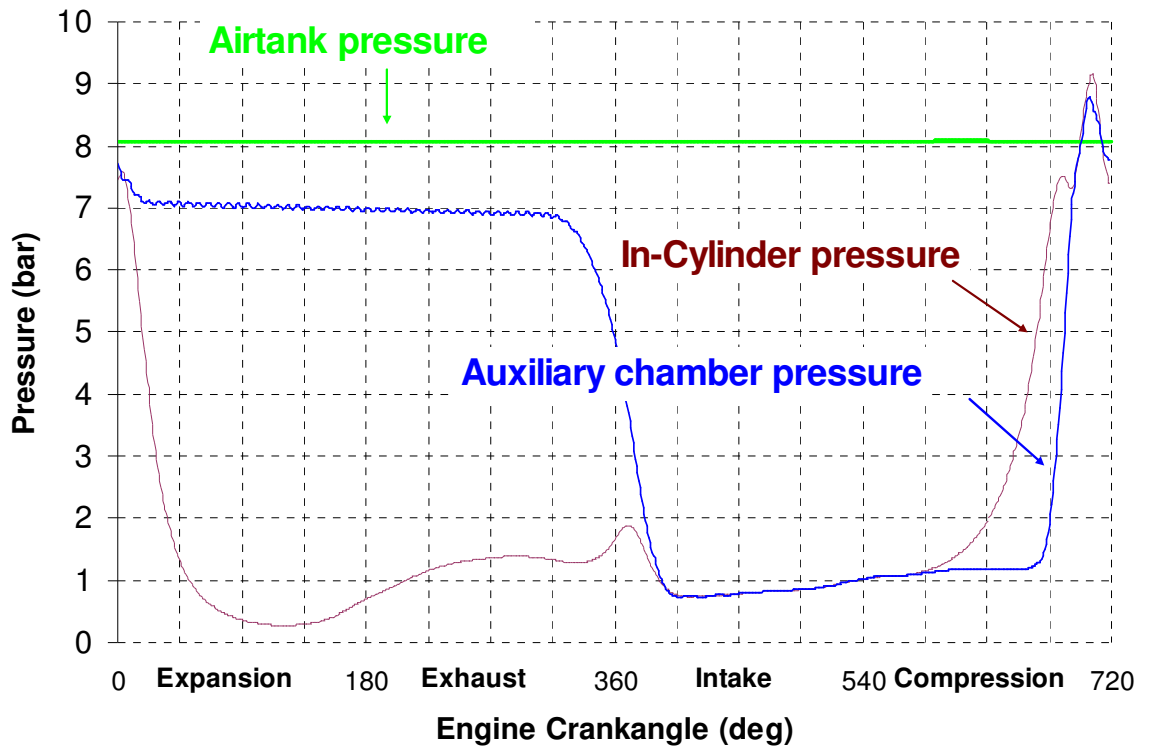


Figure 4.22: Pressure diagram for compression mode

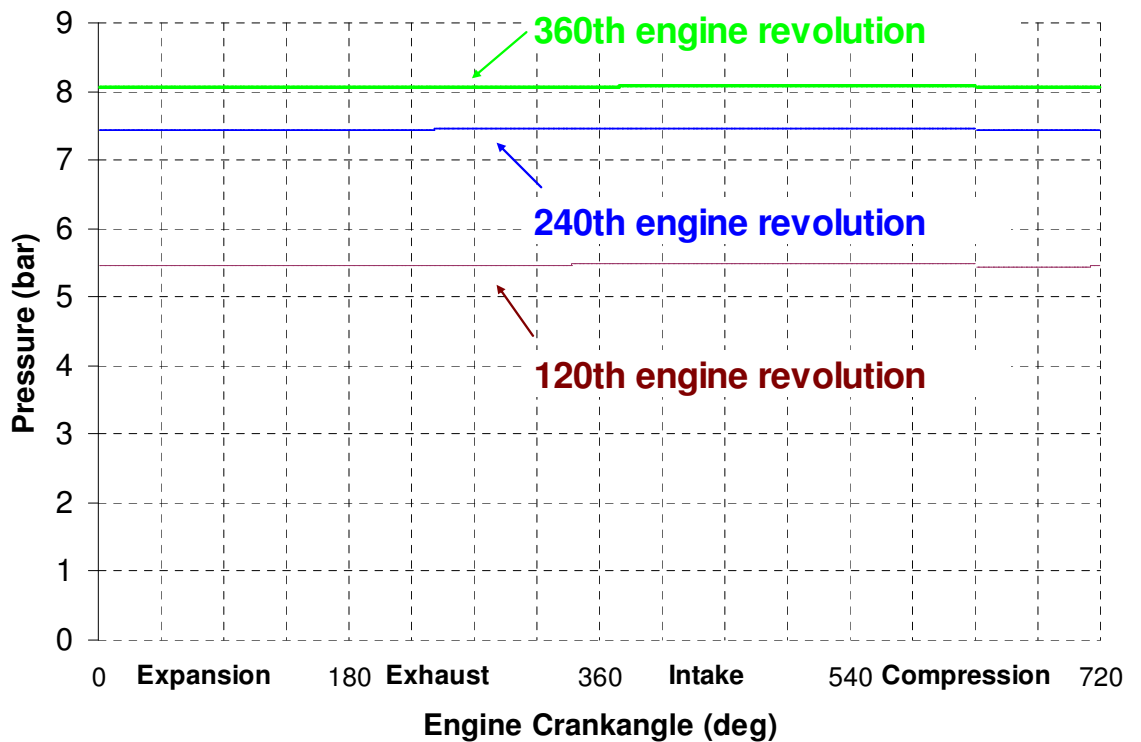


Figure 4.23: Air tank pressure during the CM operation at 1500 rpm

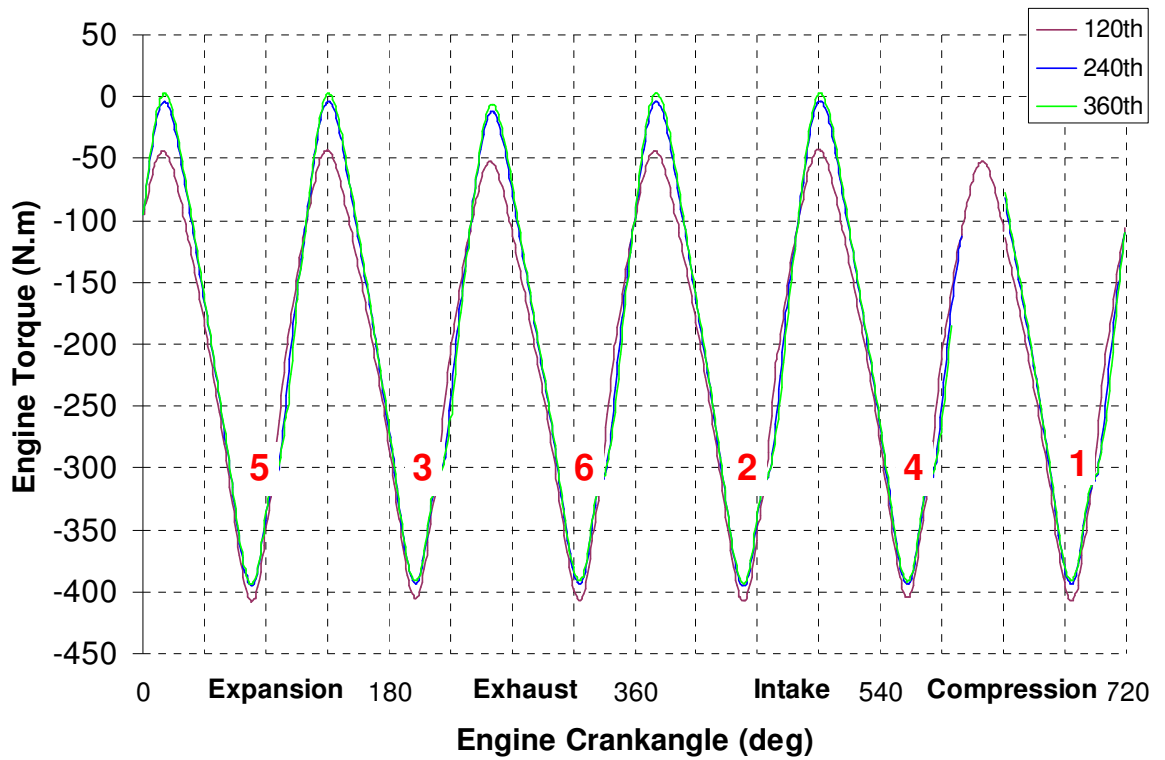


Figure 4.24: Braking torque for 1500 rpm engine speed

Figure 4.23 shows air tank pressure at 120th, 240th and 360th engine revolutions at 1500rpm engine speed during the CM operation. The results show that the air tank can be charged from 1 bar to 8.1 bar within 14.4 seconds at 1500rpm engine speed.

Figure 4.24 shows the corresponding engine braking torque values at 120th, 240th and 360th engine revolutions at 1500rpm engine speed. The cylinder number is included in the diagram to show the firing order of 6 cylinders. At 120th engine revolution, according to Fig.4.23 and Figure 4.24, the tank pressure has reached to 5.5 bar and the peak braking torque of cylinder 5 reaches 407 Nm. The tank pressure reaches 8.1bar after 360 engine revolutions, the peak braking torque from the cylinder 5 approaches 393 Nm.

The maximum air tank pressure is limited to 9.5 bar by the effective compression ratio defined by the auxiliary chamber volume depending on the dimension of the sandwich block and the position of the check valve and the throttle valve.

4.3.5 Conclusions

A cost-effective pneumatic regenerative stop-star hybrid system for buses and commercial vehicles has been proposed and analysed. The concept can be realised with current

production technologies and it does not require the use of camless technologies that other air hybrid engine concepts mandate.

For an air hybrid engine with ECV, both compression mode and cranking mode operations can be operated with the use of VVEB on the intake valves, check valves and solenoid valves for transferring the compression air between the cylinders and the air tank.

However, it is concluded that the air starter is better suited for the stop-start operation because of its simplicity and easy implementation. This configuration is named as the Regenerative Engine Braking Device (RegenEBD) technology.

The engine simulation has confirmed that the RegenEBD technology can be realised by either a simple bleed type VVEB device or a more widely used compression release type Jakes Brake device. The results in Table 4.3 show that a modern diesel engine with split intake ports will be able to produce higher engine braking torque, charge up the air tank faster and store the compressed air at a higher pressure, so that more regenerative engine braking energy can be captured and used to achieve not only the stop-start operations but also provide the service air and instant boost during transient operations.

Table 4.3: Results of air hybrid concepts for a medium duty diesel engine

Configuration	Engine braking	Charge Time from 4-6 bar	Maximum Tank Pressure	Pneumatic Energy (PxV)	Cranking torque at 6.2 bar (Yuchai engine)	Cranking torque at 6.2 bar (air starter)
VVEB	77.9 Nm	4.8 s	7.4 bar	111.7 kJ	110.6 Nm	57 Nm
Jakes Brake	168.5 Nm	2.7 s	9.5 bar	143.5 kJ	X	57 Nm

Chapter 5: Experimental Studies of the Air Hybrid Engine Operation

5.1 Introduction

In order to verify the engine simulation results and demonstrate the capability of proposed air hybrid concepts, a single cylinder camless engine was equipped with the new intake systems designed for compression mode operation and tested for two different setups. In this chapter, the experimental setup and experiments are described. Then the experimental results will be presented, analysed and compared with the simulation data.

5.2 Engine Testing Equipment and Facility

5.2.1 The Single Cylinder Camless Engine

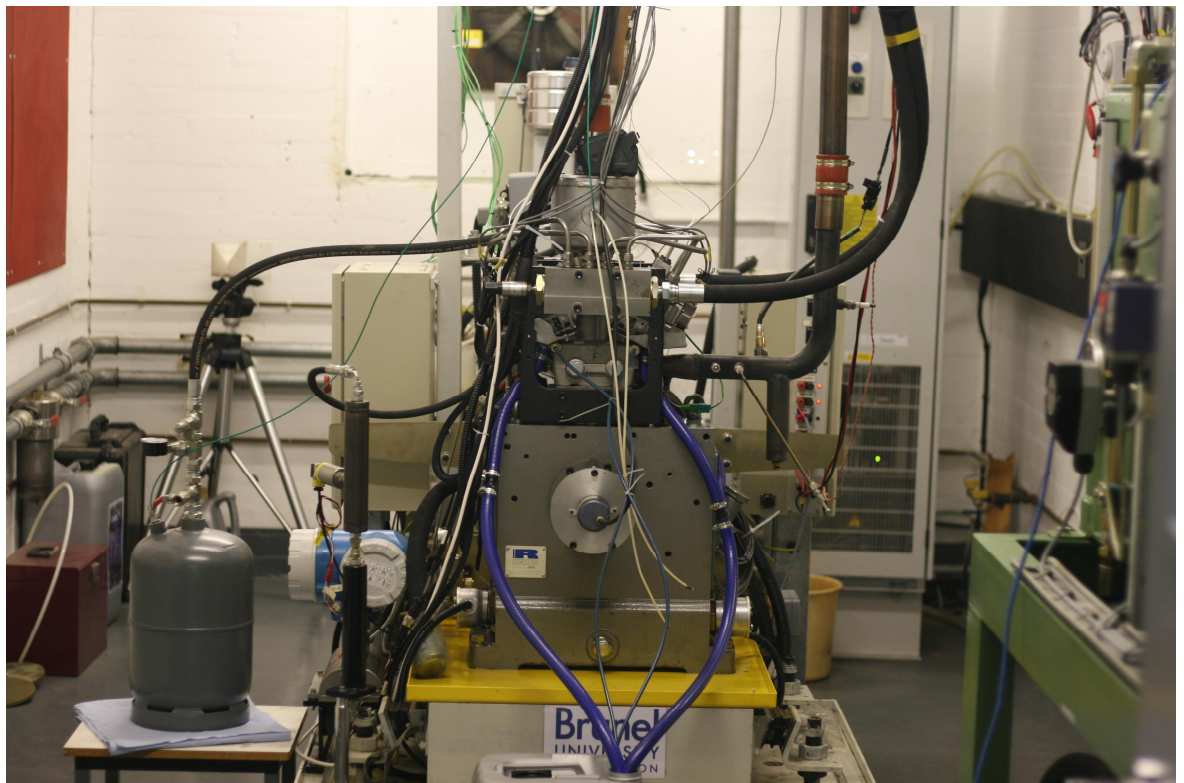


Figure 5.1: Single cylinder camless engine with electro-hydraulically actuated valves

Figure 5.1 shows a single cylinder gasoline engine equipped with 4 electro-hydraulically actuated intake and exhaust valves. The engine has a stroke of 66.94 mm, a bore of 81.6 mm and a displacement volume of 350 cm³. Its connecting rod length is 144.5 mm and its

intake and exhaust valve diameters are 27.7 mm and 30 mm respectively. The engine is capable of 4-stroke operation up to 5000 rpm. Detailed engine data are given in Table 5.1.

Table 5.1: Engine specification

Number of cylinders	1
Bore	81.6 mm
Stroke	66.94 mm
Displacement volume	350 cm ³
Total volume	385 cm ³
Clearance volume	35 cm ³
Connecting rod length	144.5 mm
Compression ratio	11:1
Valve arrangement	Overhead
Intake valve count	2
Intake valve diameter	27.7 mm
Exhaust valve count	2
Exhaust valve diameter	30 mm
One intake port volume	57 cm ³

5.2.2 Engine Control Module

5.2.2.1 R-Cube and Valve Control Unit



Figure 5.2: R-Cube



Figure 5.3: Four Valve Control Units

The Engine Control Module (ECM) is the Ricardo rapid prototype unit, R-Cube, shown in Fig.5.2. It has Dual Power Personal Computer (PC) micro-controllers and a processing speed more than 500 Million Instructions per Second (MIPS). As a central unit, R-Cube plays the main role in controlling all engine functionalities such as ignition, injection, and throttle drive by wire and valve timing. The electro-hydraulic valves are controlled by Valve Control Units (VCU), Fig.5.3.

In order to alter the valve timing and lift, R-Cube sends trigger signals via a Control Area Network (CAN) to the VCUs. Two outputs with one pulse for opening and one pulse for closing will control each of four VCUs. In order to maintain continuous control of hydraulic actuated valves, all VCUs have Uninterruptible Power Supply (UPS) power back up in the event of a power loss.

5.2.2.2 *Electro hydraulic valve actuator*

Figure 5.4 shows the electro hydraulic valve actuator which is attached to the cylinder head via a mounting block. The Electro Hydraulic Valve Actuator is essentially made up of three base components including the hydraulic actuator, the servo valve and Linear Variable Differential Transformer (LVDT). The servo valve is capable of returning engine valve to closed position if signal fails. Its maximum working pressure is 280 bar. Both intake valves and exhaust valves are attached to the actuators via rigid, threaded connector.

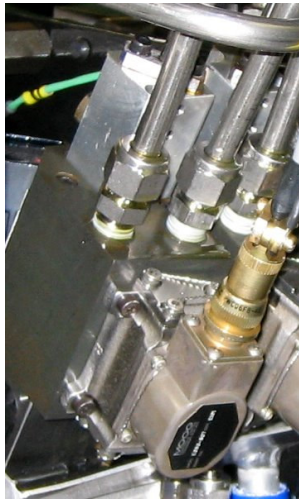


Figure 5.4: Electro hydraulic valve actuator

5.2.2.3 *Hydraulic pump unit*

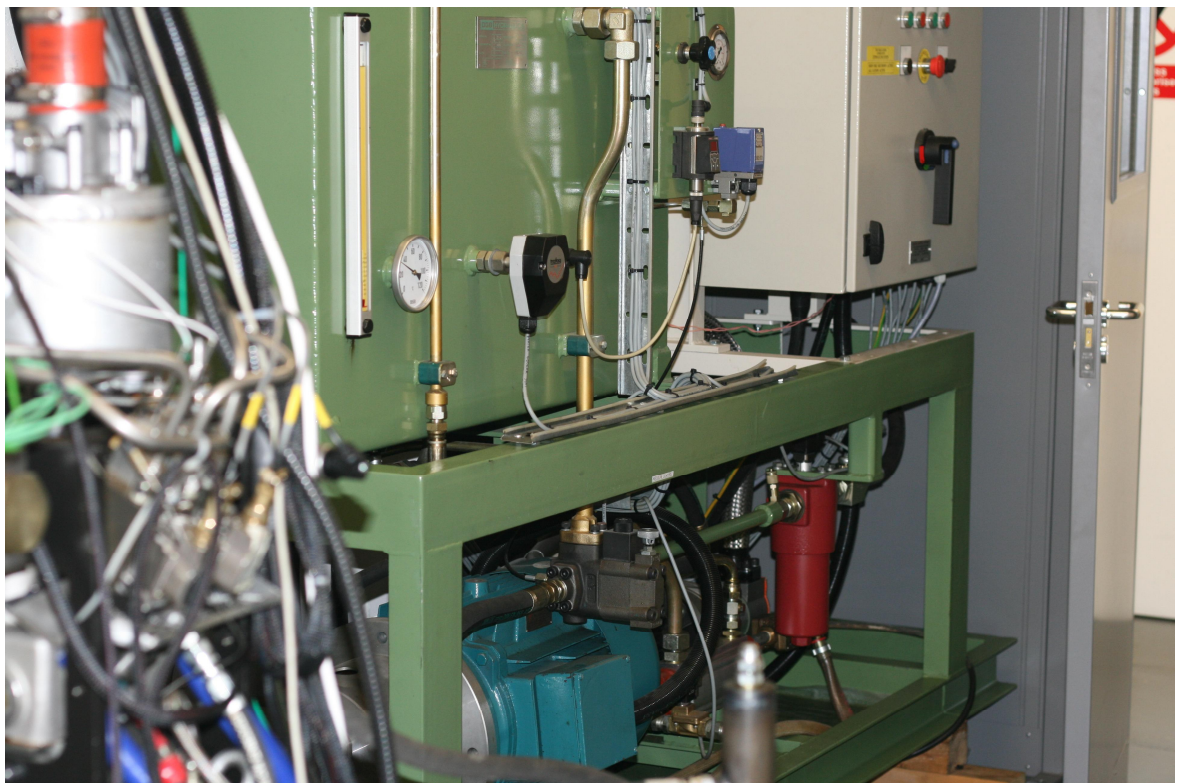


Figure 5.5: Hydraulic pump unit

Figure 5.5 shows the hydraulic power unit which is able to delivery 34 litres hydraulic oil per minute at 280 bar. There are feed and drain manifolds mounted on the engine and the oil pressure sensor is incorporated into the feed manifold. For the test of the air hybrid engine concept, hydraulic power system has been set at 100 bar hydraulic pressure to

supply clean cooled oil to the servo valves. Each of hydraulic valves can work independently with its own valve profile and hence various valve profiles can be used to optimize the performance of the air hybrid engine. The 225 litre capacity oil reservoir utilizes ISO 32 hydraulic oil which is recycled by filtering the hydraulic oil via the oil filter. Additional 10 litre bladder accumulator has been installed to function as a power supply in case of emergency, compensation for leakage, hydraulic shock absorption and pump flow supplement.

5.2.3 Air intake system

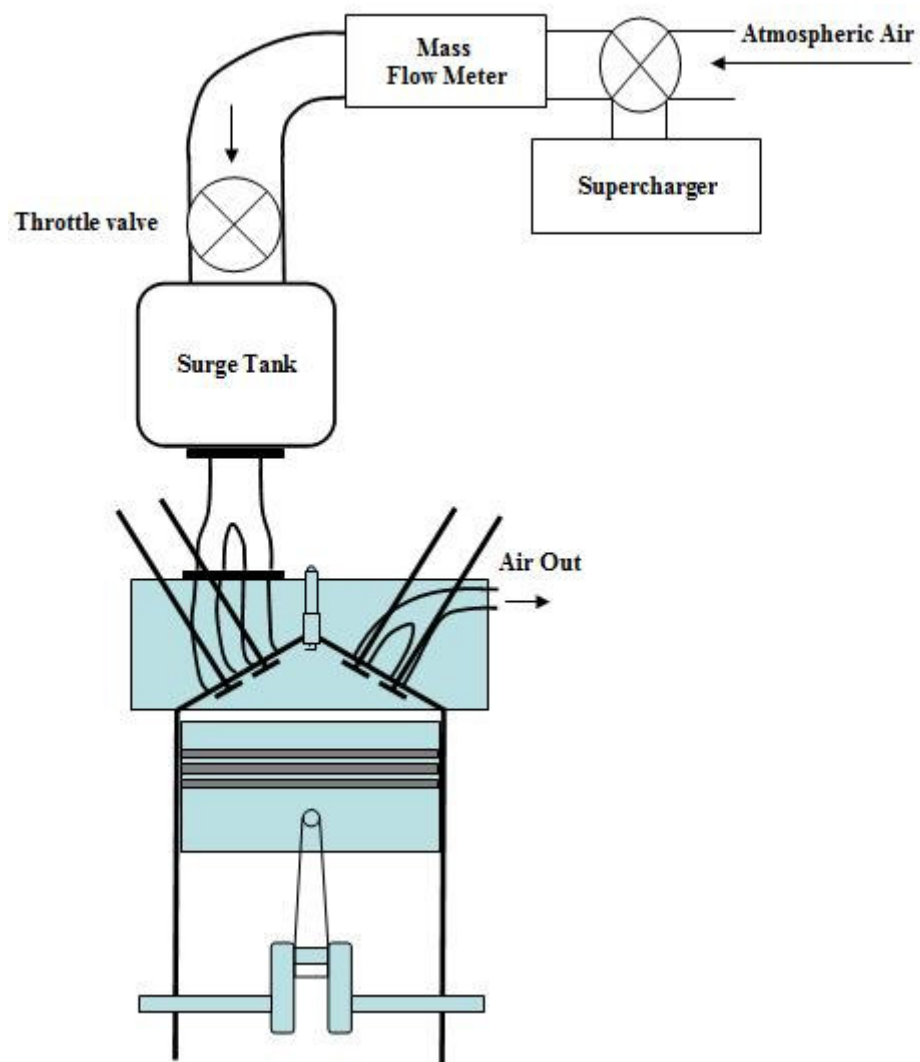


Figure 5.6: Schematic diagram of the camless engine

Figure 5.6 shows the schematic diagram of the camless engine. Test can be carried out at either Naturally Aspirated (NA) condition or boosted air intake condition. During the firing mode operation, air flows through the intake filter from atmosphere and passes through the

Hastings HFM-200/202 series mass flow meter. The mass flow meter was also used to measure the air flow rate into the air tank as described in the next section. The throttle is set at Wide Open Throttle (WOT).

5.3 Experimental Measurement and Data Analysis

5.3.1 Mass flow meter

The Hastings HFM-200/202 series mass flow meter operates on a unique thermal electric principle whereby a metallic capillary tube is heated uniformly by a resistance winding attached to the midpoint of the capillary. Two thermocouples are welded at equal distances from the midpoint and develop equal outputs at zero flow. When flow occurs through the tubing, an asymmetrical temperature created due to heat transfer from the tube to the gas on the inlet side and from the tube to the gas on the outlet side. The changes in temperatures detected by the thermocouples produce a millivolt output signal proportional to the flow rate. The maximum operational pressure is 34.5 bar and its accuracy is $\pm 1\%$ full scale.

5.3.2 In-cylinder pressure measurement

A Kistler type 6061B water-cooled piezo-electric pressure sensor is installed in the cylinder head to measure the in-cylinder pressure. A Kistler type 5011B charger amplifier converts the electrical charge produced by the pressure sensor into a proportional voltage signal. The calibrated pressure range is 0-250 bar with the operating temperature range between -50 and 350 °C.

5.3.3 Data Acquisition System

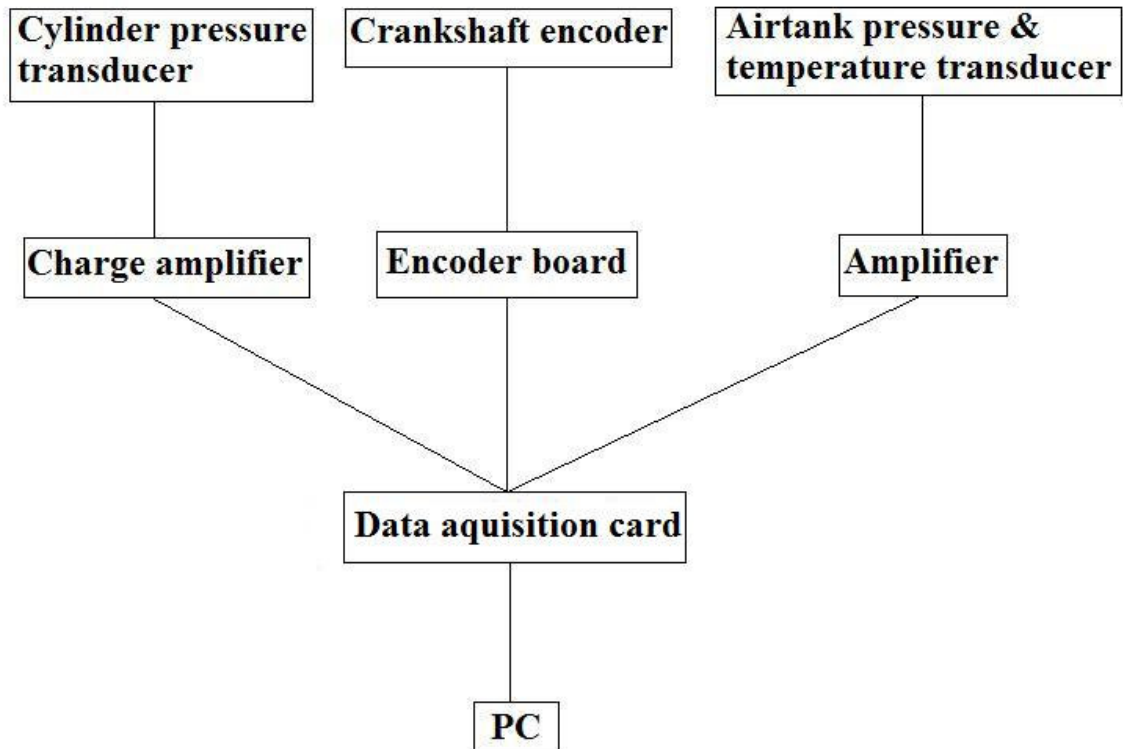


Figure 5.7: Schematic diagram of data acquisition system

The data acquisition system operates as a real-time displaying, measuring, and logging device for the in-cylinder pressure, the tank pressure, and the tank temperature readings. It comprises a National Instruments' USB data acquisition card type 6251 with 16 input channels connected to a PC and it is operated with the National Instruments Labview software from which real-time data analysis software can be developed for specific data acquisition requirements.

As shown in Figure 5.7, the crankshaft encoder and the encoder board, a part of data acquisition system, are capable of providing an output signal of 360 pulses per revolution for crankshaft angle resolution and a separate single pulse per revolution signal of the crankshaft at the TDC position of the piston. Therefore, all of pressure and temperature signals can be sampled at regular intervals and their phasing relative to the four-stroke cycle can be established.

5.3.4 The daily checks

In order to make sure that the experimental facilities worked in the same condition everyday, a few preparations were done before starting each experiment. First, coolant water and lubrication oil were preheated to 80°C. Second, it was necessary to check the water pipe was not blocked in the water-cooled cylinder pressure sensor. To keep the hydraulic oil level above the minimum range and hydraulic pressure up to 100 bar were necessary for the hydraulic valves working proper. Finally, The initial tank pressure and the initial tank temperature were measured before the start of each experiment.

5.4 Experiments on the air hybrid engine operation with a Reed Valve

5.4.1 Compression mode operation with an intake Reed Valve

In order to realise the air compression mode, a modified intake system was designed and fabricated. Figure 5.8 shows the schematic of the air hybrid engine concept with a Reed valve. Figure 5.9 illustrates the valve timing of both intake valves and exhaust valve timings for CM. It is noted that IV2 is deactivated with the corresponding intake port sealed in order to reduce the auxiliary chamber volume. During CM, IV1 opens in the normal intake stroke, air is able to flow through the Reed valve in the intake port 1. When IV1 continuously opens in the normal compression stroke, air can be compressed back into the auxiliary chamber and stopped by the Reed valve and then flowed into the airtank via the check valve.

As shown in Figure 5.10 and Figure 5.11, the sandwich box comprises a check valve, a Reed valve and a top flange to the surge tank. The metal net is installed in the sandwich box to prevent any broken parts from entering the engine in case the Reed petal fails. As mentioned above, the sandwich box is only connected to Intake Valve 1 (IV1) via one intake port shown in Figure 5.8 whilst the other intake port is sealed.

The compressed air tank, shown in Figure 12, is 13 litre in volume and equipped with a pressure and temperature transducer, two ball relief valves and a 20 bar pressure gauge. A Kistler type 4007BA20FA2 high temperature piezo-resistive pressure sensor is installed in the airtank to measure the tank temperature and tank pressure. A Kistler type 4618A2 amplifier allows to measure pressure and temperature simultaneously. The calibrated pressure range is 0-20 bar with the operating temperature range between -40 and 200 °C.

The ball relief valve with a red handle was installed to empty the charged tank manually. The other relief valve acted as a safety valve set at 12 bar. Once the tank pressure is over 12 bar, the safety valve can release the compressed air automatically. The pressure gauge was used to monitor the tank pressure in the test cell during the experiments.

A simple test of air leakage has been done when the airtank is fully charged. The tank pressure has no significant drop in an hour. Liquid has been sprayed on all the connections and joints to see if they are bubbling.

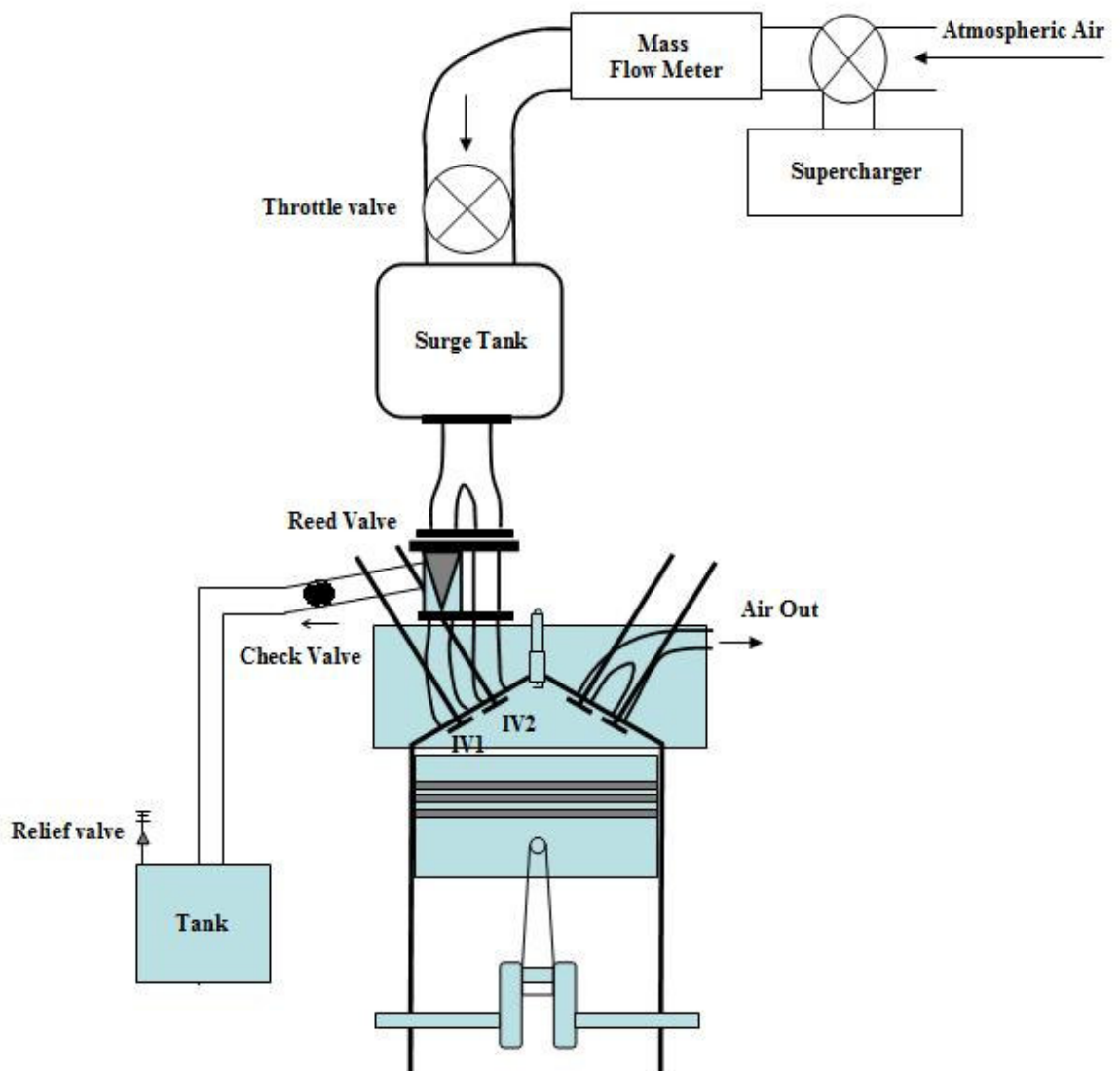


Figure 5.8: Air hybrid engine concept with a Reed valve

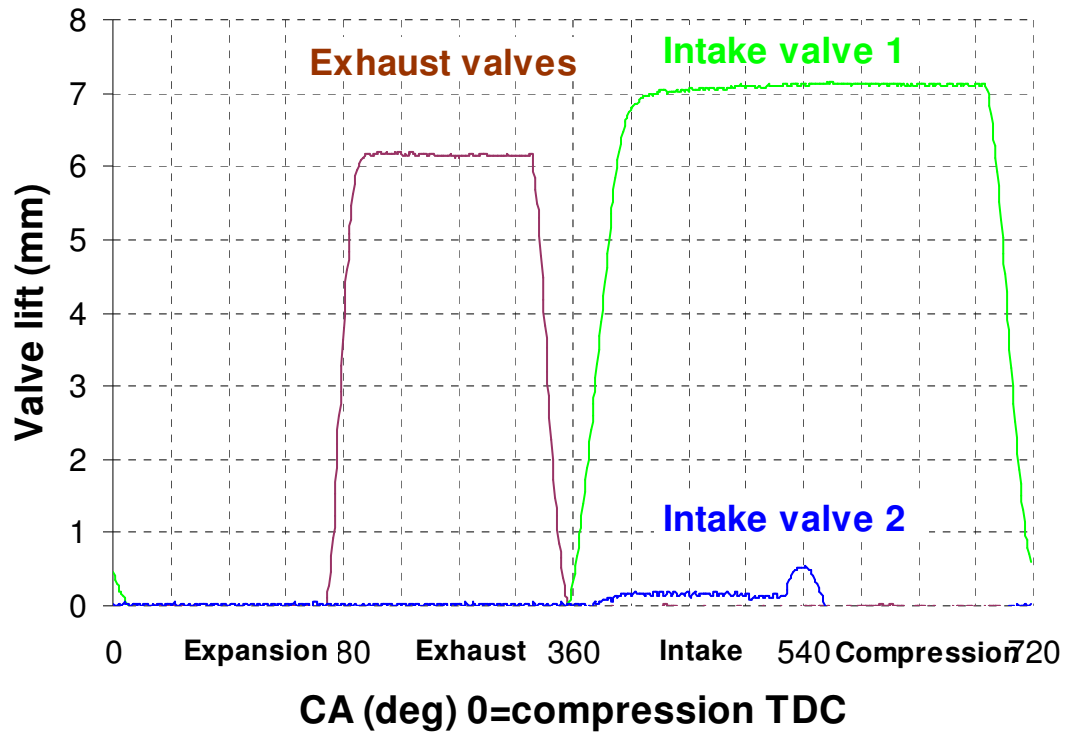


Figure 5.9: Valve timing for IV1 closing point is at 10 ATDC at 1500 rpm

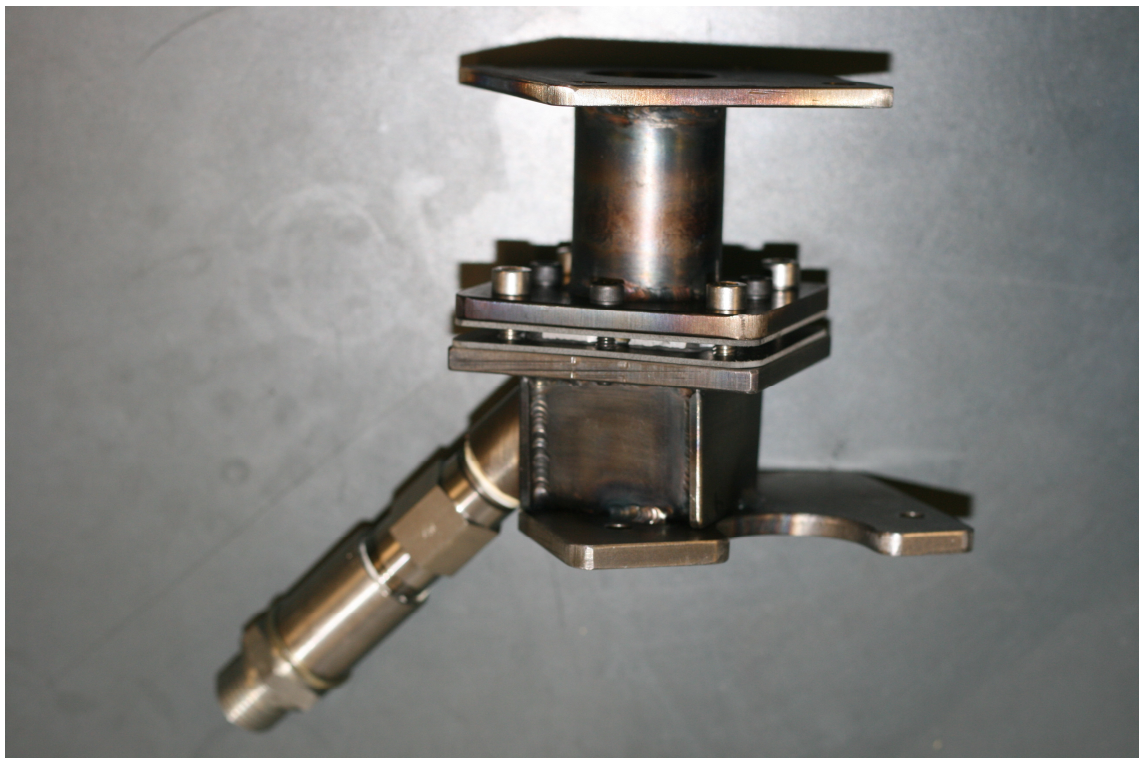


Figure 5.10: The sandwich box assembly

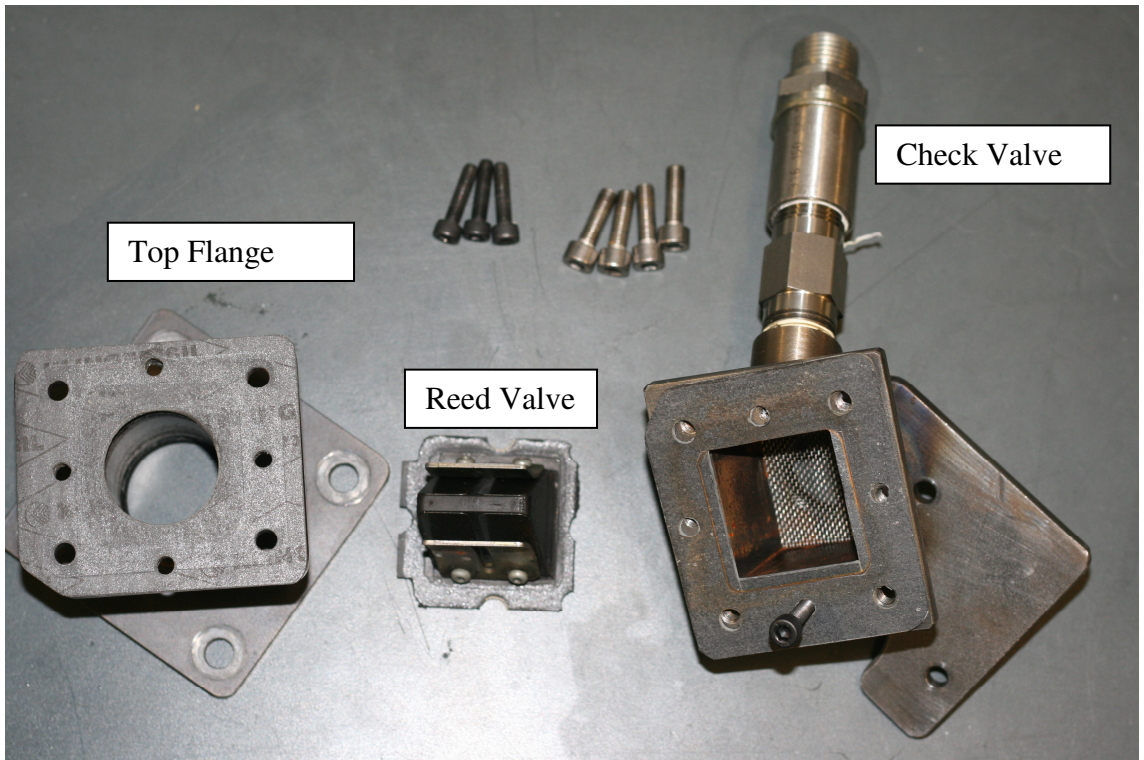


Figure 5.11: The disassembled sandwich box

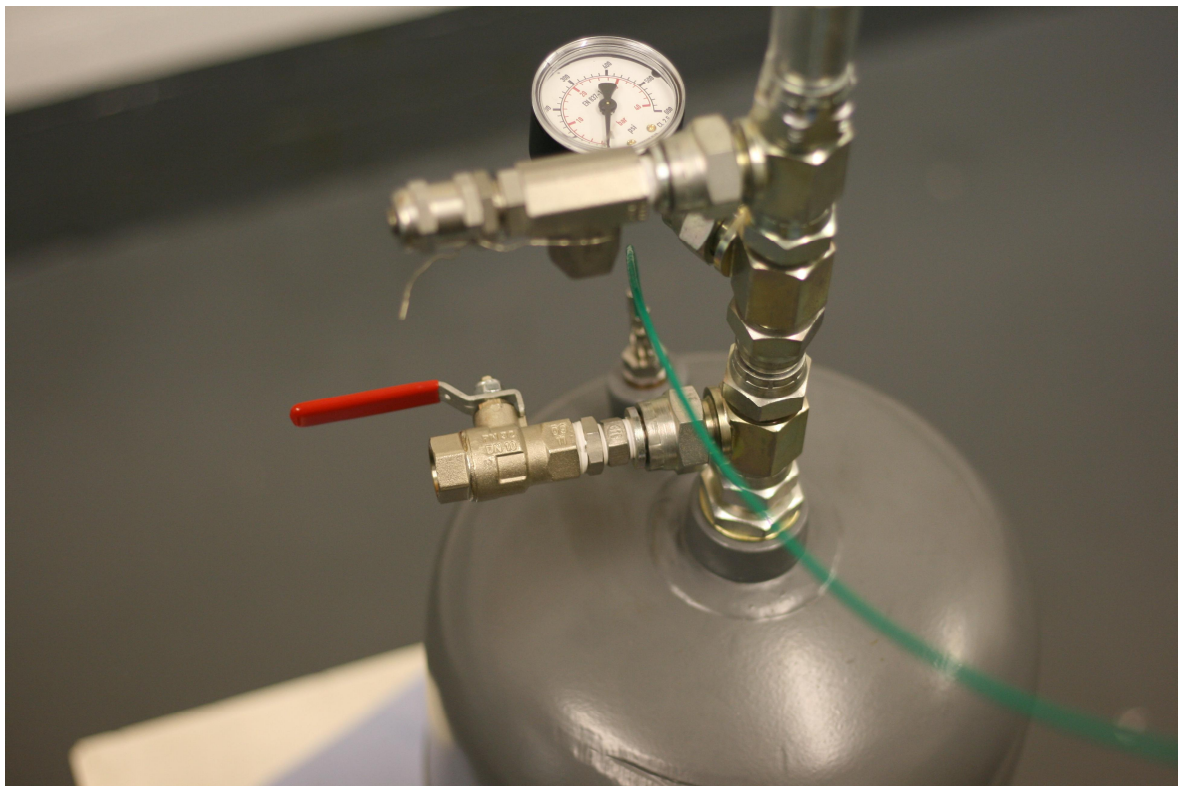


Figure 5.12: The compressed air tank

During the CM operation, the actual compression ratio (R_c) is determined by the volume of the auxiliary chamber as well as the cylinder's total clearance volume. In this concept, the sandwich box is connected to only one intake port and the surge tank. Therefore, the volume of the auxiliary chamber includes the volume of one intake port and the volume of the sandwich box. The volume of the sandwich box is determined by the position of the non-return Reed valve and the position of the one way check valve. The volume of one intake port and the sandwich box are 57 cm^3 and 40 cm^3 respectively. For the auxiliary chamber volume of 97 cm^3 , the actual compression ratio is 3.65 according to Equation 3.6. Based on the value of such an effective compression ratio, the predicted maximum pressure is 6.1 bar. Table 5.2 shows characteristics of the air hybrid engine with a Reed valve.

Table 5.2: Characteristics of the air hybrid engine with a Reed valve

R_c for air hybrid mode	3.65:1
Airtank volume	13 litre
Sandwich box volume	40 cm^3
Reed valve effective flow area	308 mm^2
Check valve diameter	12.7 mm

5.4.2 Experimental results

Figure 5.13 shows cylinder pressures for various tank pressures when the IV1 is set to close at 10 ATDC during the compression stroke at 1500 rpm. At the tank pressure of 1 bar, the cylinder pressure is the lowest in the diagram because most of the intake air is charged into the airtank in the normal compression stroke and cylinder pressure drops to below the atmospheric condition in the following normal expansion stroke until exhaust valve opens in the exhaust stroke. It is noted that the cylinder pressures suddenly go up at the start of the intake stroke when the tank pressure is above 1 bar and their peaks are proportional to the tank pressure. This is because the residual compressed air in the sandwich box from the previous cycle flows into the cylinder when IV 1 opens. Figure 5.14 shows the sensitivity of airtank pressure to various IV1 closing points for 700 engine cycles. It can be seen that higher tank pressure as well as faster charging is achieved when IV1 closes between 10° ATDC and 5° ATDC. This is also reflected in the in Figure 5.15, in which the mass of air induced in every engine cycle is shown to decrease faster with IVC at 10° ATDC and 5° ATDC since the air tank has been charged up more quickly during the first part of charging process.

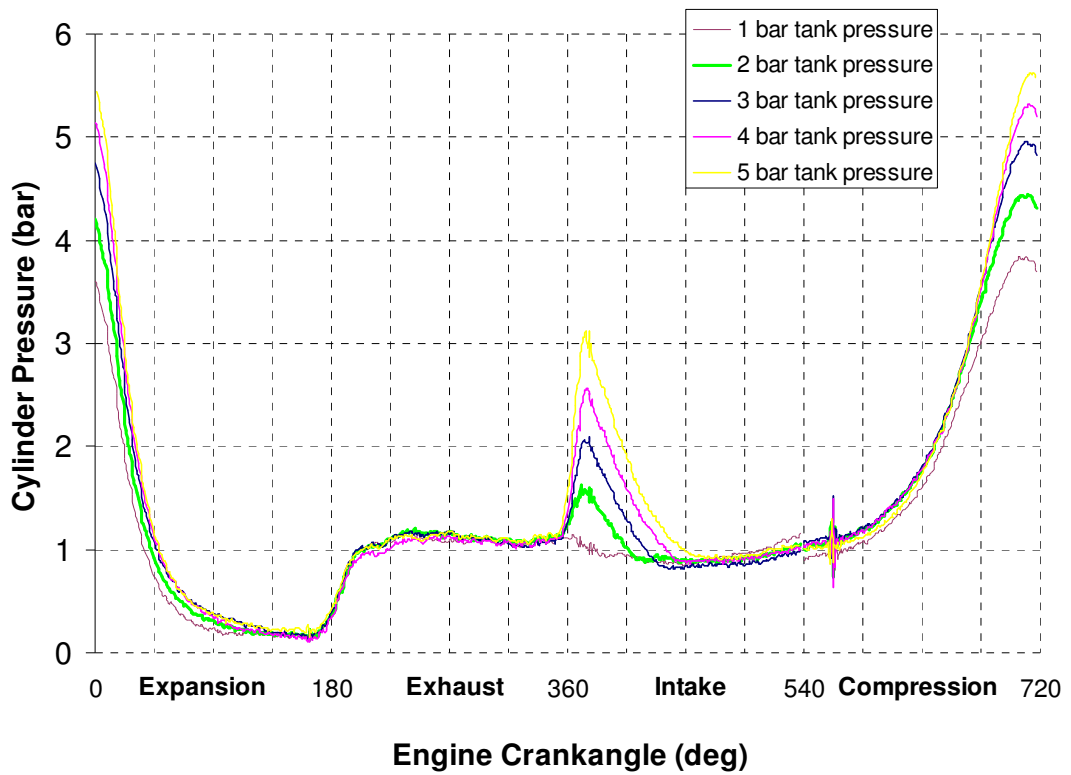


Figure 5.13: Cylinder pressure with IVC at 10 ATDC at 1500 rpm

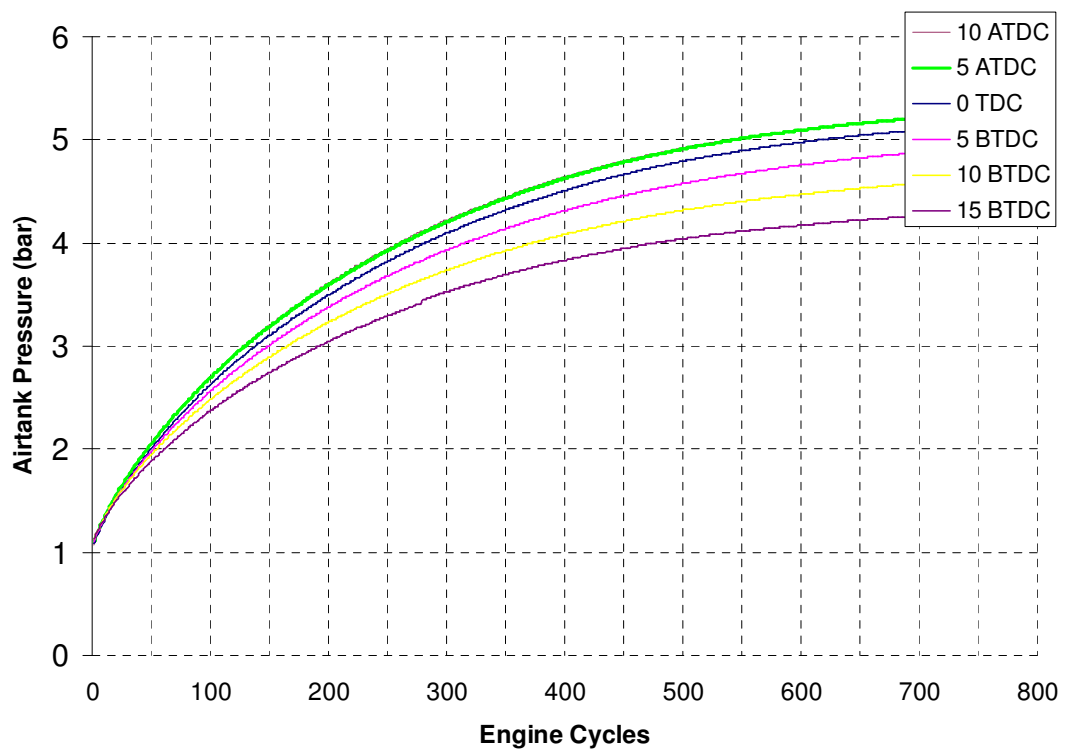


Figure 5.14: Airtank pressure histories for various IVC at 1500 rpm

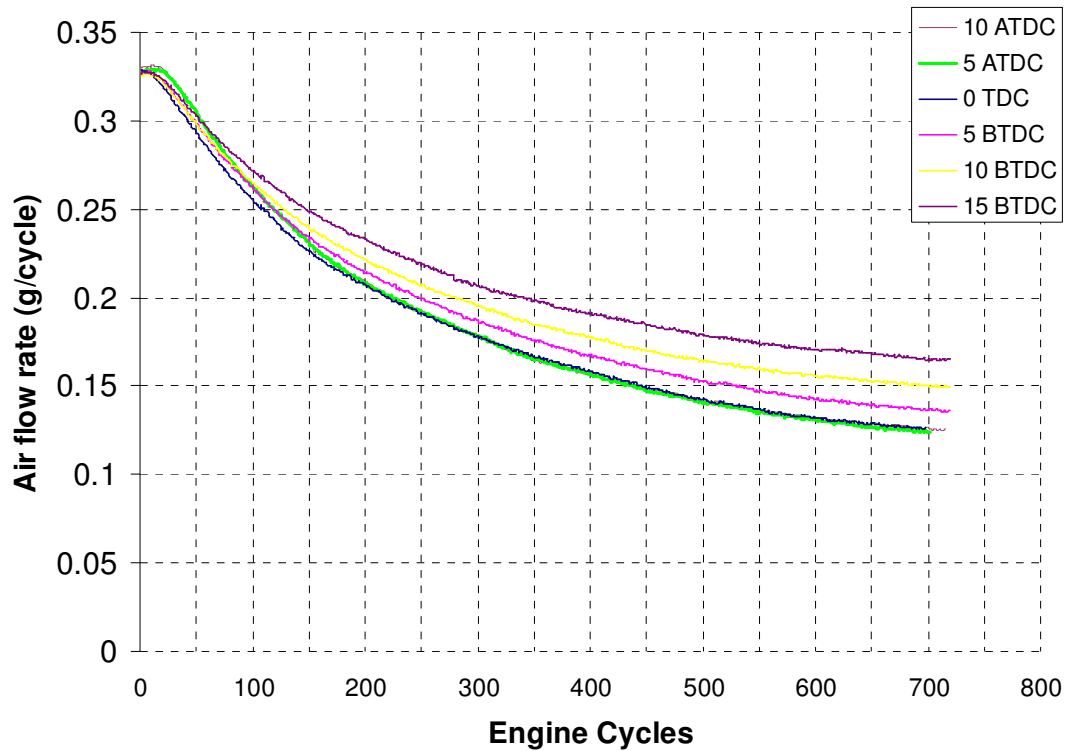


Figure 5.15: Air flow rate for various IVC timing at 1500rpm at an initial tank pressure of 1 bar

Figure 5.16 shows the amount of air mass charged into the airtank between 10° ATDC and 15° BTDC, at intervals of 5°. It is noted that for the first 15 engine cycles, the amount of air mass charged into the air tank which is calculated from the air tank pressure and temperature are slightly higher than the values of air flow rate measured by the intake air flow meter. This is because some air is drawn from the exhaust ports towards the end of the expansion process when the exhaust valves open. However, during the rest of the charging process the amount of charged air into the air tank is less than the intake air into the cylinder due to the contribution of the residual compressed air in the auxiliary chamber.

Figure 5.17 shows of the change of $imep_b$ over 700 engine cycles as the tank is charged from 1 bar for IV1 closing points between 10° ATDC and 15° BTDC, at intervals of 5°. It can be seen from the results that high braking performance is achieved while the IV1 closes at 10° ATDC and 5° ATDC. IV1 closing point is limited to 10° ATDC to avoid collision between the piston and the intake valve.

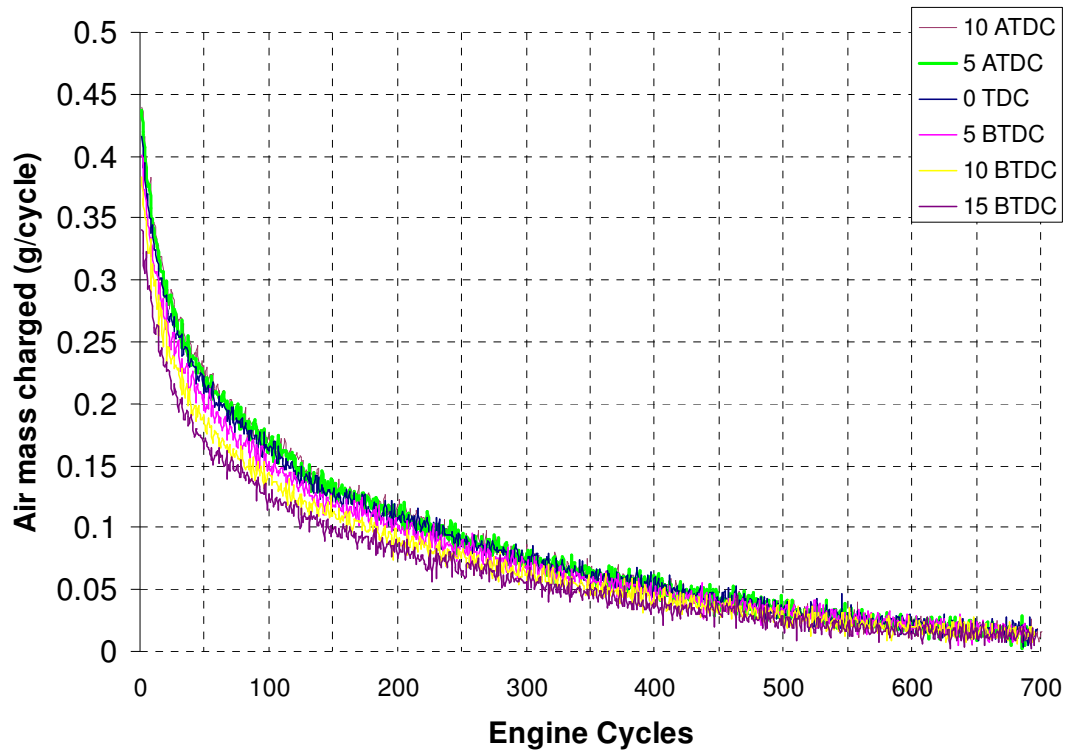


Figure 5.16: Air mass charged per cycle for various IVC at 1500 rpm with an initial tank pressure of 1 bar

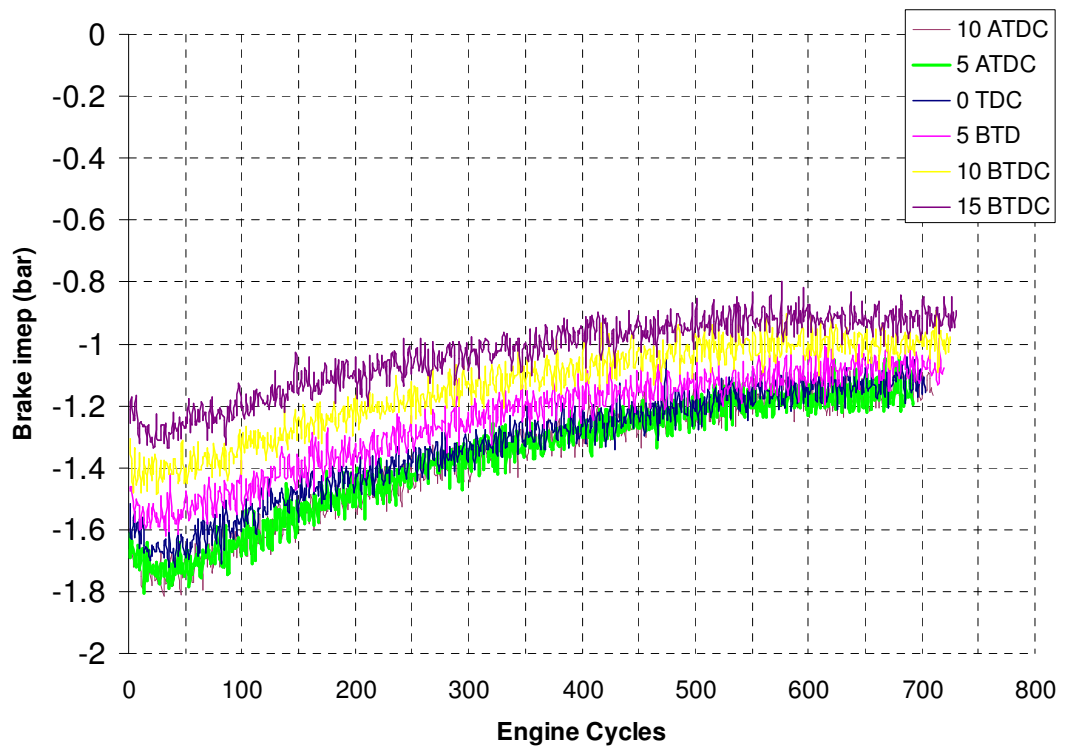


Figure 5.17: Braking imep for various IVC timing at 1500 rpm with an initial tank pressure of 1 bar

5.5 Experiments on the air hybrid engine with a split intake runner block

5.5.1 Principle of the operation

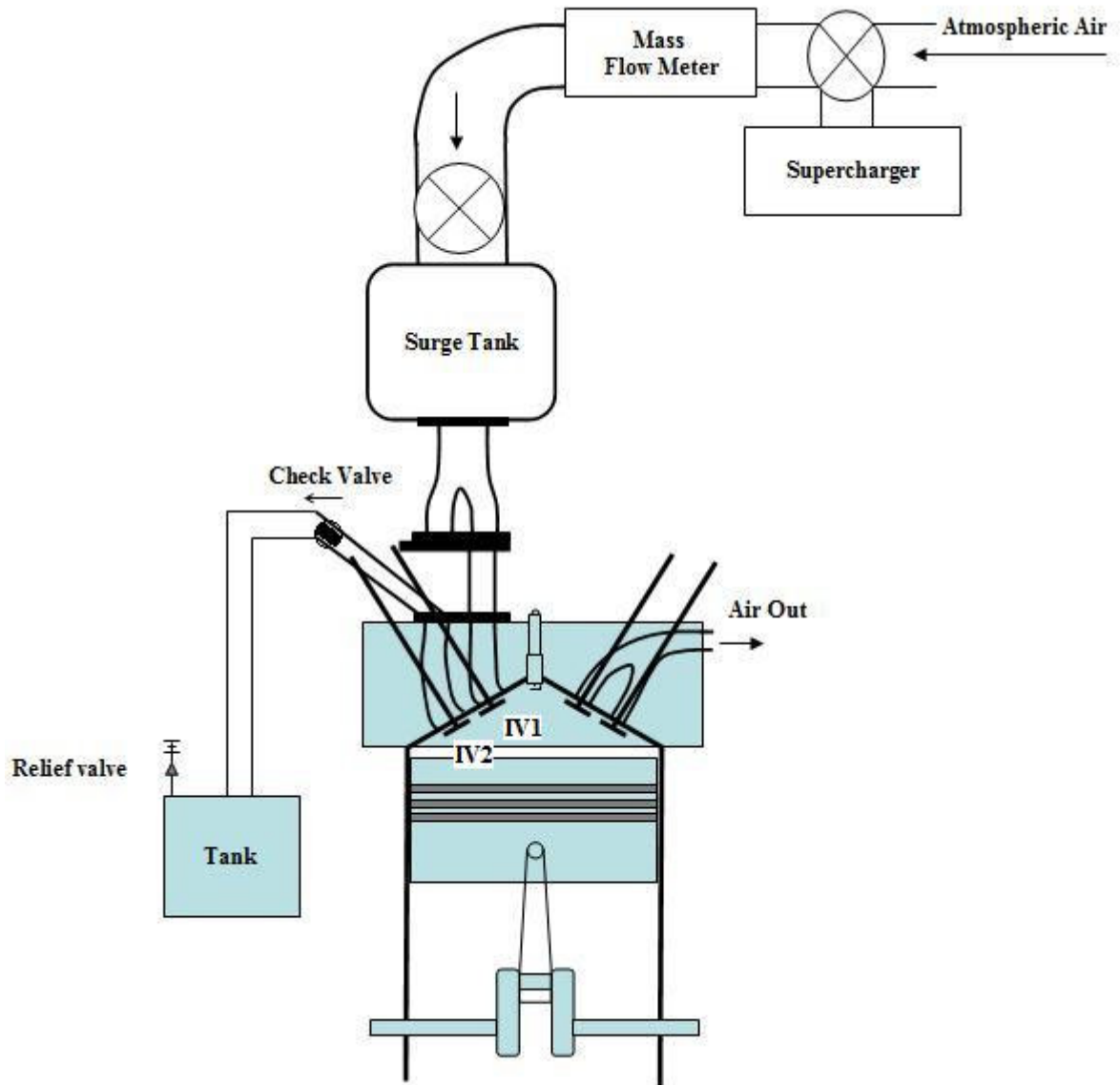


Figure 5.18: Air hybrid engine concept with a split intake runner block

In order to realise the air compression mode with higher compressed pressure in the air tank and hence pneumatic energy density, another modified intake system was designed and fabricated. As shown schematically in Figure 5.18, an additional split intake runner block was installed between the surge tank and the cylinder head. One of the intake ports is disconnected from the intake system and is connected to the airtank via a check valve and a rubber hose. The other intake port is directly connected to the air intake system.

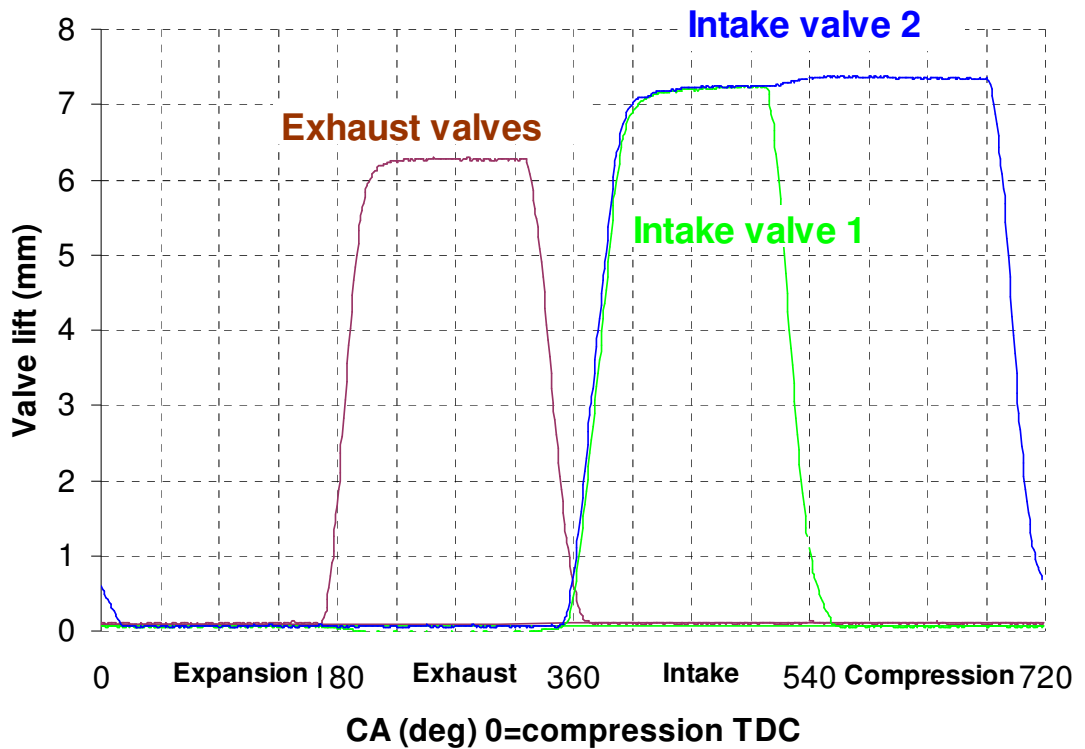


Figure 5.19: Valve timing for IV 2 closing at 15 ATDC at 1500 rpm

As shown in Figure 5.19, Intake Valve 1 (IV1) and the two exhaust valves operate at their default valve timings for the 4-stroke SI engine operation. Intake Valve 2 (IV2) has an extended opening period and remains open in the compression stroke. During the CM operation, air is sucked into the cylinder through intake port 1 and then compressed to the intake port 2 during the compression stroke. The compressed air will then pass through the check valve once the in-cylinder pressure becomes higher than the tank pressure and the charging process will continue until the air tank pressure overtakes the cylinder pressure.

Table 5.3: Dimension of additional air hybrid engine components

R_c for air hybrid mode	4.55:1
Airtank volume	13 litre
Volume between the check valve and one intake port	6.6 cm ³
Reed valve effective flow area	308 mm ²
Check valve diameter	12.7 mm

Comparing to the simulation model in Chapter 3, the throttle valve was eliminated to simplify the experimental setup. The auxiliary chamber includes the volume of one intake port which is 57 cm³ shown in Table 5.1 and the volume between the check valve and the

intake port which is 6.6 cm^3 shown in Table 5.3. According to Equation 3.6, the effective compression ratio is 4.45, which results in a predicted maximum pressure of 8.3 bar, compared to 6.1 bar for the air hybrid engine with a Reed Valve.

5.5.2 Experimental results

During the initial study, the closing time of IV2 was varied to achieve the maximum charging efficiency. Figure 5.20 shows cylinder pressures for various air tank pressures with IV2 closing at 15 ATDC at 1500 rpm. For the tank pressure at 1 bar, the cylinder pressure is the lowest in the diagram as most of air is compressed into the airtank in the compression stroke and cylinder pressure drops to vacuum condition in the following expansion stroke until exhaust valve opens in the exhaust stroke. Since the gas pressure in the auxiliary volume between IV2 and the check valve is at nearly the same pressure as in the airtank, the cylinder pressure suddenly goes up in the beginning of intake stroke as the IV2 opens. The higher the tank pressure, the more pronounced of this pressure rise during the intake stroke.

Figure 5.21 show cylinder pressures for various air tank pressures with IV2 closing at 5 BTDC at 1500 rpm. Compared to the results shown in Figure 5.20, peak cylinder pressures are typically 2 bar higher with IV2 closing at 5 BTDC as there is insufficient time for the compress air to be charged into the airtank completely.

Figure 5.22 shows the sensitivity of the airtank pressure to various IV2 closing points for 700 engine cycles. The highest tank pressures are obtained when IV2 closes at 15° ATDC and 20° ATDC, which was the most retarded timing that could be used without the valve hitting the piston. The results in Figure 5.23 show that the rate of air charge per cycle slows down as the tank pressure rises, as a result of backflow of the residual compressed air from the auxiliary volume as well as less air is compressed into the air tank during the compression stroke. The more rapid decrease in the air flow rate at retarded IV2 closing time is directly related to the faster rise in the air tank pressure seen in Figure 5.22 as IV2 is closed later. By comparing the initial air flow rate in Figure 5.15 for the Reed valve setup and that in Figure 5.23 for the split port configuration, it is noted that the air flow rate in the first three engine cycles is increased from 0.328 gram per cycle to 0.357 gram per cycle with the same IVC of 5° ATDC. Therefore, the presence of a Reed valve leads to an 8.2% reduction in the air flow rate, which would affect engines full load performance and fuel economy.

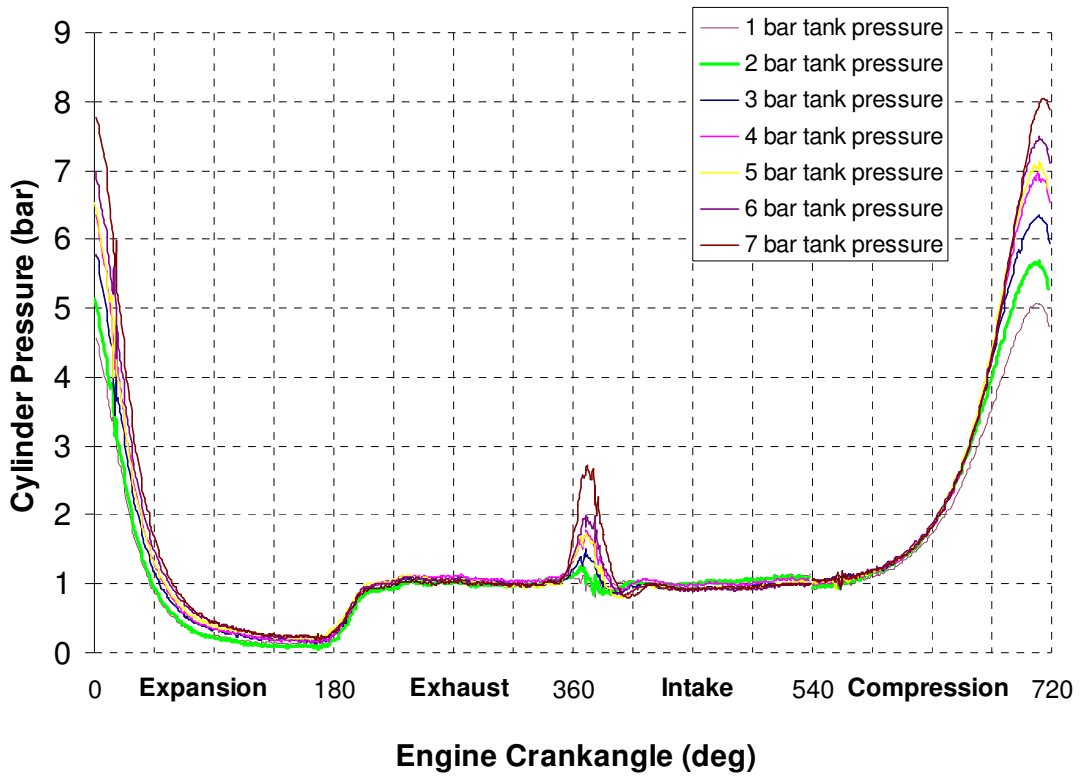


Figure 5.20: Cylinder pressure with IVC at 15 ATDC at 1500 rpm

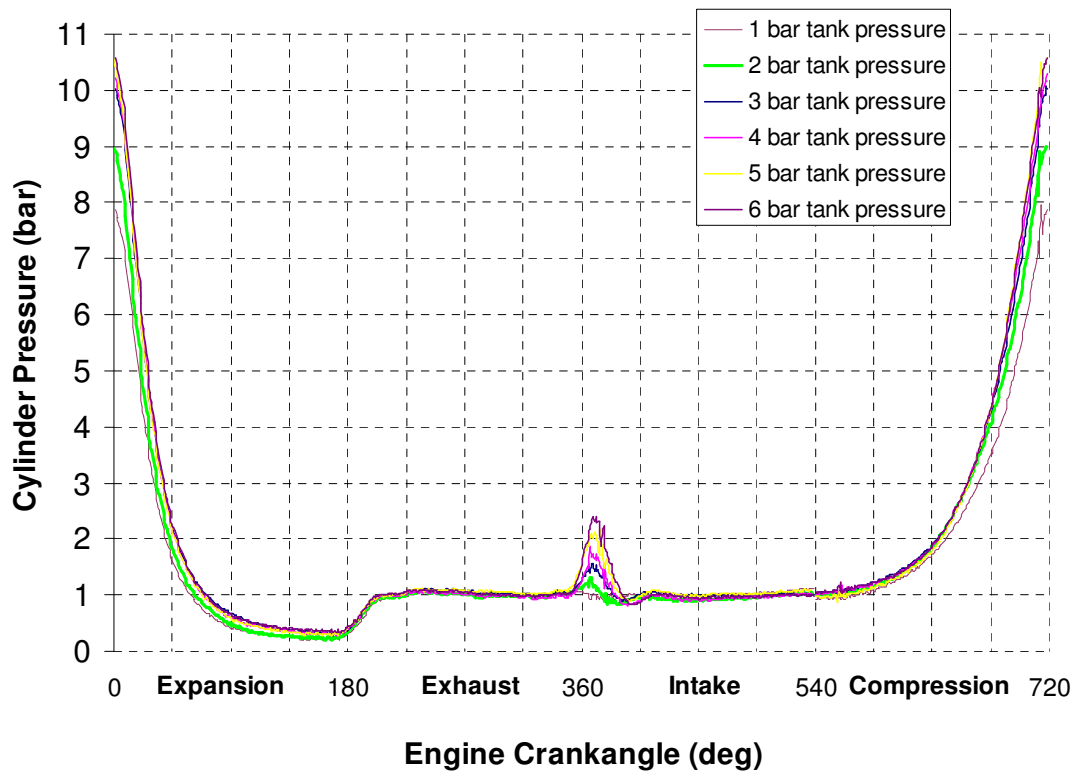


Figure 5.21: Cylinder pressure with IVC at 5 BTDC at 1500 rpm

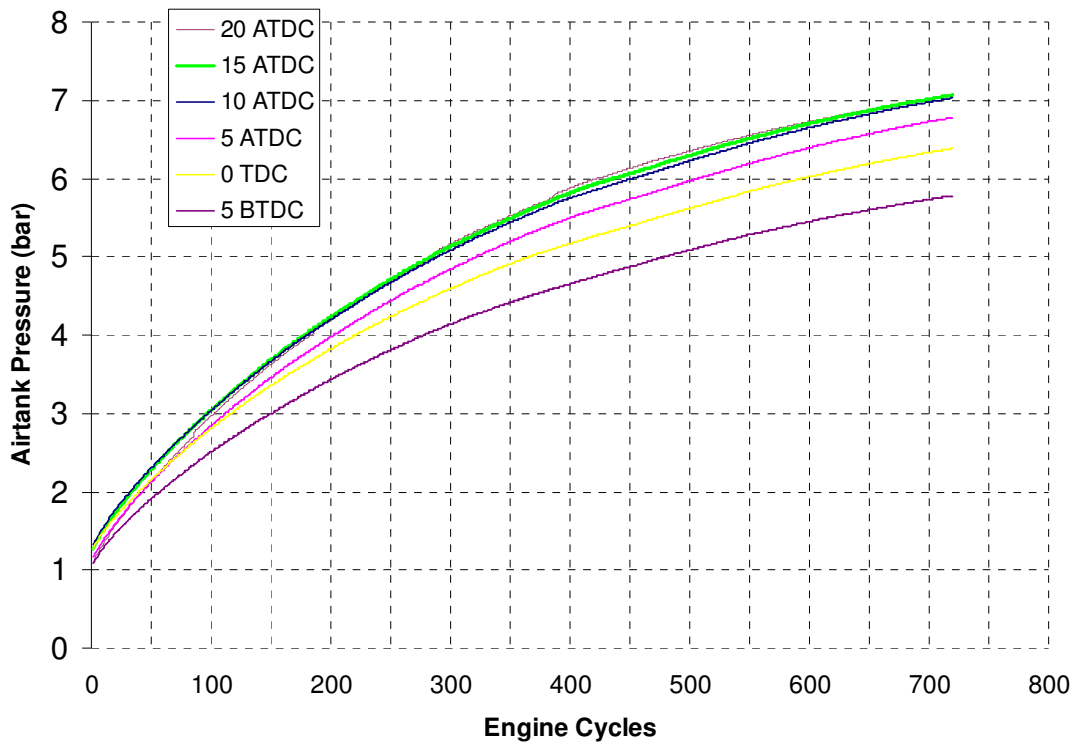


Figure 5.22: Airtank pressure for various IVC at 1500 rpm

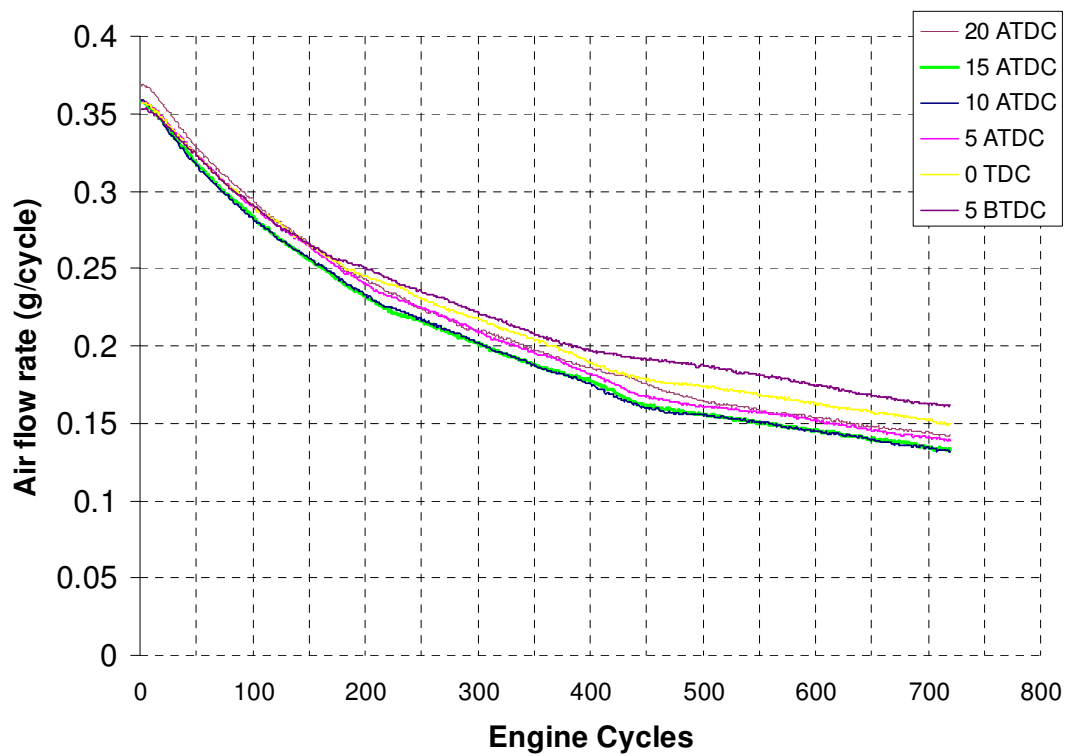


Figure 5.23: Air flow rate per cycle for various IVC at 1500rpm

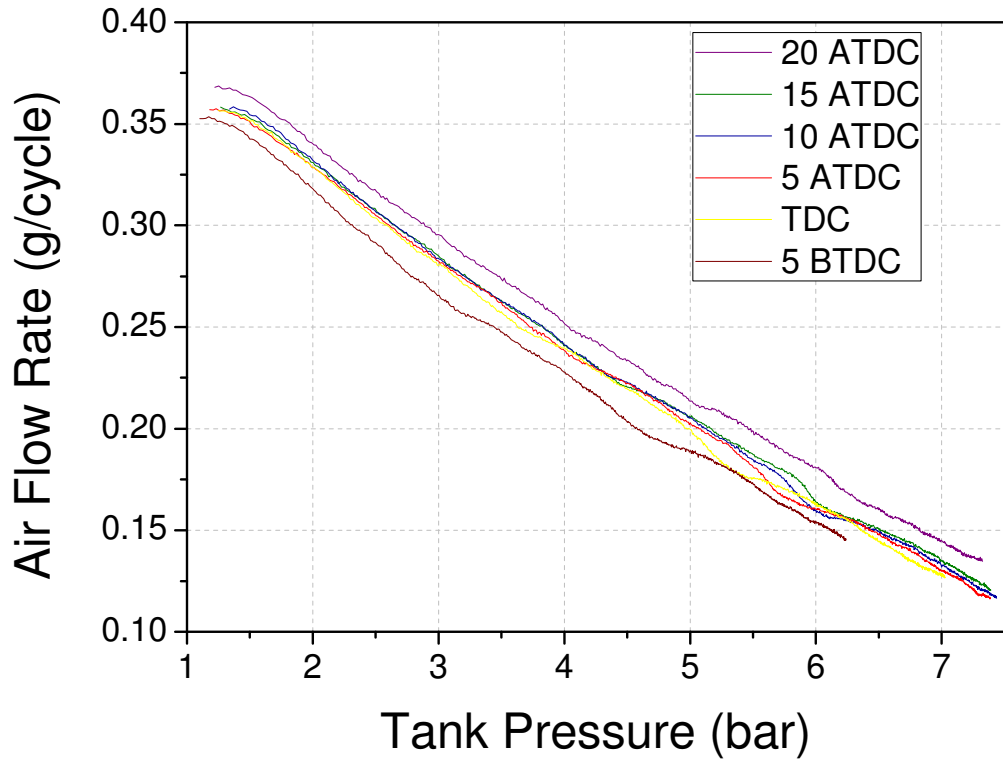


Figure 5.24: Air flow rate against tank pressure for various IVC at 1500rpm

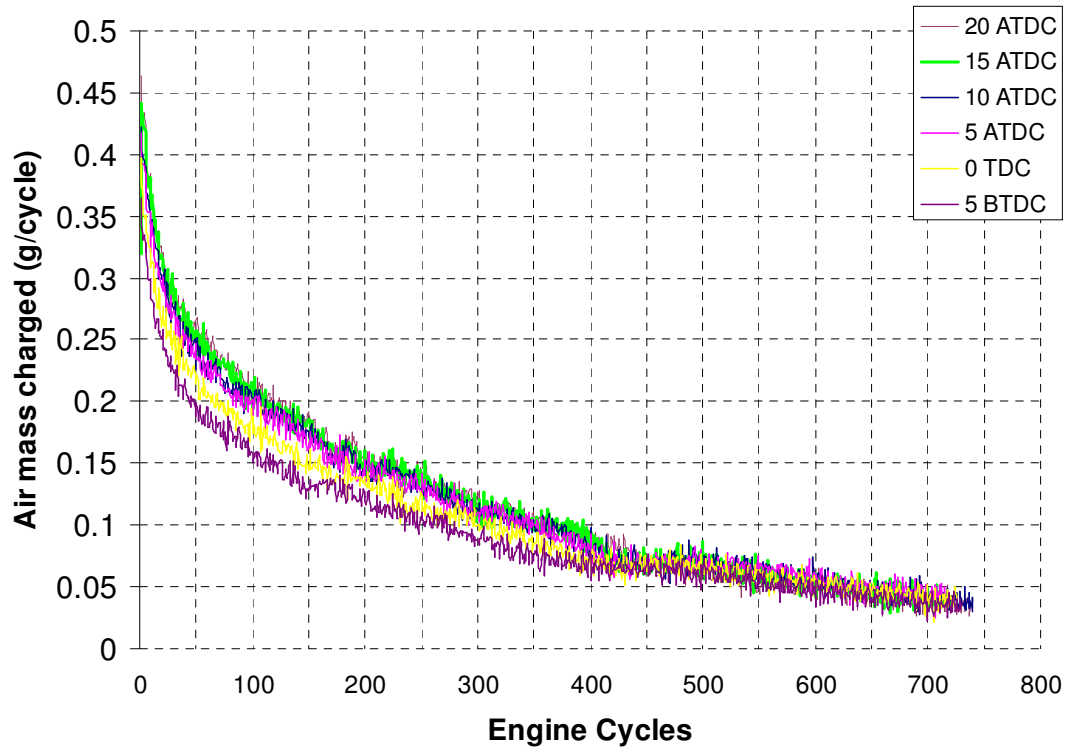


Figure 5.25: Air mass charged into the airtank per cycle for various IVC at 1500 rpm

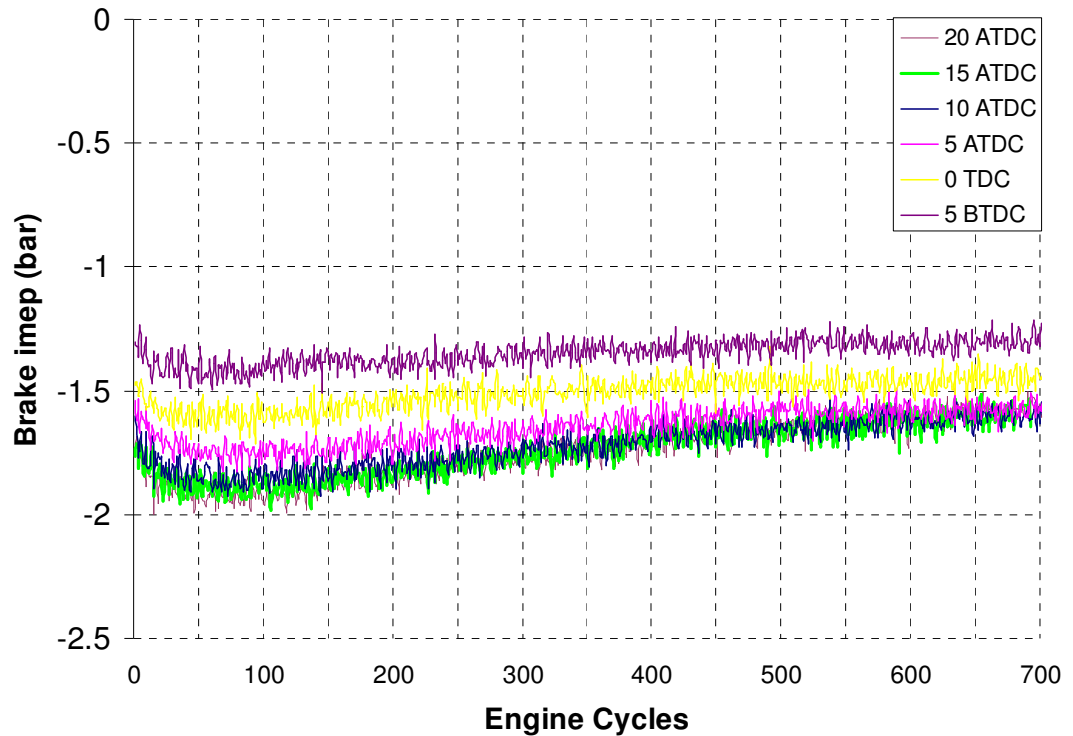


Figure 5.26: Braking imep for various IVC at 1500 rpm from an initial air tank pressure of 1 bar

There are some kinks shown in Figure 5.23 due to the decrement of the tank pressure in every engine cycle is not a constant. Figure 5.24 shows an inverse proportional relationship between the air flow rate and tank pressure since the amount of residual compressed air left in the sandwich box is proportional to the tank pressure. The air flow rate with late IVC is higher than the one with early IVC at the same tank pressure.

Figure 5.25 and Figure 5.26 show values of air mass charged into the airtank per cycle and values of braking imep (Eq.3.1) respectively for various IV closing points in more than 700 engine cycles. As expected, the value of braking imep is proportional to the air mass charged into the air tank.

Based on the results above, the IV2 closing point was fixed at 15° ATDC for the subsequent experiments and the braking torque values at 1500 rpm engine speeds.

Figure 5.27 and Figure 5.28 show air mass charged per cycle and braking imep respectively for various intake throttle valve opening which controls the air flow in to the surge tank for the engine speed between 1000 and 2000 rpm. The intake throttle valve was added to evaluate its effectiveness on the braking torque output during the CM operation

by adjusting the amount of air mass induced and therefore the amount of air charged into the airtank. It can be seen that the amount of compressed air and the braking imep generated are directly proportional to the throttle opening. Therefore, it has confirmed that the use of intake throttle can be an effective means to controlling the engine braking torque in the air hybrid engine operations. This provides the basis of the engine response map of the CM operation comprising engine braking torque values as a function of throttle positions, which is to be used for the vehicle driving cycle analysis to be presented and discussed in Chapter 6.

Table 5.4 shows an engine response map which summarises the tank pressure and the intake throttle valve opening as functions of the flow rate (g/cycle) of air mass charged for the engine speed range between 1000 and 2000 rpm. It shows the engine braking imep rather than engine braking torque for CM because of the larger flywheel as well as higher frictional losses than the production engine. The ability to control the engine braking torque enables the regenerative engine braking to be applied to a wider range of vehicle deceleration operations.

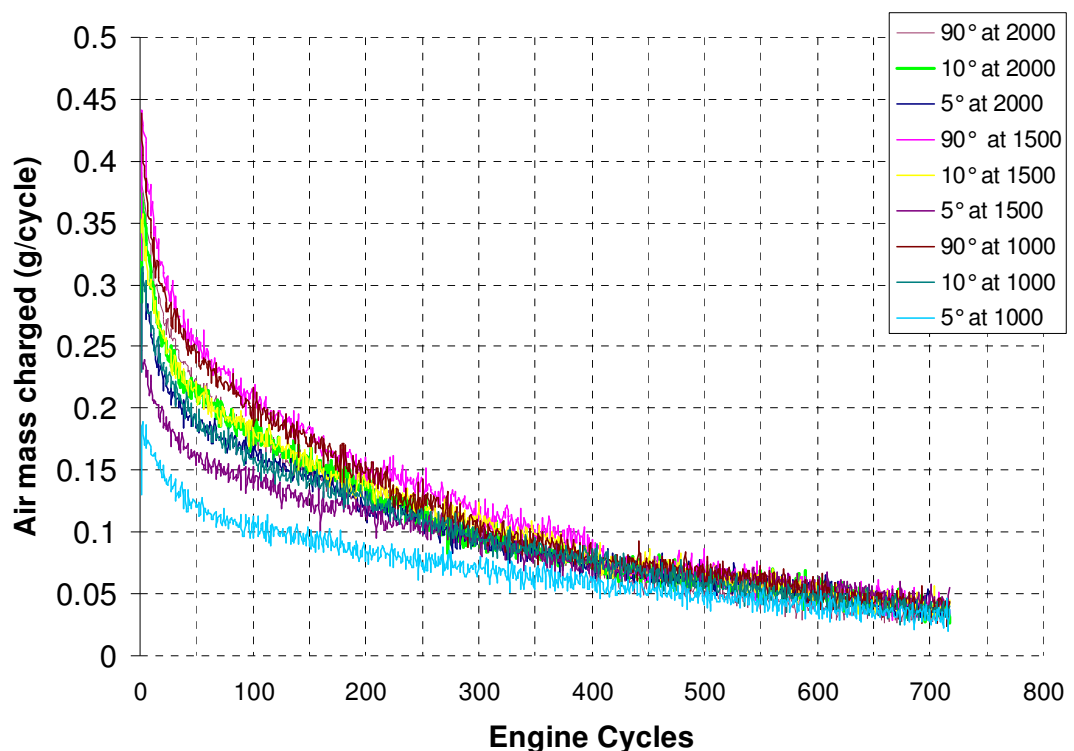


Figure 5.27: Air mass charged per cycle for various intake throttle valve opening for the engine speed range between 1000 and 2000 rpm

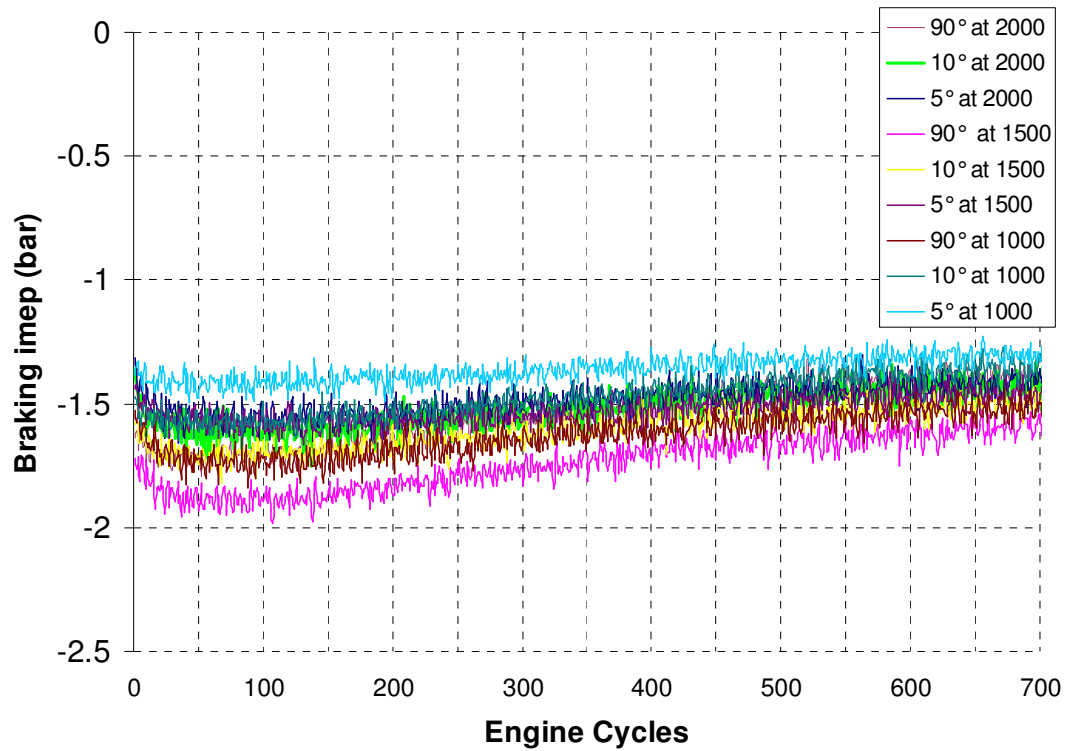


Figure 5.28: Braking imep with an initial air tank pressure of 1 bar for various intake throttle valve opening for the engine speed range between 1000 and 2000 rpm

Table 5.4: Engine response Map for the air hybrid engine with split intake ports for CM

Tank Pressure (bar)	Braking imep (bar)			Air Mass Charged (g/cycle)		
	1000 rpm	1500 rpm	2000 rpm	1000 rpm	1500 rpm	2000 rpm
1 (90°)	-1.52	-1.76	-1.67	0.438	0.44	0.421
1 (10°)	-1.46	-1.58	-1.42	0.229	0.35	0.372
1 (5°)	-1.38	-1.43	-1.31	0.129	0.25	0.259
2 (90°)	-1.82	-1.81	-1.78	0.262	0.274	0.229
2 (10°)	-1.57	-1.7	-1.64	0.172	0.216	0.223
2 (5°)	-1.36	-1.59	-1.62	0.102	0.149	0.181
3 (90°)	-1.69	-1.89	-1.71	0.185	0.2	0.176
3 (10°)	1.49	-1.72	-1.64	0.127	0.169	0.164
3 (5°)	-1.4	-1.65	-1.59	0.075	0.118	0.143
4 (90°)	-1.61	-1.83	-1.67	0.158	0.167	0.147
4 (10°)	-1.48	-1.68	-1.61	0.105	0.128	0.129
4 (5°)	-1.29	-1.58	-1.41	0.041	0.087	0.105
5 (90°)	-1.63	-1.78	-1.57	0.102	0.119	0.09
5 (10°)	-1.4	-1.55	-1.5	0.066	0.088	0.08
5 (5°)	-1.25	-1.46	-1.5	0.019	0.064	0.061
6 (90°)	-1.57	-1.76	-1.48	0.064	0.071	0.051
6 (10°)	-1.31	-1.56	-1.47	0.03	0.061	0.051
6 (5°)	x	-1.44	-1.44	X	0.044	0.034
7 (90°)	-1.43	-1.6	-1.34	0.025	0.045	0.018
7 (10°)	x	-1.45	x	X	0.015	x
7 (5°)	x	x	x	X	x	x

5.6 Evaluation of the engine simulation for the air hybrid engine with a split intake runner block

5.6.1 Engine simulation setup

In order to evaluate the accuracy of engine simulation to predict the air hybrid engine performance using the Ricardo WAVE programme, the single cylinder camless engine has been modelled to operate as an air hybrid engine with a split intake runner block. Figure 5.29 illustrate the air hybrid engine model in WAVE. The left intake port, labelled “intakeport1”, is linked to the intake manifold (“intake_manifold”) via the surge tank (“surge_tank”). The other side of intake manifold is connecting to the atmosphere (“amb1”). The left intake port is the only intake port for inducing air from the intake manifold. The right intake port, labelled “intakeport2”, is connected to the check valve and then through a hydraulic pipe (“hydraulic_pipe”) to a 13 litre air tank (“Airtank”), so that the air compressed can be charged into the airtank. All exhaust ports are connected to a single exhaust pipe to the atmosphere (“amb2”).

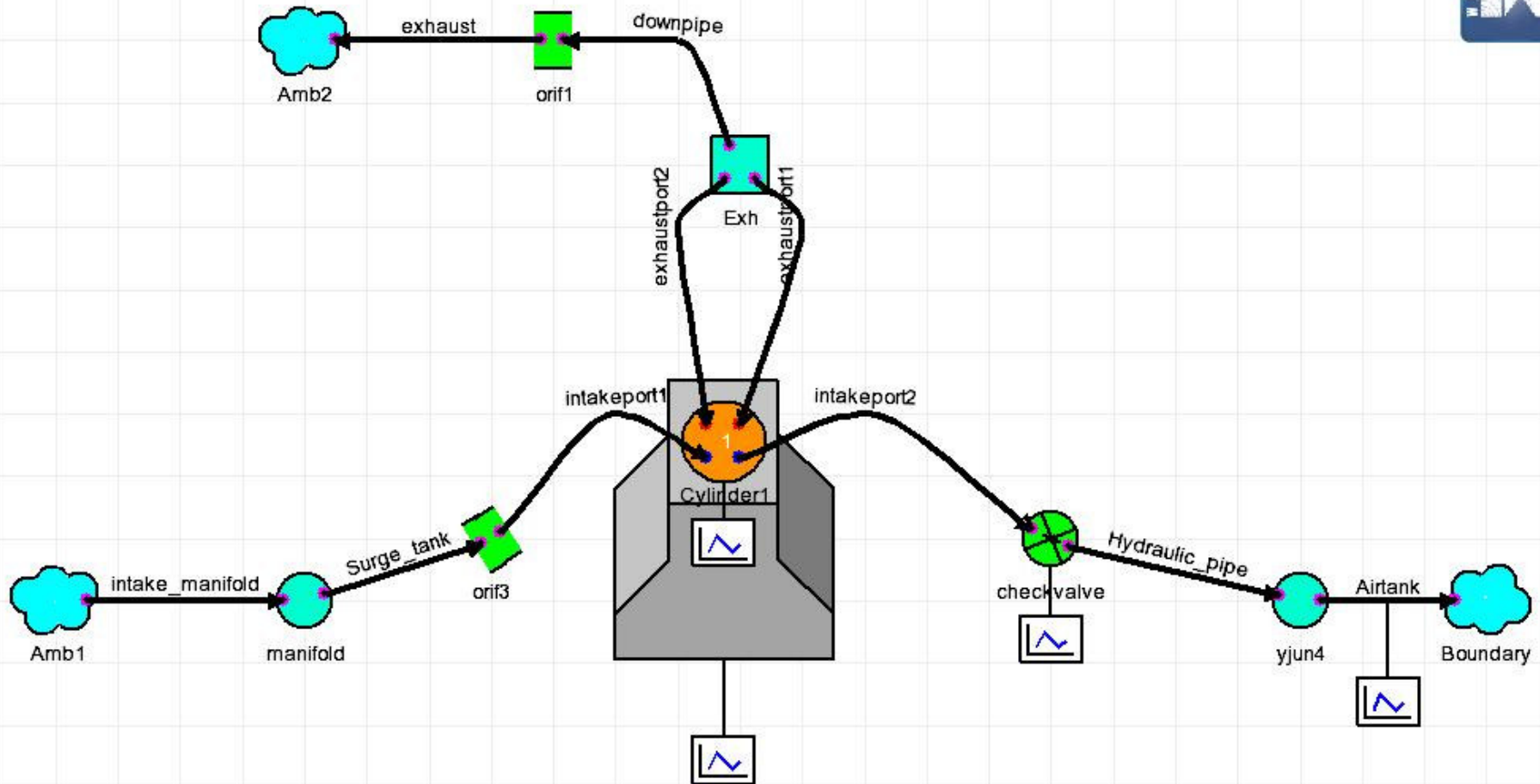


Figure 5.29: WAVE model of the single cylinder camless air hybrid engine

5.6.2 Comparison between predicted and experimental results

The comparison between the experimental and predicted results has been chosen for only one condition to verify the WAVE model. Figure 5.30 shows experimental and predicted airtank pressures at 1500 rpm engine speed over 700 engine cycles. Firstly, both the predicted and experimental airtank pressures start at the same value and follow the same curve the first couple of hundred cycles. There is a slight deviation of less than 0.14 bar between the predicted and measured airtank pressure between 200 and 250 engine cycles. The predicted and measured air tank pressures then remain the same between 300th and 600th cycles. They end up with 0.1 bar difference at 700th engine cycle. Figure 5.31 shows experimental and predicted airtank temperatures at 1500 rpm engine speed for 700 engine cycles. The predicted airtank temperature is higher than experimental airtank temperature between initial status and 600th engine cycles and it shows lower values after 600th engine cycle. The value of the thermal conductivity in the WAVE model is slightly lower than the one in the experiment which makes the speed of heat dissipation is slower in the airtank in the predicted results.

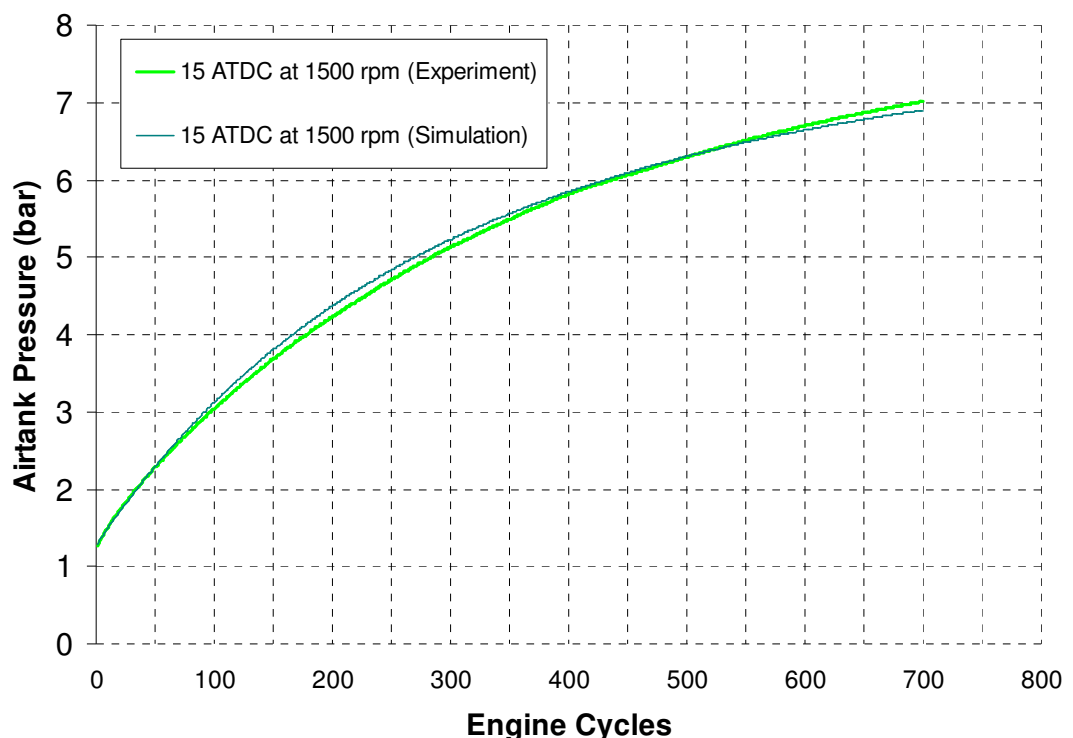


Figure 5.30: Experimental and predicted airtank pressure at 1500 rpm engine speed for 700 engine cycles

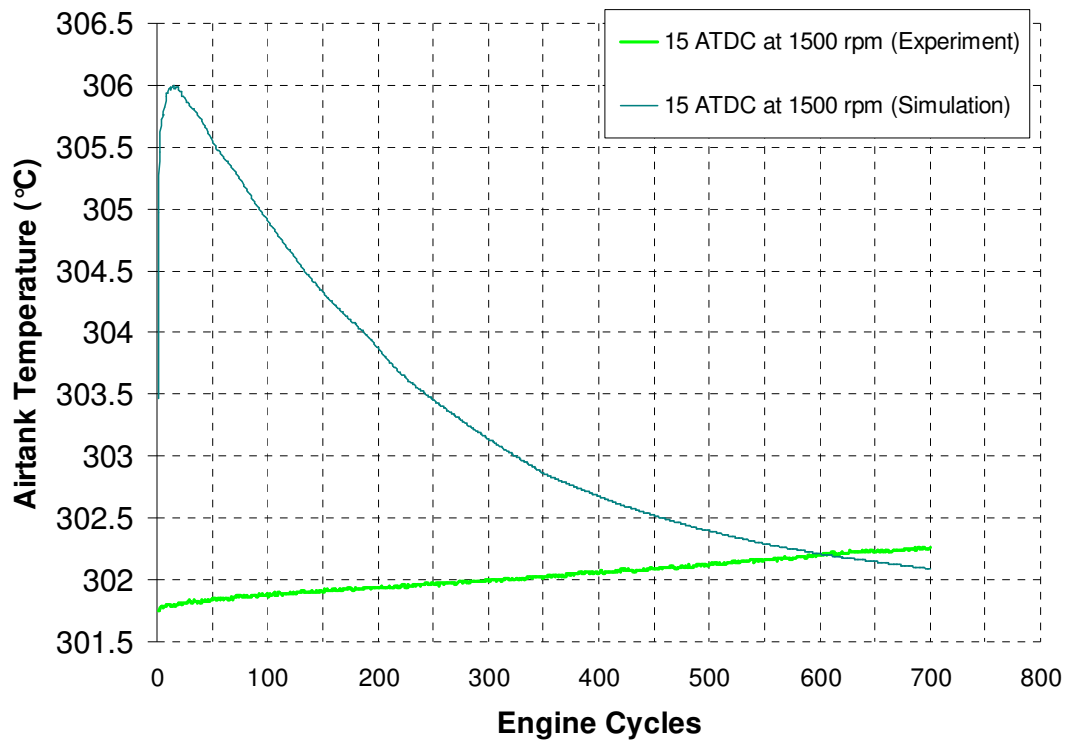


Figure 5.31: Experimental and predicted airtank temperature at 1500 rpm engine speed for 700 engine cycles

Figure 5.32 shows experimental and predicted air mass charged at 1500 rpm engine speed for 700 engine cycles. The largest difference occurs at the start of the charging process, when the measured air flow rate was 0.44 gram per cycle, 0.11 gram higher than the predicted value. This was caused by the difference in the experimental procedure and the modelling in the first 10 cycles. Otherwise, there is an excellent agreement between the measured and predicted air mass charged.

Figure 5.33 shows experimental and predicted braking imep at 1500 rpm engine speed for 700 engine cycles. Comparing to the experimental braking imep, the predicted braking imep is slightly higher than the experimental value by 0.2 bar at the beginning. They then overlap each other for the next couple of hundred engine cycles. Towards the end, the model predicts a slightly higher braking imep than experiment by 0.1 bar.

These results confirm that the air hybrid engine model using Ricardo WAVE can predict accurately the flow and performance characteristics of the compression mode operation during the air hybrid engine operations.

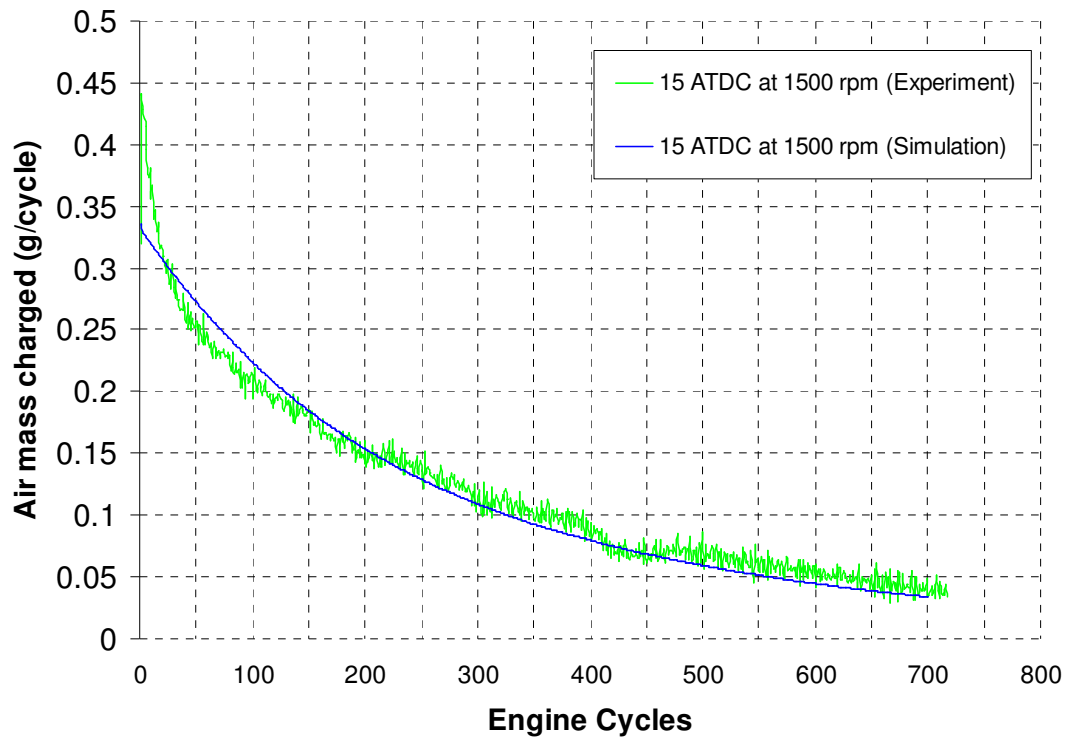


Figure 5.32: Experimental and predicted air mass charged per cycle at 1500 rpm engine speed for 700 engine cycles

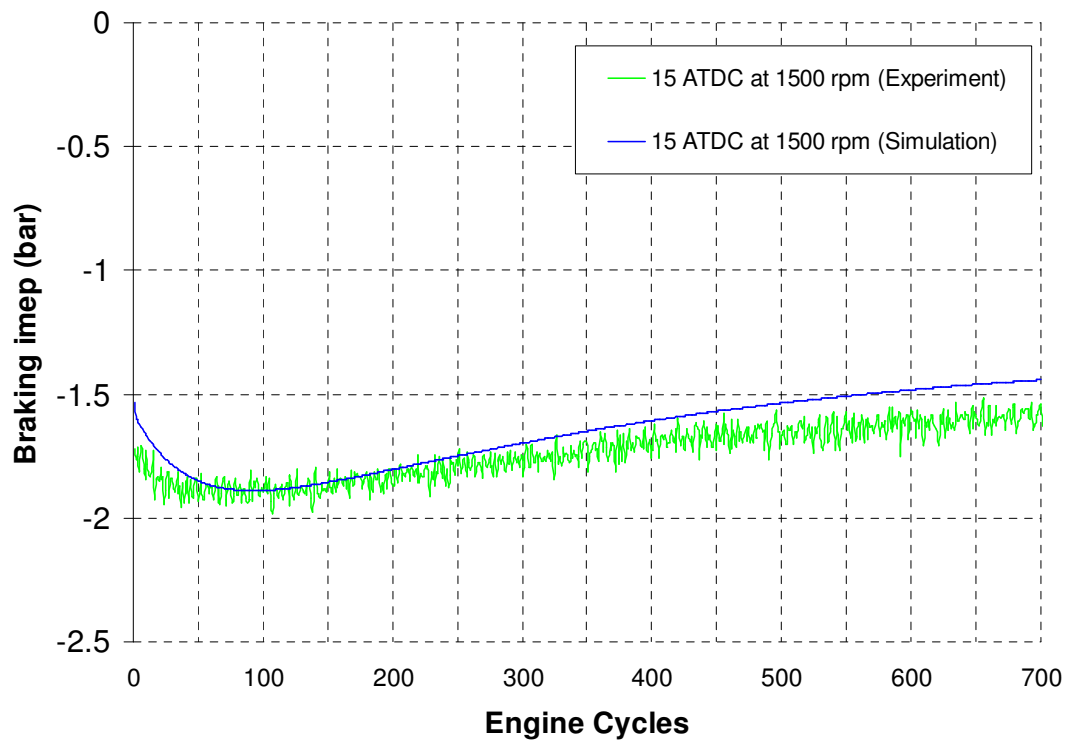


Figure 5.33: Experimental and predicted braking imep at 1500 rpm engine speed for 700 engine cycles

5.7 Summary

In this chapter, the experimental setup has been presented. Two air hybrid configurations have been designed and implemented on a single cylinder camless engine. The results have shown that both configurations were effective in the compression mode operation and could produce and collect compressed air as well as providing engine braking. However, the air hybrid engine with a Reed valve suffers from an 8.2% flow rate reduction than the split port arrangement with a port-throttle. In addition, it has been found that a port throttle valve allows the engine braking torque to be controlled according to the vehicles deceleration operation so that regenerative engine braking can be applied to a wider range of operations as well as the optimised braking performance.

Since the camless engine with a hydraulic system at present is not able to operate with the valve timings for the cranking mode operation while it is stationary, it was not possible to carry out experiments to evaluate its cranking ability of the air hybrid engine. Once such function is enabled, the future work is to achieve the air hybrid engine operations in the normal firing mode, CM and the cranking mode in driving cycles in order to evaluate its effect on fuel consumption and emissions.

Chapter 6: Driving Cycle Analysis of Air Hybrid Vehicles

6.1 Introduction

The air hybrid vehicle recovers the vehicle's kinetic energy and converts it into pneumatic energy during braking by operating the engine as an air compressor. The compressed air can then be used to crank the engine for the stop-start operation. In Chapter 3 and Chapter 4, a Ford Puma 2 litre diesel engine and a YUCHAI YC6A diesel engine have been modelled to operate as an air hybrid engine respectively and their performance has been analysed. In order to evaluate the potential fuel savings of the air hybrid engine technology and the availability of the compressed air for additional usages, a driving cycle simulation program has been developed and applied to a light duty vehicle and a city bus.

6.2 Driving Cycle Simulation Model of an Air hybrid vehicle

6.2.1 Model Overview

A vehicle driving cycle simulation model has been developed and programmed in MATLAB Simulink as shown in Figure 6.1. The symbols used and their physical representations are listed in Table 6.1. In principle, the backward vehicle driving cycle simulation approach has been adopted and it converts the vehicle velocity and the force to drive the vehicle into the engine speed and engine torque demand respectively. It can be seen from Figure 6.1 that the vehicle velocity, $v(t)$, and the vehicle acceleration, $dv(t)$, at every time step, t , during a driving cycle, are the inputs to the following four principal dynamic sub-models: (i) the longitudinal dynamic model, (ii) the aerodynamic drag force model, (iii) the rolling resistance, and (iv) the disturbance force model. The sum of the four forces is used to calculate the traction force and acts as an input to the final drive sub-model for computing the final drive speed and final drive torque demand. The transmission control sub-model then converts the final drive speed and drive torque demand into the engine speed and the engine torque demand.

During the acceleration and cruise operations, the fuel consumption is determined at every time step based on the engine's speed and torque demand, from the engine's fuel





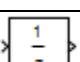
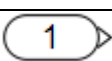
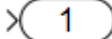




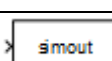

consumption data which comprises data measured experimentally and supplied by the vehicle manufacturer, as given in the Table A1 and A2 in Appendix.

The air hybrid light duty diesel vehicle using the Ford engine consumption data shown in Table A1 has a range between 750 rpm engine speed and 2000 rpm engine speed. The interpolation method is utilized in the range of engine speed given in Table A1. The idle speed of the Ford engine is 750 rpm and the engine will be cranked over 750 rpm engine speed for the stop-start mode which means the engine speed will be zero or more than 750 rpm and therefore the extrapolation method will be only utilized based on this fuel consumption data shown in A1 while the engine speed is above 2000 rpm in the light duty vehicle driving cycle simulation.

The city bus with YUCHAI YC-6A 7.25 litre diesel engine using the fuel consumption data shown in Table A2 has a range between 900 rpm engine speed and 2300 rpm engine speed and a single value of idle fuel consumption at 650 rpm engine speed. The interpolation method is utilized in the range between 900 rpm engine speed and 2300 rpm engine speed given in Table A2. The idle speed of the YUCHAI engine is 650 rpm and the engine will be cranked over 650 rpm engine speed for the stop-start mode which means the engine speed will be zero or more than 650 rpm and therefore the extrapolation method will be utilized based on this fuel consumption data shown in A1 while the engine speed is in the range of 650 rpm and 900 rpm or above 2300 rpm engine speed in the commercial vehicle driving cycle simulation.

In the drive cycle simulation model of the air hybrid vehicle, the vehicle's fuel consumption can be reduced by turning the engine off during the stop-start operation and fuel cut-off in the compressor mode during the deceleration operation. However, since fuel cut-off is used in modern diesel engines, the fuel saving consequent on the air hybrid operation is mainly achieved from the fuel consumption during the engine off period in the driving cycle.

Table 6.1 List of Symbols and their physical representations [62-68]

Block symbol	Block property	Block Description
	Constant	Output the constant specified by the constant value parameter
	Add	To add or subtract inputs
	Product	To multiply or divide inputs
	Abs	To make value 'u' as an absolute value
	Unit delay	To sample and hold with one sample period delay
	In1	To provide an input port for a subsystem or model
	Out1	To provide an output port for a subsystem or model
	Saturation	To limit input signal to the upper and lower saturation values
	Switch	To pass through input 1 when input 2 satisfies the selected criterion; otherwise, pass through input 3
	Lookup table	To perform 1-D linear interpolation of input values using the specified table
	Lookup table (2-D)	To perform 2-D linear interpolation of input values using the specified table
	To workspace	To write input to specified array or structure in MATLAB's main workspace
	Scope	To scope the selected output values

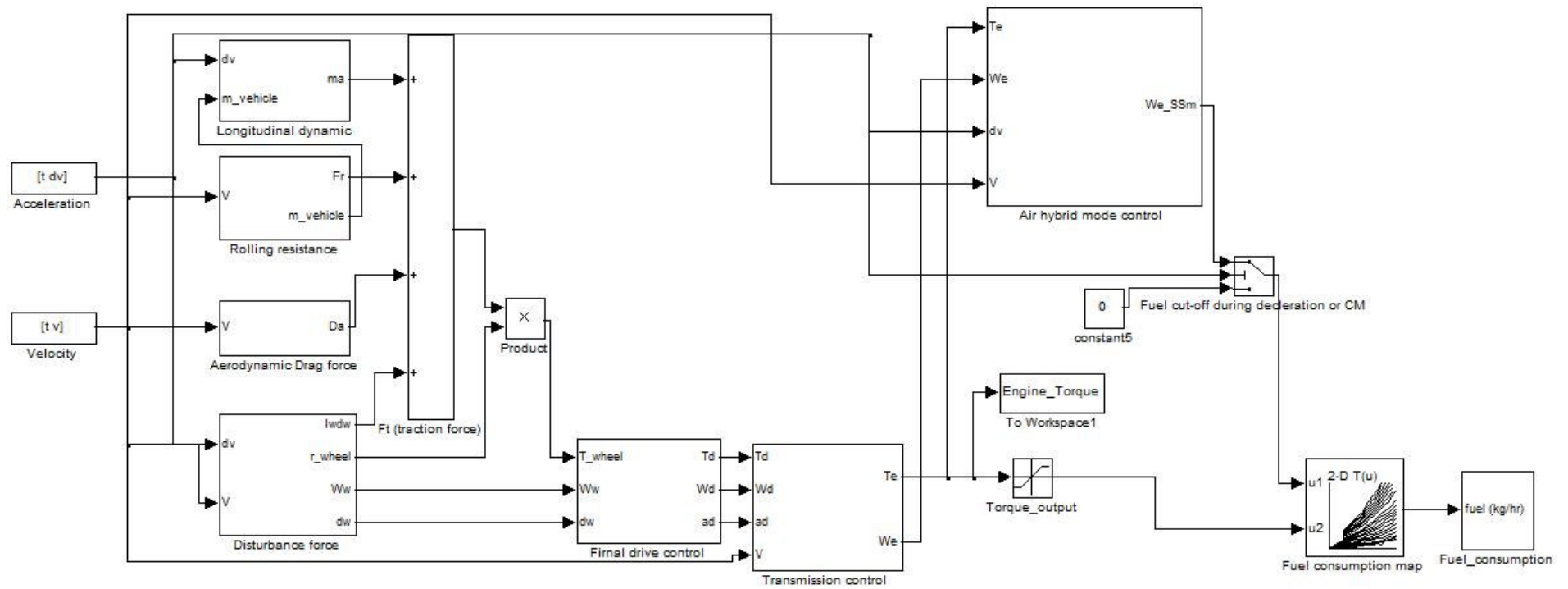


Figure 6.1: Matlab Simulink model of an air hybrid vehicle

6.2.2 Sub-models of normal vehicle operations

6.2.2.1 Longitudinal dynamics sub-model

In order to calculate the mechanical energy consumed by a vehicle in a driving cycle, a numerical driveline model is required. According to Newton's second law, the longitudinal dynamics of a road vehicle is given by

$$m_v \frac{d}{dt} v(t) = F_t(t) - (F_a(t) + F_r(t) + F_d(t)) \quad \text{Equation 6.1}$$

where m_v is the vehicle mass in Kg, t the time step, v the vehicle velocity, F_a the aerodynamic drag force and F_r the rolling resistance, and F_d the disturbance force that summarizes all other not yet specified effect. The traction force F_t is the force generated by the prime mover minus the force that is used to accelerate the rotating parts inside the vehicle and minus all friction losses in the power train. The output of the sub-model is the longitudinal force as determined by the product of the vehicle mass and its acceleration.

6.2.2.2 Aerodynamic drag force

The aerodynamic drag force acting on a vehicle in motion can be modelled as below:

$$F_a = \frac{1}{2} \cdot \rho_a \cdot v^2 \cdot A_f \cdot C_d \quad \text{Equation 6.2}$$

where ρ_a is the density of air, A_f the vehicle frontal area and C_d the aerodynamic drag coefficient. For a full-size passenger car, 0.7 m^2 the product of the A_f and C_d is often used as the average numerical value [69].

6.2.2.3 Rolling resistance

Rolling resistance, generated by a turning tyre, is opposite to the direction of motion and is proportional to the normal force on the tyre print. The value of rolling resistance can be computed by using the following equation:

$$F_r = m_v \cdot g \cdot \mu_r \quad \text{Equation 6.3}$$

where g is the gravitational acceleration and μ_r is the rolling resistance coefficient, which increases with speed as a polynomial function :

$$\mu_r = \sum_{i=0}^n \mu_i v_x^{2i} \quad \text{Equation 6.4}$$

This polynomial function is utilized to fit the experimental data [70]. Practically, the function contains two or three terms of the polynomial would be enough:

$$\mu_r = \mu_0 + \mu_1 v_x^2 \quad \text{Equation 6.5}$$

For most passenger car tyres, the reasonable values of μ_0 and μ_1 are 0.015 and $7 \cdot 10^{-6} \text{ s}^2/\text{m}^2$ respectively [70]. However, any individual tyre should be determined experimentally for obtaining its own data of μ_0 and μ_1 .

6.2.2.4 *Disturbance force*

Disturbance force represents sum of all other resistance forces during the vehicle cruise. The total inertia torque of the wheels, which has been introduced in the disturbance force model, is given by:

$$F_{m,w}(t) = \frac{I_w}{r_w^2} \frac{d}{dt} \omega_w(t) \quad \text{Equation 6.6}$$

where I_w is the rotational inertia of the wheels and axle shafts, r_w the wheel radius and ω_w the speed of all wheels, which are assumed to be identical.

6.2.2.5 *Final drive control sub-model*

Figure 6.2 shows the final drive control sub-model which indicates the process of delivering the torque, generated on the wheels from the traction force with additional inertial losses in the final driveshaft, back to the torque demand in the final driveshaft. The value of torque demand of the final driveshaft can be computed by using the following equation:

$$T_d = \frac{F_t(t) \cdot r_w}{N_f}(t) + I_d \cdot \alpha_d \quad \text{Equation 6.7}$$

where T_d is the torque demand on the driveshaft, N_f the numerical ratio of the final drive, I_d the rotational inertia of the driveshaft and α_d the rotational acceleration of the driveshaft.

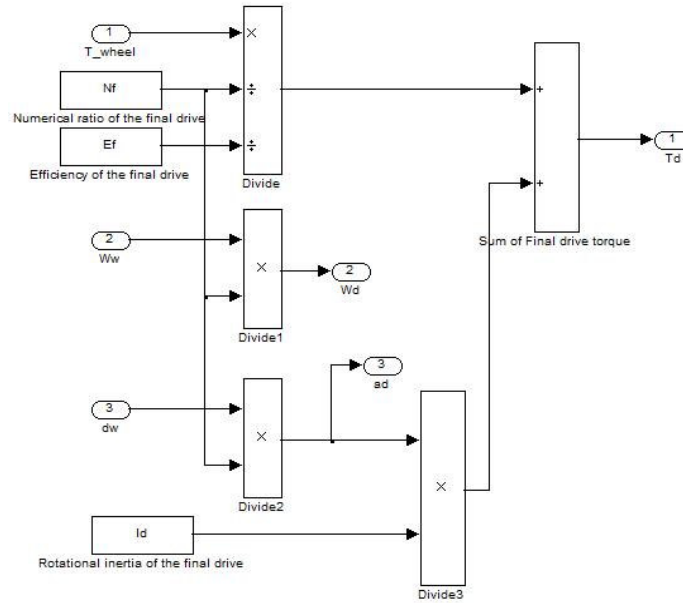


Figure 6.2: Final drive sub-model

6.2.2.6 Transmission control sub-model

Gear shifting points, derived from the vehicle velocity, have been analyzed in a logical control loop shown in the left side of the transmission control sub-model in Figure 6.3. The selected NEDC strategy is identical to that used for the legislative NEDC. Gear shifting in the cycle is performed at vehicle speed set values which are shown in Table 6.2.

Table 6.2: The NEDC strategy

$0 < v(t) < 15$ km/h	ratio=1
$15 < v(t) < 35$ km/h	ratio=2
$35 < v(t) < 55$ km/h	ratio=3
$50 < v(t) < 70$ km/h	ratio=4
70 km/h $< v(t)$	ratio=5

Once the gear number is obtained from the logical control loop, the linked 1D lookup table is capable of discovering the gear ratio in every fixed step simulation time. Furthermore, the torque demand delivered at the engine is the final driveshaft torque divided by the gear ratio of the transmission and is increased by inertial losses in the engine. The value of the engine torque demand can be computed by using the following equation:

$$T_e = \frac{T_d}{N_t} + I_e \cdot \alpha_e \quad \text{Equation 6.8}$$

where T_e is the torque demand on the engine, N_t the numerical ratio of the transmission, I_e the rotational inertia of the engine and α_e the rotational acceleration of the engine.

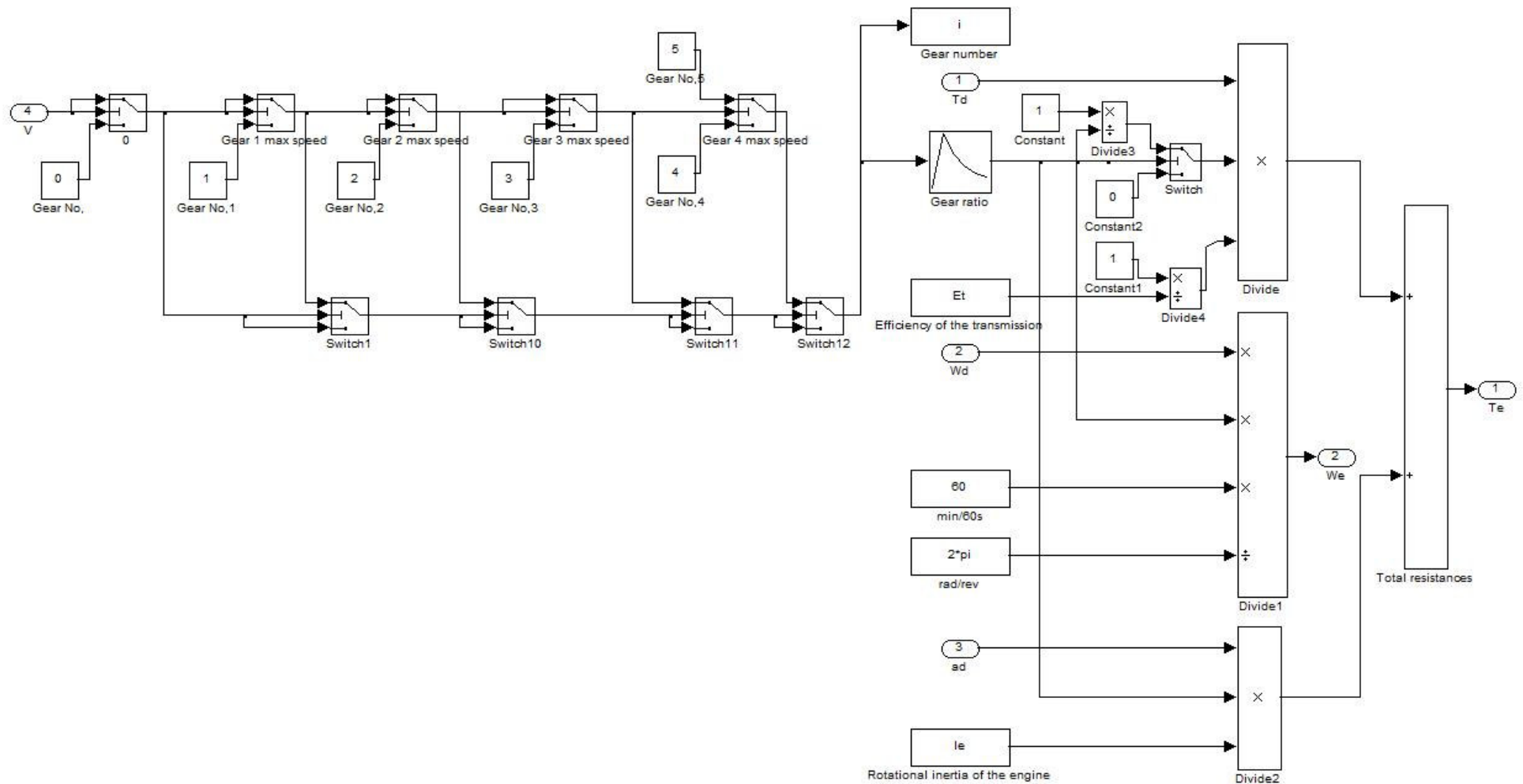


Figure 6.3: Transmission control sub-model

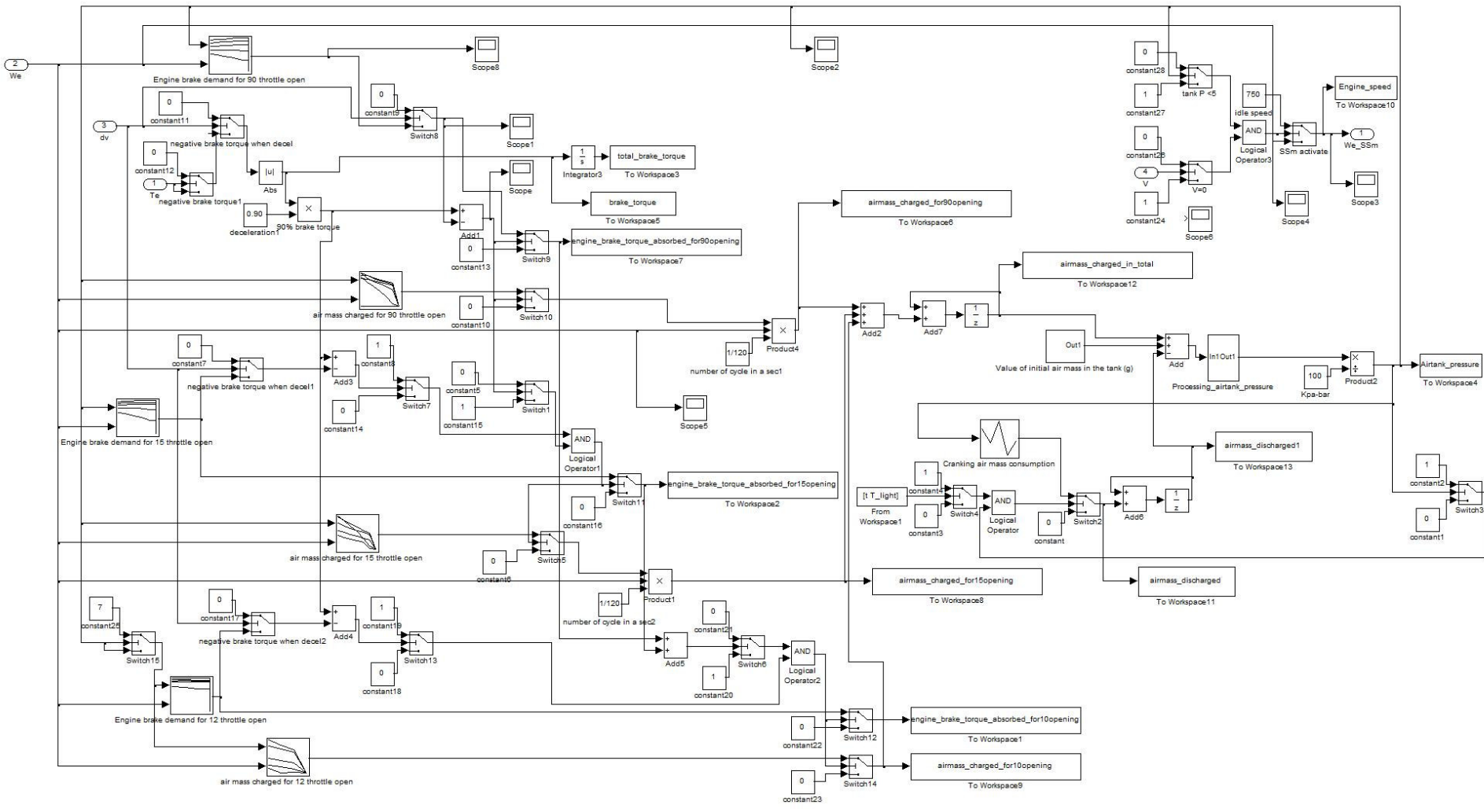


Figure 6.4: Air hybrid mode control sub-model

6.2.3 Air Hybrid Control sub-model

The air hybrid mode control sub-model, shown in Figure 6.4, includes an energy management algorithm, which activates the air compressor mode during deceleration only if the kinetic braking energy is higher than the engine braking torque that can be generated by the compression mode operation. Thus, it is necessary to compute and store the engine braking torque at every engine speed during the whole driving cycle. The air compressor mode is switched on only if the engine braking torque is less than 90% of the kinetic braking energy. The amount of air stored is then computed via the engine's compressor mode response map produced by the air hybrid engine simulation programme described in Chapter 3 or Chapter 4.

In order to capture as much kinetic braking energy as possible, an intake throttle valve has been added to the intake system upstream of the intake manifold so that the amount of air into the engine can be regulated. The maximum engine braking torque in the compressor mode is achieved while the throttle valve is fully open at 90°. When the throttle valve is partial open, it leads to smaller engine braking torque and less air stored in the air tank. By lowering the engine braking torque, a greater amount of kinetic braking energy can be recovered. During the compressor mode operation, three engine response maps for throttle valve opening at 90°, 15° and 12° are included for the three control loops as shown in Fig.6.4.

From the top left to the bottom left, the three control loops have been executed to find out if 90% of kinetic braking energy is bigger than the engine braking torque in the sequence of throttle valve opening at 90°, 15° and 12°. Each loop inputs both the engine speed and the tank pressure into two 2D lookup tables to generate two outputs, the engine braking torque demand and the amount of compressed air storage, by using the interpolation and extrapolation method in every fixed step simulation time during a deceleration phase.

The airtank pressure is an indicator to decide if the stop-start mode is to be activated. The airtank pressure block shown in the right hand side of Figure 6.4 is monitored in the whole driving cycles and the engine is turned off only if the airtank pressure is above the minimum pressure required to crank start the engine while the vehicle is stationary. The response map for the cranking mode will contain the data of engine cranking speed and compressed air mass consumption. The sum of compressed air production during CM and

consumption during the cranking mode determines the airtank pressure, hence a positive value will represent a successful stop-start operation.

6.2.4 Airtank pressure control loop

In order to validate the WAVE model, a comparison between the experimental data and simulation results has been done and presented in Chapter 5. During the experimental studies, it was found that due to heat loss the airtank had nearly constant temperature close to ambient. Therefore, the airtank temperature is assumed to be at the room temperature in the driving cycle analysis. This would be the worst scenario, as in practice, the air tank can be insulated to reduced heat loss and a heat recuperator may be used to maximise the capture of the thermal energy. In addition, the air tank is assumed to undergo the isothermal process during the charging and discharging process. Subsequently, airtank pressure at the end of each braking and motoring engine cycle is described by the following two equations:

$$p_t = \frac{(m_t + m_c) \cdot R \cdot T_t}{V_t} \quad \text{Equation 6.9}$$

$$p_t = \frac{(m_t - m_c) \cdot R \cdot T_t}{V_t} \quad \text{Equation 6.10}$$

where m_c is the mass of the air charge, m_t is the mass of compressed air stored in the airtank, V_t is the airtank volume which is 40 litres in the model and T_t is the temperature of the airtank which has been set 25° Celsius as a constant temperature. This is different from Chapter 3 and Chapter 4, where an adiabatic process was assumed and hence the compressed air would be at higher temperatures. If the heat recuperator is utilized in the model, higher energy regeneration efficiency would be expected.

6.3 Driving cycle analysis of an air hybrid Light Duty Diesel Vehicle

6.3.1 Vehicle data

A Ford Mondeo vehicle with a 2.0litre diesel engine has been chosen for the driving cycle analysis of the air hybrid light duty diesel vehicle. The relevant vehicle data are listed in Table 6.3.

Table 6.3: Ford Mondeo Vehicle data

Kerb weight	1557 kg
Total vehicle weight (2 ppl)	1707 kg
Aerodynamic drag coefficient	0.35
Frontal area	2.48 m ²
Air density	1.225 kg/m ³
Wheel Radius	0.3 m
Rolling resistance coefficient	0.013
Wheel Inertia	0.4
Airtank volume	40 litres
Airtank weight	26.8 kg
Starting tank pressure	6 bar
1st gear ratio	3.077
2nd gear ratio	1.864
3rd gear ratio	1.241
4th gear ratio	0.842
5th gear ratio	0.62
6th gear ratio	0.497
Final drive ratio	4.071
Tyres (rev/km)	518

6.3.2 Engine response map for the compressor mode operation

Table 6.4 Ford Puma Diesel Engine response Map during the CM operation

Tank Pressure (bar)	Engine Braking Torque (Nm)					Air mass charged (g/cycle)				
	100 rpm	500 rpm	1000 rpm	1500 rpm	2000 rpm	100 rpm	500 rpm	1000 rpm	1500 rpm	2000 rpm
4 (90°)	-31.96	-39.42	-46.84	-53.89	-59.21	1.27	1.43	1.44	1.34	1.20
4 (15°)	-31.91	-38.53	-43.05	-46.12	-48.70	1.20	1.18	0.94	0.68	0.49
4 (12°)	-31.90	-37.62	-39.25	-40.41	-42.67	1.18	0.96	0.52	0.28	0.16
5 (90°)	-30.77	-40.11	-48.11	-55.24	-60.49	1.04	1.20	1.33	1.33	1.18
5 (15°)	-30.68	-38.97	-43.75	-46.75	-49.34	1.04	1.04	0.84	0.61	0.42
5 (12°)	-30.71	-37.86	-39.39	-40.41	-42.76	0.99	0.84	0.44	0.21	0.01
6 (90°)	-28.87	-40.49	-48.96	-56.30	-61.61	0.86	1.08	1.22	1.24	1.10
6 (15°)	-28.67	-38.97	-44.13	-47.14	-49.84	0.85	0.93	0.75	0.54	0.36
6 (12°)	-28.85	-37.41	-39.29	-40.25	-42.79	0.83	0.73	0.36	0.14	0.02
7 (90°)	-26.39	-40.19	-49.51	-57.09	-62.51	0.65	0.96	1.12	1.15	1.04
7 (15°)	-26.15	-38.39	-44.29	-47.40	-50.15	0.65	0.81	0.67	0.47	0.30
7 (12°)	x	x	x	x	x	x	x	x	x	x
8 (90°)	-23.47	-39.46	-49.86	-57.74	-63.24	0.41	0.84	1.03	1.07	0.97
8 (15°)	-23.42	-37.72	-44.26	-47.48	-50.38	0.40	0.68	0.61	0.40	0.24
8 (12°)	x	x	x	x	x	x	x	x	x	x
9 (90°)	-20.23	-38.92	-50.03	-58.24	-63.86	0.09	0.72	0.94	1.01	0.91
9 (15°)	-20.33	-37.00	-44.11	-47.46	-50.53	0.10	0.58	0.54	0.34	0.02
9 (12°)	x	x	x	x	x	x	x	x	x	x

The diesel engine is assumed to operate according to 3rd air hybrid engine concept presented in Chapter 3. As explained above, an air hybrid operation engine map needs to be generated prior to the start of the driving cycle analysis. The map is made up the

amount of air mass charged (g/cycle) as a function of both engine braking torque and tank pressure during the compressor mode operation. This engine response map is generated by running steady-state simulations of the engine compression mode operation as discussed in Chapter 3 and it is shown in Table 6.4.

6.3.3 Engine response maps for the cranking mode operation

During the cranking mode operation, compressed air is released from the air tank and allowed to expand in the cylinder in the normal intake stroke to crank the engine, as described in Chapter 3. Assuming the whole cylinder is filled up with the compressed air released from the air tank, the amount of air released from the air tank can be calculated from the ideal gas equation:

$$p_t \cdot V_c = m_c \cdot R \cdot T_t \quad \text{Equation 6.11}$$

where p_t is the absolute air tank pressure, V_c is the volume of the cylinder, m_c is the amount of air mass released from the air tank and T_t is the air tank temperature. During the cranking mode operation, the engine is assumed to be accelerated from standstill to normal idle speed due to the expansion work of the compressed air. Cranking time and the amount of compressed air consumed are dependent on the gas force exerted and cylinder volume at a given speed,

$$F_G = p_t \times A \quad \text{Equation 6.12}$$

where p_t is the air tank pressure and A is the piston area. Assuming that the air tank supplies 10 bar gas pressure on the piston with a diameter of 86 mm, the resulting gas force F_G is 5227N.

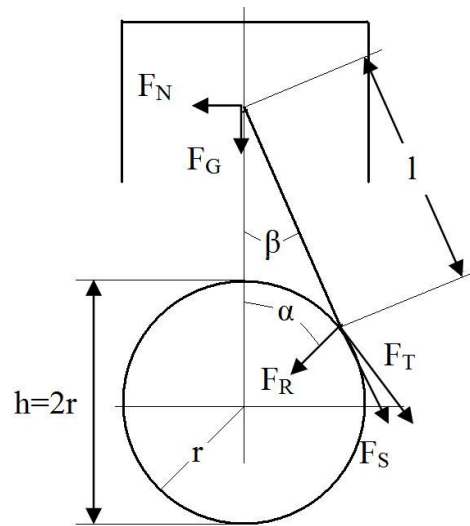


Fig 6.5: Gas-force components shown on a basic crankshaft assembly

Figure 6.5 shows the relation between the gas force F_G and tangential force F_T which could be computed by using Equation 6.8:

$$F_T = F_G \times \sin(\alpha + \beta) / \cos \beta \quad \text{Equation 6.13}$$

where α is the crankshaft angle and β is the pivoting angle of the connecting rod. Values of tangential force F_T , vary with the crank angle (CA) and could be computed from Equation 6.14, 6.15 and 6.16 shown below.

$$\sin \beta = \lambda \sin \alpha \quad \text{Equation 6.14}$$

$$\cos \beta = \sqrt{1 - \lambda^2 \cdot \sin^2 \alpha} \quad \text{Equation 6.15}$$

where λ is the ratio of the half stroke γ and the length of the connecting rod l , i.e.

$$\lambda = \gamma / l \quad \text{Equation 6.16}$$

Gas torque T_G is computed by using

$$T_G = F_T \times r \quad \text{Equation 6.17}$$

from which the angular acceleration, $d\omega/dt$, can be calculated as follows.

$$T_G - T_F = I \frac{d\omega}{dt} \quad \text{Equation 6.18}$$

where, T_F is the friction torque, I is the moment of engine inertia., The friction torque T_F is calculated by the 1-D engine simulation model in WAVE to have a constant value of

11.18Nm for the 2.0litre diesel engine during the cranking operation. The value of the friction torque varies with engine speed and temperature. In [58], it shows the temperature is a significant factor which affects the value of the friction torque. The limitation has been shown in this simple simulation due to the utilization of the constant value of the friction torque. According to Table 6.5, the moment of engine inertia for Ford PUMA 2 litre diesel engine is set to 0.17 kg*m².

Table 6.5: Typical specific engine inertia [71]

Engine Type	Specific Inertia [kg*m ² /l]
Racing gasoline	0.01
Motorcycle	0.03
Light duty, single flywheel	0.085
Light duty, dual flywheel	0.11
Heavy duty diesel	0.18

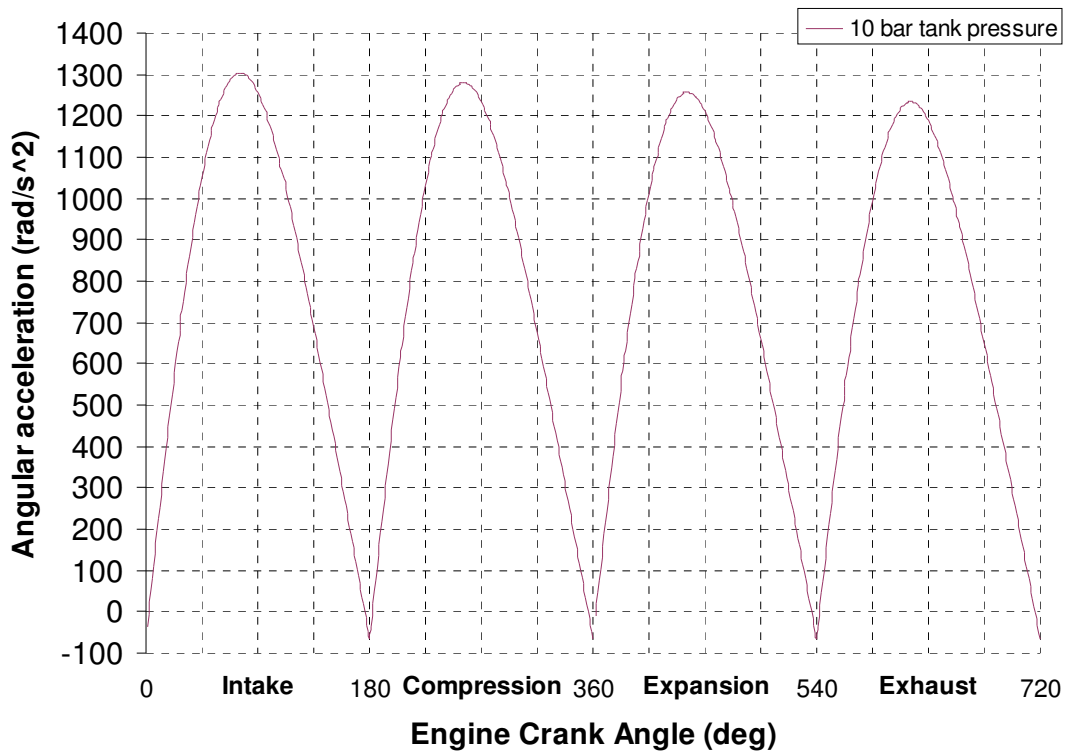


Figure 6.6: Angular acceleration against engine crank angle

For the cranking mode, values of the angular acceleration $d\omega/dt$ are shown in Figure 6.6 at the tank pressure of 10 bar during one engine cycle. It is noted that peak values of the angular acceleration gradually decrease from the intake stroke to the exhaust stroke because the compressed air in the airtank is released into the four cylinders in the same sequence as engine firing order, starting from Cylinder 1 in its intake stroke. Negative

values of the angular acceleration happened for engine crank angles around TDC and BDC when gas torque is smaller than the friction torque.

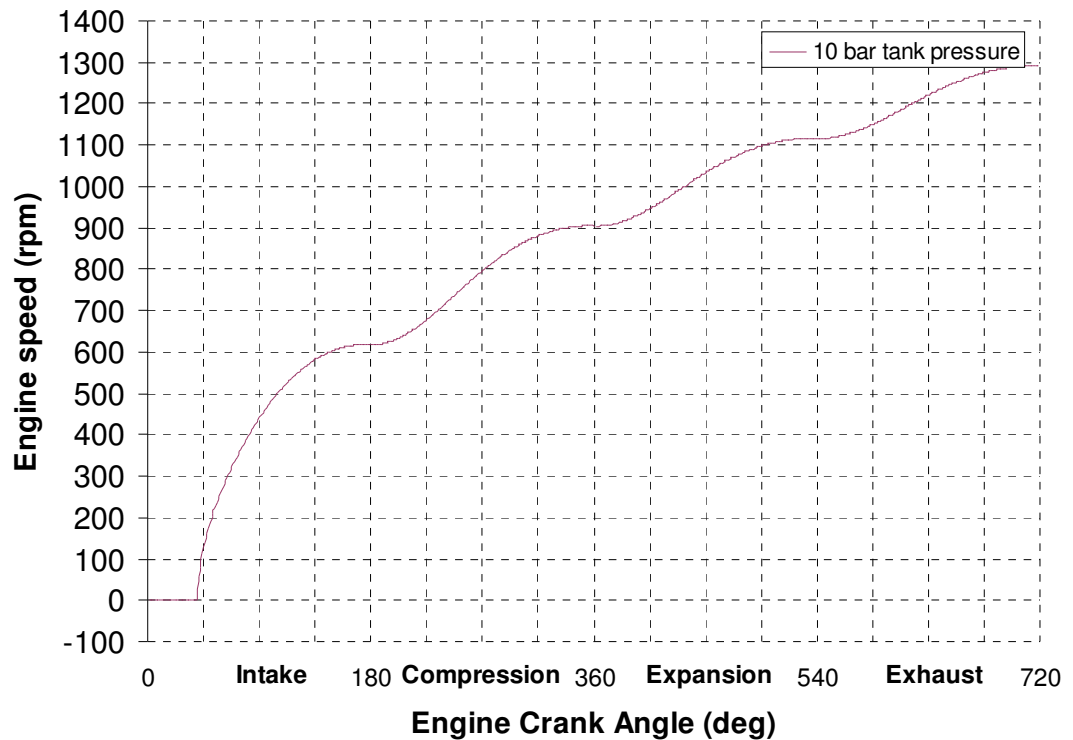


Figure 6.7: Engine cranking speed against engine crank angle

Figure 6.7 shows the engine cranking speed against engine crank angle assuming the starting position of Cylinder 1 at 40° ATDC in the intake stroke. The cranking order is Cylinder 1, Cylinder 3, Cylinder 4 and Cylinder 2 in one engine cycle. The results show that it takes 160 ms for this engine to reach 1290 rpm engine speed at 10 bar air tank pressure. This seems in line with the experimental observations reported in [49], in which a twin cylinder engine was cranked to 1500 rpm in less than 100ms by compressed air through a dedicated electro-hydraulic actuated valve at 10 bar tank pressure. Figure 6.8 shows the predicted engine cranking speed for the tank pressure range between 5 and 10 bar, at interval of 1 bar. It is noted that it takes 67 ms for the engine to reach 617 rpm during the intake stroke of Cylinder 1 at the tank pressure of 10 bar. This is followed by another 39ms before it reaches 904 rpm during the intake stroke of Cylinder 3. Thus, it takes a total 106 ms to crank start the engine to 904 rpm. Since the normal idle speed is 750 rpm, only the first two cylinders (cylinders 1 and 3) need to be operated in the cranking mode by the compressed air at the airtank pressure of 10 bar. Once the engine has reached the idle speed after the first revolution, the control valve can be turned off whilst the engine valve train could be switched from the cranking mode to the normal firing

mode. The air mass consumption and the engine idle speed at various airtank pressures will be discussed in the next paragraph.

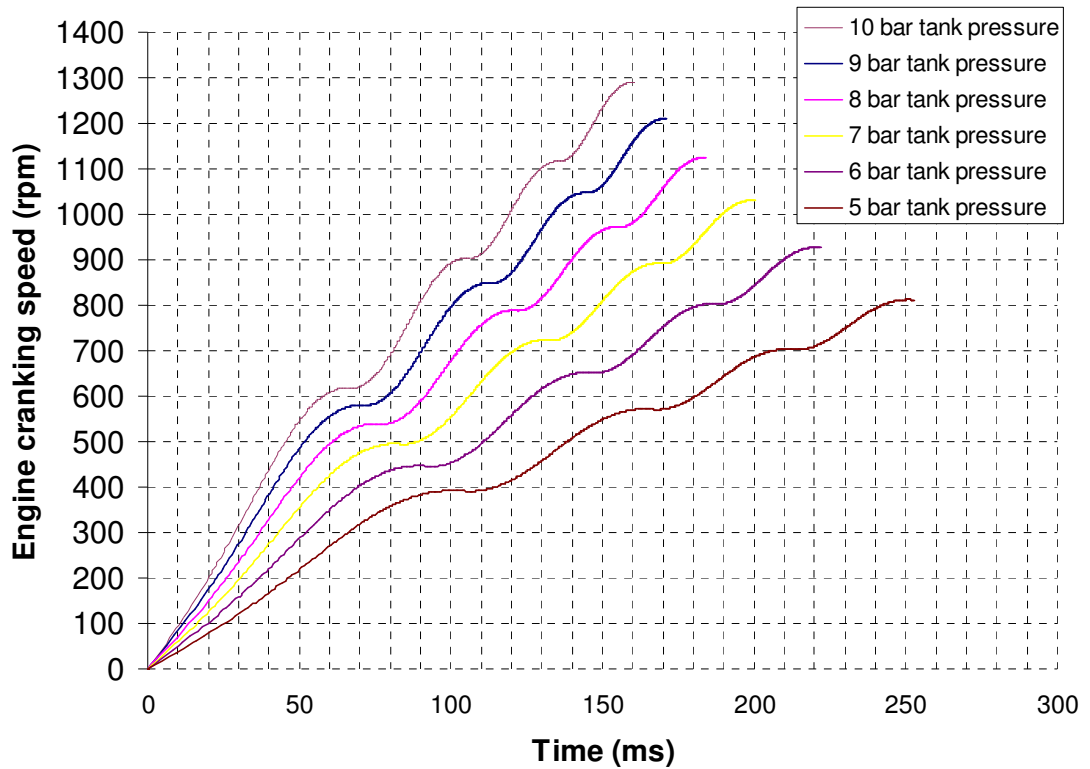


Figure 6.8: Engine cranking speed against time for one engine cycle

Table 6.6: Ford Puma Engine response Map for the cranking mode

Tank Pressure (bar)	Time consumption (ms)	Released air mass (g)	Final engine speed (rpm)	Numbers of cylinders cranked
10	97.6	14.5	904	2
9	113.4	13.0	848	2
8	121.9	11.6	787	2
7	169.5	15.1	891	3
6	187.8	12.9	802	3
5	252.9	14.3	811	4

Table 6.6 shows the engine response map for the cranking mode. The minimum engine speed is 750 rpm in the range of the tank pressures. Numbers of cylinders cranked by the compressed air are dependent on the air tank pressure. The cranking period is consequent upon the angular acceleration and numbers of cylinders cranked. Compressed air consumption during cranking is then determined by the tank pressure and numbers of cylinders cranked. The minimum tank pressure of 5 bar has been chosen so that the engine can be cranked to above 800 rpm in 252.9 ms in an engine cycle. The maximum tank pressure of 10 bar has been chosen for the safety issue and therefore the relief valve can be

activated at the 10 bar pressure on the air tank. This engine response map is implemented in the air hybrid control sub-model.

6.3.4 New European Driving Cycles for light duty vehicles

The NEDC is a driving cycle consisting of four repeated ECE-15 driving cycles and an Extra-Urban Driving Cycle (EUDC) which occupied 780 and 400 seconds respectively. The cycle pattern can be seen in A2 in Appendix.

ECE-15 is an urban driving cycle including characteristics an average speed of 18.7 km/h, a maximum speed of 50km/h and a distance of 4.052 km for duration of 195 seconds. The city driving conditions are characterized by low vehicle speed, low engine load and low exhaust gas temperature. The cycle pattern can be seen in Figure A3 in Appendix.

The EUDC is a high speed driving mode. It consists of an average speed of 62.6 km/h, a maximum speed of 120km/h and a distance of 6.955 km for duration of 400 seconds. The cycle pattern can be seen in Figure A4 in Appendix. For low power vehicles, the maximum speed of alternative EUDC cycle is 90 km/h. It can be seen in Figure A5 in Appendix.

6.3.5 Results and analysis

6.3.5.1 Air Hybrid Vehicle Speed and Load Analysis

Figure 6.9 shows the engine speed profiles during the NEDC for the air hybrid vehicle operation (blue line) and the normal vehicle operation (brown line). The difference between these two vehicle operations is that the air hybrid engine is switched off whilst the engine idles at 750 rpm engine speed when the vehicle is stationary.

Next, the engine load is calculated and shown in Figure 6.10. The negative brake torque regions correspond to the deceleration period and their values represent the braking energy that could be recovered.

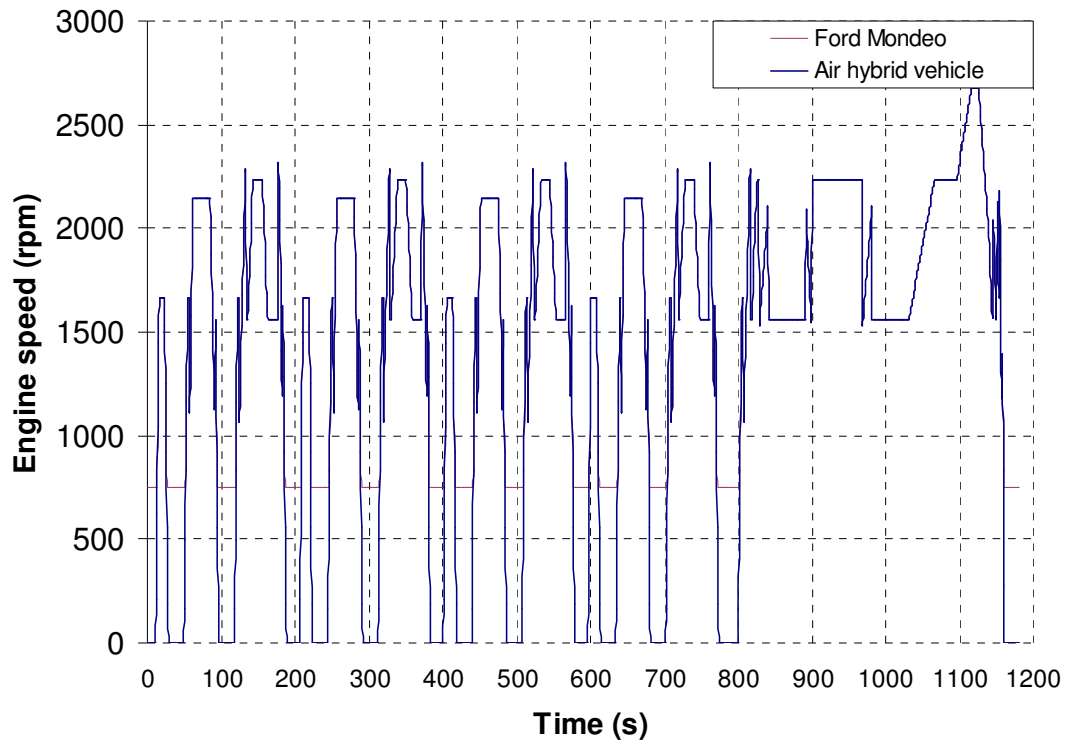


Figure 6.9: Engine speed throughout the NEDC

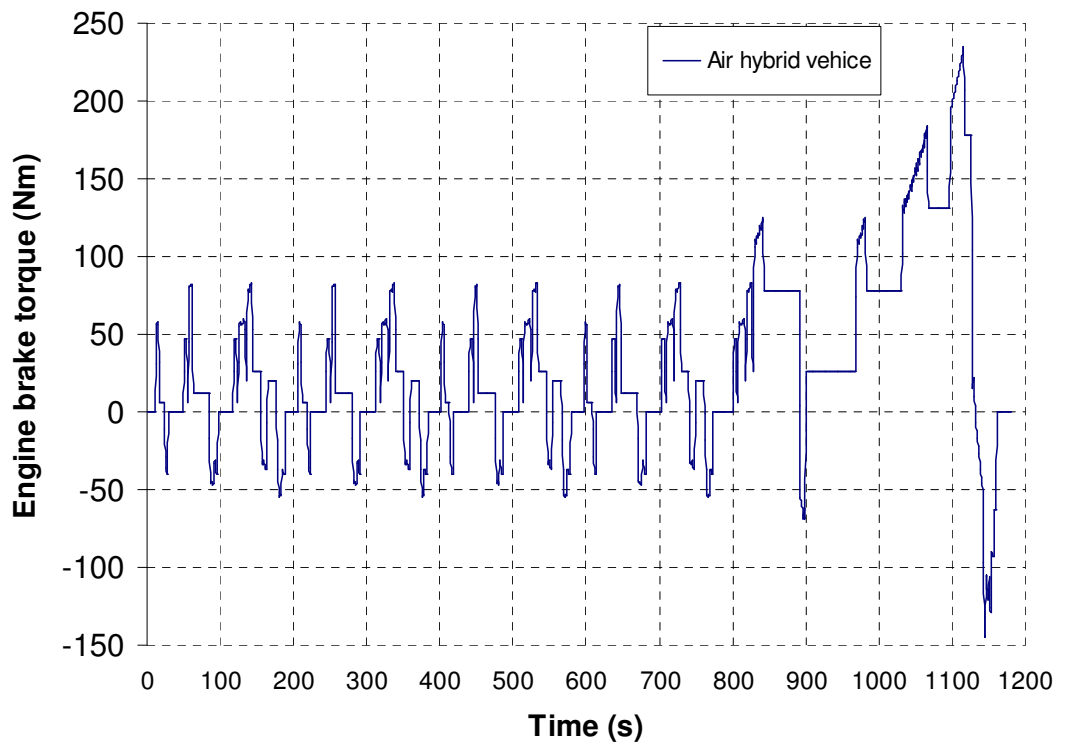


Figure 6.10: Engine load during the NEDC

6.3.5.2 Compression braking

In order to illustrate the amount of braking energy that can be recovered during the compression mode operation, Figure 6.11 shows the engine compression torque in relation to the engine load for wide open throttle (90°), partially opened (15°) and closed throttle (12°) during the NEDC. They show that 19.0% of braking energy can be captured at WOT and 9.8% at partially opened throttle respectively. With partially closed throttle valve at 12°, no braking energy is captured.

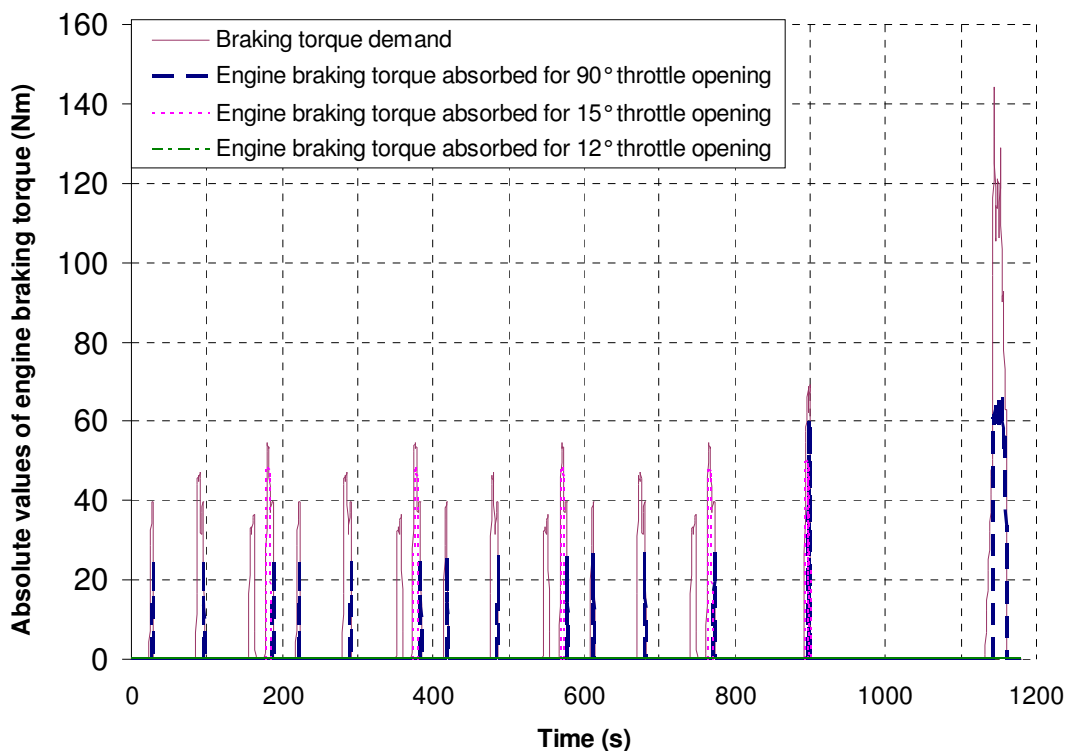


Figure 6.11: Absolute value of engine braking torque output in comparison with engine braking torque captured during the NEDC

In order to illustrate the details of the braking energy recovery process, Figure 6.12 and Figure 6.13 show one ECE-15 driving cycle and one EUDC. As mentioned before, ECE-15 is characterized by low engine load and therefore partial opened throttle (15°) is assisted to create low braking engine torque demand. In Figure 6.12, 10.9% of total braking energy is absorbed between 181 and 183 seconds with partially opened throttle at 15°. Furthermore, 5.7% of total braking energy is absorbed in 28th, 96th and 188th seconds at WOT. None of total braking energy is absorbed with partially closed throttle at 12°. The throttle valve installed in the intake manifold would increase the ability of braking energy absorption by 192% in ECE-15 low speed driving cycle.

Figure 6.13 shows the high speed Extra Urban Driving Cycle between 780 and 1180 second. With WOT, braking energy is absorbed in 897th and 899th and between 1143 and 1160 seconds. It occupies 44.8% of total braking energy in EUDC. Furthermore, 7.6% of total braking energy in EUDC is absorbed between 894 and 896 seconds and in 898th second with partially opened throttle at 15°. Again, there is no need to open the throttle at 12° with high braking engine torque in EUDC.

Figure 6.14 shows the compressed air charging process during the NEDC. Out of the total compressed air supplied to the air tank, 92.7 grams is collected with WOT and 72.8 grams with partially opened throttle. According to the results, the compression braking with the partially closed throttle setting of 12° is not necessary when a 2.0litre diesel powered D segment car is driven in the NEDC.

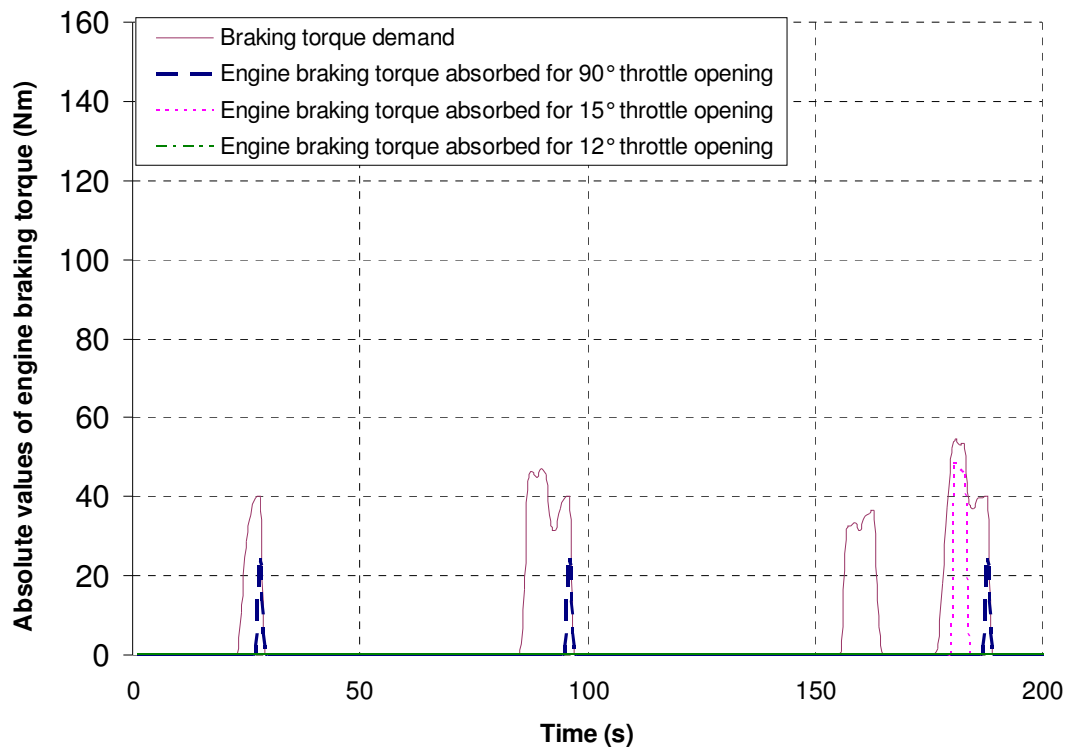


Figure 6.12: Details of the compression braking mode in one ECE-15 driving cycle

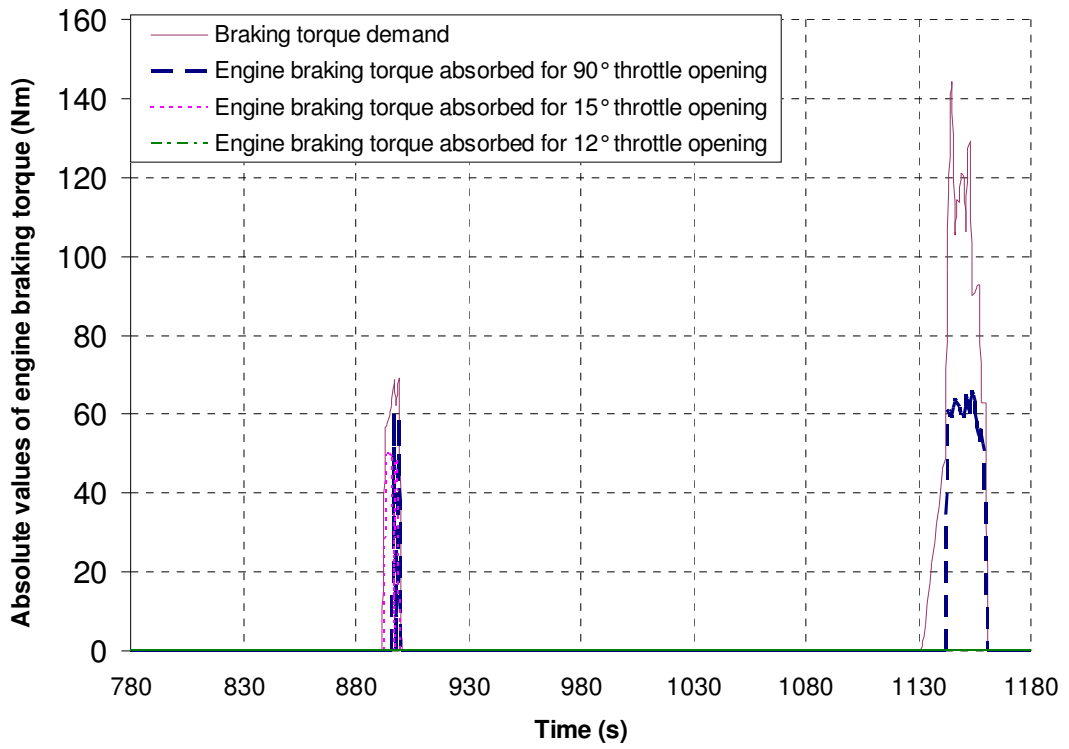


Figure 6.13: Details of the compression braking mode in a EUDC

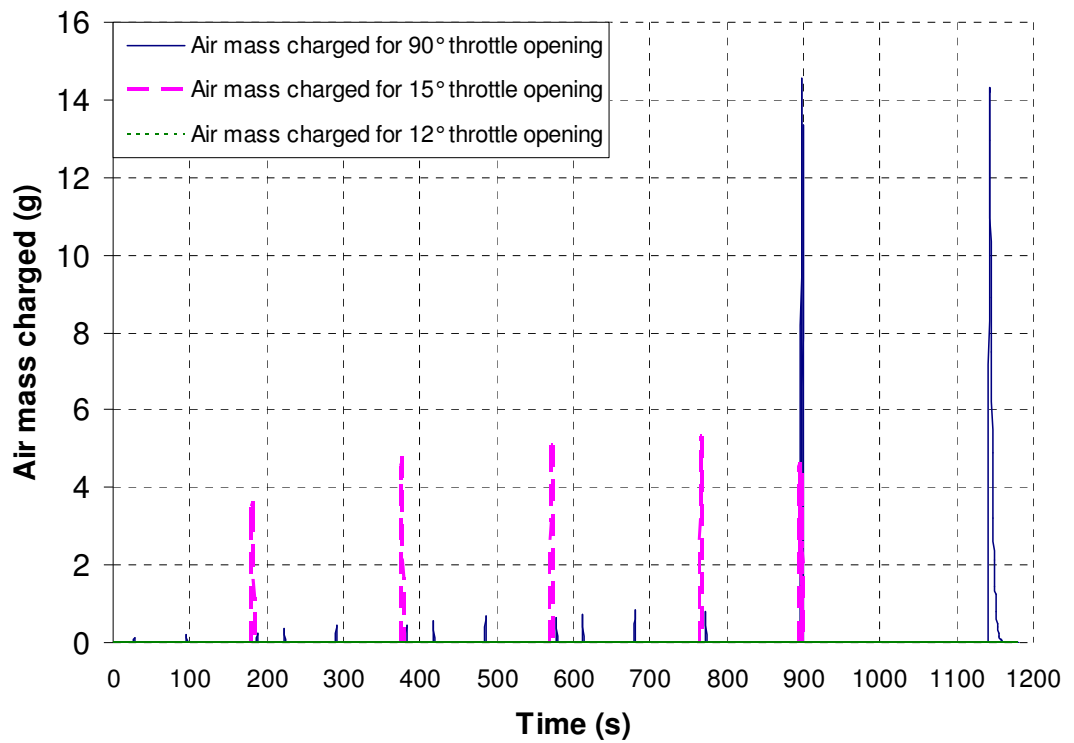


Figure 6.14: Air mass captured for various throttle valve opening throughout the NEDC

6.3.5.3 Engine cranking and compressed air usage

Figure 6.15 shows air mass discharged from the airtank at the initial tank pressure of 10 bar throughout the NEDC. In Figure 6.15, each air mass discharge event represents a successful stop-start operation. According to the results, all 13 possible stop-start operations throughout NEDC can be realised, which means there is enough compressed air captured and stored in the airtank.

Figure 6.16 shows airtank pressure profiles throughout the NEDC in various tank sizes between 10 and 40 litres in an interval of 10 litres. In all cases, with the initial airtank pressure set at 10 bar, final airtank pressure returns to above 10 bar at the end of the cycle. However, the tank pressure falls below 5 bar, the minimum pressure for cranking, between 400 and 700 seconds for a 10 litre air tank, during which stop-start mode operation is not realised. Therefore, the minimum tank size capable of activating stop-start mode operation throughout the NEDC is 20 litres. The weight of the airtank can be scaled down from 26.8kg to 13.4kg.

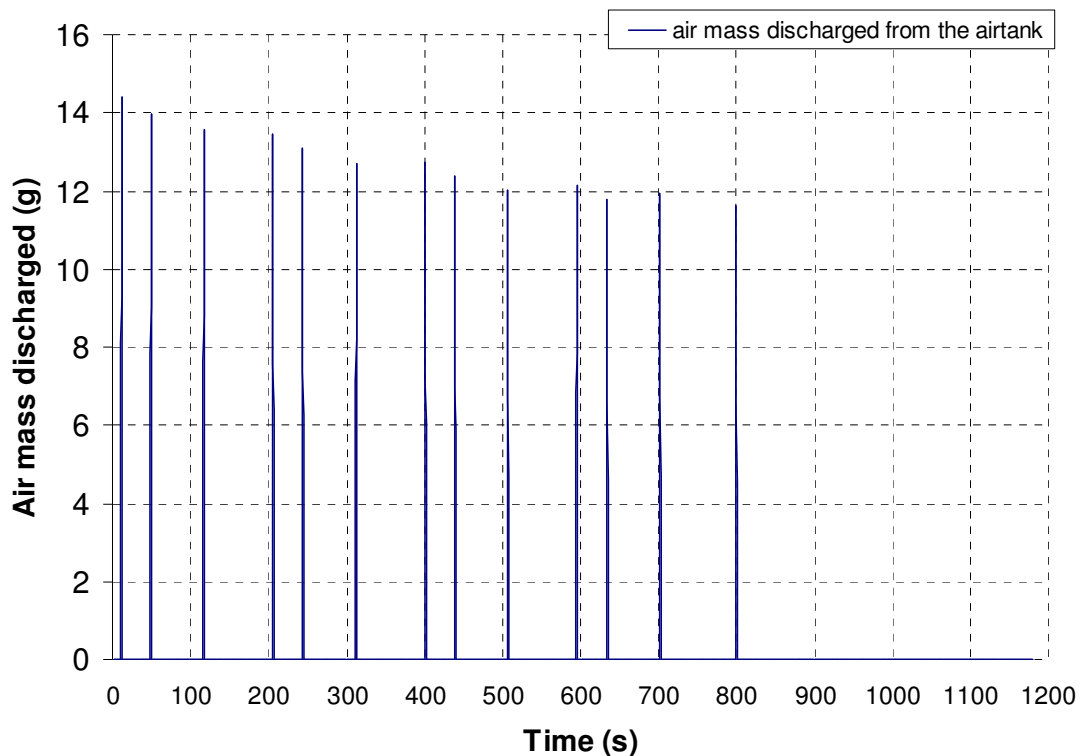


Figure 6.15: Air mass discharged throughout the NEDC

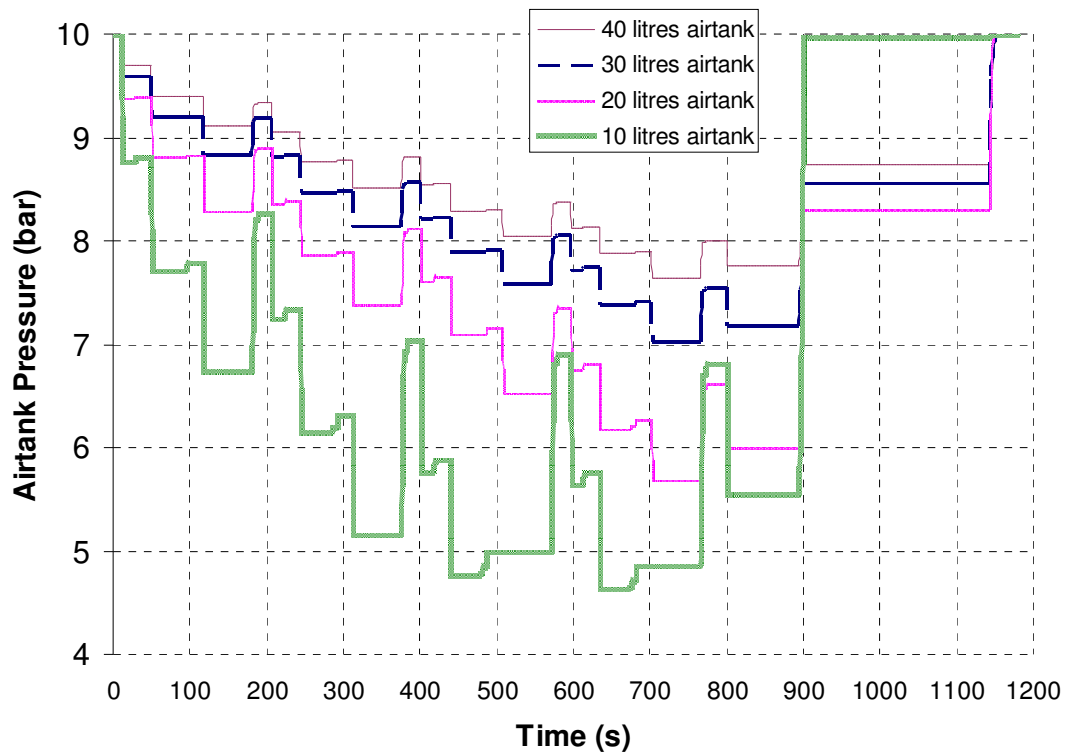


Figure 6.16: Airtank pressure variation in various tank sizes throughout the NEDC

6.3.5.4 Fuel consumption

Figure 6.17 shows a comparison of fuel consumption over the NEDC between the standard vehicle and air hybrid vehicle. Standard vehicle operation during the NEDC consumes 677 grams of fuel. The air hybrid vehicle uses 631.2 gram of fuel, which represents a 6.8% reduction in fuel consumption as a result of the regenerative stop-start operations. This is in-line with the 6% fuel consumption predicted for a similar diesel vehicle equipped with a stop-start system [6]. However, since the air hybrid technology can convert the free vehicle kinetic energy to provide instant supply of compressed air. Compared to the general downsized engine, it has the additional benefit to enable highly downsized engine to be used for further improvement in fuel economy without the loss in performance and greater emissions associated with turbo-lag.

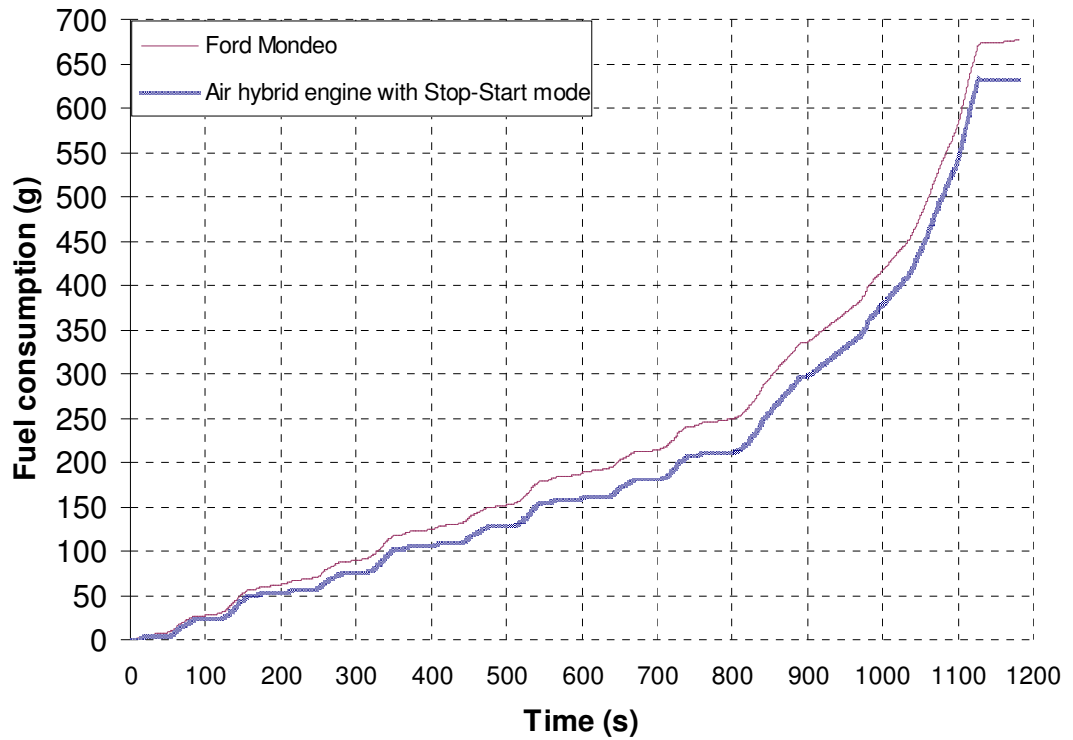


Figure 6.17: Fuel consumption throughout the NEDC

6.4 Driving Cycle Analysis of a City Bus

6.4.1 Bus data

A city bus with a YUCHAI YC-6A 7.25 litre diesel engine was chosen for the London transport bus driving cycle analysis of the air hybrid heavy duty diesel vehicle. The relevant bus data are listed in Table 6.7.

Table 6.7: City bus data

Kerb weight	16500 kg
Aerodynamic drag coefficient	0.5
Frontal area	5.69 m ²
Air density	1.225 kg/m ³
Wheel Radius	0.508 m
Rolling resistance coefficient	0.013
Airtank volume	151 litres
Starting tank pressure	6 bar
1st gear ratio	6.9
2nd gear ratio	4.13
3rd gear ratio	2.45
4th gear ratio	1.49
5th gear ratio	1
Final drive ratio	5.125
Air starter	15 kg

6.4.2 YUCHAI YC6A 7.25 litre diesel engine response map for the compressor mode operation

The diesel engine is assumed to operate according to the first air hybrid concept for the joint intake port engine presented in Chapter 4. As explained above, an air hybrid operation engine map needs to be generated prior to the start of the driving cycle analysis. The map is made up the amount of air mass charged (g/cycle) as a function of both the engine braking torque and tank pressure during the compressor mode operation. This engine response map is generated by running steady-state simulations of the engine compression mode operation as discussed in Chapter 4 and it is shown in Table 6.8 for the YC6A diesel engine.

Table 6.8: YUCHAI YC6A Diesel Engine response Map during the CM operation

Tank Pressure (bar)	Engine Braking Torque (Nm)					Air mass charged (g/cycle)				
	100 rpm	500 rpm	1000 rpm	1500 rpm	2000 rpm	100 rpm	500 rpm	1000 rpm	1500 rpm	2000 rpm
4	-72.06	-85.05	-104.80	-126.30	-140.70	3.12	3.16	2.84	2.38	1.79
5	-66.85	-77.91	-97.33	-114.10	-134.90	2.28	2.45	2.20	1.67	1.42
6	-61.38	-71.64	-87.66	-111.00	-129.20	1.79	1.93	1.60	1.45	1.09
7	-56.74	-66.00	-83.26	-107.60	-123.60	1.60	1.59	1.37	1.24	0.80

6.4.3 Engine response maps for the cranking mode operation

An Ingersoll Rand air starter (SS175) has been chosen as the starting motor for the cranking mode operation. Its performance characteristics are given in Figure 6.18. At each tank pressure, the amount of air mass used during each cranking operation is calculated from the air flow at maximum horse power shown in Figure 6.18 for a cranking period of 1 second. Figure 6.19 shows and the potential number of starts at various tank pressures and for different tank sizes.

SS175 Performance Information

Pressure PSI (bar)	Breakaway Torque ft-lb (Nm)		Speed @ Max HP RPM		Max Power HP (kw)	Flow @ Max HP SCFM (L/s)
	B Ratio	E Ratio	B Ratio	E Ratio		
90 (6.2)	30 (41)	42 (57)	3500	2500	10 (7)	300 (142)
120 (8.3)	38 (51)	54 (73)	3800	2700	14 (10)	400 (189)
150 (10.3)	46 (62)	70 (95)	4100	2800	18 (13)	500 (236)

Figure 6.18: SS175 air starter performance information [61]

SS175 Number of Starts per Tank

(Assuming 1-Second Crank Time @ 90 PSI)

Max Tank Pressure (psi)	300	17	26	35	44	52	61	70	79	20	Max Tank Pressure (bar)
	270	15	23	31	38	46	53	61	69	18	
	240	13	20	26	33	39	46	52	59	16	
	210	11	16	22	27	33	38	44	49	14	
	180	9	13	17	22	26	31	35	39	12	
	150	7	10	13	16	20	23	26	29	10	
	120	4	7	9	11	13	15	17	20	8	
	90	2	3	4	5	7	8	9	10	6	
		40	60	80	100	120	140	160	180		Gallons Liters
		151	227	302	378	454	529	605	680		
		Tank Size									

Figure 6.19: SS175 air starter number of starts per tank [61]

6.4.4 Millbrook London Transport Bus (MLTB) Drive Cycle

MLTB drive cycle is a real world drive cycle based on logged data of a bus in service in central London. Two phases, a medium speed ‘Outer London’ phase simulating a journey from Brixton Station to Trafalgar Square and a low speed ‘Inner London’ phase simulating a journey from Trafalgar Square to the end of Oxford Street, make up the MLTB drive cycle. Outer London Phase and Inner London Phase include a nominal distance of 6.45 km for a duration of 1,380 seconds and a nominal distance of 2.47 km for a duration of 901 seconds respectively. The cycle pattern, shown in Figure A6 in Appendix, covers an entire distance of 8.92 km for a duration of 2281 seconds.

6.4.5 Results and discussion on YUCHAI air hybrid engine

6.4.5.1 Air Hybrid Vehicle Speed and Load Analysis

Figure 6.20 shows the engine speed profiles during the MLTB drive cycle for the air hybrid vehicle operation (blue line) and the normal vehicle operation (brown line). The difference between these two vehicle operations is that the air hybrid engine is switched off whilst the engine idles at 650 rpm engine speed when the vehicle is stationary.

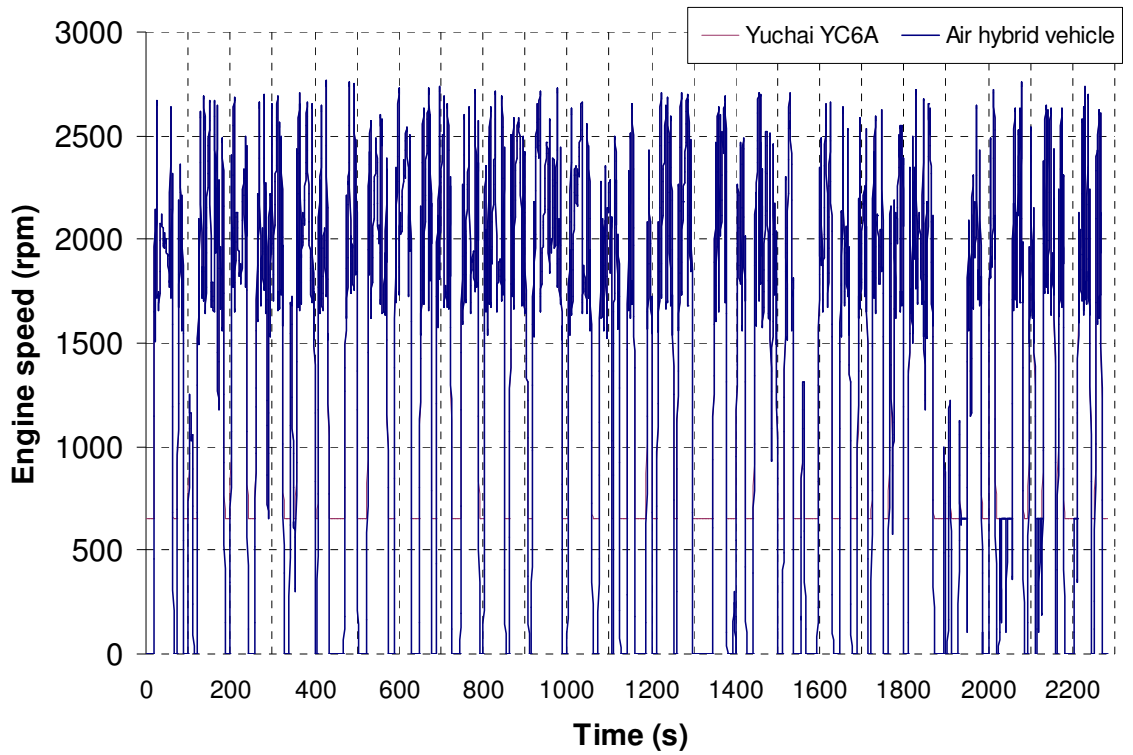


Figure 6.20: Engine speed throughout the MLTB drive cycle

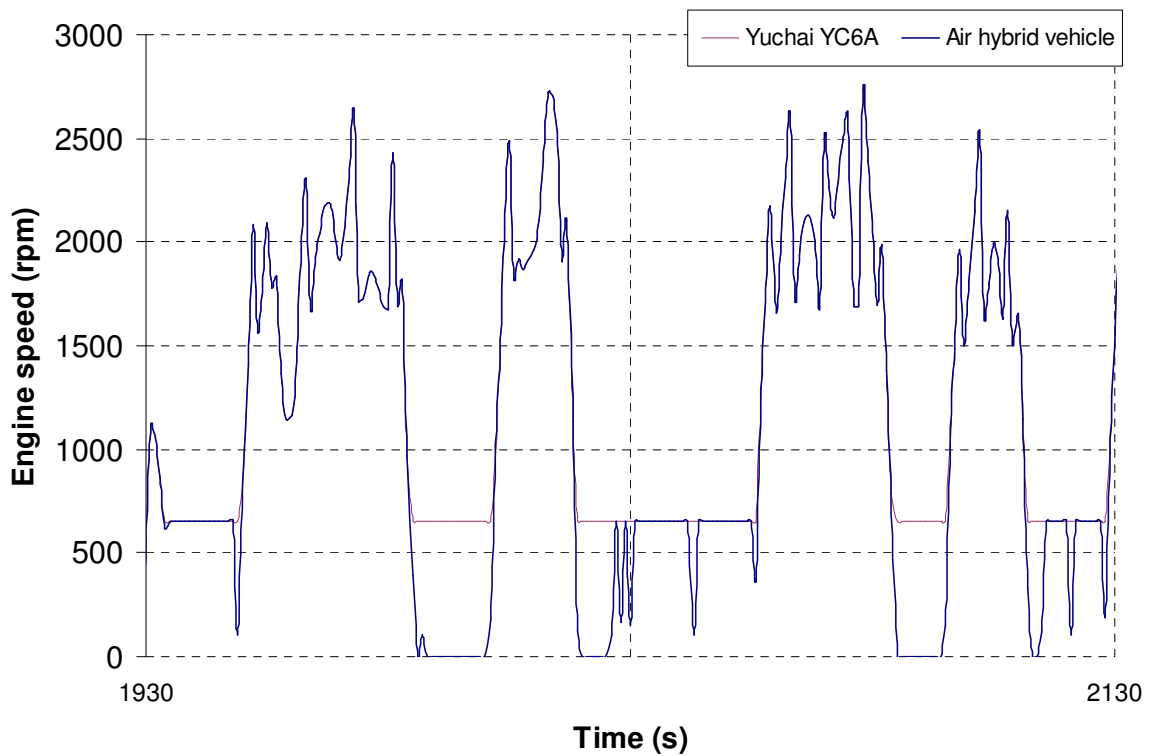


Figure 6.21: Engine speed between 1930 and 2130 seconds of the MLTB drive cycle

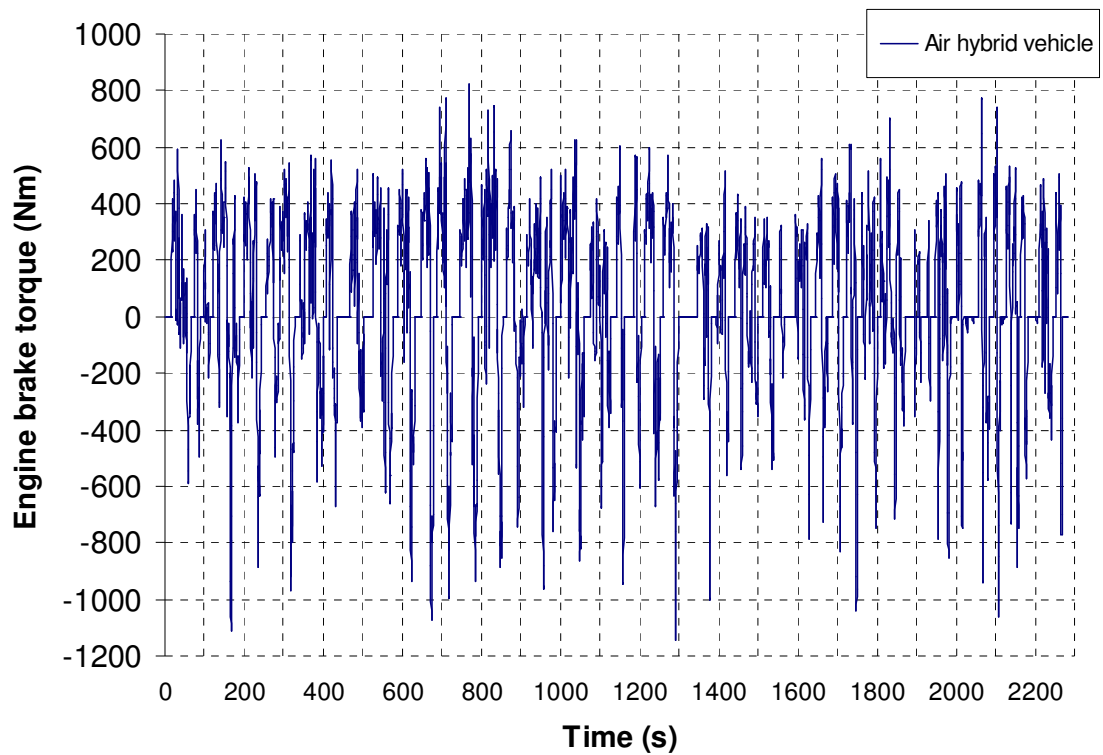


Figure 6.22: Engine load during the MLTB drive cycle

Figure 6.21 shows that in some periods of time between 1930 and 2130 seconds the engine is allowed to idle while the vehicle is stationary. This is an indication that there is insufficient tank pressure for the cranking mode operation. In order to further improve the effectiveness of regenerative compressed air production and hence the subsequent utilisation for stop-start operations, it would be desirable to implement the 2nd concept for an engine with split intake ports presented in Chapter 4.

Next, the engine load is calculated and shown in Figure 6.22. The negative brake torque regions correspond to the deceleration period and their values represent the braking energy that could be recovered.

6.4.5.2 Compression braking

In order to illustrate the amount of braking energy that can be recovered during the compression mode operation, Figure 6.23 shows the engine compression torque in relation to the engine load during the MLTB drive cycle. It shows that 26.8% of braking energy has been captured. Figure 6.24 shows the compressed air charging process during the MLTB drive cycle. There is 7427.4 grams of compressed air supplied to the air tank.

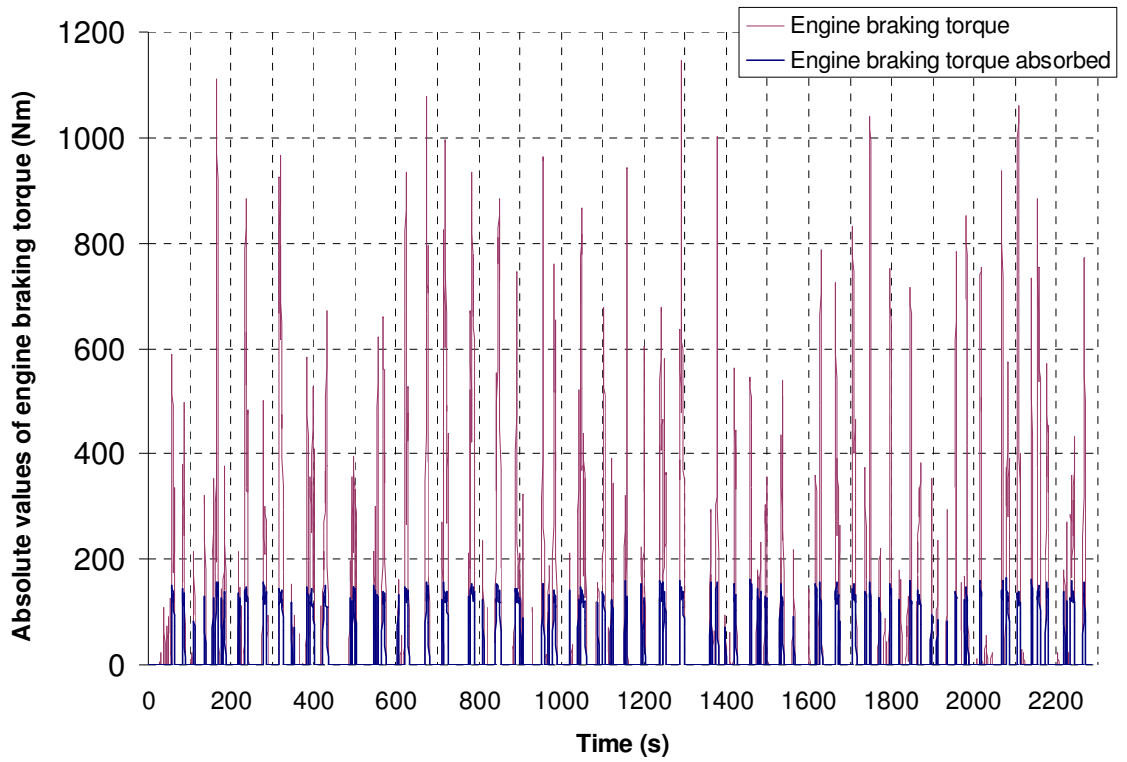


Figure 6.23: Absolute value of engine braking torque output in comparison with engine braking torque captured during the MLTB drive cycle

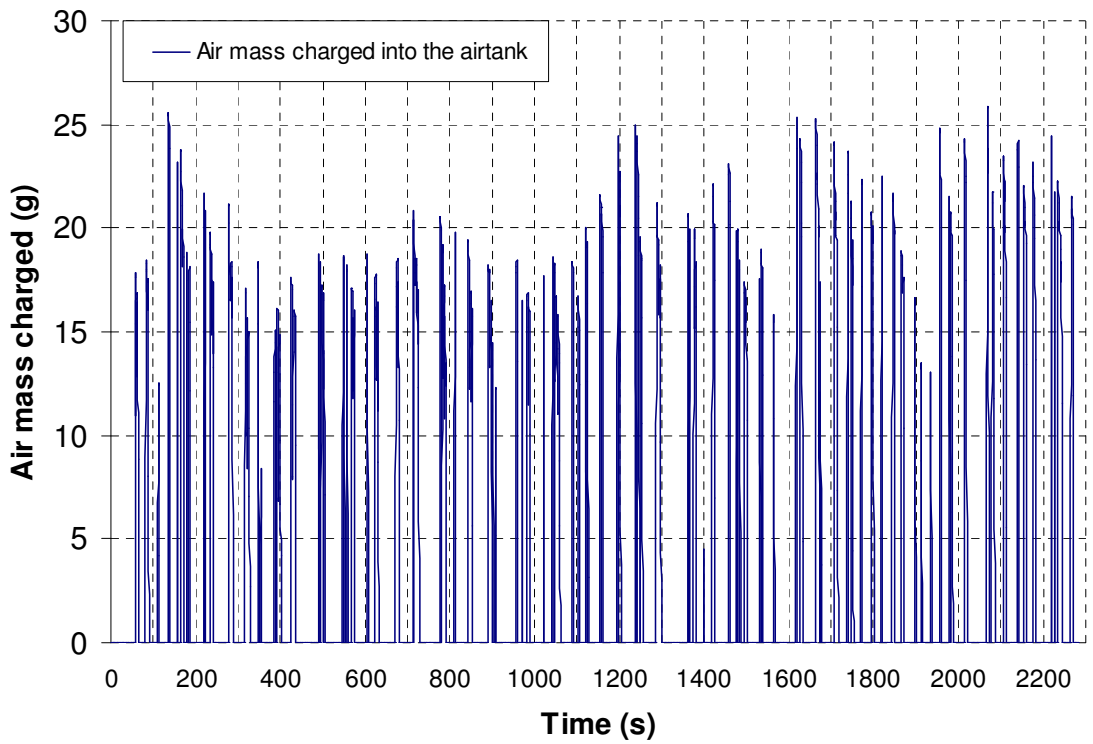


Figure 6.24: Air mass captured and stored in the airtank throughout the MLTB drive cycle

6.4.5.3 Engine cranking and compressed air usage

Figure 6.25 shows the temporal profile of the air mass discharged from the airtank at an initial tank pressure of 7.4 bar throughout the MLTB drive cycle. In total, 7711.6 grams of compressed air are consumed by the air starter to crank the engine.

Figure 6.26 shows the airtank pressure variation throughout the MLTB drive cycle in a 151 litres airtank. The initial airtank pressure has been set at 7.4 bar, the maximum pressure that can be achieved during the compression mode operation. However, Figure 6.27 shows airtank pressure falls below 5.2bar in some periods of time between 1930 and 2130 seconds of the MLTB drive cycle when the engine will not be able to operate in the stop-start mode.

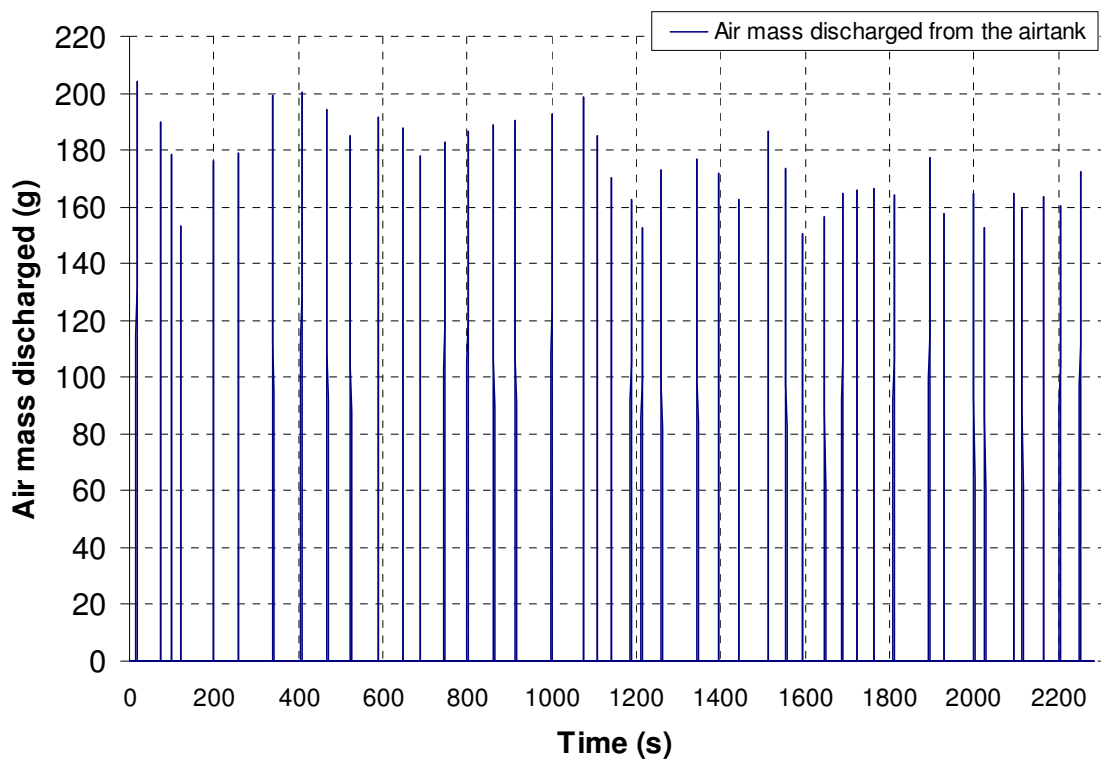


Figure 6.25: Air mass discharged from the airtank throughout the MLTB drive cycle

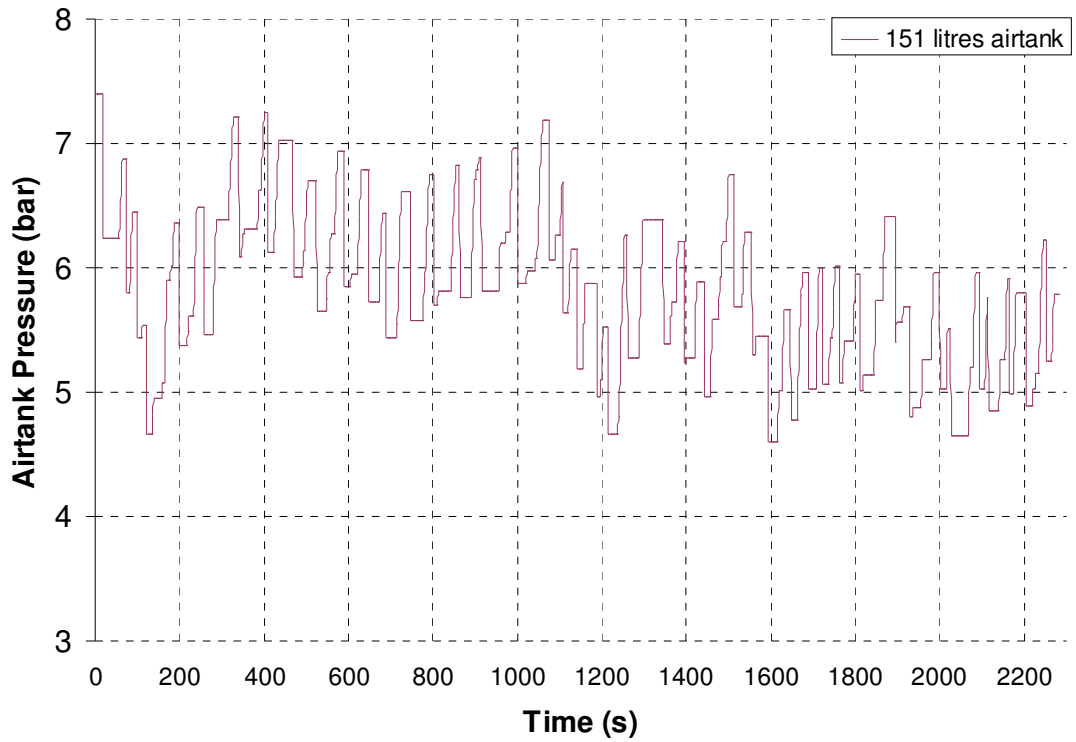


Figure 6.26: Airtank pressure variation throughout the MLTB drive cycle

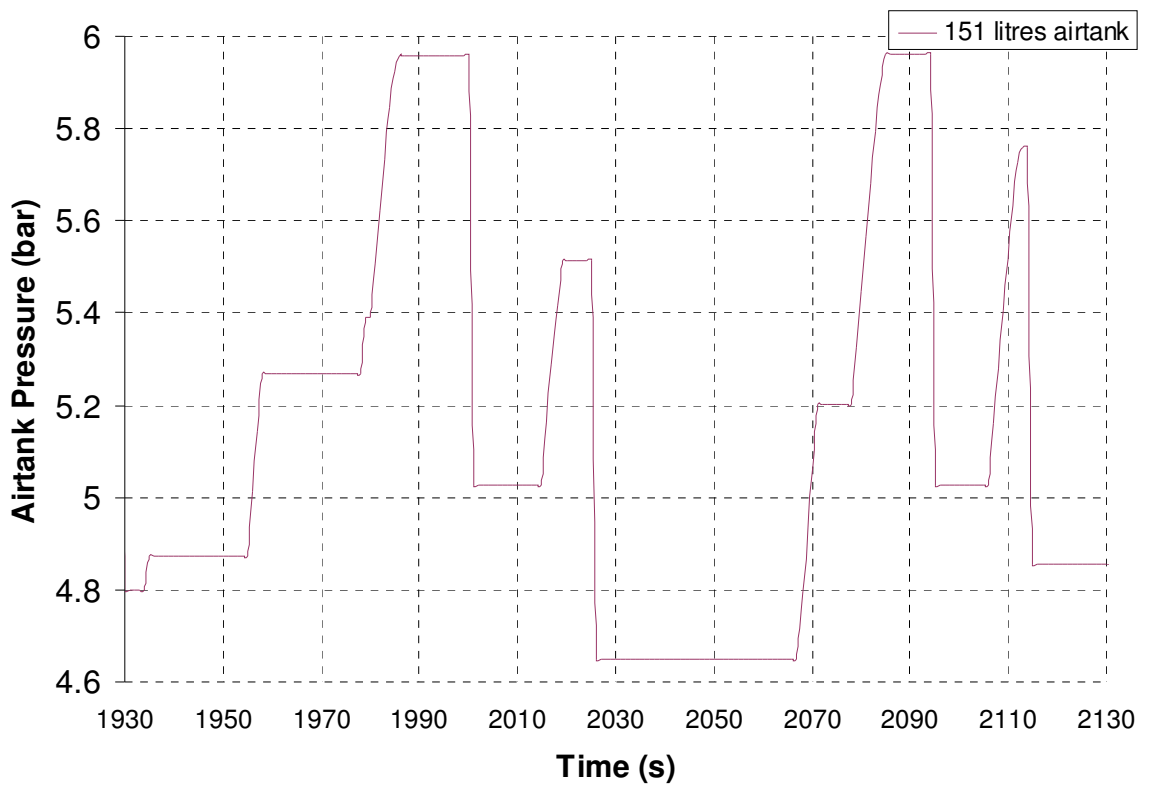


Figure 6.27: Airtank pressure variation between 1930 and 2130 seconds of the MLTB drive cycle

6.4.5.4 Fuel consumption

Figure 6.28 shows a comparison of fuel consumption over the MLTB drive cycle between the standard vehicle and air hybrid vehicle. Standard vehicle operation during the MLTB drive cycle consumes 3888.4 grams of fuel based on the engine's fuel consumption data provided by YUCHAI. The air hybrid vehicle uses 3645.4 gram of fuel, which represents a 6.2% reduction in fuel consumption as a result of the regenerative stop-start operations. Furthermore, the Deceleration Fuel Cut-Off (DFCO) function has been applied in Yuchai YC6A diesel engine with its limitation of 850 rpm engine speed. It means if the engine speed is lower than 850 rpm during the deceleration, it switches back to the firing mode. The RegenEBD system stops fuel injection during the whole deceleration process and saves 25.6 grams fuel more which is 10.5% in the amount of total fuel saving. On the other hand, idle fuel saving is 217.4 grams which is 89.5% in the amount of total fuel saving.

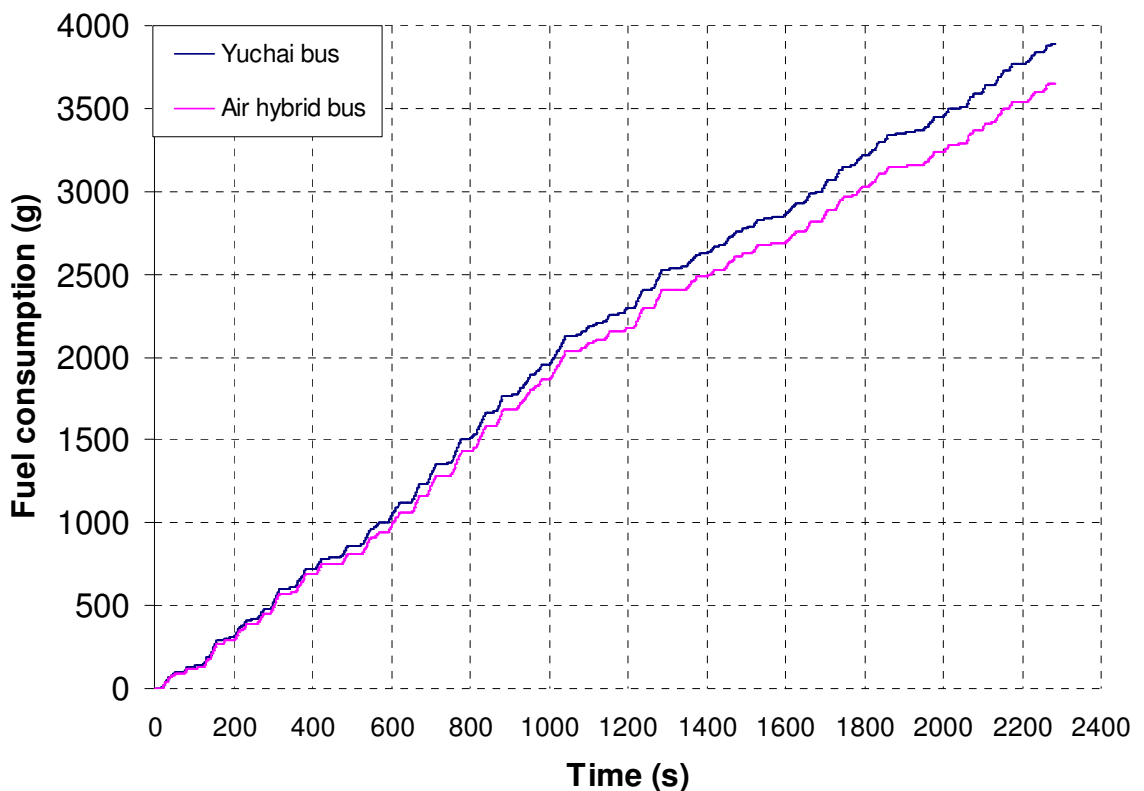


Figure 6.28: Fuel consumption throughout the MLTB drive cycle

According to a report to Department for Transport by Sciotech [72], the city diesel bus has an average fuel consumption of 50 litre/100km and produces 160kg/100km CO₂ emissions. For the typical mileage of 45000 km/year per vehicle, even a conservative assumption of 5% improvement in fuel consumption by the air hybrid engine technology can reduce CO₂

emission by 3.6 tons as well as a fuel saving of 1125 litres per year per vehicle. Taking the UK fleet as 50,000 city buses this would equate to 180000 tons of CO₂ per annum and or 12.4 million gallons of diesel over the bus fleet per year, a not inconsiderable amount of savings.

6.4.6 Analysis of the potential of the current alternator/battery system for HGVs

6.4.6.1 Reality check for starting energy and hence equivalent fuel required for starting

The starting energy (E_s) required for Heavy Goods Vehicles (HGVs) can be modelled as below:

$$E_s = m_f \cdot LHV \cdot \eta_b \cdot \eta_{al} \cdot \eta_{ch} \cdot \eta_{dis} \cdot \eta_{st} \quad \text{Equation 6.19}$$

where m_f is fuel mass required for each engine start, LHV the lower heating value, η_b the engine braking efficiency, η_{al} the alternator efficiency, η_{ch} the battery charging efficiency, η_{dis} the battery discharging efficiency, η_{st} starter motor efficiency. The reality check equation for the fuel consumption of starting can be computed by the equation:

$$m_f = [E_s \div (\eta_b \cdot \eta_{al} \cdot \eta_{ch} \cdot \eta_{dis} \cdot \eta_{st})] \div LHV \quad \text{Equation 6.20}$$

The starting Energy (E_s) is 6 kJ scaled from Bosch data (3.75kJ for a 4.5 litre engine). The lower heating value (LHV) is 44 kJ per gram. The engine braking efficiency (η_b) and the alternator efficiency (η_{al}) are assumed to be 30% and 65% respectively. The battery charging efficiency (η_{ch}) and the fast battery discharging efficiency (η_{dis}) at maximum discharge current are 70% and 47% respectively [73]. The starter motor efficiency (η_{st}) is between 10-30% and 20% is assumed for warm-start [74]. According to Equation 6.20, it can be computed that 10.62 grams fuel mass is required for each engine start.

For MLTB driving cycle, there are 50 stop-starts, hence the fuel required for the stop-start operations will be 531 grams. Therefore, the fuel saving without regenerative energy recovery is determined as the value of original fuel consumption subtract the sum of fuel consumption without idle and the fuel required for the stop-start operations. Following the analysis above, there will be no fuel saving by adopting the current alternator/battery system for HGVs.

6.4.6.2 Battery charging ability

In the case of a HGV (DAF LF55 18 tonne truck) which utilizes an 80 Amp alternator and two 125Ah/12V batteries. The maximum charging current for the automotive battery should be less than 10% of the battery capacity, typically around 5 Amps for the protection of the battery from damage. In addition, the state of charge (SOC) of battery should maintain at 84% \pm 1% through on-line monitoring for a stop-start system. However, assuming a more aggressive charging current of 25 Amps at 28 Volts. Hence the value of the battery charging ability from a current belt-driven alternator during the 6 seconds braking is 4200 J. When the battery charging efficiency (η_{ch}), the fast battery discharging efficiency (η_{dis}) and the starter motor efficiency (η_{st}) are taken into account, the amount of energy for starting is about 276 J, compared with 6000J starting energy. The current alternator/starter stop-start system will have little capacity to produce regenerative energy.

6.4.6.3 Durability of Battery and Starter Motors

As the battery will be subject to 50 times of duty cycles in a single trip, the life time of the battery will be dramatically reduced. As Figure 6.29 below shows, that the current battery will last 20,000 cycles. If a bus needs 8 trips in a day, 50 working days is the maximum before it is completely dead.

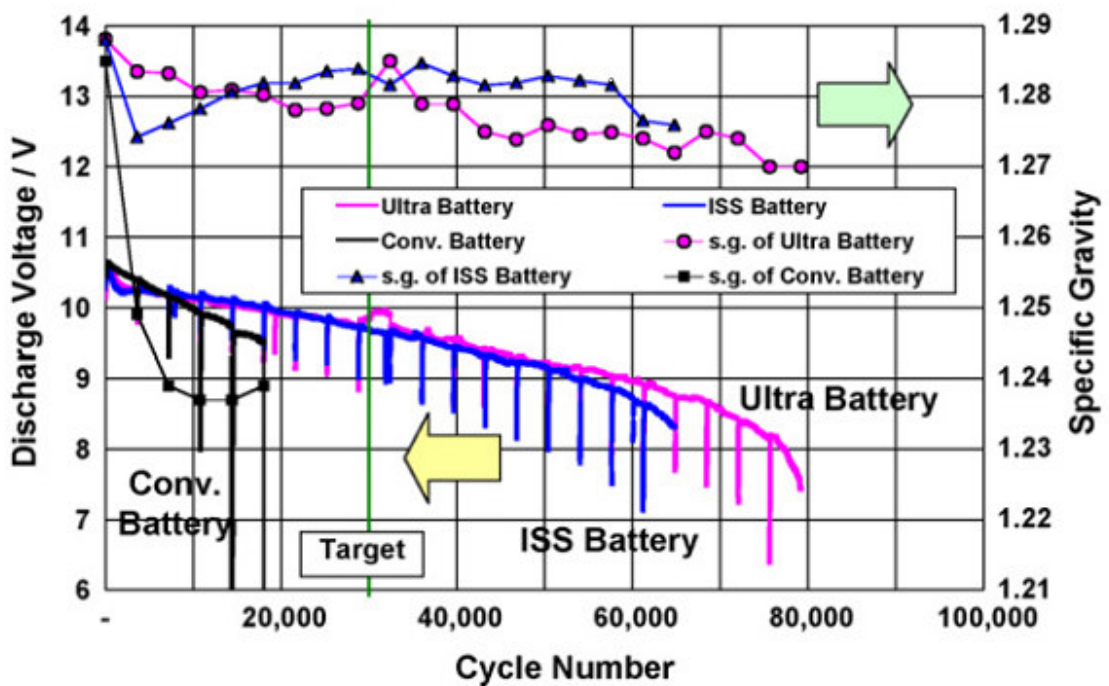


Figure 6.29: Discharge voltage against battery cycle number [75]

There is no starter motors for commercial vehicles that can withstand the substantially increased number of operations required either. (200 stop-start x 300=60000 cycles/year)

6.5 Summary

The proposed regenerative air hybrid engine technology reduces fuel consumption by a combination of regenerative stop-start and supply of service air for free using the braking energy. It exploits the functional capability of the current engine design to operate as a compressor, capturing and storing braking energy as compressed air during braking and replenishing after each deceleration. It is not dependent on hybrid electric technology, but simply extends the functionality of the existing engine with the important new role of capturing the braking energy for regenerative stop-start operation and supply of boost air for downsized engine operation and service air for commercial vehicles.

In this chapter, an air hybrid driving cycle simulation program has been developed and applied to assess the fuel saving potentials of a light duty vehicle and a medium duty vehicle. The light duty vehicle is modelled as passenger car driving in the NEDC which is a steady state driving cycle with infrequent stop-start operations, whereas the medium duty vehicle chosen is a city bus running in a real world driving cycle. It is found that the passenger car can achieve about 5% fuel economy benefit from regenerative stop-start operation using the production oriented air hybrid technology. For a 2.0litre engine, it is noted that a 10 litre air tank will be large enough to sustain the regenerative stop-start operations during the driving cycle. In the case of the city bus modelled, much greater fuel saving of 6.5% can be achieved during a real world driving cycle because of the greater braking energy and frequent stop-start operations.

Furthermore, additional fuel savings of 3% in heavy duty trucks have been demonstrated by downshifting during acceleration from the instant supply of compressed air by Bendix in an independent study [76].

CO₂ saving from any new technology is crucially driven by two factors: affordable economics and high volume uptake. The proposed air hybrid concept exploits the novel integration of existing production components and will cost no more than a few thousand pounds, making it a more efficient, affordable, engine-only, quick-to-market, low-carbon alternative to the hybrid electric vehicles, in particular medium and heavy duty vehicles.

Finally, there are additional benefits of air hybrid engine technology to provide assistance in overcoming turbo lag, improving driving performance, and reducing emissions.

The current battery and starter motors in commercial vehicles will not be able to withstand the frequent charge and discharge operations for a bus driving cycle.

Even if the future battery could be made to sustain such frequent charge and discharge cycles, the belt driven stop-start system does not offer any improvement in fuel economy benefit due to insignificant regenerative energy recovered.

To achieve similar functions and abilities of RegenEBD, much more expensive and complex mild electric hybrid system is required, including a large generator/motor and the associated drive train, larger NiMH or even Lithium Ion batteries and power electronics.

Chapter 7: Conclusions and Further Work

7.1 Conclusions

In this work, novel air hybrid engine concepts have been proposed and presented. Their performance characteristics have been studied by utilizing Ricardo's WAVE 1D gas dynamics simulation package and the results are then used in the air hybrid engine sub-model. A four-cylinder Ford PUMA 2 litre diesel engine have been modelled to operate in four air hybrid engine configurations and their braking and motoring performance of each configuration are analysed and compared. A Yuchai YC6A engine is modelled to operate with RegenEBD modes with a bleed type engine braking device (VVEB) and a compression release engine braking device (Jakes Brake). The experimental test of the air hybrid engine operation with separate intake ports or joint intake ports have been carried out on a single cylinder camless engine. Furthermore, the experimental results are compared with simulation results in order to validate the accuracy of the predicted air hybrid engine results. Finally, backward air hybrid vehicle driving simulation has been developed and then applied to exploit the performance and potential of a light duty vehicle in the NEDC and a city bus in the London Bus Route driving cycle.

7.1.1 Predicted Air Hybrid Engine Performance

7.1.1.1 Air hybrid concept 1 with Reed valve for a light duty diesel engine

- I. For the CM operation, the sensitivity of predicted $CATC_b$ and $imep_b$ against various active IVC points has been explored. The results show that maximum $CATC_b$ and maximum $imep_b$ are realized when the active IVC is at 50° ATDC, at which maximum amount of air is charged into the airtank and the engine produces the highest braking power.
- II. The compressed air can be used to crank start the engine or to provide driving torque through the EM operation. Although the maximum starting torque can be achieved when the ECV remains open throughout the intake stroke, it is found that the specific motoring and cranking torque per unit air mass is optimised when the closing point of the ECV is set at 80° BBDC. In order to maximise the driving torque output during the EM operation, the opening period of one of the intake valves needs to be shifted to the early compression stroke by means of a CPS device.

- III. The regenerative efficiency of this air hybrid concept is found to be between 19-25% for air tank pressures of 5-15 bar.

7.1.1.2 Air hybrid engine concept 2 with a port throttle for a light duty diesel engine

- I. This air hybrid concept dispenses with the need of high speed capability of the ECV so that low cost solenoid valves and much simpler control can be used. Furthermore, the replacement of Reed Valves with port throttles eliminates the flow restriction and durability problems associated with 1st concept. The analytical study has shown that 2nd air hybrid concept will be suited for regenerative stop and start operations by means of two independent intake cam profile switching devices.
- II. The compression mode characteristics of this air hybrid concept is the same as that of the first concept.
- III. During the cranking operation, the ECV remains open. The amount of the compressed air supplied to the engine is controlled by the timing of the intake valve linked to the compressed air supply. For as a standard intake cam design, the optimum air usage is obtained with the take valve opening at 70° ATDC.

7.1.1.3 Air hybrid engine concept 3 for a light duty diesel engine

- I. The significant improvement of air hybrid engine concept 3 is that the engine can work as either an air compressor or an air expander using the same valve settings. The first two air hybrid concepts would require that both intake valves utilize a CPS mechanism. In contrast, only one intake valve (IV6) is required to adopt a CPS mechanism for the CM and the cranking mode operation which minimizes modification and saves cost. This air hybrid concept has therefore been selected in the vehicle driving simulation in Chapter 6.
- II. Due to the on-off valve (ECV) being moved to the other intake port, the auxiliary chamber volume is reduced, resulting in a higher real compression ratio to 6.8. The higher real compression ratio leads to higher maximum tank pressure and hence higher energy density in the air tank.
- III. During both compression braking and engine cranking operations, it is found that the both braking specific imep and motoring specific imep are optimised when the intake

valve used to capture the compressed air (IV6) is set to close at 70° ATDC, for a standard opening duration of 240 CA.

7.1.1.4 Air hybrid engine 4 with joint intake ports for a light duty diesel engine

- I. This concept is formulated for an engine with joint intake ports and mandates the extended opening of both intake valves during the CM operation through a more sophisticated CPS device. The air hybrid system is able to charge its 40 litre air tank from 6.8 bar tank pressure to 8 bar tank pressure in 4.8 seconds in CM. However, it suffers from much reduced maximum air tank pressure due to the larger auxiliary chamber volume of the joint intake port.
- II. In order to operate the engine in the cranking mode, the opening event of the exhaust valves needs to be shifted to the compression stroke in order to minimise the negative compression work.
- III. Therefore, this concept is least practical and of lowest performance than the first 3 concepts.

7.1.1.5 RegenEBD Technology with VVEB

- I. The air hybrid engine concept is implemented through the RegenEBD technology in a bus diesel engine using a commercial bleed-type engine braking device, VVEB.
- II. During the CM operation, the VVEB device keeps intake valves open at 1.25 mm off the valve seats. By installing a Reed valve in each cylinder, an air tank of 150litre can be charged from 1bar to 7.1bar within 9.6 seconds at 1500rpm engine speed. The engine is capable of generating braking torque of 200Nm during the compression mode operation.
- II. The regenerative stop-start is achieved by a standard air starter, which assuming 1-second crank time is able to provide 2 start-up operations with a 151 litres air tank at 6.2 bar [61].

7.1.1.6 RegenEBD Technology with a compression release engine braking device

I. The air hybrid engine concept is implemented through the RegenEBD technology in the same bus diesel engine using a compression release engine braking device on one of the intakes valves

II. In conjunction with the split intake ports design, the use of compression release engine braking device doubles the engine braking torque during the compression mode operation, so that more and faster regenerative braking energy recovery can be realised.

7.1.2 Experimental Validation of Air Hybrid Concepts

7.1.2.1 The air hybrid engine operation with a Reed Valve

In this configuration, the compression mode operation is achieved by the extended intake valve opening and a Reed valve, with the other intake valve disabled. It is found that the best braking performance is achieved when the intake valve closes at between 10° ATDC and 15° BTDC. The maximum braking mean effective pressure is between 2-2.8 bar.

7.1.2.2 The air hybrid engine with a split intake runner block

I. The compression mode operation is realised by admitting air through one intake port and valve (IV1) and then compressing the air into the airtank via the other intake port and intake valve (IV2), in a similar way to the 3rd concept presented for the light duty diesel engine. The measured tank pressure results indicate that the compression mode is most efficient when IV2 closes around 15° ATDC.

II. Further experiments have demonstrated that the engine braking torque can be effectively controlled by means of an intake throttle. This has been incorporated into the light duty vehicle driving cycle simulation studies so that different engine braking force can be applied to the vehicle according to the braking requirement.

IV. The comparison between the experimental results and the predicted values by 1D engine simulation shows excellent agreement in air tank pressure, air mass flow rate and the braking imeps.

7.1.3 Vehicle simulation

7.1.3.1 Driving cycle analysis of an air hybrid Light Duty Diesel Vehicle

A Ford Mondeo car is used to evaluate the effect of air hybrid engine operation on the fuel economy through the NEDC.

- I. The minimum tank size capable of activating stop-start mode operation throughout the NEDC is found to be 20 litres, 10 times of the engine displacement volume.
- II. The result shows 19% and 9.8% braking torque captured while the throttle valve opening is at 90° and 15° respectively. While the throttle valve opening is 12°, there is no braking torque captured.
- III. While the throttle valve opening is at 90° and 15° for CM, there are 92.7 and 72.8 gram air mass charged respectively. While the throttle valve opening is at 12° for CM, there is no air mass charged. Therefore, 12° throttle valve opening is not included in the vehicle simulation.
- IV. During the NEDC, the fuel consumption is reduced from 677 grams to 631.2 gram, which represents a 6.8% reduction in fuel consumption as a result of the regenerative stop-start operations. However, since the air hybrid technology can provide instant supply of compressed air, it has the additional benefit to enable highly downsized engine to be used for further improvement in fuel economy without the loss in performance and greater emissions associated with turbo-lag.

7.1.3.2 Driving cycle analysis of a city bus

Modelling of a city bus fitted with a YUCHAI 7.25 litre diesel engine has been performed throughout the MLTB driving cycles.

- I. The results show that 26.8% of braking energy has been captured with the fixed VVEB setup.
- II. There is 7427.4 grams of compressed air supplied to the air tank. In total, 7711.6 grams of compressed air are consumed by the air starter to crank the engine.
- III. During the MLTB drive cycle, the fuel consumption is reduced from 3929.5 grams to 3674.6 grams, which represents a 6.5% reduction in fuel consumption as a result of the regenerative stop-start operations. Additional fuel savings of 3% in heavy duty trucks can be achieved by downshifting during transient operation and reduced use of engine driven compressors.

7.1.4 Overall Conclusions

CO₂ saving from any new technology is crucially driven by two factors: affordable economics and high volume uptake. The proposed air hybrid concept exploits the novel integration of existing production components, making it more efficient, affordable, engine-only, quick-to-market, low-carbon alternative to the hybrid electric vehicles, in particular for medium and heavy duty vehicles, or even SUVs with downsized engines.

Compared to the current battery alternator/starter stop-start system, the RegenEBD technology for the buses provides at least twice the fuel savings and is a more robust and durable technology. Furthermore, it offers additional benefits of improved engine performance, low emission and less maintenance.

Finally, Yuchai Machinery Company has recently successfully demonstrated the RegenEBD technology in a bus. The bus is able to capture the compressed air in an air tank and uses an air starter to achieve stop-start operations during some demonstrations runs on a public road.

7.2 Further work

- (i) It would be desirable to extend the light duty vehicle driving cycle analysis to larger vehicles, including large SUVs and light good vehicles, such as Ford Transit Van, under different driving cycles that reflect more closely the real world driving.
- (ii) The bus driving cycle analysis should also be carried out for a bus with a modern split intake diesel engine equipped with a compression release RegenEBD. If additional information on the usage of compressed air can be obtained, the potential for RegenEBD to provide the service air can be assessed in place of the engine driven compressor.
- (iii) Provided that information can be obtained on the vehicles with highly downsized engines, the potential of the regenerative compressed air supply for improve transient performance and fuel economy benefits should also be investigated.
- (iv) The use of a heat recuperator should be investigated if direct engine cranking by compressed air to be used, in order to increase the crank work and reduce engine cooling due to expansion of air.
- (v) In order to validate the modelling work on the engine cranking by compressed air, it would be useful to carry out such experiments on the single cylinder camless engine,

once the engine and valve control systems have been updated to enable open valve starting experiments.

- (vi) To implement the concepts on engines and vehicles of different designs in order to evaluate fully its potential for fuel savings and improved vehicle performance.

References

1. “Euro 5 and Euro 6 standards: reduction of pollutant emissions from light vehicles”, obtained from http://europa.eu/legislation_summaries/environment/air_pollution/l28186_en.htm, last visited December 2010.
2. “Commission plans framework to ensure the EU meets its target for cutting CO₂ emissions from cars”, obtained from <http://europa.eu/rapid/pressReleasesAction.do?reference=IP/07/155&format=HTML&aged=0&language=EN&guiLanguage=en>, last visited December 2010.
3. “Energy and climate change”, obtained from http://europa.eu/press_room/press_packs/climate/index_en.htm, last visited December 2010.
4. “Commercial vehicles and CO₂, the business of fuel economy”, obtained from <http://www.automobile-industry.eu/>, last visited March 2010.
5. Van Basshuysen, R. and Spicher, U.[et al.], “Gasoline Engine with Direct Injection”, p.7, Vieweg+Teubner, ISBN 978-3-8348-0670-3, 2009.
6. Millo F., Badami M., Ferraro C.V. and Rolando L., “Different hybrid powertrain solutions for European diesel passenger cars”, SAE paper 2009-24-0064.
7. Smyth, J. and Douglas, R., “Meeting Tomorrow’s Challenges: The Role of the IC Engine”, SAE paper 2004-21-0080, 2004.
8. Kelly, K., Mihalic, M. and Zolot, M., “Battery Usage and Thermal Performance of the Toyota Prius and Honda Insight for Various Chassis Dynamometer Test Procedures”, NREL Internal Report, 2001.
9. Kelly, K., Mihalic, M. and Zolot, M., “Battery Usage and Thermal Performance of the Toyota Prius and Honda Insight for Various Chassis Dynamometer Test Procedures”, NREL Internal Report, 2001.

10. Hellman, K., Peralta, M. and Piotrowski, G. "Evaluation of a Toyota Prius Hybrid System (THS)", United States Environmental Protection Agency EPA420-R-98-006, 1998.
11. Chatroux, D. "Toyota PRIUS: focus on Continuous Variable Transmission and battery costs", Advances in Hybrid Powertrains, Paris, 2008.
12. "London's hybrid bus trials - the results", obtained from <http://www.cvengineering.com/>, last visited December 2010.
13. "Future Fuels & Power", obtained from <http://www.v63.net/truckandbusbuilder/index.html>, last visited December 2010.
14. Husted, H., "A Comparative Study of the Production Applications of Hybrid Electric Powertrains", SAE paper 2003-01-2307, 2003.
15. Tamai, G., Hoang, T., Taylor, J., Skaggs, C. and Downs, B., "Saturn Engine Stop-Start System with an Automatic Transmission", SAE paper 2001-01-0326, 2001.
16. Aoki, K., Kuroda, S., Kajiwara, S., Sato, H. and Yamamoto, Y., "Development of Integrated Motor Assist Hybrid System: Development of the 'Insight', a Personal Hybrid Coupe", SAE paper 2000-01-2216, 2000.
17. Baseley, S., Ehret, C., Greif, E. and Kliffken, M., "Hydraulic Hybrid Systems for Commercial Vehicles", SAE paper 2007-01-4150, 2007.
18. Kepner, R., "Hydraulic Power Assist – A Demonstration of Hydraulic Hybrid Vehicle Regenerative Braking in a Road Vehicle Application", SAE paper 2002-01-3128, 2002.
19. Batavia, B., "Hydraulic Hybrid Vehicle Energy Management System", SAE paper 2009-01-1772, 2009.
20. "Hydraulics & pneumatics", obtained from <http://www.hydraulicspneumatics.com/200/Issue/Article/False/38545/Issue>, last visited March 2011.
21. "Hybrid Concept", obtained from <http://www.innas.com/Assets/files/Hybrid%20brochure.pdf>, last visited March 2011.

22. Achten, P., "The Hybrid Transmission", SAE paper 2007-01-4152, 2007.
23. "Hybrid Technology Technical Articles", obtained from <http://www.parker.com/portal/site/Market-Tech/menuitem.2ac544c4aa325776de92b210237ad1ca/?vgnextoid=2ebcf84ab14ba210VgnVCM10000048021dacRCRD&vgnnextfmt=default&display=literature&vgnnextcat=Technical+Articles&querypotential=abc#>, last visited March 2011.
24. "Chrysler, EPA Ink Deal To Develop Hydraulic Hybrid Minivan", obtained from http://www.trucktrend.com/features/news/2011/163_news110119_chrysler_hydraulic_hybrid_minivan/index.html, last visited May 2011.
25. "The History of Compressed Air Vehicle", obtained from <http://www.aircarfactories.com/air-cars/compressed-air-history.html>, last visited March 2011.
26. Pneumatic Options Research Library, obtained from <http://www.aircaraccess.com>, last visited March 2011.
27. Broderick, J., "Combined internal-combustion and compressed-air engine", US Patent 1013528, January 1912.
28. Brown, R., "Compressed air engine", US Patent 3765180, October 1973.
29. Higelin, P. and Charlet, A., "Thermodynamic cycles for a new hybrid pneumatic-combustion engine concept", 5th International Conference on Internal Combustion Engines (ICE2001), Naples, Italy, HM1-2201-01-033, 2001.
30. Higelin, P., Charlet A. and Chamaillard, Y., "Thermodynamic simulation of a hybrid pneumatic-combustion engine concept". International Journal of Applied Thermodynamics, March 2002, vol.5, no.1, pp.1-12, 2002.
31. Higelin, P., Vsile, I., Charlet, A. and Chamaillard, Y., "Parametric Optimization of a New Hybrid Pneumatic-Combustion Engine Concept", International Journal of Engine Research, vol.5, no.2, pp.205-217, 2004.

32. Ivanco, A., Chamaillard, Y., Charlet, A. and Higelin, P., “Energy Management Strategies for Hybrid-Pneumatic Engine based on sliding window pattern recognition”, *Advances in Hybrid Powertrains*, Paris, 2008
33. Ivanco, A., Charlet, A., Chamaillard, Y. and Higelin, P., “Energy Management Strategies for Hybrid-Pneumatic Engine Studied on an Markov Chain Type Generated Driving Cycle”, SAE paper 2009-01-0145, 2009.
34. Brejaud, P., Charlet, A., Chamaillard, Y. and Higelin, P., “Pneumatic-Combustion Hybrid Engine: A Study of the Effect of the Valvetrain Sophistication on Pneumatic Modes”, *Oil & Gas Science and Technology – Rev. IFP*, Vol.65, No.1, pp.27-37, 2010.
35. Schechter M. and Levin, M., “Camless Engine”, SAE paper 1996-96-0581, 1996.
36. Turner, J., Kenchington, S. A. and Stretch, D. A., “Production AVT Development: Lotus and Eaton's Electrohydraulic Closed-Loop Fully Variable Valve Train System”, *Fortschritt Berichte - VDI Reihe 12 Verkehrstechnik Fahrzeugtechnik*, vol.1, issue 566, pp.331-346, 2004.
37. Allen, J. and Law, D., “Production Electro-Hydraulic Variable Valve-Train for a New Generation of I.C. Engines”, SAE paper 2002-01-11089, 2002.
38. Tai, C. and Tsao, T., “Using Camless Valvetrain for Air Hybrid Optimization”, SAE paper 2003-01-0038, 2003.
39. Kang, H., Tai, C., Smith, E., Wang, X., Tsao, T., Stewart, J. and Blumberg, P., “Demonstration of Air-Power-Assist (APA) Engine Technology for Clean Combustion and Direct Energy Recovery in Heavy Duty Application”, SAE paper 2008-01-1197, 2008.
40. Psanis, C., “Modeling and Experiments on Air Hybrid Engine Concept for Automotive Applications”, Thesis for the degree of PhD, Brunel University, July 2004.
41. Trajkovic, S., Milosavljevic, A., Tunestal, P. and Johansson, B., “FPGA Controlled Pneumatic Variable Valve Actuation”, SAE paper 2006-01-0041, 2006.
42. Trajkovic, S., Tunestal, P. and Johansson, B., “Investigation of Different Valve Geometries and Valve Timing Strategies and their Effect on Regenerative Efficiency

- for a Pneumatic Hybrid with Variable Valve Actuation”, SAE paper 08SFL-0329, 2008.
43. Trajkovic, S., Tunestal, P. and Johansson, B., “Simulation of a Pneumatic Powertrain with VVT in GT-Powertrain and Comparison with Experimental Data”, SAE paper 2009-01-1323, 2009.
 44. Trajkovic, S., Tunestal, P. and Johansson, B., “Vehicle Driving Cycle Simulation of a Pneumatic Hybrid Bus Based on Experimental Engine Measurements”, SAE paper 2010-01-0825, 2010.
 45. Trajkovic, S., “The Pneumatic Hybrid Vehicle A New Concept for Fuel Consumption Reduction”, Thesis for the degree of PhD, Lund Institute of Technology, ISSN 0282-1990, 2010.
 46. Hancock, D., Fraser, N., Jeremy, M., Sykes, R. and Blaxill, H., “A New 3 Cylinder 1.2l Advanced Downsizing Technology Demonstrator Engine”, SAE paper 2008-01-0611, 2008.
 47. Lumsden, G., OudeNijeweme, D., Fraser, N. and Blaxill, H., “Development of a Turbocharged Direct Injection Downsizing Demonstrator”, SAE paper 2009-01-1503, 2009.
 48. Fraser, N., Blaxill, H., Lumsden, G. and Bassett, M., “Challenges for Increased Efficiency through Gasoline Engine Downsizing”, SAE paper 2009-01-1053, 2009.
 49. Donitz, C., Vasile, I., Onder, C. and Guzzella, L., “Realizing a Concept for High Efficiency and Excellent Driveability: The Downsized and Supercharged Hybrid Pneumatic Engine”, SAE paper 2009-01-1326, 2009.
 50. Turner, J., Bassett, M., Pearson, R., Picher, G. and Douglas, K., “New Operating Strategies afforded by Fully Variable Valve Trains”, SAE paper 2004-01-1386, 2004.
 51. Ricardo WAVE 8.1 WAVE Knowledge Centre: What is WAVE?, 2009.
 52. “Ricardo WAVE software”, obtained from <http://www.ricardo.com/en-gb/What-we-do/Software/Products/WAVE/>, last visited October 2010.
 53. Ma T. and Zhao H., Method of operating an internal combustion Engine

- Europe (Granted 29/08/07)- Patent No. 1747351; UK, France, Germany, Italy.
 - U.S. (Granted 03/06/08)- Patent No. 7,380,525
 - China (Granted 30/09/09)- ZL200580020515.7
54. Lee, C., Zhao, H. and Ma, T., “A Low Cost Air Hybrid”, *Oil & Gas Science and Technology – Rev. IFP*, Vol.65, No.1, pp.19-26, 2010.
55. Lee, C., Zhao, H. and Ma, T., “The Performance Characteristics of an Production Oriented Air Hybrid Powertrain”, *SAE Int. J. Engines*. 3(1):609-619, 2010.
56. Ma, T., Zhao, H., Engine for an Air Hybrid Vehicle, UK Priority Application (Filed 24/06/10) - Patent Application No. GB1010649.0
57. Huber, R., Klumpp, P. and Ulbrich, H., “Dynamic Anlysis of the Audi Valvelift System”, SAE paper 2010-01-1195, 2010.
58. Henry, R., Lequesne, B., Chen, S., Ronning, J. and Xue, Y., “Belt-Driven Starter-Generator for Future 42-Volt Systems”, SAE paper 2001-01-0728, 2001.
59. Zhou, Q. and Houldcroft, J., “Cold engine cranking torque requirement analysis”, SAE paper 2007-01-1967, 2007.
60. Private communication with China Yuchai International Limited.
61. “Vane Starters (Ingersoll Rand)”, obtained from http://www.ingersollrandproducts.com/IS/product.aspx-am_en-4250, last visited March 2010.
62. MATLAB 7.8 (R2009a): Simulink Block Library 7.3: Sources, July 2009.
63. MATLAB 7.8 (R2009a): Simulink Block Library 7.3: Sinks, July 2009.
64. MATLAB 7.8 (R2009a): Simulink Block Library 7.3: Continuous, July 2009.
65. MATLAB 7.8 (R2009a): Simulink Block Library 7.3: Discontinuous, July 2009.
66. MATLAB 7.8 (R2009a): Simulink Block Library 7.3: Math Operations, July 2009.
67. MATLAB 7.8 (R2009a): Simulink Block Library 7.3: Lookup Tables, July 2009.

68. MATLAB 7.8 (R2009a): Simulink Block Library 7.3: Port & Subsystems, July 2009.
69. Guzzella L. and Sciarretta A., “Vehicle Propulsion Systems: Introduction to Modeling and Optimization”, p.27, Springer, ISBN 978-3-540—25195-8, 2007.
70. Jazar, R., “Vehicle Dynamics: Theory and Application”, p.119, Springer, ISBN 978-0-387-74243-4, 2008.
71. Ricardo WAVE 8.0 reference library, user manuals: vehicle driveline model: 3.5 engine, August 2010.
72. ScioTech, “Economics of bus driveline”, Department for Transport (DfT): www.dft.gov.uk/pgr/roads/environment/research/cqvcf/economicsofbusdrivelines, last visited January 2011.
73. Battery University, obtained from <http://batteryuniversity.com/>, last visited February 2011.
74. “Using DC motors in fighting robots”, obtained from <http://homepages.which.net/~paul.hills/Motors/Motors.html>, last visited February 2011.
75. “Understanding Stop-Start Idle Elimination and emerging Energy storage Solution”, obtained from <http://community.nasdaq.com/News/2010-11/understanding-stopstart-idle-elimination-and-emerging-energy-storage-solutions.aspx?storyid=44921>, last visited Feb 2011
76. BENDIX, “BENDIX Energy Management Improves Fuel Savings, Vehicle Performance”, obtained from http://www.bendix.com/media/documents/press_releases/2010/Energy_Mgmt_System_Update_2010_a.pdf, last visited January 2011.

Appendix

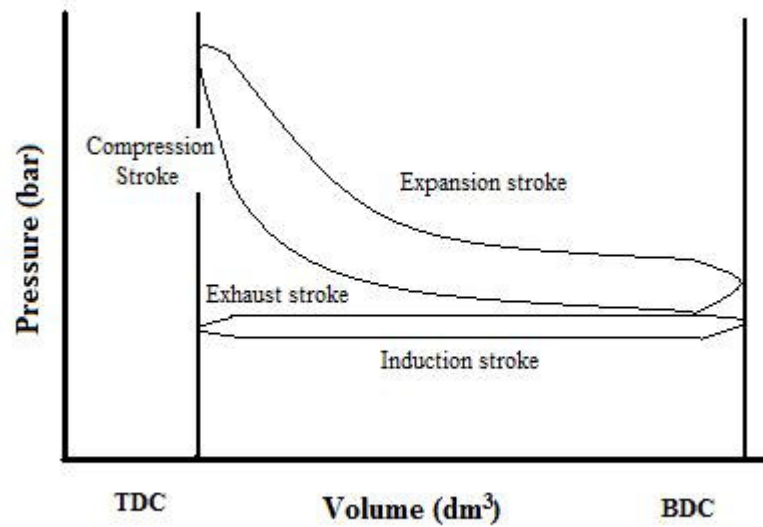


Figure A1: PV diagram

Table A1: Puma 2.0TCDi data

Rpm	Nm	kg/hr	rpm	Nm	kg/hr	rpm	Nm	kg/hr
750	0	0.43	2000	63.63	3.352	3000	270.19	18.986
750	7.95	0.49	2000	79.42	4.057	3000	284.61	20.429
750	15.9	0.57	2000	95.62	4.746	3000	355.763	26.596
750	23.85	0.76	2000	111.54	5.404	3250	0	2.13
750	31.8	0.89	2000	126.99	6.494	3250	3.15	2.431
750	39.75	1.05	2000	143.22	6.83	3250	7.65	2.492
750	47.7	1.1	2000	158.94	7.295	3250	15.53	3.097
750	55.65	1.27	2000	175.22	7.937	3250	31.67	4.35
750	63.61	1.35	2000	190.99	8.53	3250	47.8	5.103
750	71.56	1.48	2000	206.4	9.171	3250	63.58	6.321
750	79.51	1.67	2000	222.39	9.893	3250	79.31	7.043
750	87.46	1.75	2000	238.49	10.566	3250	95.16	8.261
750	95.41	1.89	2000	254.45	11.335	3250	111.35	9.367
750	103.36	2.07	2000	270.56	12.249	3250	127.37	10.682
750	111.31	2.31	2000	286.17	12.73	3250	143.12	11.692
750	119.26	2.47	2000	302.24	13.932	3250	158.88	12.975
750	127.21	2.63	2000	318.77	14.494	3250	175.33	13.856
750	135.16	2.84	2000	327.05	15.215	3250	190.82	14.898
750	143.11	3.01	2000	408.813	19.819	3250	206.46	15.94
750	151.06	3.23	2250	0	1.454	3250	222.93	17.303
810	0	0.482	2250	3.46	1.488	3250	238.68	18.506
810	20	0.735	2250	8.1	1.742	3250	254.7	19.548
810	40	1.035	2250	15.73	2.026	3250	268.4	21.311
810	60	1.405	2250	32.34	2.619	3250	335.5	26.793
810	80	1.819	2250	48.12	3.596	3500	0	2.024

810	100	2.212	2250	63.86	3.885	3500	2.88	2.286
810	132	3.159	2250	79.95	4.734	3500	8.2	2.927
1000	0	0.493	2250	95.6	5.52	3500	15.63	3.628
1000	2.53	0.507	2250	111.66	6.161	3500	31.68	4.654
1000	7.89	0.577	2250	127.44	7.091	3500	47.82	5.472
1000	15.72	0.779	2250	143.34	7.556	3500	63.43	6.754
1000	31.86	1.137	2250	159.43	8.149	3500	79.43	7.732
1000	47.38	1.446	2250	175.11	8.951	3500	95.42	9.175
1000	63.68	1.779	2250	190.94	9.816	3500	111.28	10.377
1000	79.82	2.166	2250	206.81	10.746	3500	127.3	11.772
1000	95.42	2.438	2250	222.79	11.452	3500	143.38	13.295
1000	111.01	2.801	2250	238.76	12.253	3500	159.21	14.738
1000	127.32	3.25	2250	254.49	13.215	3500	174.63	14.979
1000	143.42	3.699	2250	270.66	13.696	3500	191.04	16.822
1000	157.73	4.196	2250	286.39	14.498	3500	206.41	17.864
1000	197.163	6.035	2250	302.23	15.46	3500	222.82	19.387
1250	0	0.662	2250	318.47	16.261	3500	238.52	20.83
1250	2.56	0.761	2250	328.22	16.983	3500	249.51	22.113
1250	8.18	0.847	2250	410.275	21.67	3500	311.888	28.083
1250	15.74	0.877	2500	0	1.564	3800	0	3.115
1250	31.72	1.416	2500	2.24	1.748	3800	3.09	3.336
1250	47.63	1.555	2500	7.89	1.953	3800	8.26	3.673
1250	63.7	2.129	2500	16.11	2.329	3800	15.83	4.09
1250	79.88	2.529	2500	32.01	3.259	3800	31.93	5.356
1250	95.16	3.049	2500	47.8	3.772	3800	47.87	6.446
1250	111.25	3.474	2500	63.92	4.366	3800	63.79	7.825
1250	127	3.923	2500	79.8	4.991	3800	79.73	9.236
1250	143.2	4.308	2500	95.77	6.081	3800	95.67	10.711
1250	159.02	4.821	2500	111.35	6.69	3800	111.44	12.186
1250	174.83	5.254	2500	127.36	7.572	3800	127.65	13.228
1250	190.8	5.751	2500	143.45	8.662	3800	143.16	14.27
1250	206.72	6.376	2500	159.4	9.079	3800	159.24	15.552
1250	212.67	6.616	2500	174.95	10.025	3800	175.21	17.075
1250	265.838	8.23	2500	190.94	10.49	3800	191.24	18.438
1500	0	0.668	2500	206.74	11.692	3800	206.81	19.961
1500	2.72	0.782	2500	222.97	12.654	3800	223	21.725
1500	7.46	0.829	2500	238.86	13.616	3800	226.98	22.125
1500	15.97	1.095	2500	254.86	14.337	3800	283.725	27.997
1500	31.77	1.555	2500	270.6	15.46	4000	0	3.151
1500	48	1.936	2500	286.21	16.582	4000	2.47	3.352
1500	63.47	2.365	2500	302.35	17.704	4000	7.89	4.186
1500	79.57	3.522	2500	312.02	18.345	4000	15.97	5.34
1500	95.43	3.49	2500	390.025	23.789	4000	31.87	6.014
1500	111.43	4.035	2750	0	1.609	4000	47.92	7.04
1500	127.04	4.644	2750	3.56	1.778	4000	63.69	8.37
1500	142.97	5.077	2750	7.94	2.208	4000	79.49	9.733
1500	158.97	5.574	2750	15.84	2.498	4000	95.66	11.24
1500	175.03	6.103	2750	32.03	3.388	4000	111.33	13.068
1500	190.86	6.6	2750	47.73	4.029	4000	127.37	14.11
1500	206.42	7.145	2750	63.97	4.718	4000	143.55	15.312
1500	222.48	7.739	2750	79.59	5.808	4000	159.27	16.595
1500	238.26	8.284	2750	95.32	6.674	4000	175.18	18.118
1500	254.5	9.101	2750	111.23	7.38	4000	190.87	19.641
1500	271.88	9.694	2750	127.02	8.406	4000	212.49	22.366
1500	339.85	12.48	2750	143.13	9.191	4000	265.613	27.959
1800	0	0.902	2750	159.03	10.249	4200	0	3.371
1800	3.48	1.009	2750	174.83	11.227	4200	4.7	3.737

1800	8.21	1.082	2750	190.65	12.333	4200	7.91	4.138
1800	15.76	1.342	2750	206.73	13.375	4200	15.97	4.763
1800	31.69	1.88	2750	222.58	14.097	4200	32.16	6.158
1800	47.45	2.509	2750	238.81	15.379	4200	47.77	7.489
1800	63.47	3.054	2750	254.82	16.341	4200	63.84	9.044
1800	79.21	3.64	2750	270.35	17.143	4200	79.82	10.502
1800	95.76	4.281	2750	286.12	18.345	4200	95.72	12.106
1800	111.56	4.891	2750	293.68	19.307	4200	111.62	13.388
1800	127.5	5.468	2750	367.1	24.562	4200	127.22	14.751
1800	143.19	6.045	3000	0	1.966	4200	143.24	16.033
1800	159.15	6.606	3000	2.99	2.298	4200	159.43	17.957
1800	174.92	7.231	3000	8.12	2.316	4200	175.35	19.32
1800	191.01	7.792	3000	15.84	2.818	4200	190.54	21.404
1800	206.96	8.482	3000	31.42	4.029	4200	238.175	26.55
1800	222.97	9.139	3000	47.88	4.542	4500	0	4.086
1800	238.73	9.716	3000	63.65	5.44	4500	3.97	4.603
1800	254.77	10.486	3000	79.65	6.257	4500	8.29	4.747
1800	270.65	11.496	3000	95.58	7.396	4500	16.01	5.661
1800	286.67	11.929	3000	111.43	8.261	4500	32.03	7.216
1800	302.2	12.65	3000	127.08	9.416	4500	47.8	8.547
1800	324.3	13.932	3000	143.21	10.602	4500	63.87	10.278
1800	405.375	17.523	3000	158.89	11.612	4500	79.65	12.234
2000	0	1.019	3000	174.9	12.253	4500	95.68	13.949
2000	2.36	1.112	3000	190.81	13.536	4500	111.13	14.911
2000	7.79	1.33	3000	206.71	14.818	4500	127.32	16.114
2000	16.01	1.578	3000	222.88	15.94	4500	143.26	17.957
2000	31.68	2.237	3000	238.63	16.983	4500	160.9	20.362
2000	47.84	2.794	3000	254.52	17.784	4500	201.125	24.569

Table A2: YUCHAI YC6A data

rpm	Nm	kg/hr	rpm	Nm	kg/hr	rpm	Nm	kg/hr
2296	792	42.21	1900	335	14.76	1300	749	20.46
2297	734	38.91	1899	239	11.57	1300	500	14
2296	672	35.45	1699	999	36.31	1299	350	10.15
2297	594	31.06	1701	899	32.1	1300	248	7.86
2295	395	21.71	1700	848	30.13	1100	986	23.76
2296	278	16.47	1700	499	18.1	1097	898	21.41
2295	196	13.11	1699	349	13.42	1098	848	20.21
2100	867	40.45	1700	748	26.71	1099	749	17.81
2100	805	37.06	1700	249	10.41	1099	499	11.92
2099	738	33.85	1496	998	31.31	1097	350	8.63
2098	650	29.72	1501	898	27.81	1098	250	6.53
2098	434	20.68	1499	847	26.13	897	848	18.02
2099	303	15.5	1499	747	23.18	896	763	15.88
2098	217	12.26	1499	499	15.95	898	722	15.05
1898	957	39.73	1498	349	11.82	896	638	12.95
1900	887	36.33	1498	250	9.11	896	423	8.45
1899	816	33.02	1300	1000	27.4	896	297	6.08
1899	719	28.88	1300	898	24.58	897	212	4.63
1900	478	19.81	1299	849	23.2	650	0	1.2

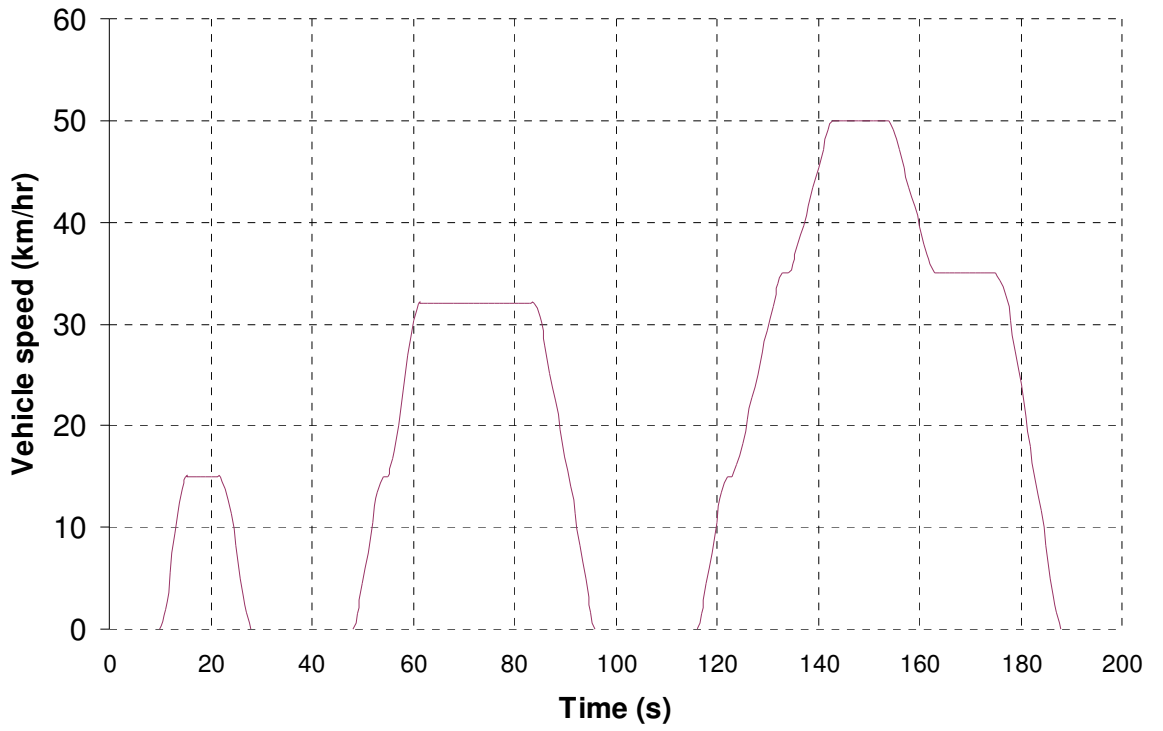


Figure A2: ECE-15 driving cycle time-speed diagram

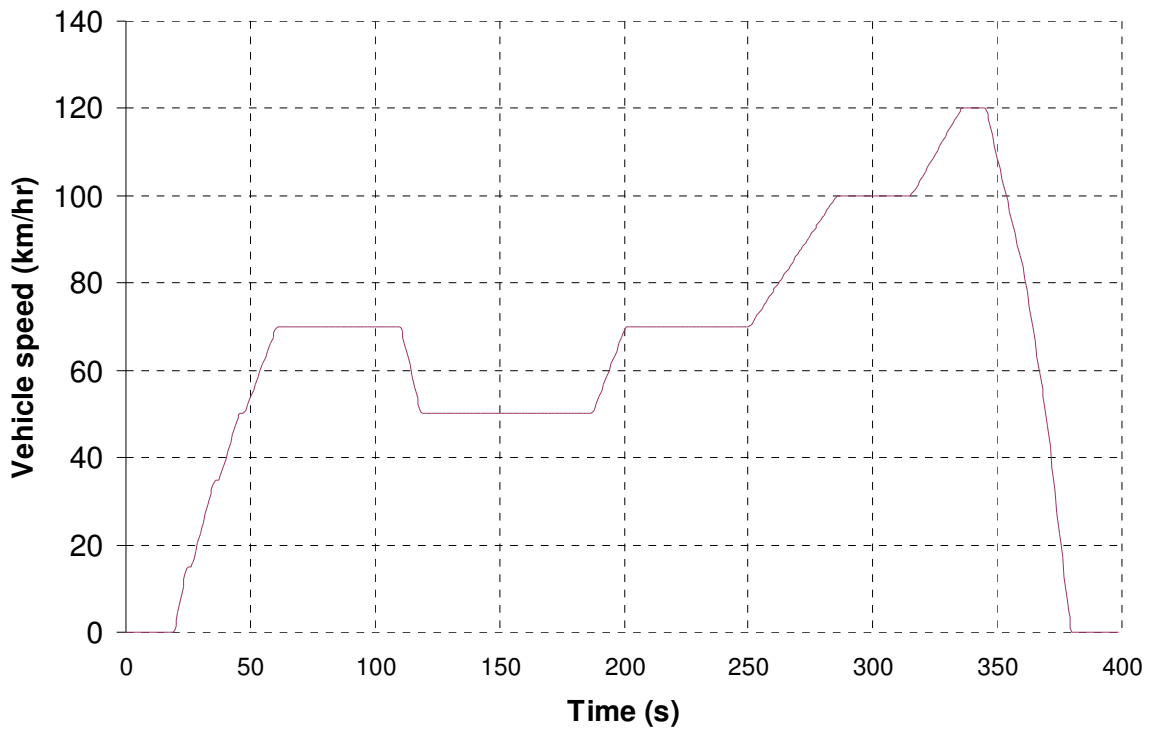


Figure A3: EUDC time-speed diagram

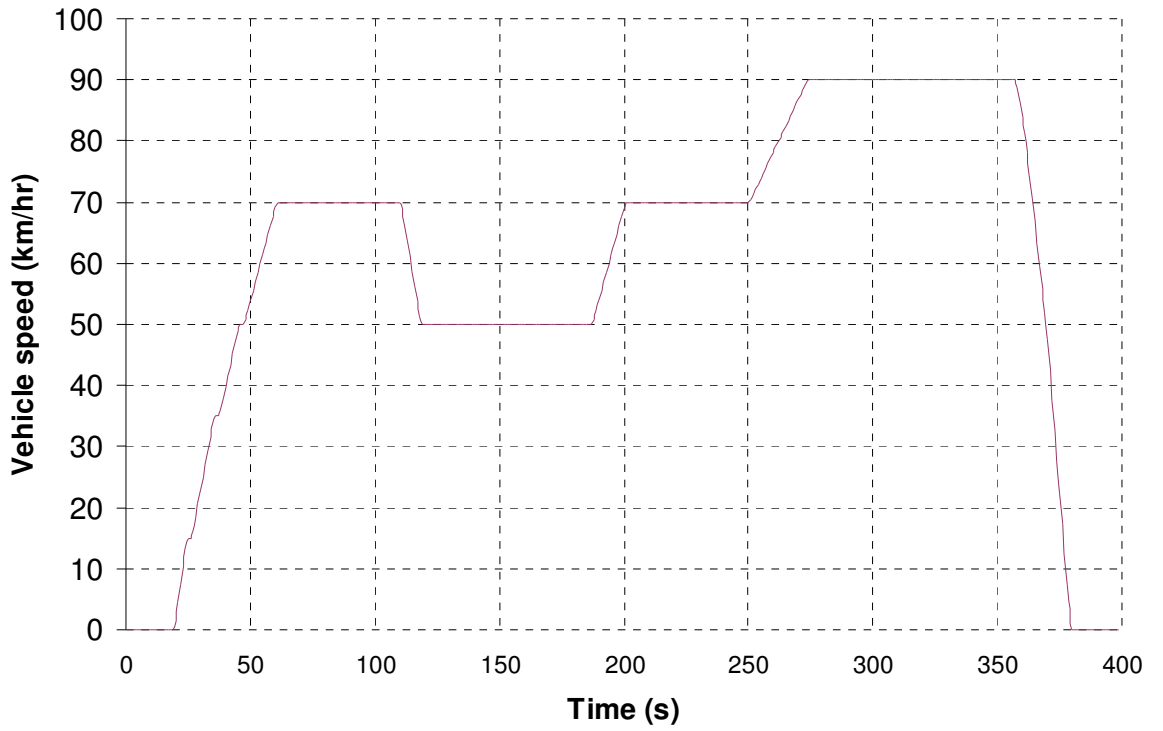


Figure A4: EUDCL time-speed diagram

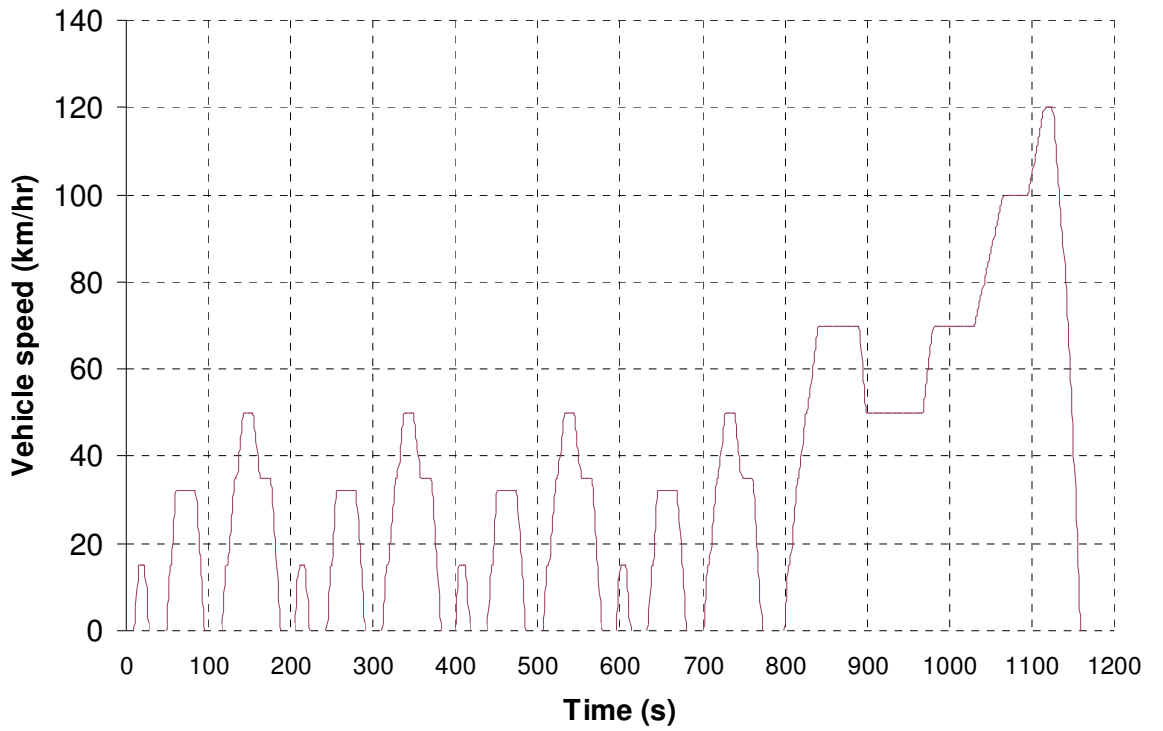


Figure A5: NEDC time-speed diagram

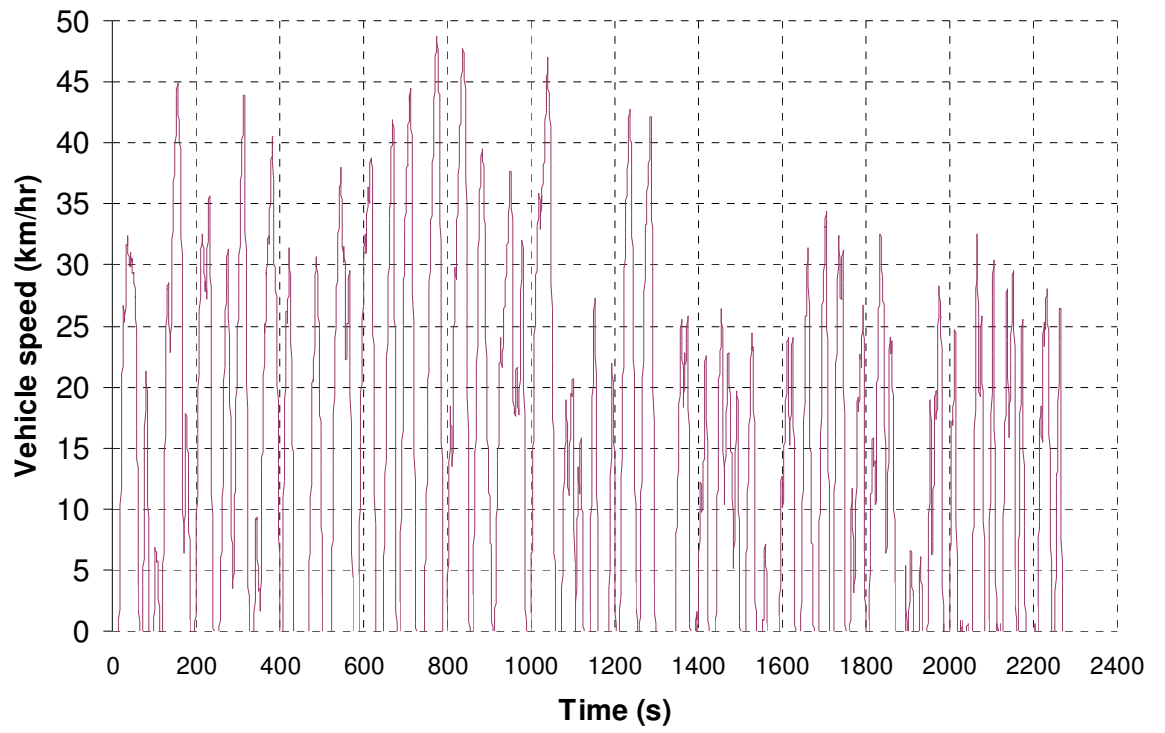


Figure A6: MLTB driving cycle time-speed diagram